NONLINEAR DYNAMICS OF FLEXIBLE CARTESIAN MANIPULATORS

A thesis Submitted for the Degree of

Doctor of Philosophy

By

BARUN PRATIHER
(Roll No: 04610301)

Department of Mechanical Engineering
Indian Institute of Technology Guwahati
India-781039
December, 2008

Dedicated

TO

MAA Saraswati and Lord Krishna

To my lovely Parents

Mrs. Shyamarani Pratiher

Mr. Mohananda Pratiher

To my sweet sisters and brother

Jhuma Pratiher and Tumpa Porel

Biplab Pratiher

Department of Mechanical Engineering
Indian Institute of Technology Guwahati
India-781039

Certificate

It is certified that the work contained in this thesis entitled "Nonlinear Dynamics of Flexible Cartesian Manipulators" submitted by Mr. Barun Pratiher to the Indian Institute of Technology Guwahati for the award of the degree of Philosophy has been carried out under my supervision in the Department of Mechanical Engineering, Indian Institute of Technology Guwahati. This work has not been submitted elsewhere for the award of any other degree or diploma.

The thesis, in my opinion, has reached the standard fulfilling the requirements for the award of the degree of Doctor of Philosophy in accordance with the regulations of the Institute.

(Dr. Santosha K. Dwivedy)
Professor
Department of Mechanical Engineering
Indian Institute of Technology Guwahati
India-781039

ACKNOWLEDGEMENTS

First of all, I would like to express my deepest and wholeheartedly thank to Prof. Santosha K. Dwivedy for his excellent supervision and kindness throughout this work. His patience as an advisor, unlimited energy while teaching, promptness while reviewing all my writing, and passion for research are to be commended and worth emulating. I am always gratitude to him for the endless freedom, encouragement, and motivation which he has provided to achieve this goal.

Then, I express my deep sense of gratitude to the chairman of my doctoral committee and head of the Department, Prof. Uday S. Dixit for his valuable advice and kind help. Also, I would like to extend my appreciation to my doctoral committee members Prof. R. Tiwari and Prof. S. Talukdar for their constructive criticisms and helpful suggestions which make thesis improvement.

I would like to express my thank to my friend Mr. Sachin Kumar Singh for helping me in my critical situations including financial crisis times. I also extend my thank to my friends Mr. Lalsangzela Sailo, Sandip Mondal, Mr. Soumen Dhara, all research scholars in the Department of Mechanical Engineering and my other friends for their lot of help to complete my work successfully.

Most importantly, I would like to thank my parents, Mrs. Shyamarani Pratiher and Mr. Mohananda Pratiher for their love, blessing, encouragement and never-ending kindness which made everything easier to achieve. My sweet sisters Jhuma and Tumpa and my lovely brother Biplab Pratiher were always a source of untiring love, support and affection in all walks of life.

(Barun Pratiher)

ABSTRACT

In this work, the nonlinear dynamic analyses of flexible Cartesian manipulators with elastic, viscoelastic and magnetoelastic beam materials for different applications are carried out. From exhaustive literature review, it is observed that though Cartesian manipulator has been used in many applications such as space exploration, hazardous nuclear power plant, micro surgery, precision manufacturing, and in many other industrial applications, very limited research has been carried out to enhance their productivity by making them lightweight or flexible, as these flexible manipulators cause severe vibration problems. Hence, in this work, an attempt is made to study the flexible Cartesian manipulator and develop some strategy to control the vibration of the presently used elastic manipulators by incorporating viscoelastic and magnetoelastic manipulator.

Here, single-link flexible Cartesian manipulator with a payload has been modeled either as an transversely vibrating Euler-Bernoulli beam with roller-support at one end and tip mass at the other end, or as a transversely vibrating cantilever beam with end mass. The roller-supported end is assumed to have periodic motion. In some analyses, to simulate applications like welding, spraying, metal cutting etc. when the endeffector of the manipulator is in contact with the work environment, and has been subjected to forces from the environment, the endeffector of the manipulator has been modeled as a point mass subjected to harmonically varying axial tip force. In this work, 9 different flexible Cartesian manipulator models have been studied.

Here, D' Alembert's principle is used to derive the spatial governing equation of motion for elastic, viscoelastic and magnetoelastic manipulators, which is discretized into their temporal equations of motion by using generalized Galerkin's method. These nondimensional temporal equations of motion contain many nonlinear terms which include cubic geometric and inertial terms due to large transverse deflection, nonlinear damping

terms, and nonlinear parametric excitation terms along with linear stiffness, damping, forcing and parametric excitation terms.

Due to the presence of many nonlinear terms, the perturbation methods viz., first and second order method of multiple scales, and method of normal forms are used to reduce the second order temporal equation of motion to a set of first order differential equations, which are then reduced to a set of nonlinear algebraic equation for steady state condition. For different resonance conditions, these reduced equations are solved numerically to find the steady state response of the systems. Taking various physical system parameters such as amplitude and frequency of support motion; mass ratio (ratio of mass of the payload and the beam); static and dynamic amplitude and frequency of axial force and magnetic field; viscous damping; loss factor; material conductivity and relative permeability of the material numerical simulations have been carried out to find the transient and steady state response, their stability and critical bifurcations. Time response, frequency response, instability regions, phase portraits, Poincare's section, and basins of attraction are used to analyze the system behaviour for different resonance conditions.

Initially, study has been carried out to investigate the vibration of harmonically varying roller-supported elastic manipulators with and without periodically varying axial force. It is observed that when the operating frequency of the system is closer to the fundamental natural frequency and/or near twice and thrice the fundamental natural frequency of the system, the system has a tendency to vibrate violently and undergo catastrophic failure if the operating frequency exceed critical bifurcation limit. To attenuate this vibration of the manipulator passively, study has been carried out by taking viscoelastic material in place of elastic material. Finally, to actively control the vibration of the manipulator, exhaustive investigation is carried out by taking five different models of Cartesian manipulators with magnetoelastic material. Here, the manipulator is modeled both as cantilever and roller-supported Euler-Bernoulli beam with tip mass.

From the present analyses it is observed that the viscoelastic and magnetoelastic manipulators have significant potential to reduce the vibration of the manipulators. Hence, these lightweight flexible manipulators can be used effectively to lower the cost, to increase the speed of operations, and to enhance the productivity of the system in many industrial and other applications. The obtained perturbation results are compared with the results obtained by numerically solving the temporal equation of motion and with the previously published experimental results which are found to be in good agreement. Hence, though a few free vibration experiments are required to find the system characteristics, instead of carrying out other expensive experiments and computationally solving the temporal equation of motion which are tedious and time consuming, one may use the developed simplified reduced equations in the present work for finding the frequency response, and the critical bifurcation points for different resonance conditions. The findings of this thesis will serve as guidelines and will find extensive applications in the design, manufacturing, and control of flexible Cartesian manipulator for precision positioning and constrained motion without any vibration.

CONTENTS

Abstract v

List of Figures xi

Nomenclature xxiii

List of publications from this thesis xxiv

1 INTRODUCTION 1

1.1 Introduction 1

1.2 Goal of present work 9

1.3 Methodology 10

1.4 Organization of thesis 11

2 REVIEW OF LITERATURE 13

2.1 Introduction 13

2.2 Literatures review on the flexible robotic manipulator 13

2.2.1 Application of flexible manipulator 14

2.2.2 Modeling of single-link flexible Manipulator 15

2.2.3. Effect of payload 20

2.2.4 Modeling as Rayleigh and Timoshenko beam 21

2.2.5 Shape optimization 21

2.2.6 Multi-link manipulator 22

2.2.7 Nonlinear analysis of flexible manipulators 22

2.2.8 Control of flexible manipulator 23

2.2.9 Flexible Cartesian manipulator 25

2.2.10 Dynamics of Base excited Systems 27

2.2 Literature review on beams with viscoelastic material 28

2.3 Literature review on magnetoelastic beams 31

2.4 Literature review on parametrically exited systems 33
2.5 Summary 38
3 ELASTIC CARTESIAN MANIPULATOR 39
3.1 Introduction 39
3.2 Mathematical modeling 40
3.3 Cartesian manipulator without axial tip force 46
3.3.1 Analysis 46
3.3.2 Numerical results and discussions 51
3.4 Cartesian manipulator with harmonically varying axial tip force 62
3.4.1 Analysis 62
3.4.2 Numerical results and discussions 68
3.5 Summary 84
4 Viscoelastic Cartesian manipulator 87
4.1 Introduction 87
4.2 Mathematical modeling 88
4.3 Cartesian manipulator without axial tip force 92
4.3.1 Analysis 92
4.3.2 Numerical results and discussions 98
4.4 Cartesian manipulator with harmonically varying axial tip force 109
4.4.1 Analysis 109
4.4.2 Numerical results and discussions 113
4.5 Summary 129
5 Magnetoelastic Cartesian manipulator 133
5.1 Introduction 133
5.2 Mathematical modeling 134
5.3 Cantilevered manipulator with axial force considering small transverse deflection 142
5.3.1 Analysis 142

5.3.2 Numerical results and discussions 145
5.4 Cantilevered manipulator with static and dynamic magnetic field 155
5.4.1 Analysis 155
5.4.2 Numerical results and discussions 158
5.5 Cantilevered manipulator without axial force 166
5.5.1 Analysis 166
5.5.2 Numerical results and discussions 168
5.6 Cantilevered manipulator with harmonically varying tip force 176
5.6.1 Analysis 176
5.6.2 Numerical results and discussions 180
5.7 Roller-supported manipulator without axial force 193
5.7.1 Analysis 193
5.7.2 Numerical results and discussions 198
5.8 Summary 213
6 Conclusions and Scopes of Future works 215
6.1 Conclusions 215
6.2 Scope of Future works 225
7 References 227

LIST OF FIGURES

Figures	Contents	Page No.
Fig. 1.1	A heavy weight SCARA robot.	2
Fig. 1.2	A heavy weight Cartesian robot.	2
Fig. 1.3	Prostate Biopsy Robot in Closed High-Field MRI Scanner.	2
Fig. 1.4	Multi-role flexible robot for hazmat handling, search and rescue, and hostage rescue operation.	2
Fig. 3.1	Schematic diagram of a single-link Cartesian manipulator with payload subjected to harmonically varying axial force	40
Fig. 3.2	Frequency response curve for simple resonance case for mass ratio $\overline{m}$ =1.8787 and base excitation $\overline{Z}$ =0.00372.	52
Fig. 3.3	Time history, phase portrait and Poincare's' map at the critical point B (Fig. 3.2) where (i), (iii) and (v) represent for transient response and (ii), (iv) and (vi) represent the steady state response with initial point 0.326, 0.1.	54
Fig. 3.4	Time history, phase portrait and Poincare's' map at the point $A^{/}$ (Fig. 3.2) where (i), (iii) and (v) represent the transient response and (ii), (iv) and (vi) represent the steady state response with initial point 0.055, 0.1.	55
Fig. 3.5	Frequency response curve for simple resonance case for mass ratio $\overline{m}$ =1.8787;(i) $\overline{Z}$ =0.0125, (ii) $\overline{Z}$ =0.05.	56
Fig. 3.6	Frequency response curve for simple resonance case for mass ratio $\overline{Z}$ =0.02; (i) $\overline{m}$ =0.5656, and (ii) $\overline{m}$ =4.6968.	58
Fig. 3.7	Frequency response curve for sub harmonic resonance with mass ratio $\overline{m}$ = 0.5656 and $\overline{Z}$ = 0.2.	59
Fig. 3.8	Frequency response curve for subharmonic resonance for mass ratio $\overline{m}$ =0.5656; (i) $\overline{Z}$ =0.1, (ii) $\overline{Z}$ =0.01	60
Fig. 3.9	Frequency response curve for sub harmonic resonance case with $\overline{Z}$	61

=0.05; (i) $\bar{m}$ = 0.3757, (ii) $\bar{m}$ = 2.8181

Fig. 3.10 (a) Time history for trivial fixed-point response and (b) Projection of the trajectories in plane $p_s - q_s$ with $\bar{Z}$ =0.2 and mass ratio $\bar{m}$ =0.5656. 61

Fig. 3.11 Frequency response curve of a Cartesian manipulator with payload (P_o equal to zero) for $\bar{m}$ =2.0, $\bar{Z}$ =0.00372. 69

Fig. 3.12 Basins of attraction for $\bar{\omega}_1 = 0.80$ as key in Fig. 3.11. 69

Fig. 3.13 Frequency response curve for $\bar{m}$ =2.0, $\bar{Z}$ =0.00372; (i) $\bar{P}_0 = 0.167$, and (ii) $\bar{P}_0 = 0.333$. 70

Fig. 3.14 Time response and Poincare's map at the point B' (Fig.3.13 (i)) where (i), (ii) represents transient and (iii), (iv) represents steady state response of the system with initial condition $q = 0.33, \dot{q} = 0.01$. 71

Fig. 3.15 Time responses and Poincare's maps with three different initial conditions (i, iv) B, (ii, v) A, and (iii, vi) C as key in Fig.3.13 (i). 72

Fig. 3.16 Frequency response curve for $\bar{m}$ =2.0 and $\bar{P}_0 = 0.167$; (i) $\bar{Z}$ =0.00744, and (ii) $\bar{Z}$ =0.0298. 73

Fig. 3.17 Frequency response curve for $\bar{Z}$ =0.00372 and $\bar{P}_0 = 0.167$; (i) $\bar{m}$ =1.0, and (ii) $\bar{m}$ = 4.0. 73

Fig. 3.18 Frequency response curve for $\bar{m}$ =2.0, and $\bar{P}_0 = 0.0$; (i) $\bar{P}_1 = 0.033$ (ii) $\bar{P}_1 = 0.167$, (iii) $\bar{P}_1 = 0.25$, (iv) $\bar{P}_1 = 0.333$. 74

Fig. 3.19 Time responses and phase portraits with three different initial conditions (i, iv) A, (ii, v) B, and (iii, vi) C as key in Fig.3.18 (ii) 75

Fig. 3.20 Frequency response curve for $\bar{m}$ =2.0, and $\bar{P}_1 = 0.167$; (i) $\bar{P}_0 = 0.167$, (ii) $\bar{P}_0 = 0.334$. 76

Fig. 3.21 Frequency response curve for $\bar{P}_0 = 0.167$, and $\bar{P}_1 = 0.167$; (i) $\bar{m}$ =1.0, (ii) $\bar{m}$ = 4.0. 77

Fig. 3.22 Influence of phase angle (ϕ) on the frequency responses for $\bar{m} = 2.0$, 78

$\bar{P}_0 = 0.0$, $\bar{P}_1 = 0.167$, and $\bar{Z} = 0.0298$; (i) $\phi = 0$, (ii) $\phi = \frac{\pi}{6}$, (iii) $\phi = \frac{\pi}{2}$ and (iv) $\phi = \pi$.

Fig. 3.23 Influence of amplitude of Base excitation ($\bar{Z}$) on the frequency responses for $\bar{m} = 2.0$, $\bar{P}_0 = 0.0$, $\phi = 0$, and $\bar{P}_1 = 0.167$; (i) $\bar{Z} = 0.00372$, (ii) $\bar{Z} = 0.00744$. 79

Fig. 3.24 Time response and Poincare's maps corresponding to point A (i, iv); time responses and phase portraits corresponding to points B (ii, v), and C (iii, vi). Key as in Fig. 3.23(i). 80

Fig. 3.25 Time responses and phase portraits three different points initial conditions (i, v)A_1, (ii, vi)A_2, (iii, vii)A_3, and (iv, viii)A_4 as key in Fig.3.23 (i). 81

Fig. 3.26 Basins of attraction for $\bar{\omega}_1 = 0.70$ as key in Fig. 3.22(ii). 82

Fig. 3.27 Influence of amplitude of dynamic load ($\bar{P}_1$) on the frequency response curve for $\bar{m} = 2.0$, $\bar{P}_0 = 0.0$, $\phi = 0$, $\bar{Z} = 0.0298$; (i) $\bar{P}_1 = 0.333$, (ii) $\bar{P}_1 = 0.499$. 82

Fig. 3.28 Influence of amplitude of static load ($\bar{P}_0$) on the frequency response curve for $\bar{m} = 2.0$, $\bar{Z} = 0.0298$, $\phi = 0$, $\bar{P}_1 = 0.167$; (i) $\bar{P}_0 = 0.167$, (ii) $\bar{P}_0 = 0.334$ 83

Fig. 3.29 Influence of mass ratio ($\bar{m}$) on the frequency response curve for $\bar{Z} = 0.0298$, $\bar{P}_0 = 0.0$, $\phi = 0$, $\bar{P}_1 = 0.167$; (i) $\bar{m} = 1.0$, (ii) $\bar{m} = 4.0$. 84

Fig. 4.1 Schematic diagram of a single-link viscoelastic Cartesian manipulator with payload *M* subjected to harmonically varying axial force. 88

Fig. 4.2 Equivalent spring-mass-damper system with Kelvin-Voigt model. 97

Fig. 4.3 Frequency response curve for viscoelastic manipulator with $\bar{m} = 1.8787$, $\bar{Z} = 0.00372$; (i) $\delta = 0.02$ (ii)) $\delta = 0.05$. 99

Fig. 4.4 Time response, and phase portrait for the critical points A (key as in Fig. 100

4.3(i)) where (a, c) are the transient response, and (b, d) are the steady state response.

Fig. 4.5 Time response, phase portrait and Poincare's map for the critical points B' (key as in Fig. 4.3 (i)) where (a, c, e) are the transient response and (b, d, f) are the steady state response. 101

Fig. 4.6 Steady state time response (a) and phase portrait (b) for the critical points C' (key as in Fig. 4.3 (i)). 102

Fig. 4.7 Steady state time response (a) and phase portrait (b) for the critical points D (key as in Fig. 4.3 (i)). 102

Fig. 4.8 Frequency response curve for elastic beam for $\bar{m} = 1.8787$, $\bar{Z} = 0.00372$. 103

Fig. 4.9 Frequency response for the equivalent spring-mass-damper system (i) $\zeta = 0.05$, ii) $\zeta = 0.1$,(iii) $\zeta = 0.2$, and (iv) $\zeta = 0.5$. 103

Fig. 4.10 Effect of loss factor (δ) on the frequency response curve for $\bar{m} = 1.3333$, $\bar{Z} = 0.0333$; (i) δ = 0.05, (ii) δ = 0.1(iii) δ = 0.2, and (iv) δ = 0.5. 104

Fig. 4.11 Effect of amplitude base excitation ($\bar{Z}$) on the frequency response curve for $\bar{m} = 1.333$, $\delta = 0.05$;(i) $\bar{Z}$ =0.00667, (ii) $\bar{Z}$ =0.1667. 105

Fig. 4.12 Effect of mass ratio ($\bar{m}$) on the frequency response curve for δ = 0.05, $\bar{Z}$ =0.0333; (i) $\bar{m}$ =0.6667, (ii) $\bar{m}$ =2.6667. 106

Fig. 4.13 Effect of loss factor (δ) on the frequency response curve for $\bar{m} = 0.667$, $\bar{Z} = 0.333$; (i) δ = 0.0, (ii) δ = 0.01, (iii) δ = 0.05, and (iv) δ = 0.1. 107

Fig. 4.14 Effect of amplitude of base excitation ($\bar{Z}$) on the frequency response curve for $\bar{m} = 0.667$, δ = 0.05; (i) $\bar{Z}$ = 0.1667, (ii) $\bar{Z}$ = 0.6667. 108

Fig. 4.15 Effect of mass ratio ($\bar{m}$) on the frequency response curve for δ = 0.05, $\bar{Z}$ =0.333; (i) $\bar{m}$ = 0.50, (ii) $\bar{m}$ =1.0. 108

Fig. 4.16 Influence of material loss factor (δ) on the frequency response curves for $\bar{m} = 1.0$, $\bar{P}_0 = 0.0$, and $\bar{Z} = 0.0166$. 114

Fig. 4.17 Basins of attraction (i) $\bar{\omega}$ equal to 0.7 (ii) $\bar{\omega}$ equal to 1.1. Key as in Fig. 4.16 for δ equal to 0.1. 116

Fig. 4.18 Time responses and phase portraits for points A, B, and C for δ equal to 0.15. Key as in Fig. 4.16. 116

Fig. 4.19 Influence of amplitude of support motion ($\bar{Z}$) on the frequency response curves for $\bar{m} = 1.0$, $\bar{P}_0 = 0.0$, $\bar{Z} = 0.0166$. 118

Fig. 4.20 Influence of amplitude of static load ($\bar{P}_0$) on the frequency response curves for $\bar{Z} = 0.0166$, $\bar{m} = 1.0$, $\delta = 0.15$. 118

Fig. 4.21 Influence of payload mass ($\bar{m}$) on the frequency response curves for $\bar{Z} = 0.0166$, $\bar{P}_0 = 0.0$, $\delta = 0.15$ 118

Fig. 4.22 Frequency response curves for material loss factor δ = 0.2, $\bar{m} = 1.0$, $\bar{P}_0 = 0.0$, $\bar{P}_1 = 0.3624$. 119

Fig. 4.23 Influence of material loss factor (δ) on the frequency response curves for $\bar{m} = 1.0$, $\bar{P}_0 = 0.0$, $\bar{P}_1 = 0.3624$. 119

Fig. 4.24 Influence of dynamic loading ($\bar{P}_1$) on the frequency response curves for $\bar{m} = 1.0$, $\bar{P}_0 = 0.0$, $\delta = 0.15$. 121

Fig. 4.25 Influence of static loading ($\bar{P}_0$) on the frequency response curves for $\bar{m} = 1.0$, $\bar{P}_1 = 0.3624$, $\delta = 0.15$. 121

Fig. 4.26 Influence of payload ($\bar{m}$) on the frequency response curves for $\bar{P}_0 = 0.0$, $\bar{P}_1 = 0.3624$, $\delta = 0.15$. 121

Fig. 4.27 Influence of material loss factor (δ) on the frequency response curves for $\bar{m} = 1.0$, $\bar{P}_0 = 0.0$, $\bar{P}_1 = 0.3624$, $\bar{Z} = 0.0166$; (i) $\delta = 0.0$, (ii) $\delta = 0.1$, (iii) $\delta = 0.15$, (iv) $\delta = 0.2$. 123

Fig. 4.28 Basins of attraction for (i) $\bar{\omega}_1$ equal to 0.7 (ii) $\bar{\omega}_1$ equal to 0.8. Key as in Fig. 4.27 (iii). 124

Fig. 4.29 Influence of phase angle (ϕ) on the frequency response curves for 125

	$\bar{m}=1.0$, $\bar{P}_0=0.0$, $\bar{P}_1=0.3624$, $\delta=0.15$, $\bar{Z}=0.0166$; (i) $\phi=\pi/4$, (ii) $\phi=\pi/2$, (iii) $\phi=5\pi/6$, (iv) $\phi=\pi$.	
Fig. 4.30	Time response, phase portrait and Poincare's map for the A, B, and C key as Fig. 4.29(iii).	126
Fig. 4.31	Influence of amplitude of base excitation ($\bar{Z}$) on the frequency response curves for $\bar{m}=1.0$, $\bar{P}_0=0.0$, $\bar{P}_1=0.3624$, $\delta=0.15$; (i) $\bar{Z}=0.0083$, (ii) $\bar{Z}=0.0332$.	127
Fig. 4.32	Influence of amplitude of dynamic loading ($\bar{P}_1$) on the frequency response curves for $\bar{m}=1.0, \delta=0.15$, $\bar{P}_0=0.0$, $\bar{Z}=0.0166$; (i) $\bar{P}_1=0.5436$, (ii) $\bar{P}_1=0.7248$.	127
Fig. 4.33	Influence of payload ($\bar{m}$) on the frequency response curves for $\delta=0.15$, $\bar{P}_0=0.0$, $\bar{Z}=0.0166$, $\bar{P}_0=0.0$, $\delta=0.15$, $\bar{P}_1=0.3624$; (i) $\bar{m}=0.5$, (ii) $\bar{m}=2.0$.	129
Fig. 4.34	Influence of static force ($\bar{P}_0$) on the frequency response curves for, $\bar{m}=1.0, \delta=0.15$, $\bar{P}_1=0.3624$, $\bar{Z}=0.0166$; (i) $\bar{P}_0=0.3624$, (ii) $\bar{P}_0=0.7248$.	129
Fig. 5.1	Schematic diagram of a magnetoelastic Cartesian manipulator with payload subjected to harmonically varying axial tip force.	134
Fig. 5.2	Schematic diagram of magnetoelastic cantilevered manipulator beam with tip mass subjected to harmonic axial load.	138
Fig. 5.3	Schematic diagram of magnetoelastic cantilevered manipulator	139
Fig. 5.4	Schematic diagram of magnetoelastic cantilevered manipulator subjected to both static and dynamic magnetic fields.	140
Fig. 5.5	Schematic diagram of a magnetoelastic cantilevered manipulator subjected to harmonically varying tip force with small deflection	141
Fig. 5.6	The region of instability in magnetic field for cantilever beam.	147

Fig. 5.7 Influence of the static axial force on the transition curves in magnetic field for cantilever beam without tip mass (I) c_d = 0.0 (II) c_d = 0.2 N-s/m, and (III) c_d = 0.4 N-s/m; (a) P_0 = 5 N and (b) P_0 =10 N. 147

Fig. 5.8 Influence of the mass ratio on the transition curves in magnetic field for cantilever beam with tip mass for $P_0 = 1.0$, (I) c_d = 0.0 (II) c_d = 0.2 N-s/m, and (III) c_d = 0.4 N-s/m; (a) $\overline{m}$ =0.1 and (b) $\overline{m}$ =0.2. 148

Fig. 5.9 Time response for (a) point C (b) point B and (c) point A; key as in Fig. 5.7(b, I). 148

Fig. 5.10 Influence of the magnetic field on the transition curves in periodic axial force field for $P_0 = 1.0$, $\overline{m}$ = 0, (I) c_d = 0.0 (II) c_d = 0.2 N-s/m, and (III) c_d = 0.4 N-s/m; (a) B_m = 0.3 Am^{-1} and (b) B_m =1.3 Am^{-1}. 149

Fig. 5.11 Influence of the static axial force on the transition curves in periodic axial force field for B_m = 0.3, M = 0, (I) c_d = 0.0 (II) c_d = 0.2 N-s/m, and (III) c_d = 0.4 N-s/m; (a) P_0 = 5 N and (b) P_0 = 10 N. 149

Fig. 5.12 Influence of the mass ratio on the transition curves in periodic axial force field for B_m = 0.3 Am^{-1} and P_0 = 1.0 N, (I) c_d = 0.0 (II) c_d = 0.2 N-s/m, and (III) c_d = 0.4 N-s/m; (a) $\overline{m}$ =0.1 and (b) $\overline{m}$ =0.2. 150

Fig. 5.13 Time response for (a) point C (b) point B and (c) point A; key as in Fig. 5.10(a, II). 150

Fig. 5.14 Influence of the magnetic field on the transition curves for P_0 = 1.0 N, M = 0, (I) c_d = 0.0 (II) c_d = 0.2 N-s/m, and (III) c_d = 0.4 N-s/m; (a) B_m = 0.3 Am^{-1} and (b) B_m = 1.3 Am^{-1}. 152

Fig. 5.15 Influence of the periodic axial force on the transition curves for P_1 = 1.0 N, M = 0, (I) c_d = 0.0 (II) c_d = 0.2 N-s/m, and (III) c_d = 0.4 N-s/m; (a) P_0 = 5 N and (b) P_0 = 10 N. 152

Fig. 5.16 Influence of the mass ratio in periodic axial force on the transition 153

curves for $P_0 = 1.0$ N, B_m = 0.3 Am^{-1}, (I) c_d = 0.0 (II) c_d = 0.2 N-s/m, and (III) c_d = 0.4 N-s/m; (a) Fig. $\overline{m}$ =0.1 and (b) $\overline{m}$ =0.2.

Fig. 5.17 Influence of the mass ratio in magnetic field on the transition curves for $P_1 = 1.0$ N, $P_0 = 1.0$ N, (I) c_d = 0.0 (II) c_d = 0.2 N-s/m, and (III) c_d = 0.4 N-s/m; (a) $\overline{m}$ =0.1 and (b) $\overline{m}$ =0.2. 153

Fig. 5.18 Time response for (a) point C (b) point B and (c) point A; key as in Fig. 5.10(a, II). 154

Fig. 5.19 Region of instability in the presence of magnetic field for $M = 0.0, c_d = 0.0$. 159

Fig. 5.20 Frequency response curves for $M = 0.02$ kg, $c_d = 0.01$ N-s/m, $B_s = 0.1$ Am^{-1}, $B_d = 0.3$ Am^{-1}, and σ =10^2 Vm^{-1}. 159

Fig. 5.21 (a) Time response for the point A and (b) time response for the point B as marked in Fig.2. 160

Fig. 5.22 (a) Transient response and (b) steady state time response for the point C. 161

Fig. 5.23 Influences of B_d on the frequency response curves for $M = 0.02$ kg, $c_d = 0.01$ N-s/m, $B_s = 0.1$ Am^{-1}, and σ =10^2 Vm^{-1}. 162

Fig. 5.24 Influences of M on the frequency response curves for $M = 0.02$ kg, $c_d = 0.01$ N-s/m, $B_s = 0.1$ Am^{-1}, and σ =10^2 Vm^{-1}. 162

Fig. 5.25 Influence of c_d on instability region for $M = 0.0$, (I) $c_d = 0.0$ N-s/m, (II) $c_d = 0.02$ N-s/m, (III) $c_d = 0.03$ N-s/m. 162

Fig. 5.26 Influences of c_d on the frequency response curves for $M = 0.02$ kg, $B_s = 0.1$ Am^{-1}, and σ =10^2 Vm^{-1}. 162

Fig. 5.27 Influence of B_s on instability region for $M = 0.0$ kg, $c_d = 0.0$, (I) $B_s = 0.05$ Am^{-1}, (II) $B_s = 0.1$ Am^{-1} (III) $B_s = 0.2$ Am^{-1}. 163

Fig. 5.28 Influence of B_s on the frequency response curves for $M = 0.02$ kg, $c_d = 0.01$ N-s/m, $B_d = 0.1$ Am^{-1}, and σ =10^2 Vm^{-1}. 163

Fig. 5.29 Influence of B_d for $M = 0.02$ kg, $c_d = 0.0$, $B_s = 0.2$ Am^{-1}, σ =10^2 Vm^{-1}, (I) $B_d = 0.05$ Am^{-1} (II) $B_d = 0.1$ Am^{-1} (III) $B_d = 0.2$ Am^{-1}. 165

Fig. 5.30 Fig. 5.30. Influence of B_S on frequency response curve for $B_d = 0.2$ Am^{-1}, $M = 0.02$ Kg, σ =10^2 Vm^{-1}, $c_d = 0.01$ N-s/m. 165

Fig. 5.31 The region of instability of a cantilever beam in magnetic field. 169

Fig. 5.32 (a) Time response for the point A and (b) time response for the point B (points A and B are marked in Fig. 5.31). 169

Fig. 5.33 Effect of the magnetic field strength (B_m) on the frequency response curves for $M = 0.02$ kg, $c_d = 0.01$ N-s/m, $\mu_r = 3000$, $\sigma = 10^7$ Vm^{-1}; (a) $B_m = 0.20$ Am^{-1}, (b) $B_m = 0.25$ Am^{-1}, (c) $B_m = 0.30$ Am^{-1}, (d) $B_m = 0.35$ Am^{-1}. 170

Fig. 5.34 (a) Time response for the point A and (b) time response for the point B (A and B points are marked in Fig.5.33(c)). 171

Fig. 5.35 (a) Transient response and (b) steady state time response for the point C with magnetic field (solid line) and without magnetic field (dotted line). 172

Fig. 5.36 Influence of damping on frequency response curve for $M = 0.02$ kg, $\mu_r = 3000$, $\sigma = 10^7$ Vm^{-1}, $B_m = 0.30$ Am^{-1}; (a) $c_d = 0.02$ N-s/m, (b) $c_d = 0.03$ N-s/m. 172

Fig. 5.37 Influence of mass ratio ($\overline{m}$) on frequency response curve for $c_d = 0.01$ N-s/m, $\mu_r = 3000$, $\sigma = 10^7$ Vm^{-1}, $B_m = 0.30$ Am^{-1}; (a) $M = 0.01$ kg, (b) $M = 0.015$ kg. 173

Fig. 5.38 Effect of relative permeability (μ_r) of the material on the frequency response curve $M = 0.02$ kg, $c_d = 0.01$ N-s/m, $\sigma = 10^7$ Vm^{-1}, $B_m = 0.30$ Am^{-1}; (a) $\mu_r = 2.0$, (b) $\mu_r = 7.0$. 174

Fig. 5.39 Effect of material conductivity (σ) on the frequency response curve for $M = 0.02$ kg, $c_d = 0.01$ N-s/m, $\mu_r = 2500$, $B_m = 0.30$ Am^{-1}; (a) 175

$\sigma = 10^2$ Vm^{-1}, (b) $\sigma = 10^6$ Vm^{-1}.

Fig. 5.40 Frequency response curves for $M = 0.02$ kg, $P_0 = 0.2$ N, $B_m = 0.30$ Am^{-1}. 181

Fig. 5.41 (a) Time responses (b) phase portraits corresponding to the points A, B and C. Key same as in Fig. 5.40. 182

Fig. 5.42 (a) Transient time responses and (b) steady state time responses corresponding to point E as marked in Fig. 5.40. Dotted line represents the response without magnetic field and solid line represents the response with magnetic field. Key same as in Fig. 5.40. 183

Fig. 5.43 Effect of the B_m on the frequency response curves for $M = 0.02$ kg, and $P_0 = 0.2$ N. 184

Fig. 5.44 Effect of the amplitude of static axial load (P_0) on the frequency response curves for $M = 0.02$ kg, $B_m = 0.25$ Am^{-1}. 184

Fig. 5.45 Influence of M on the frequency response curves for $P_0 = 0.2$ N, $B_m = 0.30$ Am^{-1}. 185

Fig. 5.46 Frequency response curves for $M = 0.02$ kg, $P_0 = 0.2$ N, $P_1 = 0.2$ N, $B_m = 0.0$. 186

Fig. 5.47 Effect of B_m on the frequency response curves for $M = 0.02$ kg, $P_0 = 0.2$ N, $P_1 = 0.2$ N. 186

Fig. 5.48 (a) Transient time responses and (b) steady state time responses for point A marked in Fig. 5.47 with B_m equal to 0.30 Am^{-1}. Dotted line represents the response without magnetic field and solid represent the response with magnetic field. 187

Fig. 5.49 Effect of P_1 on the frequency response curves for $M = 0.02$ kg, $P_0 = 0.2$ N, $B_m = 0.3$ Am^{-1}. 188

Fig. 5.50 Effect of P_0 on the frequency response curves for $M = 0.02$ kg, $P_1 = 0.2$ 188

N , $B_m = 0.30$ Am^{-1}.

Fig. 5.51 Influence of M on the frequency response curves for $P_0 = 0.2$ N, $P_1 = 0.2$ N, $B_m = 0.30$ Am^{-1}. 189

Fig. 5.52 Frequency response curves for $M = 0.02$ kg , $P_0 = 0.2$ N, $P_1 = 0.2$ N, $\phi = 0$, $B_m = 0.25$ Am^{-1} . 190

Fig. 5.53 Effect of (B_m) on the frequency response curves for $M = 0.02$ kg , $P_0 = 0.2$ N, $P_1 = 0.2$ N, $\phi = 0$. 190

Fig. 5.54 Effect of P_1 on the frequency response curves for $M = 0.02$ kg , $P_0 = 0.2$ N , $B_m = 0.25$ Am^{-1}, $\phi = 0$. 191

Fig. 5.55 Effect of P_0 on the frequency response curves for $M = 0.02$ kg , $P_1 = 0.2$ N , $B_m = 0.25$ Am^{-1}, $\phi = 0$. 191

Fig. 5.56 Influence of M on the frequency response curves for $P_0 = 0.0$ N, $P_1 = 0.2$ N, $B_m = 0.25$ Am^{-1}, $\phi = 0$. 192

Fig. 5.57 Effect of ϕ on the frequency response curves for $M = 0.02$ kg , $P_0 = 0.2$ N, $P_1 = 0.2$ N, $B_m = 0.25$ Am^{-1}. 192

Fig. 5.58 Frequency response curve for $M = 0.02$ kg $B_m = 0.30$ Am^{-1}, $c_d = 0.01$ N-s/m^2 , $Z = 0.0025$ m. 199

Fig. 5.59 Basin of attraction (i) for $\bar{\omega}_1 = 0.9$ and (ii) $\bar{\omega}_1 = 1.1$. Key as in Fig. 5.59. 199

Fig. 5.60 Influence of payload on the critical value of B_m. 200

Fig. 5.61 (i) Time response , (ii) phase portrait and (iii) Poincare's map for the points A, B, C key as in Fig. 5.59. 201

Fig. 5.62 Influence of magnetic field strength (B_m) on the frequency response curves for $M = 0.02$ kg , $c_d = 0.01$ N-s/m , $Z = 0.0025$ m. 202

Fig. 5.63 Influence of amplitude of base motion (*Z)* on the frequency response curves for $M = 0.02$ kg , $c_d = 0.01$ N-s/m , $B_m = 0.30$ Am^{-1}. 202

Fig. 5.64 Influence of damping (c_d) on the frequency response curves for $B_m = 0.30$ Am^{-1}, $Z = 0.005$ m, $M = 0.02$ kg. 203

Fig. 5.65 Influence of tip mass (M) on the frequency response curves for $B_m = 0.30$ Am^{-1}, $c_d = 0.01$ N-s/m , $Z = 0.005$ m. 203

Fig. 5.66 The influence of magnetic field strength (B_m) on frequency response curves for $M = 0.02$ kg , $c_d = 0.01$ N-s/m . 204

Fig. 5.67 Influence of damping (c_d) on the frequency response curves for $M = 0.02$ kg , $B_m = 0.3$ Am^{-1}. 205

Fig. 5.68 Influence of tip mass (M) on the frequency response curves for $B_m = 0.30$ Am^{-1}, $c_d = 0.01$ N-s/m , $Z = 0.005$ m. 205

Fig. 5.69 Influence of base excitation (Z) on the frequency response curves for $M = 0.04$ kg , $c_d = 0.01$ N-s/m , $B_m = 0.20$ Am^{-1}; (i) $Z = 0.00125$ m, (ii) $Z = 0.0025$ m, (iii) $Z = 0.005$ m, (iv) $Z = 0.01$ m. 207

Fig. 5.70 Time response (i, iv, vii), phase portrait (ii, v, viii), and Poincare's map (iii, vi, ix) for points A, B and C key as Fig. 5.69(iii). 209

Fig. 5.71 Influence of phase angle (ϕ) on the frequency response curves for $M = 0.04$ kg , $B_m = 0.20$ Am^{-1}, $c_d = 0.01$ N-s/m , $Z = 0.005$ m; (i) $\phi = \pi/6$ (ii) $\phi = \pi/3$, (iii) $\phi = \pi/2$, (iv) $\phi = \pi$. 210

Fig. 5.72 Basin of attraction for $\bar{\omega}_1 = 0.7$. Key as in Fig. 5.69 (iv). 211

Fig. 5.73 Influence of magnetic field strength (B_m) on the frequency response curves for $M = 0.04$ kg , $c_d = 0.01$ N-s/m , $Z = 0.005$ m; (i) $B_m = 0.10$ Am^{-1}, (ii) $B_m = 0.30$ Am^{-1}. 212

Fig. 5.74 Influence of tip mass (M) on the frequency response curves for $B_m = 0.20$ Am^{-1}, $Z = 0.005$ m, $c_d = 0.01$ N-s/m ; (i) $M = 0.01$ kg , (ii) $M = 0.02$ kg . 213

NOMENCLATURE

A Cross-section area of the beam

B_0 Periodically varying transverse magnetic field

B_m Amplitude transverse magnetic field

B_d Amplitude of dynamic magnetic field

B_s Amplitude of static magnetic field

c_d Damping constant of elastic and magnetoelastic martial

d Width of the beam

E Young's modulus of the elastic beam

E_1 Real part of the Young's modulus of the viscoelastic beam

E_2 Imaginary part of the Young's modulus of the viscoelastic beam

h Thickness of the beam

I Cross-sectional moment of inertia of the beam

L Length of the beam

M Tip mass of the cantilever beam or payload of the manipulator

P Periodic axial force

P_0 Amplitude of static axial force

P_1 Amplitude of dynamic axial force

P_c Critical buckling load

s Reference variable along the beam

$u(\xi,t)$ Longitudinal displacement of the beam element $d\xi$

$v(\xi,t)$ Transverse displacement of the beam element $d\xi$

x, y Newtonian Cartesian reference frame

Y_b Support motion at the roller-supported end of the manipulator

Z Amplitude of support motion

η,ξ Integration variables

δ Material loss factor

χ_m Magnetic susceptibility

μ_0 Permeability of the vacuum

μ_r Relative Permeability

ρ Mass per unit length of the beam

σ Material conductivity of the beam

Ω_1 Frequency of support motion

Ω_2 Frequency of transverse magnetic field

Ω_3 Frequency of harmonically varying axial force

ω_s,ω_e Fundamental natural frequency

$\bar{()}$ Nondimensional ()

LIST OF PUBLICATIONS FROM THIS THESIS

1. B. Pratiher and S. K. Dwivedy, Nonlinear Response of a Flexible Cartesian Manipulator Subjected to a Pulsating Axial Force, Nonlinear Dynamics, DOI 10.1007/s11071-008-9431-6, 2008 (Online available).
2. B. Pratiher and S. K. Dwivedy, Nonlinear Vibration of a Magneto-Elastic Cantilever Beam with Tip Mass, ASME, Journal of Vibration and Acoustics 131,(2009)02011-1-9.
3. B. Pratiher and S. K. Dwivedy, Nonlinear dynamics of a soft magnetoelastic Cartesian manipulator, International Journal of Nonlinear Mechanics (in press)
4. B. Pratiher and S. K. Dwivedy, Nonlinear Vibration of a Single Link Viscoelastic Cartesian Manipulator, International Journal of Nonlinear Mechanics Vol. 43, 683-696, 2008.
5. B. Pratiher and S. K. Dwivedy, Nonlinear dynamics of flexible single –link Cartesian Manipulator, International Journal of Nonlinear Mechanics 42, 1062-1073, 2007.
6. B. Pratiher and S. K. Dwivedy, Parametric instability of a cantilever beam with magnetic field and periodic axial load, Journal of Sound and Vibration, 305, (4-5), 904-917, 2007.
7. B. Pratiher and S. K. Dwivedy, Dynamic Stability of a Soft Magneto-elastic Cantilever Beam with Tip Mass, Journal of Vibration and Control (Under review).
8. B. Pratiher and S. K. Dwivedy, Study of Large Vibration of a Magneto-Elastic Cantilever Beam with End Mass Subjected to Periodic Axial Load, Journal of Sound and Vibration (Under review)

Chapter 1

INTRODUCTION

1.1 Introduction

Nowadays, the use of robotic manipulators has been increased significantly in the application of space exploration, hazardous nuclear power plant, surgical operations, micro and macro fabrications, and in many other precision industrial applications to avoid human fatigue due to repetitive, monotonous, tedious, dangerous and contagious work environments. According to Robot Institute of America, an industrial robot can be defined as a reprogrammable, multifunctional manipulator designed to move materials, parts, tools, or specialized devices through variable programmed motions for the performance of a variety of tasks. A robotic manipulator is the mechanical component of the robot which is used to perform the intended task of the robot. It consists of mechanical links and joints capable of producing controlled movement in various directions. Mainly, manipulators may be grouped into revolute type or prismatic type depending on the types of joints used in the construction of the manipulators. As extensive studies have been made for revolute types of manipulators, in the present work focus has been made on the Cartesian manipulators which have only prismatic joints and can reach any position in its rectangular workspace by prismatic motions of the links. Figure 1.1 shows a SCARA robot where the joint between the first and second link is shown to be of prismatic type. Similarly, Fig. 1.2 shows two Cartesian manipulators with two prismatic joints.

It has been observed that the existing industrial robotic manipulators (e.g., Figs. 1.1 and 1.2) are heavy, bulky and hence, have high inertia effects, high power consumption, which leads to low operating speed and high cost. Hence, in order to lower the cost of the manipulator and to improve the productivity and operation time, one should go for light weight manipulators. These light weight manipulators have been particularly required in space exploration purpose, where the launching cost enormously increased with slight

increase in the payload (Dubowsky, 1994). Figure 1.3 shows another application where a flexible manipulator may be used for prostate biopsy scanning purpose. Also, in the 21st century to meet the security challenges, Fig. 1.4 shows a light weight robotic manipulator which has been designed to work in explosive ordnance disposal, removal of hazardous materials, search-and-surveillance operations, hostage rescue and other vital law enforcement tasks for bomb squads, SWAT teams, military units and others similar applications.

Fig. 1.1. A heavy weight SCARA robot (http://users.aber.ac.uk/jnw/CS364/5.php)

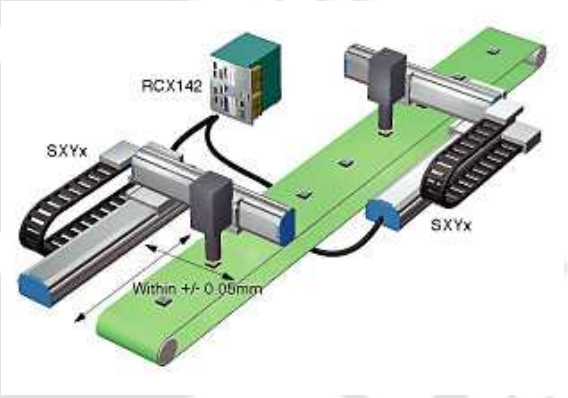

Fig. 1.2. A heavy weight Cartesian robot (www.yamaha-motor.co.jp)

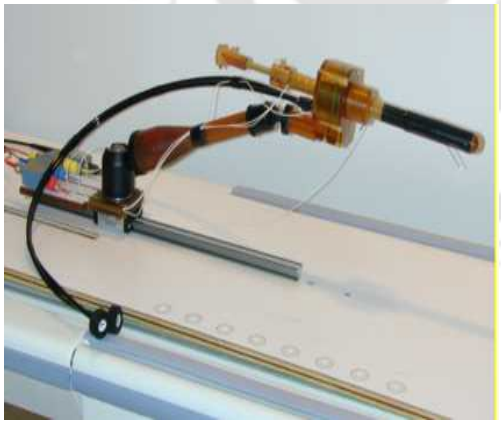

Fig.1.3. Prostate Biopsy Robot in Closed High-Field MRI Scanner (www.cisst.org/ .../ AxelRobot/AxelRobot.htm)

Fig. 1.4. Multi-role flexible robot for hazmat handling, search and rescue, and hostage rescue operation.(www.armedforces-int.com/)

These manipulators are flexible and studies on the lightweight and flexible manipulators over the conventional heavy weight rigid manipulators have been increased spectacularly in the recent years for their large operational speed, low cost, low power consumption, and better transportability. The reduction of the component weight or manipulator having flexible links and joints allows the manipulators to move faster and carry heavier loads with longer links. But, the main disadvantage of flexible manipulator is the vibration problem due to low stiffness of the manipulator and it has been shown particularly for space application that several cumulative hours may be spent to damp down the vibration (Dubowsky, 1994).

Due to the importance and usefulness of using lightweight flexible robotic manipulator, recently, many researchers have been trying to solve the vibration problem associated with the manipulator. Efforts have been made to improve their dynamic models, provide better control strategy to attenuate vibration of the flexible manipulator. As will be clear from the literature survey presented in the next chapter, most of the works on flexible Cartesian manipulators have been limited to the study of the free and forced vibration of the linear system. But during high speed operation or when the manipulator is more flexible, a linear dynamic model will no longer be valid and there is a need to develop more accurate nonlinear mathematical model of the system.

The problem associated with the flexible manipulator may be clubbed into two categories depending on the application of the manipulator. In the first category, the operations may be of pick and place type and in second category, the endeffector of the manipulator is constrained to move in the work environment. In case of pick and place type of operation, one requires a quick settling time for the flexible manipulator to control the free vibration response and to reduce the idle time to start the next operation. It is always desirable to avoid undue vibration as in many cases like precision manufacturing, it will spoil the job, in case of microsurgery it may cause serious fatal injuries to the patient, and in nuclear power plant it may lead to serious consequences. In space applications, in the absence of damping, several cumulative hours may be spent to start the next operation. In this case,

the vibration may originate due to the torque, force or initial motion applied to the flexible link of the manipulator. In the second category as the endeffector is in contact with the environment, it is subjected to a force from the environment. For example, in many precision industrial applications such as spraying, painting, welding, grinding, polishing or metal cutting, the endeffector is always subjected to a force from the work piece which may be constant and/or time varying depending on the nature of the work. Also, when the manipulator is constrained to move in a specified trajectory, the gripper or the endeffector is subjected to a tip force. Depending on the undulation of the workspace, while traversing the trajectory, the induced force on the end-effector may be modeled as an impulse or harmonic type of force. In addition to these applications, also to control the flexible manipulator, one may take the feedback control force equal to that of a pulsating axial force. Further, recent use of micromanipulator at the end of the flexible robotic manipulator to control the vibration may be one such example. In these cases, where the system is subjected to a time varying force, the mathematical model of the system is very complex and the system may be modeled as a nonlinear forced and/or parametrically excited system. Very few researchers have attempted to study the Cartesian manipulator of this type to attenuate the vibration.

Though the actual robot contains many links and joints, to start with, it is very important to study a single-link flexible manipulator. This flexible link may be the last link of a multi-link robotic manipulator or it may itself be a single-link manipulator. In case of the single-link Cartesian manipulator, one may model the manipulator as a cantilever beam with end mass or as a roller supported link with attached mass at the end. The attached mass in both these cases represents the endeffector with payload. As mentioned before, depending on the problems, the endeffector may be subjected to a periodically varying axial load. Similar to many control applications in frequency domain analysis, it is always advantageous to consider a harmonically varying end force for the analysis purpose.

In recent literatures, in many engineering applications, the single-link flexible manipulator with endeffector has been modeled as an Euler-Bernoulli beam with tip mass considering

small transverse deflection. In most of the cases, the manipulator has been modeled as an elastic beam and in few cases; it has been modeled as viscoelastic or composite beams.

As mentioned earlier, the large unwanted vibration is the major concern of the lightweight and flexible manipulator over the conventional rigid manipulator and research has been carried out to attenuate or remove this vibration. It may be noted that the vibration of a system can be attenuated by using several active or passive control schemes. The passive control can be performed through the modification of the dynamics of the under damped structure either by increasing damping constant or by altering the order of the structure. The altering of the order of the structure has normally been done by using viscoelastic material, tuned-mass dampers, sandwich structures, shunted piezoceramic dampers etc.

Also, this vibration can be actively controlled by using modern controller such as proportional, proportional–derivative (PD), proportional–integral-derivative (PID) controllers in the feedback control schemes. Many other observer based control schemes can also be used to control the vibration by using different actuators and sensors. In many engineering applications, studies have been carried out to control the vibration of the system actively by using smart materials such as piezoelectric patches, shape memory alloys, magneto rheological fluids and elastomers etc. In some cases, it has been observed that by using magnetoelastic beam and applying magnetic field, the vibration of the system can be reduced. The applied magnetic field directly controls the vibration of the manipulator by imposing a body force and body couple on the system. As the stiffness of the system changes actively when subjected to the magnetic field, the natural frequencies of the system also changes which helps to alter the resonant frequency of the system and hence it reduces the vibration of the system.

In the present work, in addition to the manipulators of elastic materials, uses of viscoelastic materials and magnetoelastic materials are also considered to attenuate the vibration of a single-link flexible manipulator. As extensive studies for the flexible cantilever beams with elastic and viscoelastic materials have been available in the literature, in the present work

only roller-supported Cartesian manipulators are considered for elastic and viscoelastic manipulators. For the magneto elastic manipulators, where the study has been very much limited, both cantilever and roller supported Cartesian manipulators are considered.

As the previous studies on the dynamics of the manipulators have been limited to the small transverse deflection of the elastic and viscoelastic manipulators, here attempt has been made to study the dynamics of manipulators with large transverse deflection. Hence, in case of elastic and viscoelastic manipulators, they are modeled as roller-supported Euler-Bernoulli beam with end mass. While, the motion of the roller- supported end of the beam is considered to be harmonic, the end-effector is subjected to harmonically varying axial load for some applications. In case of magnetoelastic manipulators, both small and large transverse deflection cases are studied.

This study will not only be useful for flexible manipulators, but also it will find extensive applications in other flexible structures such as appendages to space crafts (antennas, solar panels, instruments mounted on the spacecraft), components of high speed machinery, aircraft, vehicles and ships, TV towers, high rises, unstayed polemasts on ships and many other precision industrial applications. In these cases, the support or base motion may be due to the motion transmitted by the supporting structures or the intentionally fed base excitation as in case of a shaker or the natural base excitation as in the case of a vehicle moving in the undulated road, or the ship sailing in the wavy sea. It may also have an origin from the earthquake.

It may be noted that, when the slender beam vibrates in a direction perpendicular to the direction of the external forcing, for certain frequencies and amplitude of forcing parameters, the system may reduced to that of a parametrically excited system as the governing equation of motion of such system contains time-dependent excitation terms. It may be recalled that in case of forced vibration, the direction of the excitation force and the resulting oscillation takes place in the same direction and resonance occurs when the frequency of the external excitation is nearly equal to any of the natural frequencies of the

system. But, in case of linear parametrically excited systems resonance may occur, when the external frequency Ω is away from the natural frequency (ω_n). Particularly, this type of resonance occurs when $\Omega \approx \omega_m \pm \omega_n$, m, n representing the participating modes. When $m = n$, $\Omega \approx 2\omega_n$, and the resulting resonance is known as principal parametric resonance of n^{th} mode, and in other cases, it is known as combination resonance of sum or difference type depending on the addition or subtraction of the participating modes. As large transverse vibration has been considered in the present work, the resulting nonlinear system is similar to a combination of forced and linear and nonlinear parametrically excited systems. Hence, the required analysis to obtain the nonlinear response is expected to be very much complicated with many different resonance conditions. In addition to the above mentioned resonance conditions for forced and linear parametrically excited system, here, subharmonic, super harmonic and simultaneous resonance conditions may occur for the nonlinear system.

It may be noted that, the governing equation of motion of the system may be obtained by using force and moment balance methods or energy based methods. While force and moment balance methods include those of Newton's 2nd law, D' Alembert's principle, in energy methods one may use Lagrange principle or extended Hamilton's principle. Due to scalar approach, energy based methods are particularly useful for multi-degree of freedom and continuous systems. For multi-link manipulators, one may go for Newton-Euler formulation, Euler-Lagrange formulation etc. Besides these methods, one may use finite element method or lumped parameter models based on multi-body dynamics. As in the present work single-link manipulator has been considered, D' Alembert's principle has been used for finding the governing nonlinear differential equation of motion. Then the generalized Galerkin's method has been used to obtain the governing temporal equation of motion.

Unlike the linear systems, where one may use superposition theory to predict the response of one system when the response for a similar system is known, in nonlinear system, this

superposition theory will not work and hence one has to perform the analysis for each case separately. Due to the presence of many nonlinear terms in the governing equation of motion of the system, it is very difficult to find the closed form solution of the system. In such cases, one may obtain the approximate solution by using the perturbation methods. There are several perturbation methods such as the method of multiple scales (MMS), the averaging method (AM), Lindstedt-Poincare's method (LPM), and method of normal forms (MNF). One may also go for the harmonic balance method (HBM) which is most commonly used technique for the analysis of nonlinear differential equations. But this method has several limitations. To apply this method, one should have an *apriori* knowledge about the solution which will guide to select number of harmonic terms to be taken for the analysis. It is also very tedious and time consuming for making the formulation for a multi-degree-of-freedom (MDOF) nonlinear system and when higher harmonic terms have been taken into account. Further, a separate analysis is required to find the stability of the system while using the harmonic balance method. In averaging method (AV) while one needs to know *apriori* the solution to get a consistent solution, the response and stability can be determined from the same analysis. Unlike HBM and AV, in method of multiple scales which is a straight forward method, it is not required to know the solution before the analysis and it is very efficient for MDOF nonlinear analysis. In this method, the response and stability can be obtained from the same analysis. Like HBM and AV, this method can be used to determine the fixed-point, periodic solution, quasi-periodic and chaotic responses. But a few demerits of using MMS are the use of a small book-keeping parameter (ε) and increase of mathematical complexity with increase in the order of analysis.

Besides these methods, there are several other methods viz., intrinsic HBM, incremental HBM, incremental HBM with multiples time scales, multiple-time scales harmonic balance (MHB), and modified Lindstedt-Poincare method used for analysis of nonlinear systems. But these methods have been tested only for few specific nonlinear systems and their usability have not been fully explored. In the present work, the widely used first and second order method of multiples scales are used for the analysis of the nonlinear temporal

equation of motion. In some cases, method of normal forms is used. In all the resonant conditions, the results obtained by using the perturbation method are verified by numerically solving the temporal equation of motion. The obtained results are verified with the published experimental results and they are found to be in good agreement.

It may be noted that while the analysis of the linear parametrically excited system only predicts the trivial state instability regions or trivial state bifurcation points, in actual nonlinear systems, the response may be nontrivial fixed point response or it may be periodic, quasi-periodic or chaotic response. The response may be a combination of all these types of responses also. Further, these responses may be stable or unstable. Unlike linear systems, while analyzing the nonlinear dynamic system, one may observe many nonlinear phenomena such as multiple solutions; jump up and jump down phenomena, saturations, quenching, limit cycles and crisis etc (Nayfeh and Balachandran, 1995). One may observe many bifurcation phenomena such as sub-critical and super-critical pitchfork, trans-critical, saddle-node, and Hopf bifurcations, where either the number or the nature of the existing response curve changes. Hence, to analyze the system, in the present work, the time response, frequency response, phase portraits, Poincare's' sections, have been plotted for all resonance conditions. To study the multiple stable states, basin of attractions have also been plotted.

1.2 Goal of the present work

From the existing literature review related to the vibration of flexible manipulators having prismatic joints, it has been observed that though these types of manipulators can be used in a number of industrial applications; most of the studies have been limited to the free vibration analysis of the system. In some cases, the manipulator has been modeled as a linear parametrically excited system where the governing temporal equation of motion reduces to that of Mathieu-Hill's equation. Only few authors have modeled the manipulator as an Euler-Bernoulli beam with very small transverse deflection. Though it has been observed that to control the vibration, one may use beams with viscoelastic and magnetoelastic materials, no analysis has been made to study their applicability for the

Cartesian manipulator purpose. Also, the studies in these types of beams are limited to the determination of the natural frequencies, mode shapes and very few authors have investigated the parametric instability regions of simply supported beams. Hence, in this work attempt has been made to investigate the applicability of viscoelastic and magnetoelastic materials to replace the elastic manipulators for the purpose of vibration control.

As pointed out in the previous section, for practical applications in precision motion and high speed operations to increase the productivity, the flexible manipulators should be modeled considering moderately large vibration. Hence, the goal of the present work is to investigate the nonlinear dynamics of the Cartesian manipulator with large transverse deflection. To perform this analysis three types of manipulators viz., elastic, viscoelastic, and magnetoelastic manipulators are considered.

In many applications, the endeffector of the manipulator may be constrained to move in specific path where it is subjected to axial time varying load. In such applications the systems may be modeled as a parametrically excited system with moderately large vibration. Also, as pointed out in the previous section, the Cartesian manipulator may be modeled as a cantilever beam or as a roller-supported beam. As extensive analysis has been available for cantilever beam with elastic and viscoelastic materials, here, for these two cases, the manipulators are modeled as roller-supported Euler- Bernoulli beams. The magnetoelastic manipulators are modeled both as cantilevered and roller-supported Euler-Bernoulli beam with tip mass. Keeping the above points in mind, the objective of the present work is to study the nonlinear dynamics of the following flexible manipulator systems.

- Harmonically excited roller-supported elastic Cartesian manipulator with and without harmonically varying tip load
- Harmonically excited roller-supported viscoelastic Cartesian manipulator with and without harmonically varying tip load
- Cantilevered magnetoelastic manipulator with and without harmonically varying tip load

- Harmonically excited roller-supported magnetoelastic manipulator

1.3 Methodology

The governing equation of motion of the above mentioned systems have been obtained by using D' Alembert's principle. A generalized Galerkin's method has been used to discretize the governing equation of motion to obtain a set of nonlinear second order temporal equation of motion. Method of multiple scales or the method of normal forms have been used to reduce the second order temporal equation of motion to a set of nonlinear first order differential equations which are know as modulation or reduced equations. For steady state response, reduced equations have been used to determine the stability and bifurcation of the fixed point responses. Also, these equations are used to obtain periodic, quasi-periodic, and chaotic responses. The time response, phase portrait, Poincare's sections have been used to study the behaviour of the nonlinear responses of the systems for different control parameters such as amplitude of base excitation, tip or payload mass, damping constant, amplitudes of static and dynamic axial load, amplitude of static and dynamic magnetic field strength, material conductivity, permeability, and the material loss factor. The basins of attraction have been determined to illustrate the importance of initial conditions to obtain the accurate system response. Results obtained by using the method of multiple scales and method of normal forms have been verified with the results by numerically solving the temporal equation of the motion and comparing with the published experimental works.

1.4 Organization of the thesis

The structure of the thesis can be given as follows. This chapter gives an introduction to the present thesis. Also the scope of the present work is highlighted in this chapter.

In chapter 2, a critical review has been carried out to study the dynamics of the manipulators. Literature on the dynamics of elastic, viscoelastic and magnetoelastic manipulator has been thoroughly discussed. Other parametrically excited beam systems

have also been studied. The systems subjected magnetic fields have been critically reviewed. Also, review has been carried out for the dynamic analysis of the system with harmonic axial load.

In Chapter 3, the mathematical modeling of elastic Cartesian manipulator with and without sinusoidal tip load has been carried out. Method of multiple scales and method of normal forms have been used to solve the nonlinear temporal equation of motion. The results obtained by perturbation analysis have been compared with the experimental results.

Chapter 4 deals with the mathematical modeling and dynamic analyses of manipulator with viscoelastic material. The perturbation result has been compared with an equivalent elastic beam. The results have also been compared with those obtained by taking a linear Kelvin–Voigt Model.

Chapter 5 deals with the mathematical modeling and dynamic analyses of the magnetoelastic manipulators with payload. Here, the manipulator has been modeled as both cantilever and roller-supported Euler-Bernoulli beam with large transverse deflection. Investigation has been carried out to control the large vibration of the manipulators by using variable magnetic field.

In Chapter 6, the important conclusions of the present work have been summarized and the scope of the future work has also been indicated in this chapter. A Bibliography with 318 references has been given at the end of the thesis.

Chapter 2

REVIEW OF LITERATURE

2.1 Introduction

In this chapter, a comprehensive survey of the available literature on the flexible robotic manipulators is carried out. Particular emphasis is given on the study of nonlinear dynamics of Cartesian manipulators which can be modeled either as a roller-supported beam or as a cantilever beam with and without tip mass. The tip mass represents the endeffector of the manipulator. Further, as mentioned in the previous chapter, the roller-supported end is assumed to have harmonic motion and sometimes the endeffector is subjected to harmonically varying axial force.

In all these cases, the systems may be modeled as forced and/or parametrically excited systems with single and/or two frequency excitations. Hence, literature related to nonlinear forced and parametrically excited systems with single and two frequency excitations is extensively reviewed. Also, to attenuate vibration, one may replace the elastic manipulators by viscoelastic or magnetoelastic manipulators. While the literature related to flexible manipulators have been exhaustively reviewed in section 2.2, that for viscoelastic beams and magnetoelastic beams have been discussed in sections 2.3 and 2.4, respectively. As most of the cases, the system reduces to that of a parametrically excited one, hence, in section 2.5; literature related to parametrically excited systems have been briefly discussed. The summary of the literature review is presented in section 2.6.

2.2 Literature review on the flexible robotic manipulator

In this section, the literature related to the application of flexible manipulators, their modeling, and control is thoroughly investigated. While the applications of robotic manipulators is discussed in subsection 2.2.1, the three different modeling schemes, such

as assumed modes method, finite element method, lumped parameter method are discussed in subsection 2.2.2. The related issues are discussed in subsequent subsections.

2.2.1 Application of flexible manipulator

Recently, study of flexible robotic manipulators have been carried out significantly for implementing the manipulators for space exploration, mining, nuclear power plant, micro-surgical and other medical applications, and in many other precision industrial applications (Dwivedy and Eberhard (2006), Benosman and Vey (2004)). Low cost, light weight, large operational speed, low power consumption, better transportability, and safer operations due to reduced inertia are some of the advantages of using the flexible manipulators over the conventional rigid manipulators. But, the main disadvantage of flexible manipulator is the vibration problem due to the low stiffness of the manipulator. A number of researchers have been working to eliminate or attenuate the vibration of the flexible manipulators by improving the dynamic models and incorporating different control strategies. In the following subsections, a detailed literature review is carried out to demonstrate the current status of the research in this field and the importance of the studies of the dynamics of flexible robotic manipulator.

Fukuda and Kuribayashi (1984) and Fukuda (1885) studied the flexible robotic arms for the use in grinding, painting and drawing robots; and for pattern recognition with soft touching and in many similar applications. Tzou (1989) studied the control of a flexible manipulator used in space applications in order to reduce the vibration of the lightweight flexible manipulator during more complex situations. In this paper, the structural dynamics of a flexible robotic manipulator with elastic joints has been analyzed using nonlinear theoretical and finite-element methods. Alberts et al. (1992), and Krishnamurthy and Chao (1992) considered practical flexible manipulator arm for the application of space shuttle Remote Manipulator System. While Alberts et al. (1992) used finite element analysis to evaluate the effectiveness of viscoelastic damping treatments for large flexible space manipulators, Krishnamurthy and Chao (1992) used a linear quadratic regulator (LQR) technique for suppressing the vibration problem of the flexible manipulator. Cyril et al.

(1995) studied the modeling and control of a spacecraft-mounted manipulator capturing a spinning satellite. In this work, a non-linearity compensation and decoupling proportional-derivative (PD) control scheme have been adopted to analyze the control of the manipulator.

Munasinghe et al. (1999) studied the high speed precision control of robot arms for trajectory generation. Kumar et al. (2000) used flexible manipulators for micro-surgical operation. Meggiolaro and Dubowsky (2001) improved the fine positioning accuracy of a powerful flexible manipulator used for maintaining the nuclear power plant. Zhou et al. (2004) used multi-body software package ADAMS to model a flexible robot, which find application in spot-welding operation. Yoon and Kyu (2006) studied the control strategies of a flexible manipulator for hazardous operation. Liu et al. (2007) used a flexible dual-arm space robot for capturing an object. Lv et al. (2007) investigated the bending-torsion vibration of a two-link flexible manipulator used in space application.

2.2.2 Modeling of single-link flexible Manipulator

A detailed review of the literature related to dynamic analyses and control of flexible robotic manipulators has been carried out by Dwivedy and Eberhard (2006), Benosman and Vey (2004), and Gaultier and Cleghorn (1989). Park and Cho (1991) studied the general design conditions for an ideal robotic manipulator considering simple dynamics. Baruh and Tadikonda (1989) discussed various issues related to the dynamics and control of flexible robotic manipulators. Book (1990) presented a tutorial review on the mathematical modeling, design, and control of flexible manipulator arms. In his work, various types of joint control algorithms for general and tip motion has been discussed. A detailed study on dynamics and control of flexible manipulators has been found in the book of Fraser and Daniel (1991). In this book, both assumed modes method and finite element method have been used to obtain the mathematical model of the flexible manipulator. Also, adaptive and non-adaptive control schemes have been used to minimize the vibration of flexible manipulators.

Theodore and Ghosal (1995) compared the two discretization models, viz., the assumed modes method and finite element method (FEM) to efficiently represent the link flexibility of robot manipulators. It has been observed that fewer mathematical operations have been required for the inertia matrix computation in the finite element model compared to the assumed modes formulation. Also, the numerical simulation time may be greater for finite element models because the number of state space equations is more in this method compared to the assume mode method. Martin et al. (2003) used both assumed mode methods and FEM and conducted experiments to demonstrate the relative advantages of assumed mode and finite element method. From these review articles it has been apparent that the modeling of the flexible manipulators can be classified into three groups such as assumed modes method, finite element method and lumped parameter models. Some more literature related to these methods is cited in the following subsections.

2.2.2.1 Assumed mode method

In this method, the mathematical model has been obtained by representing the link flexibility as a series of truncated finite model in terms of spatial mode eigen- functions and time-varying mode amplitudes. This assumed mode method has been widely used for different boundary conditions and mode eigenfunctions. Book (1984) modeled the manipulator used in space applications as a chain of flexible links. In his work, recursive Lagrangian dynamics and assumed mode method has been used to study the vibration of the manipulator. Hasting and Book (1987) described a linear state space model for a single-link flexible manipulator and compared simulation of the model to that of the measurements made on a 4-ft-long direct drive manipulator link. Siciliano and Book (1998) studied the control of lightweight flexible manipulators. In this work, the flexible manipulator dynamics has been derived on the basis of a Lagrangian-assumed modes method.

Barbieri and Ozguner (1988) applied an extended Hamilton's principle to obtain the equation of motion and studied the unconstrained and constrained modes of vibration. Krishnamurthy et al. (1990) studied the single-link flexible manipulators with prismatic

joints using assumed mode method. Boyer and Coiffet (1996) studied the symbolic modeling of manipulators with flexible links. Authors applied the D' Alembert's principle and assumed mode method to obtain the equation of motion for an open chain flexible links. Guang and Min (2005a, 2005b) developed a mathematical model combining the dynamics of an Euler-Bernoulli beam described by the assumed mode method and hydraulic circuit dynamics. This mathematical model has been used for designing composite controllers for the flexible link. Wei et al. (2005) designed a novel piezoelectric actuator to suppress the torsional vibration of a two-link flexible space manipulator. Here, Lagrange equation and assumed mode method have been used to model the system.

Murrugarra et al. (2006) proposed the design of a PD position control scheme for a single-link flexible manipulator. In this work, they considered the link as an Euler-Bernoulli beam and the assumed mode method has been used for modeling the transversal deformation of the beam. Hua and Zhang (2007) discussed the dynamic modeling of flexible robots colliding with its working environments. The system considered is a flexible multi-link manipulator. The flexibility of each flexible link has been described by using the approach of assumed modes. Lv et al. (2007) investigated the bending-torsion vibration of a two-link flexible space manipulator. The dynamic equation of this system has been derived using the Lagrange equation and the assumed mode method.

Ahmad (2008) developed the control schemes for end-point vibration suppression and input tracking of a flexible manipulator. The dynamic model of the system has been derived by using the assumed mode method. Ahmad (2008) studied the dynamic modeling of a two-link flexible manipulator based on closed-form equations of motion. In this work, dynamic model of the system, incorporating structural damping, hub inertia and payload, has been developed using finite assumed mode methods. Ahmad et al. (2008) used angular position control approaches for a flexible manipulator considering disturbance effects in the dynamic model. Here, constrained planar single-link flexible manipulator has been considered and the dynamic model of this manipulator has been derived using the assume mode method.

2.2.2.2 Finite element analysis

Tzou (1989), Alberts et al (1992), Tokhi et al. (2000, 2001), Chung and Yoo (2002) and Martin et al. (2003) used finite element method (FEM) to derive the dynamic model of single-link flexible manipulators. Tokhi et al. (2000, 2001) found theoretically and experimentally, the dynamic characteristics such as tip displacement, velocity and settling time for a flexible manipulator. Chung and Yoo (2002) carried out the dynamic analysis of flexible manipulator using FEM. Martins et al. (2002) studied dynamic models for a single-link flexible manipulator using the finite element approach and compared the modal frequencies found experimentally to validate the FE modeling in some cases. They have used a command shaping technique to control the vibration of single-link manipulator. Mohamed and Tokhi (2004) obtained the dynamic model of a single-link flexible manipulator using FEM and then studied the feed-forward control strategies for controlling the vibration using command shaping techniques based on input shaping, low-pass and band-stop filtering. Zhou et al (2004) used multi-body software package ADAMS to acquire some important parameters from the CAD model of HT120 spot-welding robot. Dynamic model of this robot has been formulated by using finite element code.

Payo et al. (2005) proposed a nonlinear dynamic model for single-link flexible manipulators that experience large deflections and these models are developed under the assumption of a very lightweight arm with all its mass concentrated at the tip. In this work, FEM has been used to derive the nonlinear ordinary differential equations. Yoon and Kyu (2006) used an adaptive tracking controller for the vibration reduction of flexible manipulator employed in hazardous area by combining input shaping technique with sliding-mode control. Here, they used finite element analysis to model the system. Du et al. (2007) used finite element theory for investigating the theory and method for dynamic modeling of planar parallel manipulators with flexible links. Heidari and Nikoobin (2007) determined the maximum allowable dynamic load (MADL) for flexible link-flexible joint manipulators to traverse along a predefined path. The finite element method has been used to model and derive the dynamic equations of manipulator with flexible links and joints. Zhang and Li (2007) studied the modeling and position control of two robot manipulators

handling a flexible payload. In this paper, FEM has been used to model the system. Du et al. (2008) developed dynamics modeling for flexible planar parallel robots using finite element method. Here, both elastic deformations of flexible links and the coupling effects of the elastic deformations have been considered.

2.2.2.3 Lumped parameter model

Zhu et al. (1999) studied a lumped parameter model to simulate the tip position tracking of a single-link flexible manipulator. In this work, PD type controller has been used to control vibration of the flexible manipulator. Khalil and Gautier (2000) used a lumped elasticity model for flexible mechanical systems. Nissing (2000) studied the use of a spring and damper attachment to damp out vibration in a flexible single-link manipulator. Megahed and Hamza (2004) applied a variation of the finite segment multibody dynamics approach to model and simulate planar flexible link manipulator with rigid tip connections to revolute joints. The formulation employs a consistent mass matrix in order to provide better approximation than the traditional lumped masses often encountered in the finite segment approach. Ding and Selig (2004) used Holzer method for dynamic modeling of flexible manipulators. Cao and Li (2008) studied the time varying constrained flexible manipulator system. The distributed parameter model has been obtained. This model has been divided into two subsystems which include a lumped parameter subsystem describing the rigid motion and a distributed parameter subsystem expressing the vibration by virtue of the singular perturbation method.

2.2.2.4 Miscellaneous studies

Tomei and Tornambe (1993) studied the dynamic models which consist of a system of ordinary differential equations related to the desired order of approximation. In this work, the model has been obtained by using the Lagrangian approach. Shaheed and Tokhi et al. (2000, 2001) investigated the dynamic modeling of a single-link flexible manipulator considering parametric and non-parametric identification techniques. In this work, the least mean squares, recursive least squares and genetic algorithms have been used to obtain

dynamic models of the system. Karimi and Yazdanpanah (2006) studied the modeling of a single-link flexible manipulator with an arbitrarily large (infinite) number of deflection modes based on the singular perturbation method. In this work, output feedback control of the tip position has been controlled by utilizing the ε-dependent H_∞ technique. Also, Wang and Ravani (1988a, 1988b), Korayem and Basu (1994, 1994, and 2005), Yue et al. (2001), Korayem and Ghariblu (2003), Heidari (2005), Hedari and Nikoobin (2007), and Korayem et al. (2008) found the maximum allowable dynamic load for flexible-link manipulators for different system constraints.

2.2.3 Effect of payload

Performance and efficiency of the manipulator are significantly affected due to the presence of residual vibration. Payload or the mass of the endeffector has a significant role to alter the amplitude and frequency of the vibration or response of the system. Parks and Pak (1991) studied the effect of payload on the dynamics of a flexible single-link arm with actuator on one end and payload on the other end. In this work, analytical results have been compared with the experimental results and were found to be in very good agreement. The effect of payload on the vibration excitation of a flexible manipulator along a given path has been demonstrated by Tu and Rastegar (1994). Poppelwell and Chang (1996) studied the influence of offset payload on the vibration of flexible manipulator. In this paper, it has been observed that for a given payload, an off-set influences mainly the fundamental natural frequency which will affect positioning accuracy. In all the above cases, the manipulator has been modeled as an Euler-Bernoulli beam. Tokhi et al. (2000) investigated the effect of payload on the resonant frequency of a flexible single-link manipulator. Lee and Hu (2000) addressed the robust control problem for a single-link flexible robot arm with uncertain payload variations. Here, linear state-space model has been derived by using the method of separation of variables. Liu et al. (2007) studied the effect of payload collision on the dynamics and control of a flexible dual-arm space robot capturing an object. In this work, the flexible links have been modeled as Euler-Bernoulli beams and the dynamic model of this robot system has been derived by using Lagrangian formulation.

2.2.4 Modeling as Rayleigh and Timoshenko beam

When considering a short and thick beam, or plate like structures, both rotary inertia and shear deformation play a major role and affect the vibration behaviour of the system. Particularly the effects on the higher modes are very significant. But, these terms are not included in traditional Euler-Bernoulli beam. Hence, in this section, studies on shear deformation and rotary inertia effect are discussed. While Soon and Jaw (1992) and Morris and Madani (1996) considered the effect of shear deformation on the vibration behaviour of flexible manipulator, Wang and Guan (1994) and Wang et al. (1999) considered the influences of shear, rotary inertia on the vibration behaviour of flexible manipulator. Bayo (1988) and Bayo and Moulin (1989) presented the method for solution of the inverse dynamics of open-chain flexible robots. The formulation includes all the nonlinear terms due to the large rotation of the links, together with Timoshenko beam theory to model their elastic characteristics. Cheng and Yue (2004) used Timoshenko beam theory and the finite element method to derive the dynamic equation of motion of planar cooperative manipulators with link flexibility. Zuev (2005) studied a controllable mechanical system where the flexible robot manipulator has been considered as a flexible Timoshenko beam. Also, a Galerkin's approximation has been used to solve the corresponding Sturm-Liouville problem which has been constructed for the partial differential equations of motion. Loudini et al. (2007) used the concept of Timoshenko beam theory for mathematical modeling of a planar lightweight single-link flexible manipulator arm pinned at its actuated base and carrying a payload at its free end-point.

2.2.5 Shape Optimization

Wang and Russell (1965, 1992, 1997), Wang (1994), Russell (1995), Kim and Tsai (2003), Kumar et al. (2004, 2005), and Dixit et al. (2006) found the optimum shape of the manipulator by maximizing the fundamental frequency and taking into account different system constraints. While Kumar et al. (2005) and Dixit et al. (2006), used finite element method to model the flexible manipulator which has been modeled as an Euler-Bernoulli

beam, Wang and Russell, Wang and Russell used variational approach and nonlinear programming methods to obtain the optimum design of the manipulators.

2.2.6 Multi-link manipulator

Studies on the manipulators with two or more flexible links have been carried out by many researchers to avoid the severe control problems associated with the large inertia forces when the manipulator with large-mass or rigid links moves at high speed. In the following paragraph, modeling aspects of few multi-link manipulators have been discussed.

Everett et al. (1999) designed and developed two link flexible manipulators where the Lagrangian mechanics has been used to obtain the equation of motion of the manipulator. Rosado and Yuhara (1999) studied the dynamic modeling of a flexible robotic manipulator with two flexible links and two revolute joints which rotates in the horizontal plane. In this work, the equation of motion has been derived using the Newton-Euler formulation and the finite element method. Choura and Yigit (2001) obtained the mathematical model of a two-link rigid flexible manipulator carrying a moving payload mass. Here, extended Hamilton's principle has been used to derive the equations of motion and PD-type controller has been used to stabilize the system vibration. Zhang and Zhou (2006) reported the dynamic modeling and simulation of an *N*-flexible-link and *N*-flexible-joint robot. In this work, each flexible joint has been modeled as a linearly elastic torsional spring and assumed modes technique has been used to describe the deformation of the flexible-link. Zavrazhina (2007) studied the dynamic behavior of a multi-links robot manipulator.

2.2.7 Nonlinear analysis of flexible manipulators

Naganathan and Soni (1986) studied the spatial manipulators with revolute joints where the governing equations of motion have been derived including the effects of rotary inertia, shear deformation, and the effects of the gross non-linear motion of each of the links. A simple and efficient finite element has been used for the manipulator links using Timoshenko beam theory. Tzou (1989) studied the structural dynamics of a flexible robotic

manipulator with elastic joints using nonlinear theoretical and finite-element methods. In this work, dynamic contact in an elastic joint has been simulated by a nonlinear joint model represented by a set of nonlinear springs and dampers. Liu (1993) carried out the dynamic analysis of spatial robot manipulator with a prismatic link where it has been observed that the system experience a pitchfork-type bifurcation even for small disturbance amplitudes if the excitation frequency is high, or if the maximum gravitational torque and the proportional gain is sufficient close to each other. Using extended Hamilton's principle, Fung and Chang (1998) derived the nonlinear equation of motion of a two-link flexible manipulator with tip mass.

Moallem et al. (2000, 2001) carried out experiments to obtain the nonlinear behaviour of flexible manipulators. Sang and Cheng (2204) carried out the stability analysis of nonlinear bang-bang impact control for a one degree of freedom robotic manipulator based on an analysis in L_2 space. He and Lu (2005) studied the influence of passive joint on the dynamics of planar flexible underactuated manipulators. They proposed a vibration reduction method based on the internal resonance phenomenon of multi-degree nonlinear dynamic systems.

2.2.8 Control of flexible manipulator

There are several control strategies adopted by the researchers to accurately position the endeffector in the workspace. These strategies include modal reference adaptive control, self-tuning control, feed-forward control and regular PD, PID control, input shaping techniques. In this section, the literature on the control aspects of the flexible manipulator has been reviewed only very briefly since other state-of-the-art reviews are available.

Rattan et al (1988) used feed forward and computed torque control techniques to control endeffector position of a flexible manipulator. They also carried out experiments to validate the theoretical findings. Singer and Seering (1990) proposed an input shaping technique to cancel vibration generated by an impulse input. Meckl and Seering (1990) applied the same input command shaping techniques to minimize the vibration of the

manipulator. By defining an appropriate cost function, a force profile has been derived that efficiently allocates kinetic energy so that the excitation is minimized at the system resonances and maximum energy is used for system motion. Magee and Book (1993) considered a modified command filtering technique to eliminate the first two modes of vibration in a long reach flexible manipulator with position dependent parameters. In their work, the modified command filtering technique has been compared with the previous impulse command shaping technique and PD control methods to show its effectiveness for reducing the residual vibration. Lew and Trudnowski (1996) proposed an inertial force damping controller to suppress the vibrations of a micro/macro manipulator system.

Tokhi et al. (2000) found theoretically and experimentally the dynamic characteristics such as tip displacement, velocity and settling time of a flexible manipulator. They used command shaping techniques to predict the required torque to control the flexible manipulator. Here, FEM has been used to model the manipulator. Subudhi and Morris (2002) used a reduced order controller to resolve the control complexities of a manipulator with multiple flexible links and flexible joints. They used Euler–Lagrange formulation and assumed modes method to model the system. Azad and Tokhi (2003) dealt with the development of an interactive and user-friendly environment for simulation and control of flexible manipulator systems. Here, finite difference simulation algorithm of a flexible manipulator has been implemented within the Simulink environment. Tso et al. (2003) studied the vibration control for a manipulator with a single flexible link. The authors used a non-linear Lyapunov-type controller to minimize the elastic vibration of the flexible manipulator which has been measured by an optical-laser sensor system. The edited book by Wang and Gao (2003) demonstrated advance studies in design, modeling, control, and applications of flexible manipulators. Here, both link and joint flexibility have been considered and various controllers have been used to reduce the tip vibration of the manipulator.

Benosman et al. (2002) discussed the modeling and control issues in the flexible manipulator and Benosman and Vey (2004) presented a detailed literature review on the

control of flexible manipulators. Feliu and Ramos (2005) developed a new control scheme for single-link flexible arms with varying payload that uses measurement of the link deflection provided by a strain gauge placed at the base of the link. In this work, it has been observed that the developed control scheme is more robust to payload changes than control schemes based on accelerometer measurements. Mohamed et al. (2005) experimentally investigated the feed forward and feedback control schemes for vibration control of a very flexible and high-friction flexible manipulator system. In this work, the input shaping, low-pass filtering and strain feedback control techniques have been combined with the PD control for reduction of vibration of the manipulator.

Chalhoub et al. (2006) developed two robust nonlinear controllers along with a nonlinear observer to control the rigid and flexible motions of a single-link robotic manipulator. In this work, the dynamic model of the robot arm has been formulated by taking into account the rigid-body motion of the link along with its in-plane transverse deformation. Md-Zain et al. (2006) studied the hybrid learning control schemes with input shaping for vibration suppression of a flexible manipulator. They also studied the effectiveness of the control schemes in handling various payloads. Monje et al. (2007) used a fractional order controller to control single-link lightweight flexible links in the presence of payload changes. Alam and Tokhi (2008) used a GA based hybrid fuzzy logic control strategy for input tracking and vibration reduction at the end point of a single-link flexible manipulator. From their work, it has been observed that a GA-based multi-modal command shaping technique can be used effectively for vibration reduction where prior information about natural frequencies and damping ratios of a system are not available.

Though most of the above works on the flexible manipulators have been concentrated on manipulators with revolute joints, few investigators have studied the manipulators with prismatic joints. A detailed study of the flexible Cartesian manipulators has been presented in the following section.

2.2.9 Flexible Cartesian Manipulator

In this section the literature related to the modeling, design and control of flexible Cartesian manipulators have been critically examined. A Cartesian manipulator i.e., a manipulator with prismatic joint can be modeled either as a flexible beam with roller-supported end or as a flexible cantilever beam. The roller-supported end may be subjected to harmonic motion.

Buffinton and Kane (1985) modeled a flexible manipulator as a uniform beam moving longitudinally at a prescribed rate over two bilateral supports. The temporal equation of motion has been obtained by using assumed modes technique. In this work, authors have considered three different cases viz., condition with no longitudinal motion, condition with sinusoidal longitudinal motion, and condition with longitudinal motion for the purpose of repositioning. They obtained the region of instability for harmonic longitudinal motion. Yuh et al. (1989) developed the equation of motion of a link which contains both rotational and translational motion by using Lagrangian formulation. Here the simulation results have been compared with the experimental results.

Meckl and Seering (1990) used command shaping technique to generate fast motions of a Cartesian robot with minimum residual vibration and experimentally verified the obtained theoretical results. Buffinton (1992) extended their previous work (Buffington and Kane (1985)) and derived the equations of motion for flexible robot containing translationally moving elastic members that traverse a finite number of distinct support points. The results obtained in this work have been useful for the problems involved in the dynamics and control of manipulators containing highly elastic members connected by prismatic joints. Tadikonda and Baruh (1992) studied the dynamics and control of a flexible manipulator with prismatic joint. The manipulator has been modeled as a horizontally excited Euler-Bernoulli beam with a tip mass. In this work, it has been shown that by neglecting the effect of elastic motion, the rigid body motion leads to positional inaccuracies.

Love et al. (1997) used a hydraulically actuated long reach manipulator with a flexible prismatic link. In this work, both mathematical modeling and control of hydraulic actuators as well as flexible links have been taken into account to determine the natural frequencies of the manipulator. Theodore and Ghosal (1997) studied the dynamic behavior of flexible-link manipulators with prismatic joints. Here, the translating flexible link has been modeled as an axially moving Euler–Bernoulli beam. The Lagrangian formulation along with assumed mode method has been used to find the closed form equation of motion. In all these cases, the mode shapes of the system have been taken same as those of a cantilever beam.

Coleman (1998), and Coleman and McSweeney (2004) obtained the natural frequencies and eigen-spectrums of a single-link flexible Cartesian manipulator. In these cases, the manipulator has been modeled as an Euler-Bernoulli beam with left end roller supported. The endeffector of the manipulator at the right end has been modeled as a tip mass. Hou and Tsui (1998) developed a boundary point feedback control loop to stabilize the vibration of a flexible robot arm with a horizontal moving base and payload at the tip. Basher (2000, 2007) investigated the dynamic modeling of a single-link flexible robot arm having both rotational and translation motions. In the first work, the response of the modeled Euler-Bernoulli beam has been determined by using an infinite number of modes. It has been observed that the erroneous results obtained by neglecting the effects of higher order dynamics. In the latter work, author used transfer function approach and studied the effects of higher-order dynamics on the response of the same system.

2.2.10 Dynamics of Base excited Systems

In many engineering applications, it may be noted that the manipulator can be modeled as a base excited cantilever beam with attached mass at the tip. Clamped end of the cantilever beam has a harmonic excitation. Here, a detailed literature related to the dynamics of harmonically base excited cantilever beam is reported. To (1982) described the methods for calculation of natural frequencies and mode shapes of a cantilever beam with a base excitation and extended tip mass. The exact expressions for natural frequencies

and mode shapes have been determined. Zavodney and Nayfeh (1989) obtained experimentally and theoretically the non-linear response of an elastic flexible beam carrying a lumped mass at an arbitrary position. In this work, D' Alembert's principle and Galerkin's method have been used to derive the equation of motion. It has been observed that the results obtained by using method of multiple scales have found to be in good agreement with the experimental results. Pai and Nayfeh (1990) obtained the non-linear response of a laterally base excited cantilever beam using combination of the method of multiple scales and Galerkin's methods.

Lee (1995) found the instability regions of a cantilever beam with a tip mass subjected to axial sinusoidal excitation. They used Hamilton's principle and assumed mode method to derive the governing temporal equation of motion. Al-Bedoor and Khulief (1996) obtained the approximate analytical solution for an axially moving elastic beam with different end conditions. They applied the classical method of separation of variables and the method of multiple scales to solve the partial differential equation with time dependent coefficients. Zhou (1997) obtained the exact and analytical expression for eigenfrequencies and mode shapes of a cantilever beam with heavy tip mass with rotary and translation elastic support. Esmailzadeh and Jazar (1998) determined the transient vibration of a harmonically base excited cantilever beam with a lumped mass attached to its free end.

Fung et al. (1998d) developed the instability regions of an axially moving cantilever beam with a tip mass. Extended Hamilton's principle has been used to derive the equation of motion and method of multiple scales has been used to find the instability regions. Dwivedy and Kar (1999) investigated the non-linear behavior of a slender beam carrying a lumped mass at an arbitrary position under harmonic base excitation. They considered modal interactions and studied the system with internal resonances. Ozkaya and Pakdemirli (2000) found the instability regions of an axially accelerating beam with small flexural stiffness. Forehand and Cartmell (2001) studied the steady state response of the cantilever beam with tip mass subjected to sinusoidal base excitation.

2.3 Literature review on beams with viscoelastic material

It has been observed that very few works are available on the dynamic analysis of viscoelastic beams. A detailed literature review in this regard is presented here to know the state of the art in this field.

Stevens (1966, 1969) and Stevens and Evan-Iwanowski (1969) analytically and experimentally studied the effect of viscoelastic material behaviour on the instability regions of a column subjected to a periodic axial load. Genin and Radwan (1971) derived the equation of motion for transverse vibrations of a slender beam on a continuous viscoelastic foundation. Saito and Otomi (1979) investigated the stability of viscoelastically supported beam with attached mass subject to axial and tangential periodic loads. The viscoelastic end supports has been modeled as translational and rotational springs with viscoelastic damping. The instability regions have been investigated for simple and combination resonance conditions. Dost and Glockner (1982) found the dynamic stability of a viscoelastic simply supported column subjected to an axial compressive load and observed that the column may buckle when the load is well below the Euler buckling load. Gurgoze (1987) investigated the dynamic stability of the lateral vibrations of a viscoelastic beam subjected to a constant end force and a periodic displacement excitation. He applied Galerkin's method to obtain the ordinary differential equations of third order, which constitutes a Hill's system of equations. Cederbaum and Mond (1992) studied the dynamic stability of a viscoelastic column subjected to a periodic longitudinal load. Shirahatti and Sinha (1994) studied the instability regions of viscoelastic column subjected to harmonically varying axial load.

Suire and Cederbaum (1995) determined the periodic and chaotic responses of viscoelastic beams with large transverse deflection by using Boltzmann's superposition principle. Argyris et al. (1996) developed the differential equation of motion for a nonlinear visco-elastic polymer beam and studied its stability. Fung et al. (1996) obtained the instability regions of a viscoelastic beam subjected to harmonic and parametric excitations

simultaneously. They used Galerkin's method to reduce the governing equation into the third order nonlinear differential equation and the Routh-Hurwitz criterion has been applied to investigate the stability of steady state solutions for this parametric resonance condition. Lee and Oh (1995, 2005) studied the dynamics of an axially moving viscoelastic beam subjected to time varying axial load. They used extended Hamilton's principle to derive the equation of motion.

Marynowski (2002), and Marynowski and Kapitaniak (2007) investigated the non-linear vibrations of an axially moving viscoelastic beam with time-dependent tension. The Galerkin's method and the fourth order Runge–Kutta method have been used to solve the governing non-linear partial differential equation. In this case, the Poincare's maps and bifurcation diagrams have been plotted to study the vibration of the viscoelastic beam. Marynowski and Kapitaniak (2002), and Marynowski (2004, 2006) obtained the nonlinear response of beam-like model of two-dimensional axially moving web with time-dependent tension. Here, the beam has been considered as a Kelvin–Voigt model. Galerkin's method has been used to obtain the governing non-linear partial–differential equation and the fourth-order Runge–Kutta method has been used to obtain the response of the system. Chen et al. (2004) and Chen and Yang (2005) studied the stability of an axially accelerating viscoelastic beam. While Chen et al. (2004) used method of averaging to determine the instability regions, Chen and Yeh (2005) applied method of multiple scales to study the stability of the system. Shih and Yeh (2005) investigated the dynamic instability of a simply supported viscoelastic beam subjected to an axially applied harmonic load. The instability regions of this model have been obtained by using the complex IHB method. The results have also been compared with the results obtained by the previous work and were found to be good agreement. Chen and Yang (2005) investigated the nonlinear response of an axially accelerating viscoelastic beams.

Kargarnovin et al. (2005) obtained the nonlinear response of Timoshenko beam on viscoelastic foundation to a harmonic moving load. It has been observed that the results of nonlinear and equivalent linear viscoelastic model are completely different at low frequencies and are in good agreement in higher frequencies. Mahmoodi et al. (2005)

derived the equation of motion of a viscoelastic nonlinear beam using both Lagrange and Hamilton's principle. Yang and Chen (2005) studied the bifurcation and chaos of an axially accelerating viscoelastic beam. In this work, the viscoelastic material has been represented as a Kelvin–Voigt model. Chen and Yang (2006a) studied the vibration and stability of an axially moving beam with hybrid supports (simply supported beam with torsional springs). In another work, they (2006b) determined the bifurcation and chaos of an axially accelerating transversely vibrating viscoelastic beam using 4-term Galerkin's truncation.

Gurgoze et al. (2007) derived the characteristic equation of a transversely vibrating viscoelastic cantilever beam with tip mass. From this work, it has been noted that the characteristic equation of the viscoelastic beam with a tip mass is found to be formally the same as that of the elastic beam with the tip mass. Also, the authors represented the original continuous system by an equivalent Kelvin-Voigt's spring-mass-damper system. Muscolino and Palmeri (2007) evaluated the dynamic response of an elastic beam resting on viscoelastically damped foundation under single degree of freedom moving oscillator. Mahmoodi et al. (2007) analytically found the nonlinear mode shapes and natural frequencies of a viscoelastic beam using Kelvin–Voigt model. In this work, hinged–hinged and hinged–clamped boundary conditions have been considered. Further they have investigated (Mahmoodi et al. (2008)) the nonlinear vibration of a directly excited cantilever beam which has been modeled as an inextensible viscoelastic Euler–Bernoulli beam experimentally. In their work, the viscoelastic beam has been considered as a Kelvin–Voigt damping model. They compared their experimental and theoretical work and found them to be in good agreement. Ding and Chen (2008) obtained the instability regions of an axially accelerating viscoelastic beam. Here, the finite difference method has been used to determine numerically the instability regions for principal parametric resonance and these results are in good agreement with their analytical results.

Also, the vibration of an elastic beam can be attenuated actively by using piezoelectric patches (actuator and sensors), magnetorheological fluid, and magnetorheological

elastomer or by applying the magnetic field on the system. In the next section, literature related to the dynamic analysis of magnetoelastic beam has been carried out.

2.4 Literature review on magnetoelastic beams

Though the magnetic field has been applied in many systems for different purposes, here the literature related to the control of vibration of beam structures using magnetic field are investigated. Moon and Pao (1968, 1969) used uniform transverse magnetic field to control the vibration of a cantilever beam. They experimentally and theoretically investigated the parametric instability regions of a cantilever beam. Eringen (1989) derived the equation of motion of an elastic beam subjected to small dynamic load and electromagnetic field. Wu et al. (1997) studied the transient response and instability regions of a cantilever beam subjected to magnetic and axial force. In this work, the equation of motion has been derived by using Hamilton's principle. Using incremental harmonic balance (IHB) method, the principal parametric instability regions have been obtained. The dynamic stability of a beam under electromagnetic excitation was determined experimentally and analytically by Chen and Yah (2001). Wu (2005a, 2005b) determined the transient behavior of a pinned-pinned beam subjected to transverse magnetic field and thermal loading using IHB method. Wang and Lee (2006) investigated the dynamic stability of a soft ferromagnetic beam-plate in a transverse magnetic field.

In all these works, authors have studied only the trivial state responses of the system. But, practically, most of the engineering structures exhibit nonlinear behaviour which can not be predicted from these analyses. Few authors have studied the nonlinear response of the elastic beam subjected to alternating electromagnetic field. Kojima and Nagaya (1985) found the nonlinear response of a cantilever beam with tip mass where the tip mass was subjected to alternating electromagnetic field. Lu et al. (1995) studied the dynamics of a magnetoelastic buckled beam subjected to an axial periodic force in a time varying transversal magnetic field. The method of multiple scales and qualitative analysis has been used to study the dynamic behaviour and stability of the steady state responses. Shih et al.

(1998) analyzed the transient vibrations of a simply supported beam subjected to both axial load and transverse magnetic field.

Liu and Chang (2006) studied the interactive behaviors between the time varying transverse magnetic field, periodic axial load and external force of a magnetoelastic beam with general boundary conditions. The dynamic analysis of this physical system has been obtained by using the characteristic orthogonal polynomials as well as the Galerkin's method. In this work, authors have shown that the vibration as well as natural frequency of the system can be reduced by suitably using magnetic field.

Wu (2007) investigated the instability regions of a simply supported beam subjected to periodic magnetic field and thermal load. He considered nonlinear strain in this analysis and derived time dependent Mathieu equation by using extended Hamilton's principle and Galerkin's method. The regions of instability have been obtained by using IHB method. It has been observed that the instability regions for the beam having large deformation are significantly different from those obtained for the beam with small deformation. Inoue and Ishida (2008) studied the dynamic characteristics of the magnetically levitated system considering the dynamics of an electromagnetic control force. In this work, the frequency response curves for the system have been obtained considering the effect of nonlinearity of the electromagnetic force.

2.5 Literature review on parametrically exited systems

From the above literatures survey, one may find that most of the cases, the system has been reduced to that of a parametrically excited system. Studies on the dynamics of parametrically excited systems have been investigated for many years. Unlike forced vibration where the resonance occurs when the external frequency is nearly equal to the natural frequency of the system, in parametrically excited system, resonance occurs when the external frequency is nearly equal to the sum or difference of the natural frequencies. When the external frequency is nearly equal to twice the natural frequency of the i^{th} mode,

it is known as principal parametric resonance of the i^{th} mode and when the external frequency is equal to the sum or difference of the m^{th} and n^{th} natural frequencies, it is called parametric resonance of sum or difference type, respectively. In a parametrically excited system, the time varying forcing term appears as a parameter or coefficient of the response term in the equation of motion.

The phenomenon of the parametric resonance was first observed by the famous physicist Michel Faraday (1831). He discovered this resonance phenomenon on the surface waves in a fluid filled cylinder when frequency of vertical external excitation was nearly twice the natural frequency of the system. The first principal parametric resonance has been observed by Beliaev (1924) for a hinge-hinge beam under periodic axial load. Stephenson (1908) is the first researcher, who has remarked that a column under the periodic axial load may be stable by a steady value of load which is twice the Euler load.

Haight and King (1971), and Barr (1971, 1980) studied the instability regions of parametrically excited systems which occur due to support motion. Carlson et al. (1980) investigated the dynamics of a parametrically excited tensioned bar with initial curvatures. Saito and Koizumi (1982) determined the stability of a horizontal beam with a concentrated mass at one end and subjected to periodic axial displacement excitation at the other end considering the effect of gravity. Huang and Hung (1984) obtained the dynamic stability for a simply supported straight beam under periodic axial excitation by using the averaging method and the Routh-Hurwitz stability criteria. Celep (1985) investigated theoretically the parametric instability of pretwisted columns subjected to static and periodic axial load.

Gurgoze (1986) studied the stability and the steady state response of a parametrically excited simply supported vertical beam. Nayfeh and Zavodney (1986), Nayfeh (1987), and Nayfeh and Jebril (1987) obtained the nonlinear response of two degree of freedom systems with quadratic and cubic non-linearities subjected to parametric excitations by using method of multiple scales. Handoo and Sundararajan (1971) and Chen and Yeh

(1995) determined analytically the instability regions in a cantilevered column under a periodic follower force at its free end. Burton and Kolowith (1988) studied experimentally the nonlinear chaotic response of a parametrically excited flexible cantilever beam.

Zavodney and Nayfeh (1988,1989), Nayfeh and Pai (1989), Neal and Nayfeh (1990) and Sanchez and Nayfeh (1990) carried out the nonlinear responses of parametrically excited systems using method of multiples scales. Yagasaki et al. (1990) analyzed the dynamics of a weakly nonlinear single-degree-of-freedom system subjected to combined parametric and external excitation. The averaging method has been used to study the stability of the system.

Parker and Lin (2001) investigated the dynamic stability of parametrically excited axially moving media subjected to multifrequency tension and speed fluctuations. Yabuno and Nayfeh (2001) theoretically obtained the nonlinear normal modes of a parametrically excited vertical cantilever beam by using the method of multiple scales. Maccari (2001) investigated nonlinear behaviour of a parametrically excited Rayleigh–Liénard oscillator by an asymptotic perturbation method based on Fourier expansion and time rescaling. Raghothama and Narayanan (2002) obtained the periodic motions of a nonlinear system with time-delay by using the incremental harmonic balance (IHB) method.

Ji and Leung (2002) studied the steady-state response of a parametrically excited Duffing system. El-Bassiouny (2002) used the multiple scales and the generalized synchronization method to solve the governing nonlinear differential equations of a two-degree-of-freedom system with multi-frequency parametric excitations in the presence of three-to-one internal resonance. Tylikowski (2003) stabilized the vibration of a parametrically excited nonlinear continuous system by using distributed piezoelectric sensors and actuators with velocity feedback. Ng and Rand (2003) investigated the phenomena of coexistence in a two-degree-of-freedom system using method of averaging and harmonic balance method.

Mailybaev et al. (2004) studied optimal shapes of elastic beams under the action of a periodic axial force. Eissa and Amer (2004) investigated the problem of suppressing the vibrations of a flexible structure subjected to parametric and external excitation at resonance. Abd El-Latif (2004) used time transformation method, for solving the differential equations of a parametrically excited system. Abdelhafez (2004) investigated analytically and numerically the steady-state response of a single degree-of-freedom nonlinear system with two-frequency parametric and self-excitations. Here, the method of multiple scales has been used to find the steady-state responses and their stability.

Bakri et al. (2004) studied the nonlinear behaviour of two degrees of freedom single-mass system with parametric excitation in one direction. In this work, they derived trivial state conditions for parametric and 1:2 internal resonances by using both harmonic balance and method of averaging. Chatjigeorgiou (2004) investigated the dynamic behaviour of parametrically excited vertical slender structures for marine applications. In this work, two different solution methodologies (finite differences approximation scheme and modal expansion solution method) have been used to study the behaviour of the system with and without damping.

El-Bassiouny (2005) investigated the response of a non-linear mechanical system with two-frequency parametric and self-excitations by using the method of multiple scales. Sinha et al. (2005) used the order reduction techniques for parametrically excited nonlinear systems. This technique has been carried out either in state space or in second order (structural) form. Zhang et al. (2005) investigated the analysis of the global bifurcations and chaotic dynamics for the nonlinear nonplanar oscillations of a cantilever beam subjected to a harmonic axial excitation and transverse excitations at the free end. Temporal equation of motion has been obtained by using Galerkin's method. Zhang and Meng (2005) studied a simplified model for the purpose of studying the resonant responses and nonlinear dynamics of idealized electro statically actuated micro-cantilever based devices in micro-electro-mechanical systems (MEMS).

El-Bassiouny (2006) suggested a non-linear control law to suppress the vibrations of the first mode of a cantilever beam when subjected to primary and principal parametric excitations. The method of multiple scales has been used to obtain a set of first-order reduced equations in terms of the amplitude and phase of the response. Maccari (2006) used the asymptotic perturbation method to analyze the principal parametric resonance of a parametrically excited Liénard system under state feedback control with a time delay. Feng et al. (2007) studied the non-linear response for a slender cantilever beam subject to axial narrow-band random excitation using method of multiple scales. Jin and Hu (2007) used method of multiple scales for solving the temporal equation of motion of a parametrically excited system subject to a narrow-band random parametric excitation. Lee et al. (2007) studied the stability analysis for nonplanar free vibrations of a cantilever beam using a nonlinear normal mode concept.

Cao and Zhang (2008) investigated the global bifurcations and chaotic dynamics of a string-beam coupled system subjected to parametric and external excitations by using the analytical and numerical approaches. Dohnal and Verhulst (2008) used first and second order averaging method to obtain the stability of a self- and parametrically excited two degrees of freedom system. Son et al. (2008) studied theoretically and experimentally the nonlinear characteristics of the parametric resonance of simply supported elastic beams. Alhazza et al. (2008) analytically and numerically investigated the effect of time delays on the dynamic stability and non-linear control of parametrically excited cantilever beams. Belhaq and Sah (2008) investigated the effect of a fast vertical parametric excitation on the self-excited vibrations in a delayed van der Pol oscillator. Wang et al. (2008) studied analytically and numerically the stability and bifurcation behaviors of a flexible beam undergoing a large linear motion with a combination parametric resonance. Yu and Yuan (2008) investigated the parameter stability and global bifurcations of a strong nonlinear system with parametric excitation and external excitations using the method of multiple scales.

Also, a detailed description on the dynamics and stability of parametrically excited system can be found in the works of Saito and Otomi (1979), Chalhoub et al (1987), Shirahatti and Sinha (1994), Chen and Yah (1995), Poppelwell and Chang (1996), Ankarali and Diken (1997), Esmailzadeh and Jazar (1998), Fung et al. (1998), Chen et al.(2004), Chen and Yang (2006), Chung et al (2004), Lee and Oh (2005), Shih and Yeh (2005), and Yang and Chen (2005). Further, the basics of parametrically excited systems can be found in the books of Bolotin (1964), Cartmell (1990), Szemplin'ska-Stupnicka (1990), Nayfeh and Mook (1995), Nayfeh and Balachandran (1995).

2.6 Summary

In this chapter review of literature related to the application, modeling, and control of flexible manipulator is carried out. It is observed that while a number of works related to flexible revolute manipulators have been available, very few literature are there for manipulators with prismatic joints. Hence, the works related to the flexible Cartesian manipulators is critically reviewed and one may summarize the works as follows.

- Flexible Cartesian manipulators can be modeled as a cantilever beam or as a beam with roller support at one end.
- While most of the authors studied rigid link Cartesian manipulator, few authors studied the manipulator as an Euler-Bernoulli beam with small transverse vibration.
- Tough these types of manipulators can be used in a number of industrial applications; most of the studies have been limited to the free vibration analysis of the system. In some cases, the manipulator has been modeled as a linear parametrically excited system where the governing temporal equation of motion has been reduced to that of Mathieu-Hill's equation.
- Though it has been observed that to passively control the vibration one may use beams with viscoelastic material and to actively control the vibration one may use magnetic field and beam with magnetoelastic materials, no analysis has been made to use these materials for manipulator purpose. Also, the studies in these types of beams are limited to the determination of the natural frequencies, mode shapes and

very few authors have investigated the parametric instability regions of simply supported beams.

- For practical applications in precision motion and high speed operations to increase the productivity of industrial manipulators, the flexible manipulators should be modeled considering moderately large vibration.
- In many applications the endeffector of the manipulator may be constraint to move in specific path where it is subjected to axial time varying load. In such applications the systems may be modeled as a parametrically excited system with moderately large vibration.

Chapter 3

ELASTIC CARTESIAN MANIPULATOR

3.1 Introduction

The present chapter deals with the nonlinear vibration of a single-link flexible elastic Cartesian manipulator. The manipulator is roller-supported at the left end which is constrained to move sinusoidally in the vertical direction. Here, two different problems are considered. In the first case, the endeffector of the manipulator is not subjected to any force and in the second case; it is subjected to a sinusoidally varying axial force.

In both the cases, the governing equations of motion are obtained using D' Alembert's principle and the generalized Galerkin's method is used to derive the temporal equations of motion. While the method of multiple scales is used to find the response for the system without axial force, for the system with harmonically varying axial load, method of normal forms is used. The steady state responses are determined for different resonance conditions. Time and frequency responses, phase portraits, Poincare's sections and basin of attractions are used to study the system response. The obtained results are compared with the experimental results and also with the results obtained by numerically solving the temporal equation of motion.

In section 3.2, the mathematical modeling of the manipulator with and without harmonically varying axial force is carried out. In section 3.3, the solution of the temporal equation of motion for the Cartesian manipulator without axial force is obtained and the numerical results are discussed. Similar analysis and discussions are carried out for the Cartesian manipulator with harmonically varying axial force in section 3.4. In section 3.5, the concluding remarks are made for the elastic manipulators.

3.2 Mathematical Modeling

Figure 3.1 shows a single-link flexible Cartesian manipulator with a payload of mass *M*. The left end of the manipulator is roller-supported which is subjected to harmonically varying support motion $Y_b(t) = Z\cos\Omega_1 t$. The right end of the manipulator is subjected to a sinusoidally varying axial force $P(t) = P_0 + P_1\cos\Omega_2 t$. The motion of the manipulator is considered to be in the vertical plane.

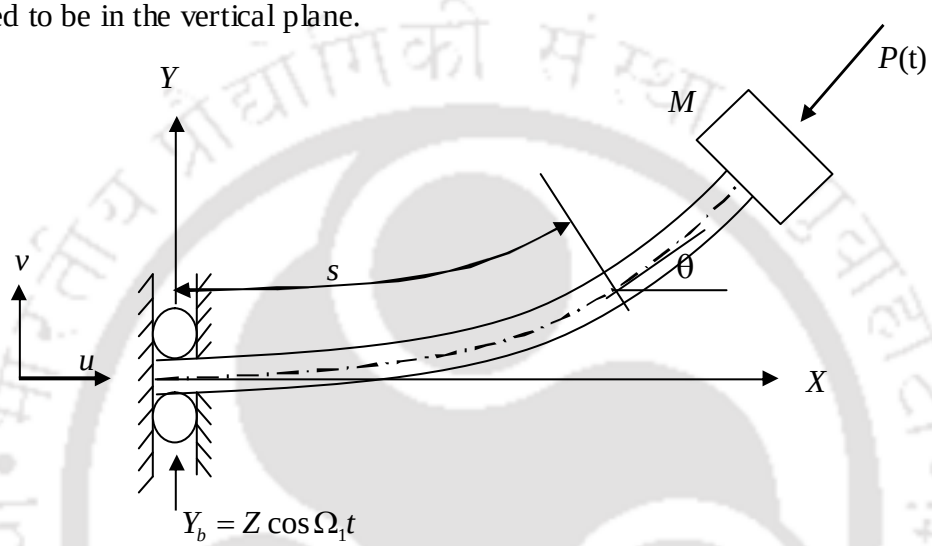

Fig. 3.1. Schematic diagram of a single-link Cartesian manipulator with payload subjected to harmonically varying axial force.

Following assumptions are considered to develop the mathematical model for the above system.

- Thickness (*h*) of the beam is considered to be very small in comparison to the length of the beam (*L*). Hence, the effects of the shear deformation and rotary inertia of the beam are neglected.
- The transverse vibration (*v*) of the beam is assumed to be purely planar. The torsional mode of the beam is neglected in this analysis.
- Payload mass is considered as a point mass which is symmetrically placed with respect to the centerline of the beam.
- The harmonically varying tip load is acting always in the tangential direction of the elastic line and the amplitude of the axial force is taken less than the critical buckling load.

Here, the Cartesian manipulator with payload is modeled as a roller-supported Euler–Bernoulli beam with a tip mass. The governing equation of motion of the present system is derived using D' Alembert's principle. Considering a small element at a distance s from the roller-supported end (Fig. 3.1) along the elastic line of the beam, the bending moment $M(s)$ of the beam can be expressed as:

$$M(s) \approx EI\left(v_{ss} + \frac{1}{2}v_s^2 v_{ss}\right). \tag{3.1}$$

Here, v is the transverse displacement of the beam. $(\,)_s$ is the first derivative with respect to s along the beam. Following Zavodney and Nayfeh (1989), and Cuvalci (1996, 2000), one may write the inextensibility condition of the beam in terms of the longitudinal displacement $u(\xi,t)$ and the transverse displacement $v(\xi,t)$ as:

$$v_s^2 + (1+u_s)^2 = 1. \quad \text{or,} \quad u(\xi,t) = \xi - \int_0^{\xi}\left(1 - v_\eta^2\right)^{\frac{1}{2}} d\eta. \tag{3.2}$$

Here, ξ, η are the integration variables. Considering the inertia forces per unit length of the beam $\rho A\ddot{u}$, and $\rho A\left(\ddot{v} + \ddot{Y}_b\right)$, in longitudinal and transverse directions, respectively and inertia forces of the tip mass in longitudinal and transverse directions as $M\ddot{u}$ and $M\left(\ddot{v} + \ddot{Y}_b\right)$, respectively, one may write equation (3.1) as follows:

$$M(s) - M_\xi(s) - M_L(s) = 0. \tag{3.3}$$

Here, $M_\xi(s)$ is the moment due to inertia force at a distance ξ from the roller-supported end and $M_L(s)$ is the moment due to inertia force for the payload at the tip of the manipulator and their expressions are given below:

$$M_\xi(s) = -\int_s^L \rho A\ddot{u}\int_s^\xi \sin\theta\, d\eta\, d\xi - \int_s^L \rho A\left(\ddot{v} + \ddot{Y}_b\right)\int_s^\xi \cos\theta\, d\eta\, d\xi, \tag{3.4}$$

$$\text{and, } M_L(s) = -M\ddot{u}\int_s^L \sin\theta\, d\xi - M\left(\ddot{v} + \ddot{Y}_b\right)\int_s^L \cos\theta\, d\xi - P(t)\int_s^L \sin\theta\, d\xi\ . \tag{3.5}$$

Considering equivalent viscous damping force $c_d\dot{v}$ due to interaction of the system with the environment and by differentiating equation (3.3) twice with respect to *s*, using the Leibniz's rule and applying the binomial expansion, one may obtain the following governing differential equation of motion.

$$EI\left(v_{ssss}+\frac{1}{2}v_s^2v_{ssss}+3v_sv_{ss}v_{sss}+v_{ss}^3\right)+\rho Av_s\left(\int_0^s\left(\dot{v}_\xi^2+v_\xi\ddot{v}_\xi\right)d\xi\right)+M\left(\ddot{v}+\ddot{Y}_b\right)v_sv_{ss}+v_sv_{ss}$$

$$\left(\rho A\ddot{Y}_b(L-s)+\int_s^L\left(\rho A\ddot{v}+c_d\dot{v}\right)d\eta\right)-v_{ss}\left(\int_s^L\rho A\int_0^\xi\left(\dot{v}_\xi^2+v_\xi\ddot{v}_\xi\right)d\xi d\eta+M\int_0^s\left(\dot{v}_\xi^2+v_\xi\ddot{v}_\xi\right)d\xi\right)+$$

$$\left(1-\frac{1}{2}v_s^2\right)\left(\rho A\left(\ddot{v}+\ddot{Y}_b\right)+c_d\dot{v}\right)+\left(P(t)v_s\right)_s=0. \qquad (3.6)$$

The boundary conditions are at $s=0$, displacement $v=Y_b$, slope $v_s=0$; at $s=L$, bending moment $EIv_{ss}=0$, and shear force $EIv_{sss}=M\left(\ddot{Y}+\ddot{v}\right)$. But it may be noted that these forces are already considered in the equation of motion.

Here, generalized Galerkin's method is used to discretize the governing equation of motion (3.6) by using the following assumed mode expression:

$$v(s,t)=r\,\psi(s)\,q(t). \qquad (3.7)$$

Here, *r*, $\psi(s)$ and $q(t)$ are respectively, the scaling parameter, admissible function of the beam and time modulation. The admissible function $\psi(s)$ is considered to be same as the eigenfunction of a cantilever beam with tip mass which can be expressed as:

$$\psi(s)=-\frac{\sin\beta L+\sinh\beta L}{\cos\beta L+\cosh\beta L}\left(\cos\beta s-\cosh\beta s\right)+\left(\sin\beta s-\sinh\beta s\right). \qquad (3.8)$$

One may find βL from the following characteristic equation.

$$1+\cos\beta L\cosh\beta L+\left(\frac{M}{\rho AL}\right)\beta L\left(\cos\beta L\sinh\beta L-\sin\beta L\cosh\beta L\right)=0. \qquad (3.9)$$

The following non-dimensional parameters are used in this analysis.

$$\bar{x}=\frac{s}{L},\ \tau=\omega_s t,\ \bar{\omega}_1=\frac{\Omega_1}{\omega_s},\ \bar{\omega}_2=\frac{\Omega_2}{\omega_s},\ \bar{r}=\frac{r}{L},\ \bar{m}=\frac{M}{\rho AL},$$

$$\bar{P}_0=\frac{P_0}{P_c},\ \bar{P}_1=\frac{P_1}{P_c},\ \chi=\frac{EI}{\rho AL^4},\ \kappa=\frac{Z}{r},\ \text{and}\ \bar{Z}=\frac{Z}{L} \qquad (3.10)$$

Here, P_c is the critical Euler buckling load for a cantilever beam, which is equal to $\left(\pi^2 E I\right)/\left(4L^2\right)$ and ω_s is the fundamental frequency of the system. Substituting equations (3.7) and (3.8) into equation (3.6) and using the generalized Galerkin's method, the resulting nondimensional temporal equation of motion is obtained as follows.

$$\ddot{q}+q+2\varepsilon\zeta\dot{q}+\varepsilon\left(\alpha_1 q^3+\alpha_2 q^2\ddot{q}+\alpha_3\dot{q}^2 q\right)$$
$$+\varepsilon\left(\alpha_4\bar{\omega}_1^2\cos\left(\bar{\omega}_1\tau\right)q^2+\alpha_5\bar{\omega}_1^2\cos\left(\bar{\omega}_1\tau\right)+\alpha_6\cos\left(\bar{\omega}_2\tau\right)q\right)=0. \qquad (3.11)$$

The expressions for the coefficients (viz., $\zeta,\alpha_1\cdots\alpha_6$) of equation (3.11) are as follows:

$$\omega_s=\sqrt{\frac{EI}{\rho AL^4}\left(\frac{h_{14}}{h_2}+\frac{P_0\pi^2}{4P_c}\frac{h_{21}}{h_2}\right)}=\sqrt{\chi\left(\frac{h_{14}}{h_2}+\bar{P}_0\frac{\pi^2}{4}\frac{h_{21}}{h_2}\right)},\zeta=\frac{c_d}{2\varepsilon\rho A\omega_s},$$

$$\alpha_1=\frac{\chi\bar{r}^2}{\varepsilon\omega_s^2}\left(\frac{h_{19}}{h_2}+\frac{h_{18}}{2h_2}+3\frac{h_{20}}{h_2}\right),\quad \alpha_2=\frac{\bar{r}^2}{\varepsilon}\left(\frac{h_3}{h_2}+\frac{h_4}{h_2}+\bar{m}\frac{h_5}{h_2}-\frac{h_6}{h_2}-\bar{m}\frac{h_7}{h_2}-\frac{h_8}{h_2}\right),$$

$$\alpha_3=\frac{\bar{r}^2}{\varepsilon}\left(\frac{h_{11}}{h_2}-\frac{h_{12}}{h_2}-\bar{m}\frac{h_{13}}{h_2}\right),\alpha_4=\frac{\bar{Z}\,\bar{r}}{\varepsilon}\left(\frac{h_{15}}{h_2}+\bar{m}\frac{h_{16}}{h_2}-\frac{h_{17}}{2h_2}\right),\alpha_5=\frac{\kappa}{\varepsilon}\left(\frac{h_1}{h_2}\right)\text{and}$$

$$\alpha_6=\frac{P_1}{M\,\omega_s^2\,L^2}\left(\frac{h_{21}}{h_2}\right).$$

Here, $h_1=\int_0^1\psi(\bar{x})d\bar{x}$, $h_2=\int_0^1[\psi(\bar{x})]^2 d\bar{x}$, $h_3=\int_0^1\left[\frac{d\psi(\bar{x})}{d\bar{x}}\left(\int_0^x\left[\frac{d\psi(\bar{\xi})}{d\bar{\xi}}\right]^2 d\bar{\xi}\right)\psi(\bar{x})\right]d\bar{x}$,

$$h_4=\int_0^1\left[\frac{d\psi(\bar{x})}{d\bar{x}}\frac{d^2\psi(\bar{x})}{d\bar{x}^2}\left[\int_x^1\psi(\bar{\xi})d\bar{\xi}\right]\psi(\bar{x})\right]d\bar{x},\quad h_5=\int_0^1\left[\frac{d\psi(\bar{x})}{d\bar{x}}\frac{d^2\psi_y(\bar{x})}{d\bar{x}^2}[\psi(\bar{x})]^2\right]d\bar{x},$$

$$h_6=\int_0^1\left[\frac{d^2\psi(\bar{x})}{d\bar{x}^2}\left(\int_x^1\int_0^\eta\left[\frac{d\psi(\bar{x})}{d\bar{\xi}}\right]^2 d\bar{\xi}d\bar{\eta}\right)\psi(\bar{x})\right]d\bar{x},\ h_7=\int_0^1\left[\frac{d^2\psi(\bar{x})}{d\bar{x}^2}\left(\int_0^x\left[\frac{d\psi(\bar{\xi})}{d\bar{\xi}}\right]^2 d\bar{\xi}\right)\psi(\bar{x})\right]d\bar{x},$$

$$h_8=\int_0^1\left[\frac{d\psi(\bar{x})}{d\bar{x}}\right]^2[\psi(\bar{x})]^2 d\bar{x},\quad h_9=\int_0^1\left[\frac{d\psi(\bar{x})}{d\bar{x}}\frac{d^2\psi(\bar{x})}{d\bar{x}^2}\left[\int_x^1\psi(\bar{\xi})d\bar{\xi}\right]\psi(\bar{x})\right]d\bar{x},$$

$$h_{10}=\int_0^1\left[\frac{d\psi(\bar{x})}{d\bar{x}}\right]^2[\psi(\bar{x})]^2 d\bar{x},\quad h_{11}=\int_0^1\left[\frac{d\psi(\bar{x})}{d\bar{x}}\left(\int_0^x\left[\frac{d\psi(\bar{\xi})}{d\bar{\xi}}\right]^2 d\bar{\xi}\right)\psi(\bar{x})\right]d\bar{x},$$

$$h_{12}=\int_0^1\left[\frac{d^2\psi(\bar{x})}{d\bar{x}^2}\left(\int_x^1\int_0^{\eta}\left[\frac{d\psi(\bar{\xi})}{d\bar{\xi}}\right]^2 d\bar{\xi}d\bar{\eta}\right)\psi(\bar{x})\right]d\bar{x},\quad h_{13}=\int_0^1\left[\frac{d^2\psi(\bar{x})}{d\bar{x}^2}\left(\int_0^{x}\left[\frac{d\psi(\bar{\xi})}{d\bar{\xi}}\right]^2 d\bar{\xi}\right)\psi(\bar{x})\right]d\bar{x},$$

$$h_{14}=\int_0^1\left[\frac{d^4\psi(\bar{x})}{d\bar{x}^4}\psi(\bar{x})d\bar{x}\right],\quad h_{15}=\int_0^1\left[(1-\bar{x})\frac{d\psi(\bar{x})}{d\bar{x}}\frac{d^2\psi(\bar{x})}{d\bar{x}^2}\psi(\bar{x})\right]d\bar{x},$$

$$h_{16}=\int_0^1\left[\frac{d\psi(\bar{x})}{d\bar{x}}\frac{d^2\psi(\bar{x})}{d\bar{x}^2}\psi(\bar{x})\right]d\bar{x},h_{17}=\int_0^1\left[\frac{d\psi(\bar{x})}{d\bar{x}}\right]^2\psi(\bar{x})d\bar{x},$$

$$h_{18}=\int_0^1\left[\left(\frac{d\psi(\bar{x})}{d\bar{x}}\right)^2\frac{d^4\psi(\bar{x})}{d\bar{x}^4}\psi(\bar{x})\right]d\bar{x},h_{19}=\int_0^1\left[\frac{d^2\psi(\bar{x})}{d\bar{x}^2}\psi(\bar{x})\right]d\bar{x},$$

$$h_{20}=\int_0^1\left[\frac{d\psi(\bar{x})}{d\bar{x}}\frac{d^2\psi(\bar{x})}{d\bar{x}^2}\frac{d^3\psi(\bar{x})}{d\bar{x}^3}\psi(\bar{x})\right]d\bar{x},\text{ and }h_{21}=\int_0^1\left[\frac{d^2\psi(\bar{x})}{d\bar{x}^2}\psi(\bar{x})\right]d\bar{x}. \qquad (3.12)$$

It is observed from the numerical values of the coefficients of the damping; forcing and nonlinear terms that they are one order less than the coefficients of the linear terms (coefficients of $\ddot{q}$ and q) which have value of unity in this case. Hence, to make all the coefficients (e.g., $\alpha_1,\alpha_2,\cdots,\alpha_6$) of the order of unity, a book keeping parameter ε which is less than one is introduced in equation (3.11). One may find that the non-dimensional temporal equation (3.11) contains linear damping term ($2\varepsilon\zeta\dot{q}$), a forced excitation term ($\alpha_5\bar{\omega}_1^2\cos(\bar{\omega}_1\tau)$) and a nonlinear parametric excitation term ($\alpha_4\bar{\omega}_1^2\cos(\bar{\omega}_1\tau)q^2$) due to the harmonically varying support motion, a parametric excitation term $\alpha_6\cos(\bar{\omega}_2\tau)q$ due to the harmonically varying axial force along with the cubic geometric (α_1q^3) and inertia ($\alpha_2q^2\ddot{q}+\alpha_3\dot{q}^2q$) terms.

It may be noted that in the absence of harmonically varying axial force, the equation of motion for the single-link Cartesian manipulator without axial force can be written by neglecting the parametric excitation term $\alpha_6\cos(\bar{\omega}_2\tau)q$ from equation (3.11) as:

$$\ddot{q}+q+2\varepsilon\zeta\dot{q}+\varepsilon\left(\alpha_1q^3+\alpha_2q^2\ddot{q}+\alpha_3\dot{q}^2q+\alpha_4\bar{\omega}_1^2\cos(\bar{\omega}_1\tau)q^2+\alpha_5\bar{\omega}_1^2\cos(\bar{\omega}_1\tau)\right)=0. \qquad (3.13)$$

One may note that the temporal equation of motions (3.11 and 3.13) contains many nonlinear terms and it is very difficult to find the closed form solution or exact solution. Hence, one may go for an approximate solution by using perturbation methods which are described in the following section. It may be noted that in case of nonlinear system as the superposition theory can not be applied, hence one will not be able to predict the solution of equation (3.13) from the solution of equation (3.11). Therefore, the solution of the systems without and with axial force should be treated separately. Here, method of multiple scales is used to solve the equation (3.13) and method of normal form is used to find the reduced equations for equation (3.11).

In the following sections, solutions of the temporal equation of motion and numerical simulations are carried out for the elastic manipulator with and without axial force.

3.3 Cartesian Manipulator without Axial Force

3.3.1 Analysis

Here, to find the solution of equation (3.13), method of multiple scales is used. Following the standard procedure (Nayfeh and Balachandran, (1995) and Nayfeh and Mook (1995)), the displacement q can be represented in terms of different time scales (T_0, T_1) and a book keeping parameter ε as follows:

$$q(\tau;\varepsilon) = q_0(T_0,T_1) + \varepsilon q_1(T_0,T_1) + O\left(\varepsilon^2\right), \tag{3.14}$$

where, $T_n = \varepsilon^n \tau$, $n = 0,1,2\cdots$, or, $T_0 = \tau$, $T_1 = \varepsilon\tau$. The first and second time derivatives are given by

$$\frac{d}{d\tau} = D_0 + \varepsilon D_1 + O\left(\varepsilon^2\right), \text{ and } \frac{d^2}{d\tau^2} = D_0^2 + 2\varepsilon D_0 D_1 + O\left(\varepsilon^2\right). \tag{3.15}$$

Here, $D_0 = \dfrac{\partial}{\partial T_0}$ and $D_1 = \dfrac{\partial}{\partial T_1}$. Substituting equations (3.14) and (3.15) into equation (3.13) and equating coefficients of like powers of ε , yields the following expressions:

Order ε^0: $D_0^2 q_0 + q_0 = 0$, (3.16a)

Order ε^1: $D_0^2 q_1 + q_1 = -2D_0 D_1 q_0 - 2\zeta D_0 q_0 - \alpha_1 q_0^3 - \alpha_2 q_0^2 D_0^2 q_0 - \alpha_3 \left(D_0 q_0\right)^2 q_0$

$$-\alpha_4 \bar{\omega}^2 \cos\left(\bar{\omega}\tau\right) q_0^2 - \alpha_5 \bar{\omega}^2 \cos\left(\bar{\omega}\tau\right). \tag{3.16b}$$

Here, as the system is subjected to only the support motion, for simplicity in equation (3.13) $\bar{\omega}_1$ is replaced by $\bar{\omega}$.

General solution of equation (3.16a) can be written as

$$q_0 = A(T_1)\exp(iT_0) + \bar{A}(T_1)\exp(-iT_0) \ . \tag{3.17}$$

Substituting equation (3.17) into equation (3.16b) leads to

$$D_0^2 q_1 + q_1 = -\left(2iD_1 A + 2i\zeta A + 3\alpha_1 A^2 \bar{A} - 3\alpha_2 A^2 \bar{A} + \alpha_3 A^2 \bar{A}\right)\exp\left(iT_0\right)$$

$$-\left(\alpha_1 - \alpha_2 - \alpha_3\right) A^3 \exp\left(3iT_0\right) - \frac{1}{2}\alpha_4 \bar{\omega}^2 A^2 \exp i\left(2+\bar{\omega}\right)T_0$$

$$-\frac{1}{2}\alpha_4\bar{\omega}^2\bar{A}^2\exp i\left(\bar{\omega}-2\right)T_0-\bar{\omega}^2\left(\alpha_4 A\bar{A}+\frac{1}{2}\alpha_5\right)\exp i\left(\bar{\omega}T_0\right)+cc\,. \qquad (3.18)$$

Here, *cc* stands for the complex conjugate of the preceding terms. Though the actual response of the system is bounded, due to the presence of secular or small divisor terms in equation (3.18), the solution of the system sometimes will not be bounded. For a bounded solution, these terms should be removed. It may be noted from equation (3.18) that it contains secular or small divisor terms when the frequency of the excitation is nearly equal to 1 ($\bar{\omega}\approx 1$) or the frequency of the excitation is nearly equal to three times the natural frequency of the system ($\bar{\omega}\approx 3$). When $\bar{\omega}\approx 1$, from equation (3.18) it can be observed that both forcing and nonlinear parametric excitation terms will contribute to the resonance condition, which may be regarded as simple resonance case. Similarly, when $\bar{\omega}\approx 3$, only nonlinear parametric term will contribute to the sub-harmonic resonance condition. These two resonance cases are studied in the following subsections.

3.3.1.1 Simple Resonance Case ($\bar{\omega}\approx 1$)

In the case of simple resonance, one may use the detuning parameter σ to express the nearness of $\bar{\omega}$ to 1 as

$$\bar{\omega}=1+\varepsilon\sigma, \qquad \sigma=O(1)\,. \qquad (3.19)$$

Substituting equation (3.19) into equation (3.18) and eliminating the secular or small divisor terms one may obtain the following equation:

$$2iA'+2i\zeta A+3\alpha_1 A^2\bar{A}-3\alpha_2 A^2\bar{A}+\alpha_3 A^2\bar{A}+\frac{1}{2}\bar{\omega}^2\alpha_4 A^2\exp i\left(-\sigma T_1\right)+$$

$$\bar{\omega}^2\left(\alpha_4 A\bar{A}+\frac{1}{2}\alpha_5\right)\exp i\left(\sigma T_1\right)=0. \qquad (3.20)$$

Substituting A in the polar form i.e. $A = \frac{1}{2}a\left(T_1\right)\mathrm{e}^{(i\beta T_1)}$ and separating the real and imaginary parts yields the following expressions:

$$a'=-\zeta a-\bar{\omega}^2\left(\frac{\alpha_4}{8}a^2+\frac{1}{2}\alpha_5\right)\sin\gamma\,, \qquad (3.21)$$

$$a\gamma' = a\sigma - \frac{3}{8}\left(\alpha_1 - \alpha_2 + \frac{\alpha_3}{3}\right)a^3 - \bar{\omega}^{-2}\left(\frac{3\alpha_4}{8}a^2 + \frac{1}{2}\alpha_5\right)\cos\gamma\,. \qquad (3.22)$$

Here, $(\ )' = \frac{\partial}{\partial T_1}$, and $\gamma = \sigma T_1 - \beta$. For steady state response (a_0, γ_0), a' and γ' are equal to zero. Eliminating γ from equations (3.21) and (3.22), one may find a fifth order polynomial in a^2, which can be expressed as:

$$Q_5 a^{10} + Q_4 a^8 + Q_3 a^6 + Q_2 a^4 + Q_1 a^2 + Q_0 = 0\,. \qquad (3.23)$$

The coefficients of the above fifth order polynomial equation in a^2 are given by the following expressions:

$$Q_0 = -\frac{1}{16}\bar{\omega}^{-8}\alpha_5^4,\ Q_1 = \frac{1}{4}\zeta^2\bar{\omega}^{-4}\alpha_5^2 + \frac{1}{4}\bar{\omega}^{-4}\sigma^2\alpha_5^2 - \frac{1}{8}\bar{\omega}^{-8}\alpha_4\alpha_3^3,$$

$$Q_2 = \frac{3}{8}\zeta^2\bar{\omega}^{-4}\alpha_4\alpha_5 + \frac{1}{8}\bar{\omega}^{-4}\sigma^2\alpha_4\alpha_5 - \frac{3}{16}\bar{\omega}^{-4}\left(\alpha_1 - \alpha_2 + \frac{\alpha_3}{3}\right)\sigma\alpha_5^2 - \frac{11}{32}\bar{\omega}^{-8}\alpha_4^2\alpha_5^2,$$

$$Q_3 = \frac{9}{64}\zeta^2\bar{\omega}^{-4}\alpha_4^2 + \frac{1}{64}\bar{\omega}^{-4}\sigma\alpha_4^2 + \frac{9}{256}\bar{\omega}^{-4}\left(\alpha_1 - \alpha_2 + \frac{\alpha_3}{3}\right)^2\alpha_5^2$$
$$-\frac{3}{32}\bar{\omega}^{-4}\sigma\left(\alpha_1 - \alpha_2 + \frac{\alpha_3}{3}\right)\alpha_4\alpha_5 - \frac{1}{128}\bar{\omega}^{-8}\alpha_4^3\alpha_5,$$

$$Q_4 = \frac{9}{512}\bar{\omega}^{-4}\left(\alpha_1 - \alpha_2 + \frac{\alpha_3}{3}\right)^2\alpha_4\alpha_5 - \frac{3}{256}\bar{\omega}^{-4}\sigma\left(\alpha_1 - \alpha_2 + \frac{\alpha_3}{3}\right)\alpha_4^2 - \frac{9}{4096}\bar{\omega}^{-8}\alpha_4^4,$$

and, $Q_5 = \frac{9}{4096}\bar{\omega}^{-4}\left(\alpha_1 - \alpha_2 + \frac{\alpha_3}{3}\right)^2\alpha_4^2\,.$ (3.24)

Equation (3.23) is an implicit equation for amplitude of the response as a function of the external detuning parameters σ (i.e. the excitation frequency), tip mass M and the amplitude of the base excitation Z. One may note from equation (3.23) that this resonance condition does not have any trivial state response (i.e., $a = 0$ is not a solution). The response of the system can be obtained either by numerically solving the fifth order polynomial equation (3.23) or numerically solving the reduced equations (3.21) and (3.22), simultaneously. Newton's method is used to solve numerically the polynomial equation (3.23) to find the response of the system. Also, the same method is used to solve the set of nonlinear algebraic equations obtained by substituting a' and γ' equal to zero in equations

(3.21) and (3.22). In all the cases, same Newton's method is used for finding the steady state response. Also, one may get the response by numerically solving the temporal equation of motion (3.13) by using Runge-Kutta method. In the present work, ODE45 function of the MATLAB has been used to numerically solve the temporal equation of motion.

The stability of the steady state fixed-point response (a_0,γ_0) can be found by superposing a perturbation (a_1,γ_1) on the singular points (a_0,γ_0) by substituting $a=a_0+a_1$, and $\gamma=\gamma_0+\gamma_1$, in equations (3.21) and (3.22) and determining the eigenvalues of the resulting Jacobian matrix (J). One may express the Jacobian matrix as follows.

$$J=\begin{bmatrix} -\zeta+\dfrac{\frac{1}{2}\alpha_4 a_0\zeta\, a_0}{\frac{1}{8}\alpha_2 a_0^2+\frac{1}{2}\alpha_5} & -\dfrac{\left(\frac{1}{8}\alpha_4 a_0^2+\frac{1}{2}\alpha_5\right)\left(\sigma a_0-\frac{3}{8}Ka_0^3\right)}{\frac{3}{8}\alpha_4 a_0^2+\frac{1}{2}\alpha_5} \\ -\frac{3}{4}Ka_0-\frac{3}{4}\dfrac{\alpha_4\left(\sigma a_0-\frac{3}{8}Ka_0^3\right)}{\frac{3}{8}\alpha_4 a_0^2+\frac{1}{2}\alpha_5}+\dfrac{\sigma a_0-\frac{3}{8}Ka_0^3}{a^2} & -\dfrac{\left(\frac{3}{8}\alpha_4 a_0^2+\frac{1}{2}\alpha_5\right)\zeta}{\frac{1}{8}\alpha_4 a_0^2+\frac{1}{2}\alpha_5} \end{bmatrix} \quad (3.25)$$

Here, $K=\left(\alpha_1-\alpha_2+\dfrac{\alpha_3}{3}\right)$. The system will be stable if the real part of all the eigenvalues of the Jacobian matrix (J) are negative. From equation (3.17), the first order nontrivial steady state approximate solution can be given by

$$q=a\cos\left(\bar{\omega}\tau-\gamma\right)+O(\varepsilon). \quad (3.26)$$

3.3.1.2 Subharmonic Resonance Case ($\bar{\omega}\approx 3$)

In this case, to describe the nearness of $\bar{\omega}$ to 3, one may use a detuning parameter σ as

$$\bar{\omega}=3+\varepsilon\sigma, \qquad \sigma=O(1). \quad (3.27)$$

Substituting equation (3.27) into equation (3.18) and by eliminating the secular or small divisor terms, one may obtain the following equation:

$$2iA'+2i\zeta A+3\alpha_1 A^2\bar{A}-3\alpha_2 A^2\bar{A}+\alpha_3 A^2\bar{A}+\frac{1}{2}\bar{\omega}^2\alpha_4 A^2\exp i\left(\sigma T_1\right)=0. \quad (3.28)$$

Here, also substituting $A = \frac{1}{2}a(T_1)e^{(i\beta T_1)}$ in equation (3.28) and separating the real and imaginary parts, one may have the following reduced equations:

$$a' = -\zeta a - \bar{\omega}^{-2}\frac{\alpha_4}{8}a^2 \sin\gamma, \tag{3.29}$$

$$a\gamma' = a\sigma - \frac{9}{8}\left(\alpha_1 - \alpha_2 + \frac{\alpha_3}{3}\right)a^3 - \bar{\omega}^{-2}\frac{3\alpha_4}{8}a^2\cos\gamma. \tag{3.30}$$

Here, $\gamma = \sigma T_1 - 3\beta$. For steady state condition, a' and γ' equal to zero. Eliminating γ from equations (3.29) and (3.30), one may find a fourth order polynomial equation in a^2 which is given by

$$a^2\left(Q_1 + Q_2 a^2 + Q_3 a^4\right) = 0. \tag{3.31}$$

The coefficients of the above polynomial are given below.

$Q_1 = 64\zeta^2\bar{\omega}^{-4} + \frac{64}{9}\sigma^2\bar{\omega}^{-4}$, $Q_2 = -16\bar{\omega}^{-4}\sigma\left(\alpha_1 - \alpha_2 + \frac{\alpha_3}{3}\right) - \bar{\omega}^{-8}\alpha_4^2$, and

$$Q_3 = 9\bar{\omega}^{-4}\left(\alpha_1 - \alpha_2 + \frac{\alpha_3}{3}\right)^2 + \frac{64}{9}\sigma^2\bar{\omega}^{-4}. \tag{3.32}$$

From equation (3.31), it may be noted that the system has both trivial ($a = 0$) and nontrivial ($a \neq 0$) solutions. Similar to previous case, to obtain the nontrivial response, one may determine the system response either by numerically solving the fourth order polynomial equation (3.31) or numerically solving the reduced equations (3.29) and (3.30), simultaneously for different system parameters.

To obtain the stability of the steady state response, one may follow the procedure given in the previous section. But, as the polar form of modulation equation (3.30) contains term like $a\gamma'$, one may note that for finding stability of the trivial state, the linearized equation will not contain the perturbation γ_1'. Hence, the stability of the trivial solutions may be obtained by converting equations (3.29) and (3.30) to their Cartesian form of modulations by introducing the transformation $p_s = a\cos\gamma$ and $q_s = a\sin\gamma$ (Nayfeh and Balachandran

(1995) and Nayfeh and Mook (1995)). Now one may obtain the resulting Cartesian modulation equations as follows:

$$p_s' = -\zeta p_s - \sigma q_s + \frac{1}{4}\alpha_4 \bar{\omega}^2 p_s q_s + \frac{9}{8} K q_s (p_s^2 + q_s^2), \tag{3.33}$$

$$q_s' = -\zeta q_s + \sigma p_s - \frac{1}{8}\alpha_4 \bar{\omega}^2 \left(3p_s^2 + q_s^2\right) - \frac{9}{8} K p_s (p_s^2 + q_s^2) \tag{3.34}$$

Here, $K = \left(\alpha_1 - \alpha_2 + \frac{\alpha_3}{3}\right)$. Stability of the steady state response (p_0, q_0) can be determined by investigating the eigenvalues of the Jacobian matrix (J) obtained by perturbing equations (3.33) and (3.34). The Jacobian matrix is given by

$$J = \begin{bmatrix} -\zeta + \frac{1}{4}\alpha_4 \bar{\omega}^2 q_0 + \frac{9}{4} K q_0 p_0 & -\sigma + \frac{1}{4}\alpha_4 \bar{\omega}^2 p_0 + \frac{9}{8} K \left(p_o^2 + q_0^2\right) + \frac{9}{4} K q_0 q_0 \\ \sigma - \frac{3}{4}\alpha_4 \bar{\omega}^2 p_0 - \frac{9}{8} K \left(p_o^2 + q_0^2\right) - \frac{9}{4} K p_0 p_0 & -\zeta - \frac{1}{4}\alpha_4 \bar{\omega}^2 q_0 - \frac{9}{4} K q_0 q_0 \end{bmatrix}. \tag{3.35}$$

The system will be stable for both trivial and nontrivial responses, if the real parts of all the eigenvalues of the Jacobian matrix (J) are negative. One may write the first order nontrivial steady state response as:

$$q = a\cos\left(\frac{1}{3}\left(\bar{\omega}\tau - \gamma\right)\right) + O(\varepsilon). \tag{3.36}$$

3.3.2 Numerical Results and Discussions

In this case, as pointed out in section 3.3.1, the system has two different types of resonance conditions viz., simple resonance and sub-harmonic resonance conditions. In all simulations, a metallic beam is considered with length L = 0.336 m, cross-section area A = 40.464×10^{-6} m^2, moment of inertia I = 8.669867×10^{-12} m^4, Young's modulus E = 1.5848×10^{11} N/m^2, damping constant c_d = 0.11 N-s/m, and mass density ρ = 7830 kg/m^3. Here, the scaling parameter ($\bar{r}$) is considered to be as 0.1. The book-keeping parameter (ε)

is taken as 0.1.The nonlinear response for this system is determined for different values of amplitude of harmonic support motion (*Z*) and payload mass *M* for the simple resonance and subharmonic resonance conditions. While the simple resonance condition is discussed in section 3.3.2.1, sub-harmonic resonance condition is discussed in section 3.3.2.2.

3.3.2.1 Simple Resonance condition ($\bar{\omega} \approx 1$)

This resonance condition takes places when the frequency of the support motion of the Ω_1 nearly equal to the fundamental frequency of the system. Figure 3.2 shows the frequency response curves for simple resonance case for the nondimensional amplitude ratio of base excitation ($\bar{Z}$) equal to 0.00372 and mass ratio $\bar{m}$ equal to 1.8787. The solid and dotted lines, respectively, represent the stable and unstable branches of the frequency response curves.

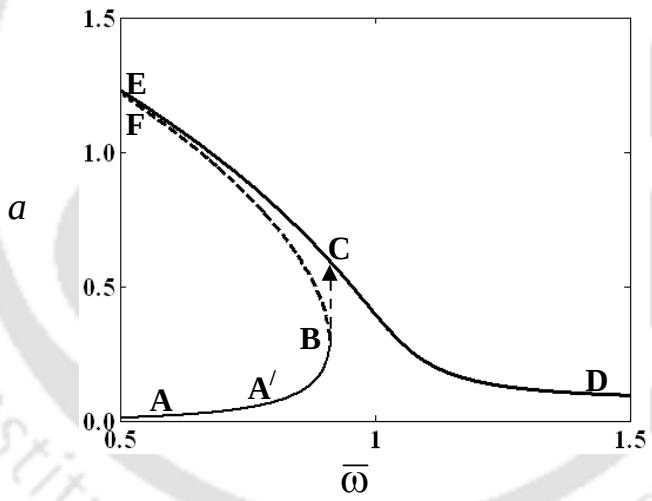

Fig. 3.2. Frequency response curve for simple resonance case for mass ratio $\bar{m}$ =1.8787 and base excitation $\bar{Z}$ =0.00372.

It is observed from the frequency response curves that the system does not possess any trivial state response. So, one may note that the manipulator will always oscillate about its equilibrium position with an amplitude equal to the nontrivial response as shown in Fig. 3.2. When the manipulator is started (e.g. at point A), with increase in frequency of external excitation, the response amplitude of the manipulator increases and it will reach a critical value at point B, which is a saddle node bifurcation point. At this point with further

increase in frequency, the system will experience a jump up phenomenon i.e. a sudden jump from point B to point C which leads to a sudden increase of amplitude. The system may fail due to this sudden jump. It is shown in Fig. 3.2 that the system experiences an upward jump at frequency $\bar{\omega}$ equal to 0.921 with a jump length equal to 0.2852. When excitation frequency is swept down (e.g. from point D), with decrease in frequency the response amplitude increases to point E. This situation may occur when the prime mover of the manipulator is stopped and in that case the system will experience a jump down phenomenon, which may lead to catastrophic failure. It is also observed that the system has a bi-stable region before the saddle-node bifurcation point B. The initial condition will play a very important role to determine the actual system response. It may be noted that in this case same system parameters are taken as that of the experimental work of Cuvalci (2000). In that work a base excited cantilever beam with a pendulum vibration absorber attached to the tip mass of the beam was considered. When the pendulum is at locked position, it can be reduced to the system considered in this work. In Cuvalci (2000), the natural frequency is observed to be at 3.07 Hz and while sweeping up the frequency, the system failed at a frequency of 2.92 Hz [Cuvalci (2000), Fig. 9(b)]. In the present work, it is observed that with same system parameters, the fundamental frequency is found to be 3.27 Hz. Also as explained before, the system undergoes a catastrophic failure at $\bar{\omega}$ = 0.921 which correspond to a frequency of 3.01 Hz. Hence, the error in the bifurcation point is very marginal and is of 3% only. More experimental results (e.g. [Cuvalci (2000), Fig. 10(a)]) are also found to be matching with the numerical results obtained in this work. So, these numerical results obtained by the method of multiple scales are in good agreement with the experimental findings. Hence, one may use equation (3.23) to find the response of any similar system instead of going for an expensive experimental work or going for a time-consuming solution of the temporal equation of motion as studied in Cuvalci (2000).

Figure 3.3 shows the time response, phase portrait, and Poincare's' section at the critical point B. The time response is obtained by solving the temporal equation of motion (3.13) using fourth order Runge–Kutta method. While the transient response (Fig. 3.3 (i), (iii), and (v)) of the system with initial point (a = 0.326, γ = 0.1) gives a beating type

phenomenon, the steady state response of the system is periodic (Fig. 3.3 (ii)). The phase portrait and Poincare's section for transient and steady state response are shown in Figs. 3.3 (iii), (v) and (iv), (vi), respectively.

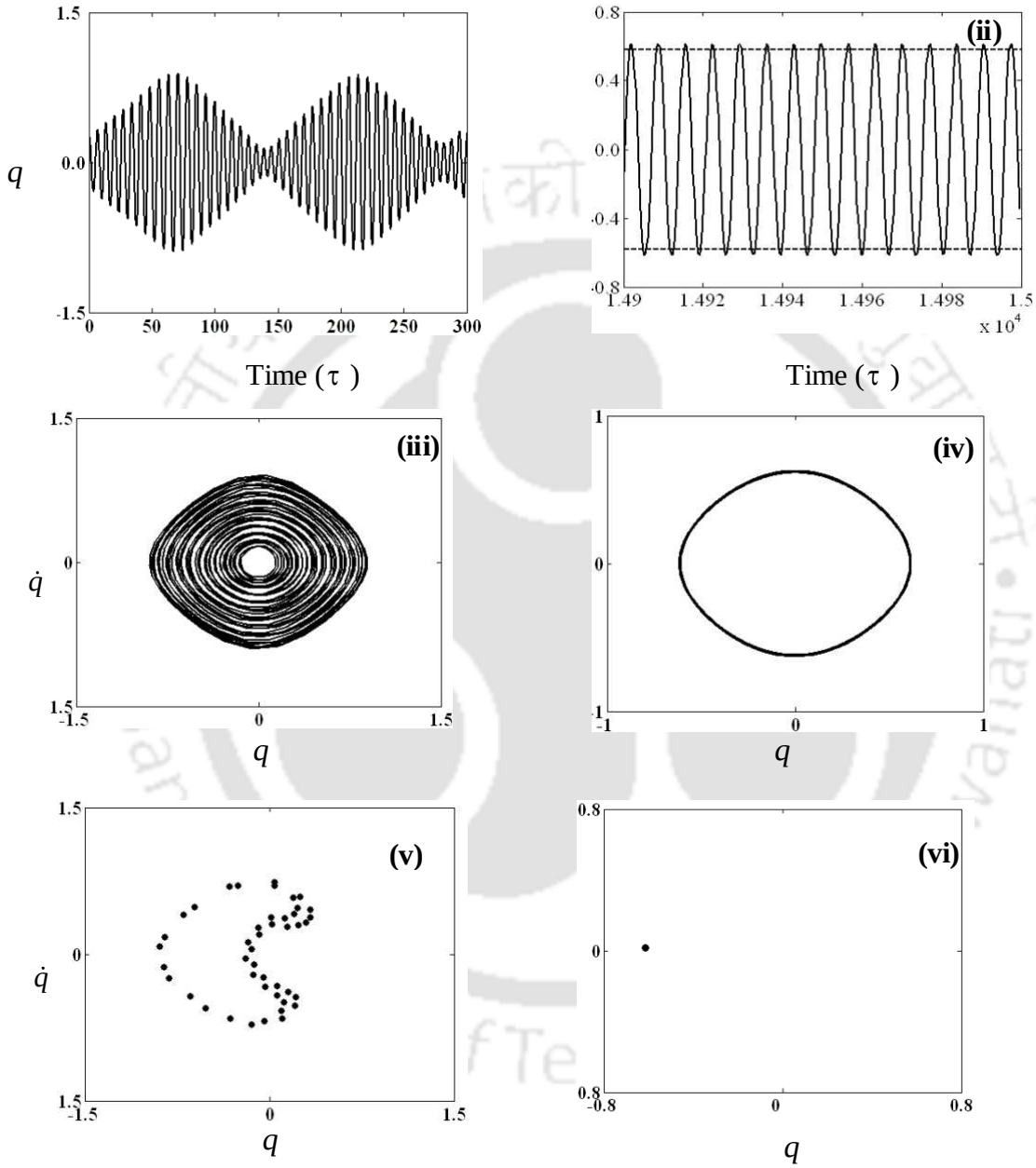

Fig. 3.3. Time response, phase portrait and Poincare's section at the critical point B (Fig. 3.2) where (i), (iii) and (v) represent for transient response and (ii), (iv) and (vi) represent the steady state response with initial point 0.326, 0.1. Dotted line in Fig.3.3.(ii) indicates the response obtained by using reduced equations

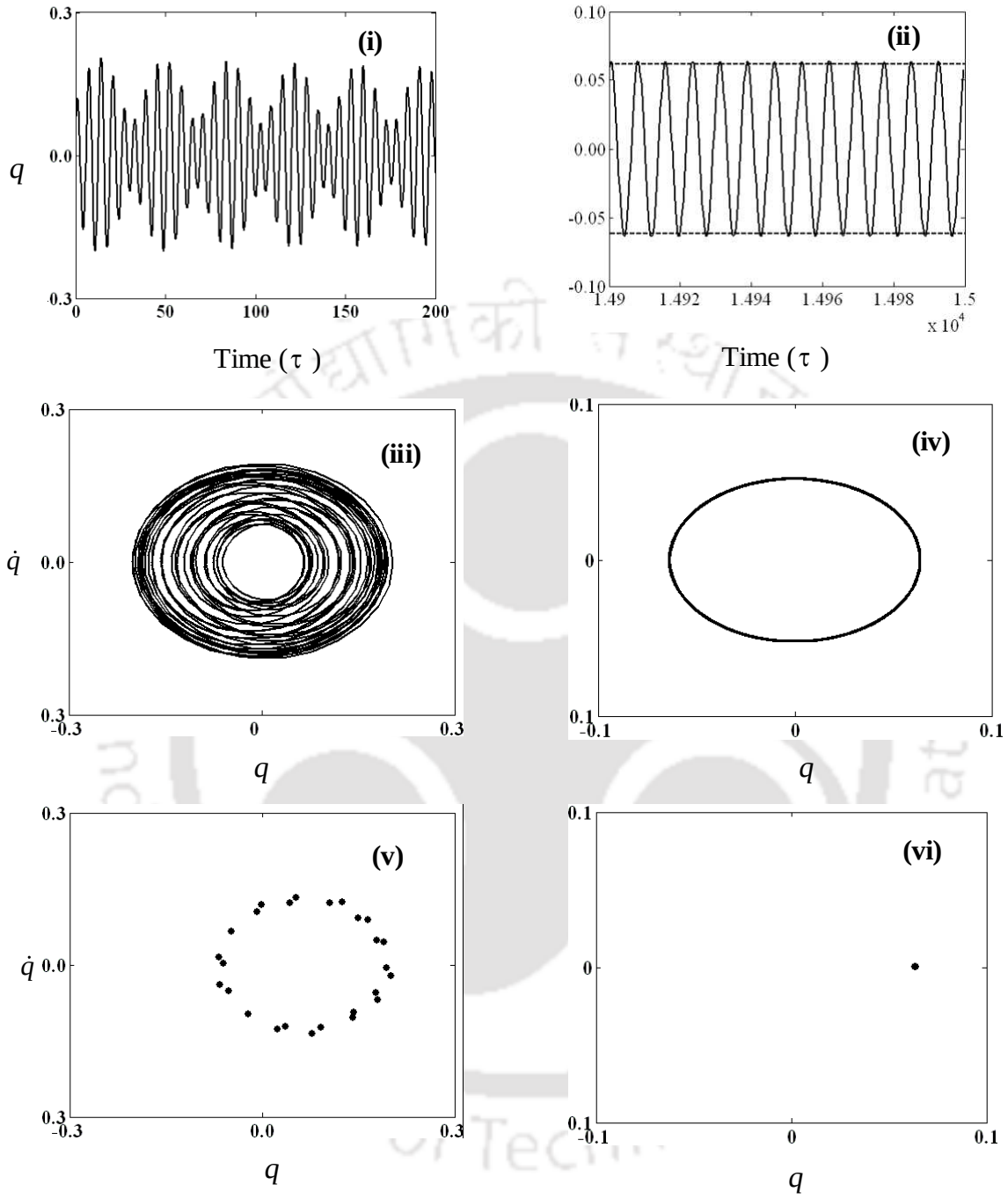

Fig. 3.4. Time response, phase portrait and Poincare's' section at the point A (Fig. 3.2) where (i), (iii) and (v) represent the transient response and (ii), (iv) and (vi) represent the steady state response with initial point 0.055, 0.1.

To compare the steady state response obtained by numerically integrating the temporal equation of motion with that found by using method of multiple scales, in Fig.3.3 (ii) the steady state response obtained by numerically solving the reduced equations (3.21) and (3.22) is superimposed which is shown by dotted line. From the Fig.3.3 (ii), it is observed that while the amplitude of the time response obtained by using reduced equation is 0.5680, the steady state response amplitude determined by numerically solving the temporal equation is found to be 0.6132. Hence, the error in the amplitude of the response is very marginal and is of 0.0794% only. Hence, the response obtained by using the method of multiple scales (Fig. 3.2 at the bifurcation point B) is in good agreement with that obtained by numerically solving the temporal equation of motion.

Figure 3.4 shows the time response, phase portrait, and Poincare's' section at the point $A^{/}$ (Fig. 3.2) which is obtained by solving the temporal equation of motion (equation (3.13)) using RK4 method. In this case, while the transient response (Fig. 3.4 (i)) of the system considering initial point as a = 0.1, γ = 0.1 displays a quasi-periodic response, the steady state response of the system is periodic (Fig. 3.4 (ii)). The phase portrait and Poincare's section for transient and steady state response are shown in Figs. 3.4(iii), (v) and (iv), (vi). Similar to previous case, here it is observed that the error in the amplitude of the response is negligible and is of 0.0523% only. Also, steady state response obtained by numerically solving the reduced equations is superimposed in Fig.3.4 (ii). Hence, one may note that the steady state response (i.e. Fig. 3.4(ii), (iv), and (vi)), obtained by numerically solving the temporal equation (3.13) of the system, is in good agreement with that obtained by using method of multiple scales as shown in Fig. 3.2 at point A.

Figure 3.5 shows the frequency response curve for two values of $\bar{Z}$ for the system with mass ratio $\bar{m}$ = 1.8787. Table 3.1 lists the variation of bifurcation points B and C for different values of amplitude ratio $\bar{Z}$. It is observed that with decrease in value of the amplitude ratio $\bar{Z}$ critical point B shifts toward $\bar{\omega}$ = 1. From Fig. 3.5 and Table 1, it may be noted that the upward jump will occur at the point of $\bar{\omega}$ equal to 0.709 and 0.850 for $\bar{Z}$

equal to 0.05 and 0.0125, respectively, and corresponding jump length equal to 0.6069 and 0.4579.

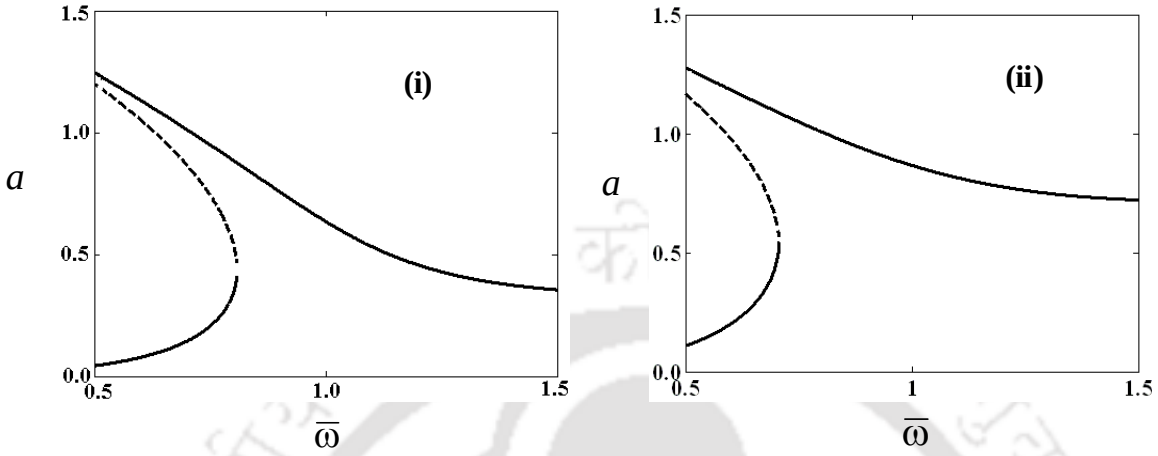

Fig. 3.5. Frequency response curve for simple resonance case for mass ratio $\bar{m}$ =1.8787; (i) $\bar{Z}$ =0.0125, (ii) $\bar{Z}$ =0.05,

Table. 3.1: Variation of the bifurcation point (B) and point C with excitation amplitude ($\bar{Z}$) for mass ratio $\bar{m}$ =1.8787.

Parameter	At critical point B		At point C		Jump
Amplitude of base excitation ($\bar{Z}$)	Response Frequency ($\bar{\omega}$)	Response Amplitude (a)	Response Frequency ($\bar{\omega}$)	Response Amplitude (a)	Length
0.2	0.518	0.6723	0.518	1.435	0.7627
0.1	0.618	0.6518	0.618	1.278	0.6262
0.05	0.709	0.5071	0.709	1.114	0.6069
0.02	0.811	0.4059	0.811	0.8968	0.4909
0.0125	0.850	0.3303	0.850	0.7882	0.4579
0.00372	0.921	0.2254	0.921	0.5680	0.3426

From Table 1, it is clear that the length BC (i.e. jump length) will decrease with decrease in the value of $\bar{Z}$. From Figs. 3.2–3.5, it is apparent that the variation in maximum response amplitude with $\bar{Z}$ is marginal. With decrease in $\bar{Z}$, the critical saddle-node bifurcation point B starts at a higher frequency and the response amplitude of the manipulator after bifurcation point is decreased with decrease in $\bar{Z}$. The stable curve CE and unstable curve BF come closer to each other with decrease in the value of base excitation $\bar{Z}$.

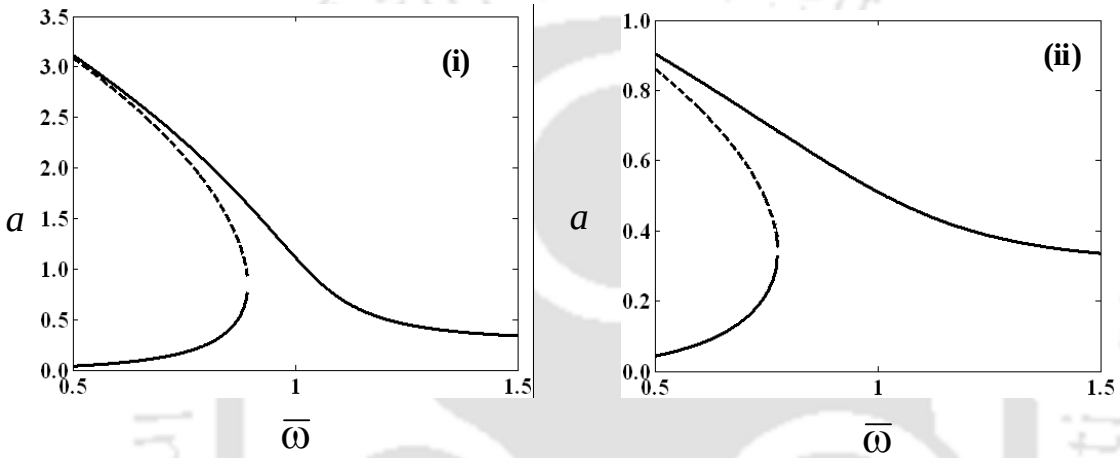

Fig. 3.6. Frequency response curve for simple resonance case for mass ratio $\bar{Z}$ =0.02; (i) $\bar{m}$ =0.5656, and (ii) $\bar{m}$ =4.6968

Table 3.2: Variation of response amplitude (a) with variation of mass ratio $\bar{m}$ for $\bar{Z}$ = 0.02.

Parameter	At critical point B		At point C		Jump length
Mass ratio ($\bar{m}$)	Frequency ($\bar{\omega}$)	Amplitude (a)	Frequency ($\bar{\omega}$)	Amplitude (a)	Variations
0.5636	0.890	0.7058	0.890	1.662	0.9562
0.9394	0.851	0.5368	0.851	1.215	0.6782
1.8787	0.811	0.4059	0.811	0.8968	0.4909
2.8181	0.79	0.3729	0.79	0.763	0.3901
3.7574	0.773	0.3132	0.773	0.6835	0.3703
4.6968	0.760	0.2836	0.760	0.6272	0.3436

Figure 3.6 shows the frequency response curves for the two different values of mass ratio $\bar{m}$ with $\bar{Z}$ equal to 0.02. Table 3.2 lists the variation of bifurcation points B and C for different values of $\bar{m}$. From Fig. 3.6 and Table 3.2, it is clearly observed that with increase in the value of the mass ratio, the critical point B moves towards left i.e. the system will fail at a lower frequency for a system with higher mass ratio. It is observed from Fig. 3.6 that the stable curve CE and unstable curve BF will merge for the value of low mass ratio. From Fig. 3.6 and Table 3.2, one may find that the maximum amplitude of the response and jump length decrease with increase in the values of mass ratio.

3.3.2.2 Subharmonic Resonance Condition ($\bar{\omega} \approx 3$)

Similar to the simple resonance case, in this case also the nonlinear frequency response curves for different values of $\bar{Z}$ and mass ratio $\bar{m}$ are studied. Unlike the simple resonance case, here the trivial response exists and it is found to be stable for a wide range of system parameters. It may be noted that subharmonic resonance case has not been studied in Cuvalci (2000). Fig. 3.7 shows the frequency response curves for $\bar{Z}$ equal to 0.2 and mass ratio $\bar{m}$ equal to 0.5656.

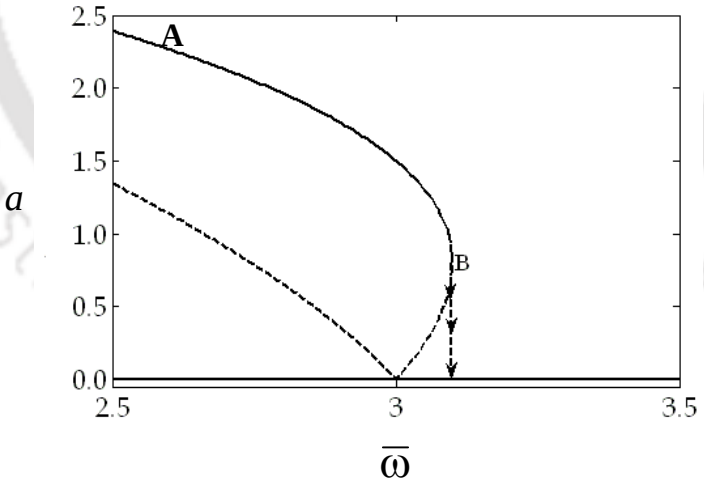

Fig. 3.7. Frequency response curve for sub harmonic resonance with mass ratio $\bar{m}$ = 0.5656 and $\bar{Z}$ = 0.2.

Similar to the previous case, here solid and dotted lines represent the stable and unstable response of the system, respectively. From Fig. 3.7, it is observed that for some initial conditions if the system response is at point A, with sweeping up the frequency at point B, the system experience a jump down phenomenon where the jump down occurs from the nontrivial solution to the stable trivial solution. Upto point B, which is a saddle-node bifurcation point, the system has a bi-stable region. After point B, the system has only a stable trivial solution.

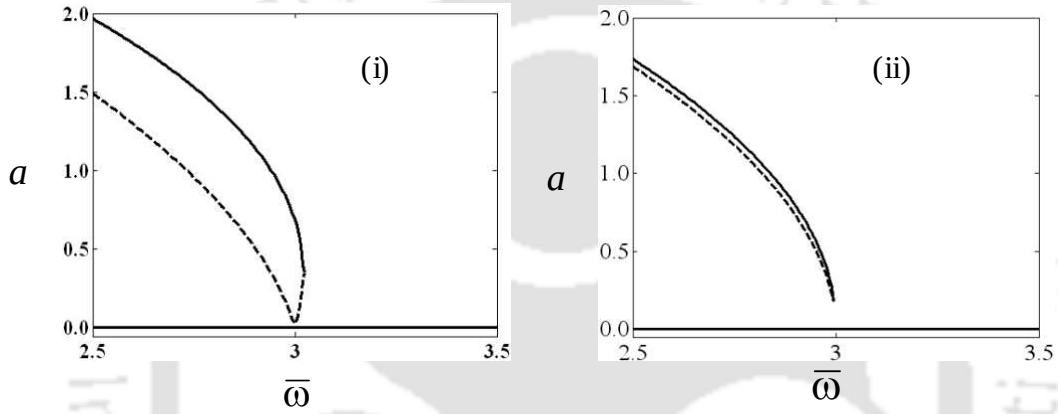

Fig. 3.8. Frequency response curve for subharmonic resonance for mass ratio $\bar{m}$ =0.5656; (i) $\bar{Z}$ =0.1, (ii) $\bar{Z}$ =0.01

Figure 3.8 shows the frequency response curves for two values of $\bar{Z}$ with mass ratio $\bar{m}$ equal to 0.5656. From Figs. 3.7 and 3.8, one may find that with decrease in $\bar{Z}$, the response amplitude of nontrivial state decreases. With decrease in $\bar{Z}$, the critical point which is a saddle-node bifurcation point shifts towards $\bar{\omega}$ = 3 and it changes from saddle-node bifurcation point to a cusp point. Also, it may be noted from Figs. 3.7 and 3.8 that with decrease in $\bar{Z}$, the stable and unstable curves come closer to each other.

Figure 3.9 shows the frequency response curves for two different values of mass ratio $\bar{m}$ with $\bar{Z}$ equal to 0.05. From this figure, it is observed that with decrease in $\bar{m}$, the amplitude of nontrivial response decreases. Similar to the effect of change in $\bar{Z}$, here also

with decrease in $\overline{m}$ the saddle-node bifurcation point shifts towards $\overline{\omega}$ =3 and it changes from saddle-node bifurcation point to a cusp point. But it may be noted that the change in mass ratio will change the value of all coefficients of the temporal equation (3.13), which will change the natural frequency of the system.

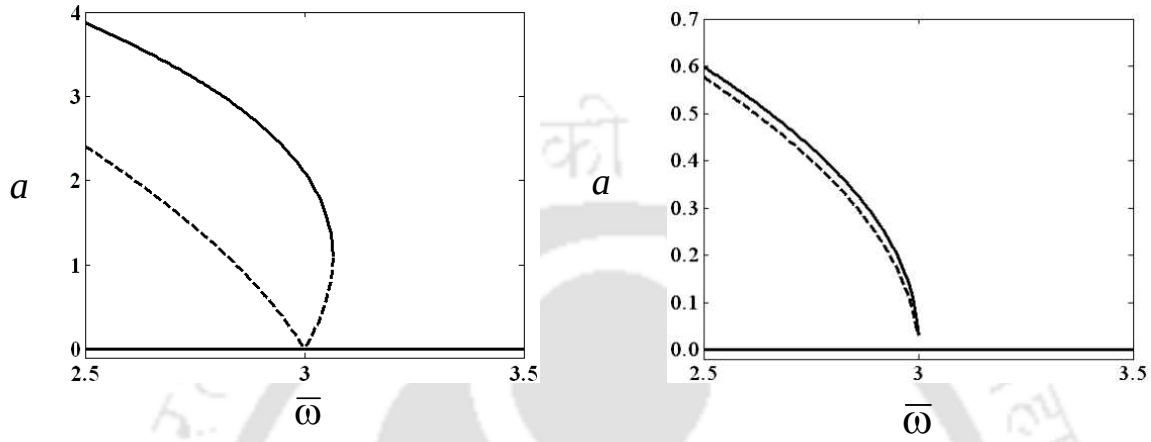

Fig. 3.9. Frequency response curve for sub harmonic resonance case with $\overline{Z}$ =0.05; (i) $\overline{m}$ = 0.3757, (ii) $\overline{m}$ = 2.8181.

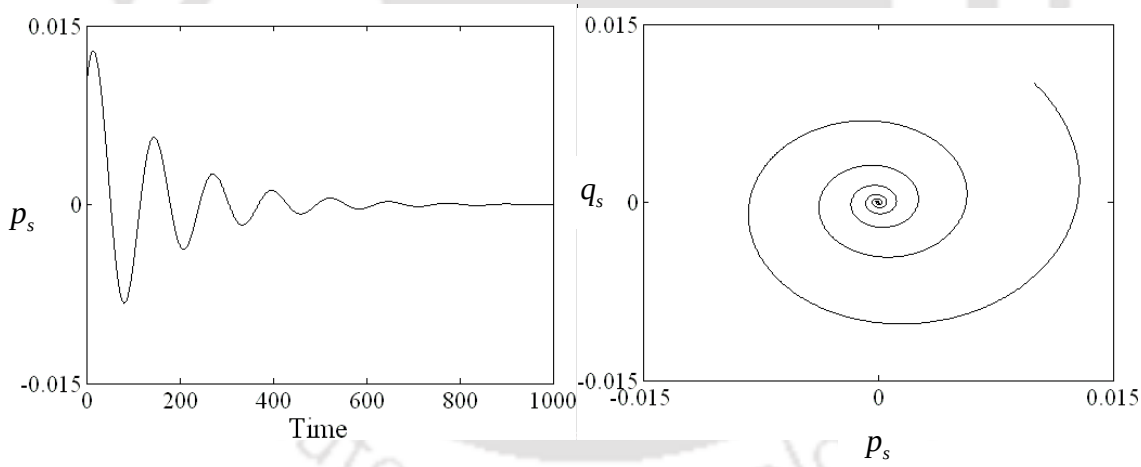

Fig. 3.10. (a) Time response for trivial fixed-point response and (b) Projection of the trajectories in plane $p_s - q_s$ with $\overline{Z}$ =0.2, and mass ratio $\overline{m}$ =0.5656.

3.4 Cartesian Manipulator with Harmonically Varying Axial Force

3.4.1 Analysis

Here, the method of normal forms is used to find the approximate solution of equation of motion (3.11). In this method, one may transform the second order temporal equation of motion into a set of first order equations to determine the uniform expansions of the solutions of equation (3.11). By putting ε equal to zero, the general solution of equation (3.11) can be given by

$$q = A\exp(i\tau) + \bar{A}\exp(-i\tau), \tag{3.37}$$

where, A is a complex number and $\bar{A}$ is the complex conjugate of A.

One may write the first time derivative of q as

$$\dot{q} = i\left(A\exp(i\tau) - \bar{A}\exp(-i\tau)\right). \tag{3.38}$$

By denoting $\xi = A\exp(i\tau)$ and $\bar{\xi} = \bar{A}\exp(-i\tau)$, equations (3.37) and (3.38), can be written as

$$q = \xi + \bar{\xi}, \quad \text{and} \quad \dot{q} = i\left(\xi - \bar{\xi}\right), \tag{3.39a, 3.39b}$$

where, ξ is a complex number and $\bar{\xi}$ is its complex conjugate.

Substituting $z = e^{i\bar{\omega}_1\tau}$, and $z_1 = e^{i\bar{\omega}_2\tau}$, and using equation (3.39) in equation (3.11), one may obtain the following equation:

$$\dot{\xi} = i\xi - \varepsilon\zeta\left(\xi - \bar{\xi}\right) + \frac{i}{2}\varepsilon\left[\alpha_1\left(\xi+\bar{\xi}\right)^3 + \alpha_2\left(\xi+\bar{\xi}\right)^2\left\{\left(\xi-\bar{\xi}\right) + 2i\dot{\xi}\right\} - \alpha_3\left(\xi-\bar{\xi}\right)^2\left(\xi+\bar{\xi}\right)\right]$$

$$+ \frac{i\,\bar{\omega}_1^2}{4}\varepsilon\left[\alpha_4\left(\xi+\bar{\xi}\right)^2\left(z+\bar{z}\right) + \alpha_5\left(z+\bar{z}\right)\right] + \frac{i}{4}\varepsilon\alpha_6\left(\xi+\bar{\xi}\right)\left(z_1+\bar{z}_1\right). \tag{3.40}$$

Now, introducing another variable η, ξ may be written as

$$\xi = \eta + \varepsilon\, h\left(\eta, \bar{\eta}, z, \bar{z}, z_1, \bar{z}_1\right) + O\left(\varepsilon^2\right), \text{and} \tag{3.41a}$$

$$\dot{\xi} = \dot{\eta} + \varepsilon\left(\frac{\partial h}{\partial \eta}\dot{\eta} + \frac{\partial h}{\partial \bar{\eta}}\dot{\bar{\eta}} + \frac{\partial h}{\partial z}\dot{z} + \frac{\partial h}{\partial \bar{z}}\dot{\bar{z}} + \frac{\partial h}{\partial z_1}\dot{z}_1 + \frac{\partial h}{\partial \bar{z}_1}\dot{\bar{z}}_1\right) + O\left(\varepsilon^2\right). \tag{3.41b}$$

Substituting equation (3.41) into the equation (3.40), yields

$$\dot{\eta} = i(\eta + \varepsilon h) - \varepsilon\zeta(\eta - \bar{\eta}) - \left(\frac{\partial h}{\partial \eta}\dot{\eta} + \frac{\partial h}{\partial \bar{\eta}}\dot{\bar{\eta}} + \frac{\partial h}{\partial z}\dot{z} + \frac{\partial h}{\partial \bar{z}}\dot{\bar{z}} + \frac{\partial h}{\partial z_1}\dot{z}_1 + \frac{\partial h}{\partial \bar{z}_1}\dot{\bar{z}}_1 \right)$$
$$+ \frac{i}{2}\varepsilon\left[\alpha_1(\eta+\bar{\eta})^3 + \alpha_2(\eta+\bar{\eta})^2\{(\eta-\bar{\eta}) + 2i\dot{\eta}\} - \alpha_3(\eta-\bar{\eta})^2(\eta+\bar{\eta})\right]$$
$$+ \frac{i\,\bar{\omega}_1^2}{4}\varepsilon\left[\alpha_4(\eta+\bar{\eta})^2(z+\bar{z}) + \alpha_5(z+\bar{z})\right] + \frac{i}{4}\varepsilon\alpha_6(\eta+\bar{\eta})(z_1+\bar{z}_1) + O(\varepsilon^2). \quad (3.42)$$

As the temporal equation of motion (3.11) contains cubic nonlinear terms, assuming h to be of third order in terms of η and $\bar{\eta}$, one may write the following equation:

$$h = \Delta_1\eta + \Delta_2\bar{\eta} + \Delta_3 z + \Delta_4\bar{z} + \Phi_1\eta z_1 + \Phi_2\bar{\eta}z_1 + \Phi_3\eta\bar{z}_1 + \Phi_4\bar{\eta}\bar{z}_1 + \Gamma_1\eta^2 z + \Gamma_2\eta\bar{\eta}z$$
$$+ \Gamma_3\bar{\eta}^2 z + \Gamma_4\eta^2\bar{z} + \Gamma_5\eta\bar{\eta}\bar{z} + \Gamma_6\bar{\eta}^2\bar{z} + \Lambda_1\eta^3 + \Lambda_2\eta^2\bar{\eta} + \Lambda_3\eta\bar{\eta}^2 + \Lambda_4\bar{\eta}^3. \quad (3.43)$$

From equation (3.42), the first order approximate solution may be written as

$$\dot{\eta} = i\eta, \text{ and } \dot{\bar{\eta}} = -i\bar{\eta}. \quad (3.44)$$

Substituting $\dot{z} = \bar{\omega}_1 e^{i\bar{\omega}_1\tau}$ and $\dot{z}_1 = \bar{\omega}_2 e^{i\bar{\omega}_2\tau}$, and using equations (3.44) and (3.43) into equation (3.42), one may get the following expression:

$$\dot{\eta} = i\eta - \varepsilon\zeta\eta + \varepsilon(\bar{\mu} + 2i\Delta_2)\bar{\eta} + i\varepsilon\left(\Delta_4 + \frac{1}{4}\alpha_5\bar{\omega}_1^2\right)\bar{z} + i\varepsilon\left(\Delta_3(1-\bar{\omega}) + \frac{1}{4}\alpha_5\bar{\omega}_1^2\right)z$$
$$+ i\varepsilon\left(\frac{1}{2}(\alpha_1 - \alpha_2 - \alpha_3) - 2\Lambda_1\right)\eta^3 + i\varepsilon\left(\frac{1}{2}(\alpha_1 - \alpha_2 - \alpha_3) + 4\Lambda_4\right)\bar{\eta}^3$$
$$+ i\varepsilon\left(\frac{3}{2}(\alpha_1 - \alpha_2 + \alpha_3) + 2\Lambda_3\right)\eta\bar{\eta}^2 + \frac{3}{2}i\varepsilon\left(\alpha_1 - \alpha_2 + \frac{\alpha_3}{3}\right)\eta^2\bar{\eta}$$
$$+ i\varepsilon\left(\frac{1}{4}\alpha_4\bar{\omega}_1^2 - \Gamma_1(1+\bar{\omega}_1)\right)\eta^2 z + i\varepsilon\left(\frac{1}{2}\alpha_4\bar{\omega}_1^2 + \Gamma_2(1-\bar{\omega}_1)\right)\eta\bar{\eta}z$$
$$+ i\varepsilon\left(\frac{1}{4}\alpha_4\bar{\omega}_1^2 + \Gamma_3(3-\bar{\omega}_1)\right)\bar{\eta}^2 z + i\varepsilon\left(\frac{1}{4}\alpha_4\bar{\omega}_1^2 - \Gamma_4(1-\bar{\omega}_1)\right)\eta^2\bar{z}$$
$$+ i\varepsilon\left(\frac{1}{2}\alpha_4\bar{\omega}_1^2 + \Gamma_5(1+\bar{\omega}_1)\right)\eta\bar{\eta}z + i\varepsilon\left(\frac{1}{4}\alpha_4\bar{\omega}_1^2 + \Gamma_6(3+\bar{\omega}_1)\right)\bar{\eta}^2 z$$
$$+ i\varepsilon\left(-\bar{\omega}_2\Phi_1 + \frac{1}{4}\alpha_6\right)\eta z_1 + i\varepsilon\left(\bar{\omega}_2\Phi_3 + \frac{1}{4}\alpha_6\right)\eta\bar{z}_1$$
$$+ i\varepsilon\left(\{2-\bar{\omega}_2\}\Phi_2 + \frac{1}{4}\alpha_6\right)\bar{\eta}z_1 + i\varepsilon\left(\{2+\bar{\omega}_2\}\Phi_4 + \frac{1}{4}\alpha_6\right)\bar{\eta}\bar{z}_1 + O(\varepsilon^2). \quad (3.45)$$

It may be noted that the above equation (3.45) does not depend on Δ_1 and Λ_2; hence both are arbitrary. It is observed that the terms containing $\eta^2\bar{\eta}, \eta\bar{\eta}z, \eta^2\bar{z}, z, \bar{\eta}z_1$ have small divisor or secular terms for simple ($\bar{\omega}_1 \approx 1$), subharmonic ($\bar{\omega}_1 \approx 3$), principal parametric ($\bar{\omega}_2 \approx 2$), and simultaneous ($\bar{\omega}_1 \approx 1$ and $\bar{\omega}_2 \approx 2$ or, $\bar{\omega}_1 \approx 3$ and $\bar{\omega}_2 \approx 2$) resonance conditions. One may choose $\Delta_2, \Delta_4, \Lambda_1, \Lambda_3, \Lambda_4,$ and Γ_1 to eliminate the nonresonance terms as follows.

$$\Delta_2 = -\frac{\zeta}{2i}, \quad \Delta_4 = -\frac{1}{4}\alpha_5\bar{\omega}_1^2, \quad \Lambda_1 = \frac{1}{4}(\alpha_1 - \alpha_2 - \alpha_3), \; \Lambda_3 = -\frac{3}{4}(\alpha_1 - \alpha_2 + \alpha_3)$$

$$\Lambda_4 = -\frac{1}{8}(\alpha_1 - \alpha_2 - \alpha_3), \quad \Gamma_1 = \frac{\frac{1}{4}\alpha_4\bar{\omega}_1^2}{(1+\bar{\omega}_1)}, \Gamma_5 = -2\Gamma_1, \Gamma_6 = -\frac{\frac{1}{4}\alpha_4\bar{\omega}_1^2}{(3+\bar{\omega}_1)},$$

$$\text{and } \Phi_4 = \frac{\frac{1}{4}\alpha_6}{(2+\bar{\omega}_1)}. \tag{3.46}$$

In the following subsections, the simple resonance case i.e. when the nondimensional frequency of base excitation $\bar{\omega}_1$ is nearly equal to 1, principal parametric resonance case i.e. when the nondimensional frequency of the axial load $\bar{\omega}_2$ is nearly equal to the 2, and simultaneous resonance case ($\bar{\omega}_1 \approx 1$ and $\bar{\omega}_2 \approx 2$) are studied. The higher order resonance conditions i.e., the subharmonic ($\bar{\omega}_1 \approx 3$) and the simultaneous resonance conditions $\bar{\omega}_1 \approx 3$ and $\bar{\omega}_2 \approx 2$ have not been studied in the present work.

3.4.1.1 Simple Resonance Case ($\bar{\omega}_1 \approx 1$ and $\bar{\omega}_2$ is away from 2)

For this simple resonance case, to express the nearness of $\bar{\omega}_1$ to 1, one may introduce the detuning parameter σ as

$$\bar{\omega}_1 = 1 + \varepsilon\sigma, \quad \text{and } \sigma = O(1). \tag{3.47}$$

Substituting equation (3.47) into equation (3.45) yields the following expression:

$$\dot{\eta} = i\eta - \varepsilon\zeta\eta + \frac{i\varepsilon}{2}\left(3\alpha_1 - 3\alpha_2 + \alpha_3\right)\eta^2\bar{\eta} + \frac{i\varepsilon\alpha_4}{2}\bar{\omega}_1{}^2\eta\bar{\eta}z + \frac{i\varepsilon\alpha_4}{4}\bar{\omega}_1{}^2\eta^2\bar{z} + \frac{i\varepsilon\alpha_5}{4}\bar{\omega}_1{}^2 z. \quad (3.48)$$

Taking $\eta = \frac{1}{2}a\exp(i\beta)$ in equation (3.48) and separating the real and imaginary parts, one may obtain the following equations:

$$\dot{a} = -\zeta a - \bar{\omega}_1{}^2\left(\frac{1}{8}\alpha_4 a^2 + \frac{1}{2}\alpha_5\right)\sin\gamma, \quad (3.49)$$

$$a\dot{\gamma} = a\sigma - \frac{3}{8}Ka^3 - \bar{\omega}_1{}^2\left(\frac{3}{8}\alpha_4 a^2 + \frac{1}{2}\alpha_5\right)\cos\gamma \ . \quad (3.50)$$

Here, $K = \left(\alpha_1 - \alpha_2 + \frac{\alpha_3}{3}\right)$, and $\gamma = \sigma\tau - \beta$. For steady state, $\dot{a} = 0$ and $\dot{\gamma} = 0$. From equations (3.49)-(3.50), one may observe that the trivial response (i.e., $a = 0$) does not exist in this case. One may find the nontrivial response of the system by numerically solving equations (3.49) and (3.50) simultaneously. To find the stability of the steady state responses, one may perturb equations (3.49) and (3.50) by substituting $a = a_o + a_1$ and $\gamma = \gamma_0 + \gamma_1$ where a_0, γ_0 are the equilibrium points, and then investigating the eigenvalues of the resulting Jacobian matrix (J). The Jacobian matrix (J) is given by

$$J = \begin{bmatrix} -\zeta + \dfrac{\frac{1}{2}\alpha_4 a_0^2\zeta}{\frac{1}{8}\alpha_2 a_0^2 + \frac{1}{2}\alpha_5} & -\dfrac{\left(\frac{1}{8}\alpha_4 a_0^2 + \frac{1}{2}\alpha_5\right)}{\frac{3}{8}\alpha_4 a_0^2 + \frac{1}{2}\alpha_5}\left(\sigma a_0 - \frac{3}{8}Ka_0^3\right) \\ -\frac{3}{4}Ka_0 + \dfrac{\sigma a_0 - \frac{3}{8}Ka_0^3}{a^2} - \frac{3}{4}\dfrac{\alpha_4\left(\sigma a_0 - \frac{3}{8}Ka_0^3\right)}{\frac{3}{8}\alpha_4 a_0^2 + \frac{1}{2}\alpha_5} & -\dfrac{\left(\frac{3}{8}\alpha_4 a_0^2 + \frac{1}{2}\alpha_5\right)\zeta}{\frac{1}{8}\alpha_4 a_0^2 + \frac{1}{2}\alpha_5} \end{bmatrix}. \quad (3.51)$$

3.4.1.2 Principal Parametric Resonance Case ($\bar{\omega}_2 \approx 2$ and $\bar{\omega}_1$ is away from 1)

In this case, one may use detuning parameter σ to express the nearness of $\bar{\omega}_2$ to 2, as

$$\bar{\omega}_2 = 2 + 2\varepsilon\sigma, \quad \text{and} \quad \sigma = O(1) \quad (3.52)$$

Substituting equation (3.52) into equation (3.45) yields the following expression:

$$\dot{\eta} = i\eta - \varepsilon\zeta\eta + + \frac{i\varepsilon}{2}\left(3\alpha_1 - 3\alpha_2 + \alpha_3\right)\eta^2\bar{\eta} + \frac{i\varepsilon\alpha_6}{2}\bar{\eta}z_1 \tag{3.53}$$

Similar to the previous case, here also putting $\eta = \frac{1}{2}a\exp(i\beta)$ in equation (3.53) and separating the real and imaginary terms, yields

$$\dot{a} = -\zeta a - \frac{\alpha_6}{4}a\sin 2\gamma, \tag{3.54}$$

$$\dot{\gamma} = 2\sigma - \frac{6}{8}\left(\alpha_1 - \alpha_2 + \frac{\alpha_3}{3}\right)a^2 - \frac{\alpha_6}{2}\cos 2\gamma. \tag{3.55}$$

Here, $\gamma = \sigma\tau - \beta$. One may note from equations (3.54)-(3.55) that the system possess both trivial and nontrivial responses. Hence, one may obtain both responses by solving equations (3.54)-(3.55) simultaneously. For steady state condition, $\dot{a} = 0$ and $\dot{\gamma} = 0$.

To obtain the stability of the steady state fixed-point response (a_0, γ_0), one may perturb the equilibrium point (a_0, γ_0) by substituting $a = a_0 + a_1$, and $\gamma = \gamma_0 + \gamma_1$, in equations (3.54) and (3.55) and finding the eigenvalues of the resulting Jacobian matrix (J). In this case the Jacobian matrix is found to be as follows.

$$J = \begin{bmatrix} -\zeta - \frac{\alpha_6}{4}\sin 2\gamma_0 & -\frac{\alpha_6}{2}a_0\cos 2\gamma_0 \\ -\frac{3}{2}\left(\alpha_1 - \alpha_2 + \frac{\alpha_3}{3}\right)a_0 & \frac{\alpha_6}{2}a_0\sin 2\gamma_0 \end{bmatrix}. \tag{3.56}$$

For this resonance condition, the system will be stable if and only if the real part of all the eigenvalues is negative.

3.4.1.3 Simultaneous Resonance Case ($\bar{\omega}_1 \approx 1$ and $\bar{\omega}_2 \approx 2$)

Following similar procedure as described in section 3.4.1.1 and 3.4.1.2, here one may use the detuning parameter σ_1, σ_2 and phase ϕ to express the nearness of $\bar{\omega}_1$ to 1 and $\bar{\omega}_2$ to 2 as given below.

$$\bar{\omega}_1 = 1 + \varepsilon\sigma_1, \quad \bar{\omega}_2 = 2 + 2\varepsilon\sigma_2, \text{ and } \bar{\omega}_2\tau = 2\bar{\omega}_1\tau + \phi, \quad \sigma_1, \sigma_2 = O(1). \tag{3.57}$$

Substituting equation (3.57) into equation (3.45), one may obtain the following equations

$$\dot{\eta} = i\eta - \varepsilon\zeta\eta + \frac{i\varepsilon}{2}\left(3\alpha_1 - 3\alpha_2 + \alpha_3\right)\eta^2\bar{\eta} + \frac{i\varepsilon\alpha_4}{2}\bar{\omega}_1{}^2\eta\bar{\eta}z + \frac{i\varepsilon\alpha_4}{4}\bar{\omega}_1{}^2\eta^2\bar{z} + \frac{i\varepsilon\alpha_5}{4}\bar{\omega}_1{}^2 z + \frac{i\varepsilon\alpha_6}{2}\bar{\eta}z_1. \quad (3.58)$$

Here also taking $\eta = \frac{1}{2}a\exp(i\beta)$ in equation (3.58) and separating the real and imaginary parts, yields the following reduced equations

$$\dot{a} = -\zeta a - \bar{\omega}_1^2\left(\frac{\alpha_4}{8}a^2 + \frac{1}{2}\alpha_5\right)\sin\gamma - \frac{1}{4}\alpha_6 a\sin(2\gamma+\phi), \quad (3.59)$$

$$a\dot{\gamma} = a\sigma_1 - \frac{3}{8}\left(\alpha_1 - \alpha_2 + \frac{\alpha_3}{3}\right)a^3 - \bar{\omega}_1^2\left(\frac{3\alpha_4}{8}a^2 + \frac{1}{2}\alpha_5\right)\cos\gamma - \frac{1}{4}\alpha_6 a\cos(2\gamma+\phi). \quad (3.60)$$

Here, $\gamma = \sigma\tau - \beta$. For steady state response (a_0, γ_0), $\dot{a}$ and $\dot{\gamma}$ equal to zero. One may obtain the response (a, γ) by numerically solving equations (3.59), and (3.60), simultaneously. It may be noted from the equations (3.59), and (3.60) that the system does not have any trivial response.

The stability of the steady state fixed-point response (a_0, γ_0) can be determined by superposing a perturbation (a_1, γ_1) on the singular points by substituting $a = a_0 + a_1$, and $\gamma = \gamma_0 + \gamma_1$, in equations (3.59), and (3.60) and finding the eigen-values of the resulting Jacobian matrix (J). The Jacobian matrix is given below.

$$J = \begin{bmatrix} -\zeta - \frac{1}{4}\bar{\omega}_1^2\alpha_4 a_0\sin\gamma_0 - \frac{1}{4}\alpha_6\sin(2\gamma_0+\phi) & -\bar{\omega}_1^2\left(\frac{1}{8}\alpha_4 a_0^2 + \frac{1}{2}\alpha_5\right)\cos\gamma_0 - \frac{1}{2}\alpha_6 a_0\cos(2\gamma_0+\phi) \\ -\frac{3}{4}\left(\alpha_1 - \alpha_2 + \frac{\alpha_3}{3}\right)a_0 - \frac{1}{4}\bar{\omega}_1^2\alpha_4\cos\gamma_0 + \bar{\omega}_1^2\frac{\left(\frac{1}{8}\alpha_4 a_0^2 + \frac{1}{2}\alpha_5\right)\cos\gamma_0}{a_0^2} & \bar{\omega}_1^2\frac{\left(\frac{3}{8}\alpha_4 a_0^2 + \frac{1}{2}\alpha_5\right)\sin\gamma_0}{a_0} + \frac{1}{2}\alpha_6\sin(2\gamma_0+\phi) \end{bmatrix}. \quad (3.61)$$

Thus for this condition, the system is stable if the real part of all the eigen-values of the Jacobian matrix (J) are negative.

3.4.2 Numerical Results and Discussions

Similar to the previous system discussed in 3.4.1, here also in all simulations, a metallic beam is considered with length L = 0.336 m, cross-section area A = 40.464×10^{-6} m^2, moment of inertia I = 8.669867×10^{-12} m^4, Young's modulus E = 1.5848×10^{11} N/m^2, damping constant c_d c = 0.11 N-s/m, and density of the beam material ρ = 7830 kg/m^3. In this case, the scaling parameter ($\bar{r}$) is taken as 0.1, and the book-keeping parameter (ε) is taken as 0.1.The response of the Cartesian manipulator with harmonically varying axial force is obtained for various system parameters such as amplitude of the harmonic base motion (Z), amplitudes of static (P_0) and dynamic (P_1) axial force, and payload mass M. In section 3.4.2.1, the simple resonance condition is discussed. The principal parametric resonance and simultaneous resonance conditions are studied in sections 3.4.2.2 and 3.4.2.3, respectively.

3.4.2.1 Simple Resonance Case ($\bar{\omega}_1 \approx 1$ and $\bar{\omega}_2$ is away from 2)

In this case, the roller-supported end of the manipulator is excited with a frequency nearly equal to the natural frequency of the system and the frequency of external axial loading is away from the first principal parametric zone. Without considering the harmonically varying force of the system, the frequency response curves for the nondimensional amplitude of base excitation ($\bar{Z}$) equal to 0.00372 and mass ratio ($\bar{m}$) equal to 2.0 is shown in Fig. 3.11. In this case, the system does not have any trivial solution. Hence, the manipulator will always oscillate with amplitude equal to the nontrivial response as shown in Fig. 3.11. One may observe from this figure that the system experience both jump up and jump down phenomenon. It may also be noted that with increase in $\bar{\omega}_1$ (i.e. from point A, Fig. 3.11) the system encounters a critical point B, which is a saddle-node bifurcation point. At this point, with further increase in nondimensional frequency $\bar{\omega}_1$, system will

undergo a jump up phenomenon. Similarly, a jump down phenomenon will occur at the point D with slight increase in non-dimensional frequency $\bar{\omega}_1$. The system has a bi-stable region between the frequency range D - B′ and in this region the initial condition will play a crucial role to find the system response which is illustrated by finding the basin of attraction as shown in Fig. 3.12. Though there are several techniques like cell-to-cell mapping, point-to-point mapping to plot the basin of attraction, here a procedure similar to that of point-to-point mapping has been used. Taking several initial points the trajectories obtained by solving the reduced equations are plotted to obtain the basin of attraction. In this case, a □ γ plane is divided into 40 (8×5) grids. The central points of these grids have been taken as the initial conditions to plot the basin of attraction.

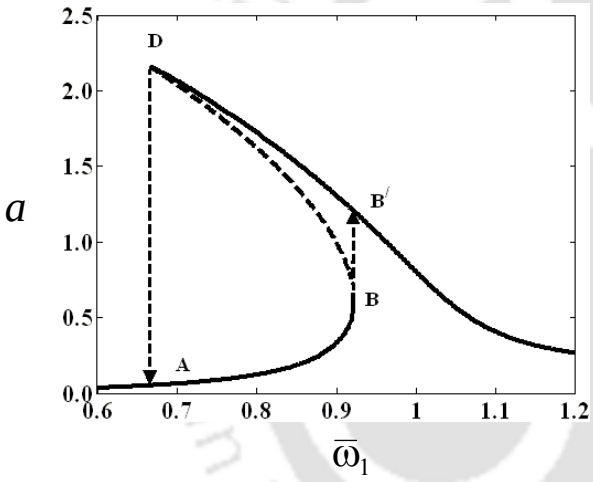

Fig. 3.11. Frequency response curve of a manipulator ($P_o = 0$)for $\bar{m}$ =2.0, $\bar{Z}$ =0.00372.

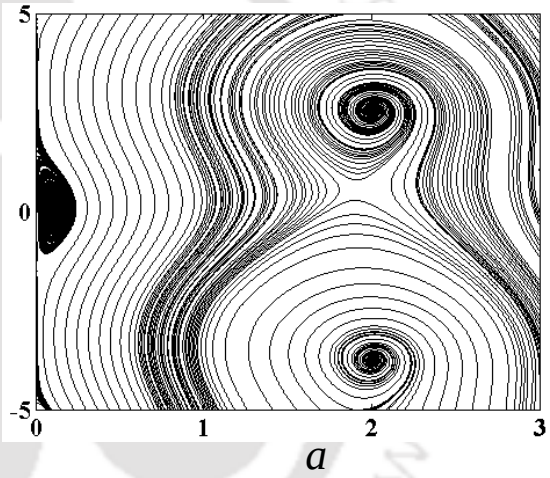

Fig. 3.12. Basins of attraction for $\bar{\omega}_1 = 0.80$ as key in Fig. 3.11.

It may be noted that in this case though the amplitude of harmonic force applied at tip of the manipulator (P_1) is not equal to zero, the response amplitude (a × scaling factor) and the saddle-node bifurcation point at B are observed to be same as that of a system without axial force as shown in Fig. 3.2. This result is in good agreement with the experimental finding of Cuvalci (2000) when the pendulum is in locked position.

Now considering the axial force, Fig. 3.13 displays the frequency response curves for two different values of the amplitude of the static load $\bar{P}_0$. It may be noted from Fig. 3.11 and Fig. 3.13 that with increase in $\bar{P}_0$, the maximum response amplitude increases. From these figures, it may be observed that for $\bar{P}_0$ equal to 0.0, 0.167, and 0.333, the bifurcation point B occurs at $\bar{\omega}_1$ equal to 0.922, 0.927 and 0.933 respectively. Hence, one may note that with increase in $\bar{P}_0$, the change in the critical value of $\bar{\omega}_1$ at which the bifurcation occurs (i.e., point B) is marginal. It may be noted that the natural frequency of the system changes with change in amplitude of static loading. So, though the change in the non-dimensional frequency is marginal, in terms of actual frequency it will be different. It is also observed that with increase in $\bar{P}_0$, both jump up and jump down length increases.

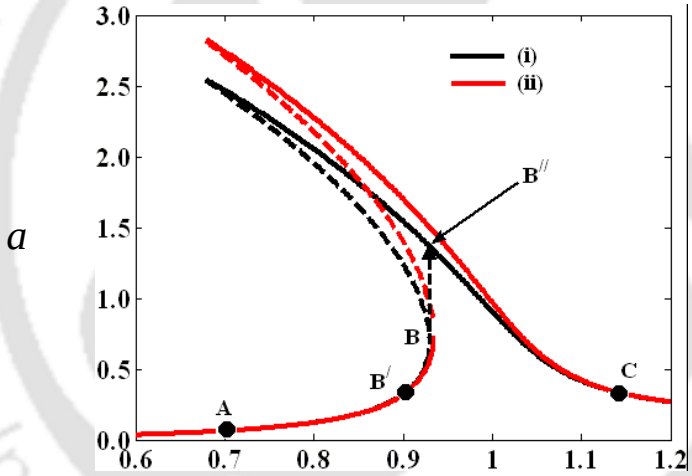

Fig. 3.13. Frequency response curve for $\frac{\bar{\omega}_1}{\bar{m}}$=2.0, $\bar{Z}$ =0.00372; (i) $\bar{P}_0 = 0.167$ and (ii) $\bar{P}_0 = 0.333$.

Figures 3.14 and 3.15 show the time response and Poincare's sections corresponding to the response at points B′, B, A, and C marked in Fig. 3.13 (i). These time responses are obtained by numerically solving the temporal equation of motion (3.11). From Fig. 3.14, which represents the time response and Poincare's section for the point B′ (i.e. $a = 0.33, \bar{\omega}_1 = 0.90$)' one may observe that with initial conditions $q = 0.33$, $\dot{q} = 0.01$,

the transient response of the system gives a beating type of phenomenon while the steady state response is periodic with amplitude of 0.345. From the steady state response, one may note that the result obtained by numerically solving the temporal equation of motion (3.11) is found to be in good agreement with that determined by using the method of normal forms (Fig. 3.14(i) at point B′).

From Fig. 3.15(i, iv), the steady state response is observed to be periodic with amplitude equal to 1.348, which is same as that shown in Fig. 3.13(i) (point B'', $a = 1.356, \bar{\omega}_1 = 0.925$). Similarly, for points A, and C in Fig. 3.13(i) the time response and Poincare's sections are also obtained by solving the temporal equation of motion (3.11). It may be noted from these figures that for points A ($a = 0.062, \bar{\omega}_1 = 0.7$, Fig. 3.13(i)) and C ($a = 0.41, \bar{\omega}_1 = 1.1$, Fig. 3.13(i)) the amplitude of steady state responses are found to be same as shown in Fig. 3.15(ii, v) and Fig. 3.15 (iii, vi).

Figure 3.16 shows the frequency response curves for two different values of $\bar{Z}$ with mass ratio $\bar{m}$ and amplitude of static load $\bar{P}_0$ equal to 2 and 0.167, respectively. With increase in $\bar{Z}$, the response amplitude increases. From the Fig. 3.13(i) and Fig. 3.16, one may observe that the saddle-node bifurcation of the system for $\bar{Z}$ equal to 0.00372, 0.00744 and 0.0298, occurs at the nondimensional frequency $\bar{\omega}_1$ equal to 0.927, 0.892 and 0.774, respectively. It may be noted that with increase in $\bar{Z}$, both jump up and jump down phenomenon occur at a lower value of $\bar{\omega}_1$ and the jump up length and jump down length will increase.

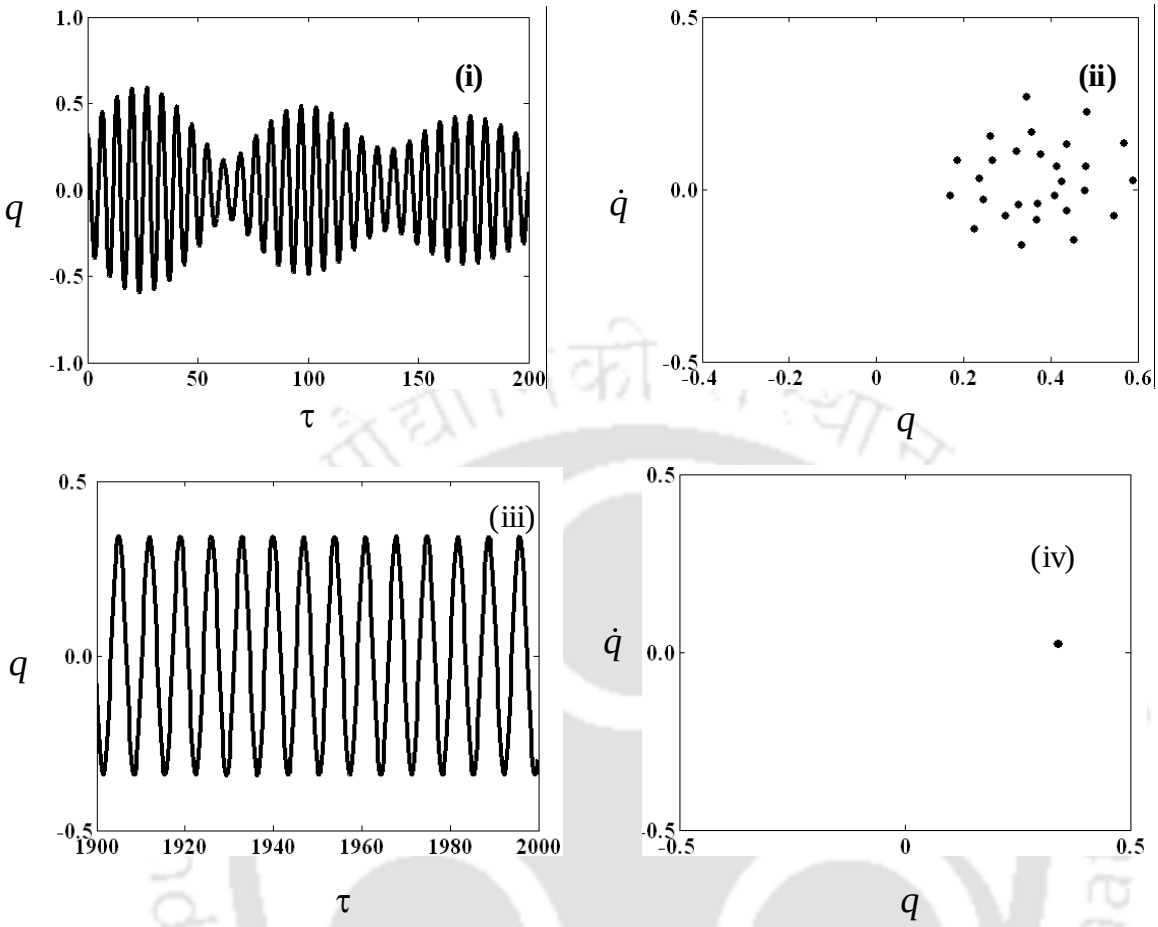

Fig. 3.14. Time response and Poincare's section at the point B' (Fig.3 (i)) where (i), (ii) represents transient and (iii), (iv) represents steady state response of the system with initial condition $q = 0.33, \dot{q} = 0.01$.

Figure 3.17 describes the effect of payload ($\bar{m}$) on the frequency response for given value of $\bar{Z}$ and $\bar{P}_0$. From Fig 3.13(i) and Fig. 3.17, one may find that with increase in $\bar{m}$, the response amplitude, the jump up and jump down lengths increases. It may also be noted that with decrease in $\bar{m}$, the critical point B starts at a lower value of nondimensional frequency $\bar{\omega}_1$.

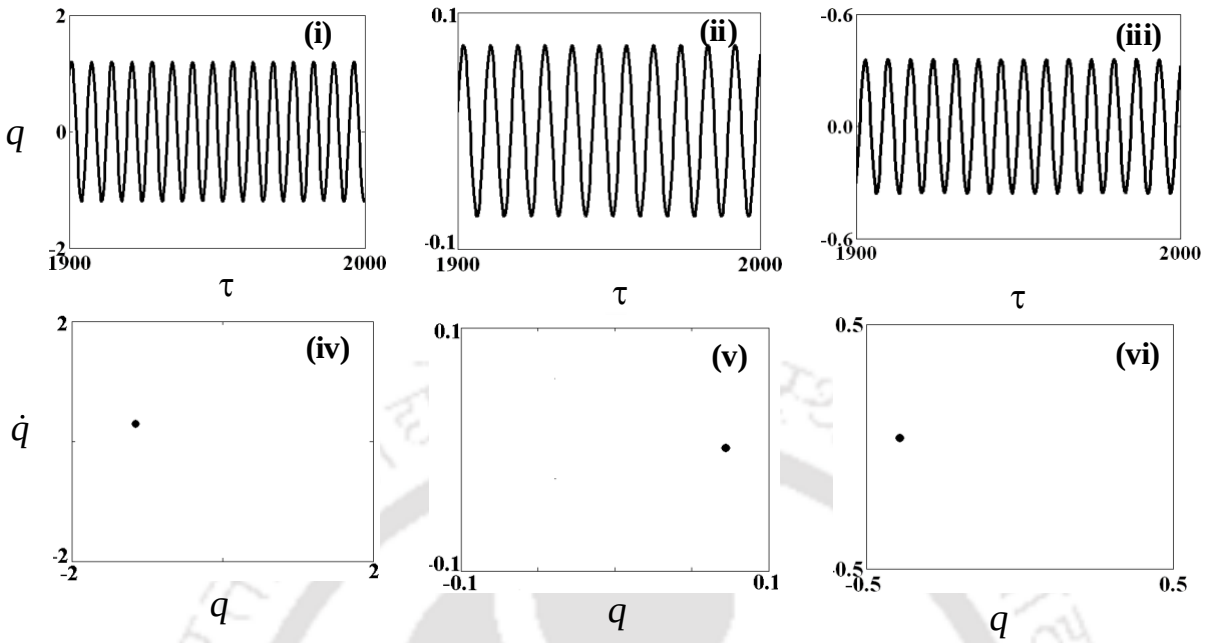

Fig. 3.15. Time responses and Poincare's sections with three different initial conditions (i, iv) B, (ii, v) A, and (iii, vi) C as key in Fig. 3.13 (i)

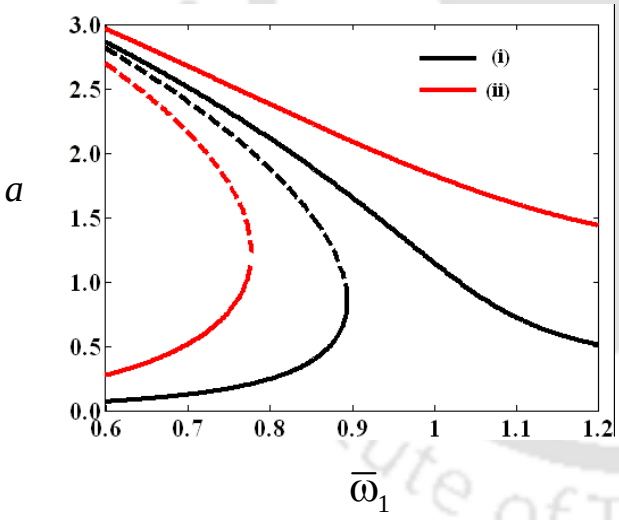

Fig. 3.16. Frequency response curve for $\bar{m}$ =2.0 and $\bar{P}_0 = 0.167$; (i) $\bar{Z}$ =0.00744 and (ii) $\bar{Z}$ =0.0298.

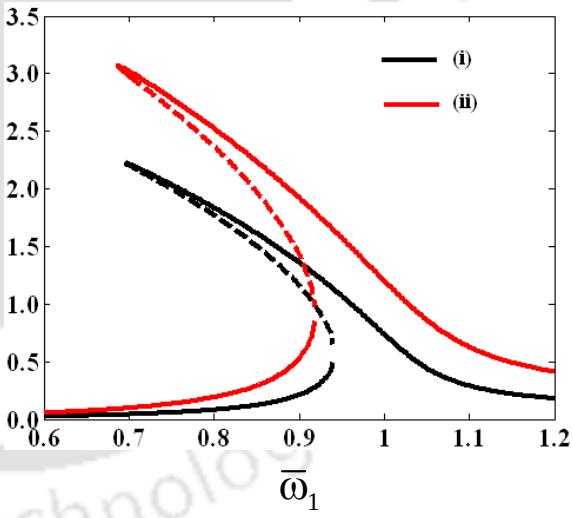

Fig. 3.17: Frequency response curve for $\bar{Z}$ =0.00372 and $\bar{P}_0 = 0.167$; (i) $\bar{m}$ =1.0 and (ii) $\bar{m}$ = 4.0.

3.4.2.2 Principal Parametric Resonance ($\bar{\omega}_2 \approx 2$ and $\bar{\omega}_1$ is away from 1)

In this case, the endeffector of the manipulator is subjected to a pulsating axial force with a frequency nearly equal to twice the natural frequency of the system and the frequency of excitation at the roller support is away from the simple resonance zone (i.e., $\bar{\omega}_1$ is away from 1). Figure 3.18 shows the frequency response curve for four different values of the amplitude of dynamic force $\bar{P}_1$ with $\bar{P}_0$ equal to zero.

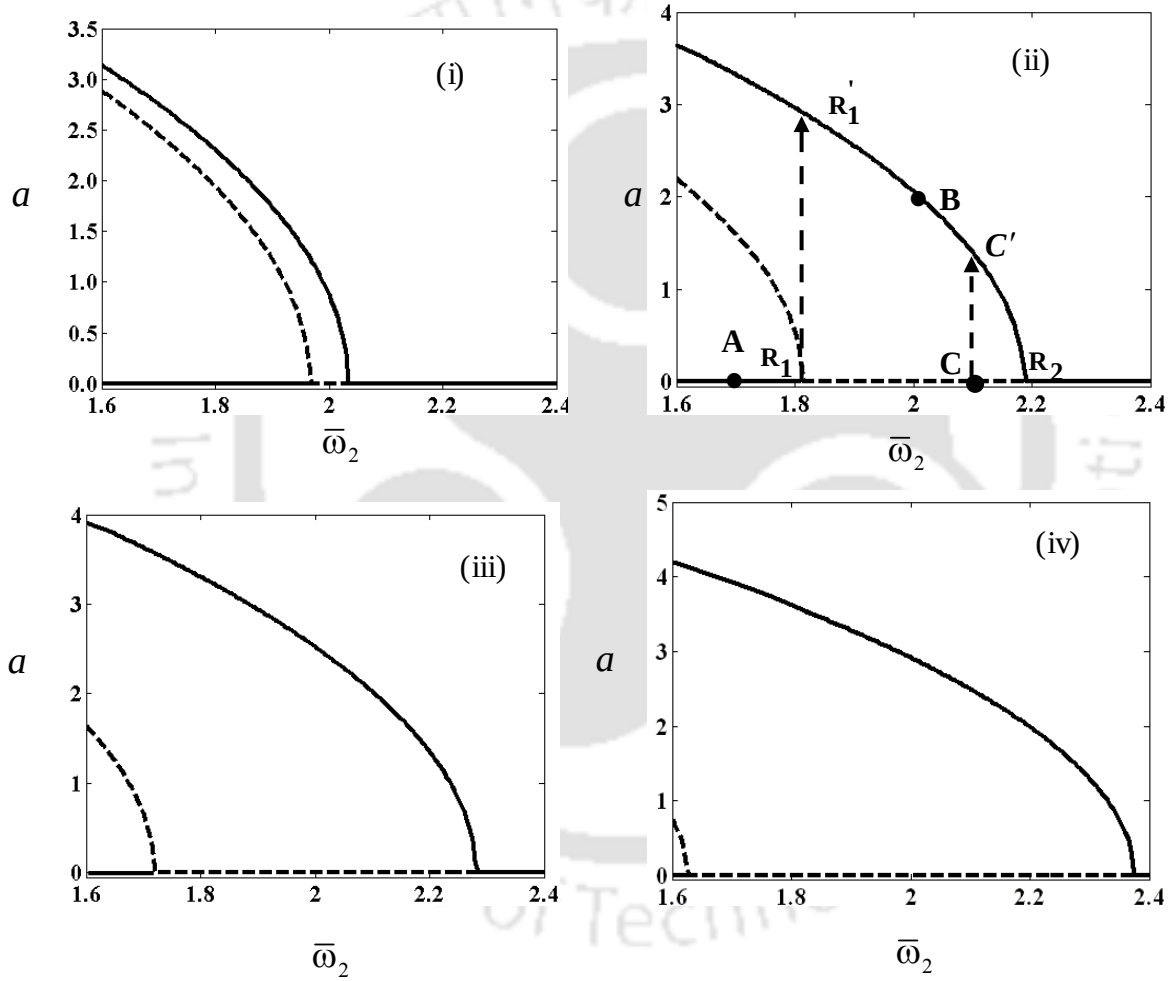

Fig. 3.18. Frequency response curve for $\bar{m}$ =2.0 and $\bar{P}_0 = 0.0$; (i) $\bar{P}_1 = 0.033$ (ii) $\bar{P}_1 = 0.167$ (iii) $\bar{P}_1 = 0.25$ (iv) $\bar{P}_1 = 0.333$.

Unlike simple resonance case, here the system has both trivial and nontrivial responses. The trivial state has sub-critical and super-critical pitchfork bifurcation points at point R_1

and R_2, respectively. These points are marked in Fig. 3.18(ii)). At R_1, the system will experience a jump up phenomenon. The trivial state is unstable between frequency range marked by points R_1 and R_2. From Fig. 3.18 one may observe that with increase in the amplitude of the dynamic loading $\bar{P}_1$ response amplitude of the system increases and the range of unstable trivial state between sub and super critical pitchfork bifurcation points R_1R_2 increases.

Like the previous case, here also one may compare the response obtained by using the method of normal forms with those found by numerically solving the temporal equation (3.11). Figure 3.19(i, iv) show the time response and phase portrait for points A (i.e. $a = 0.0, \bar{\omega}_2 = 1.7$ in Fig. 3.18(ii)) which clearly shows that the steady state response is stable trivial state which is same as that shown in Fig. 3.18(ii). Figure 3.19 (ii, v) shows the steady state response for the point B ($a = 2.062, \bar{\omega}_2 = 2.0$ in Fig. 3.18 (ii)) with initial point q =2.062, $\dot{q} = 0.001$.

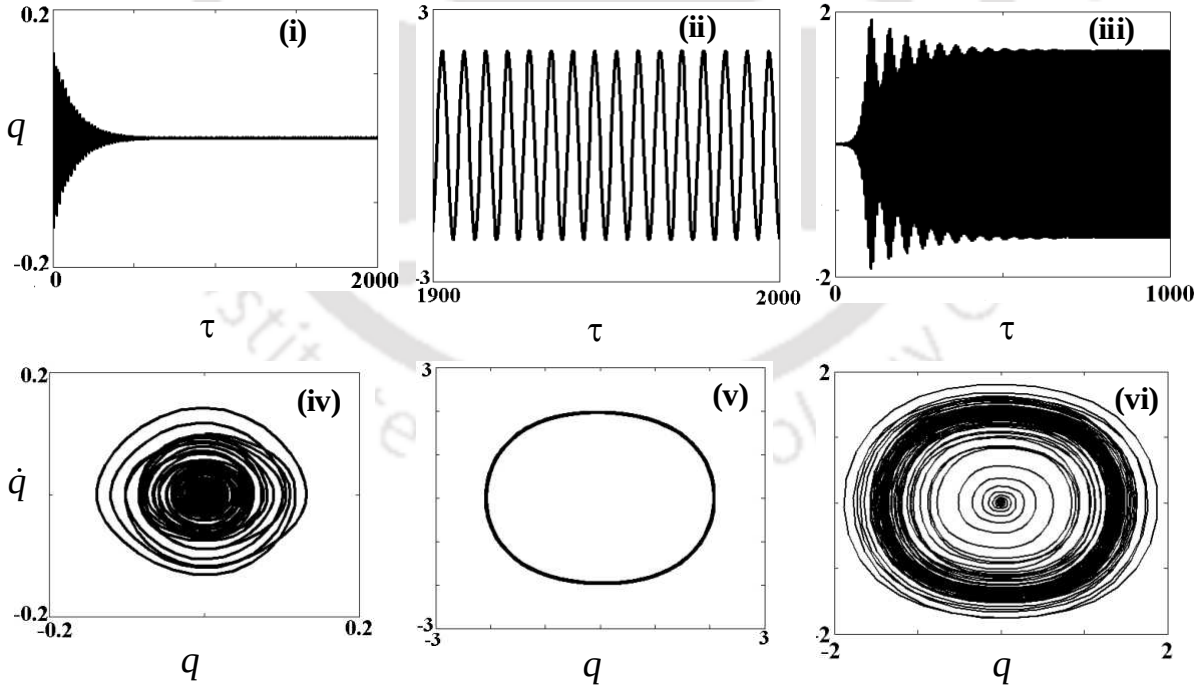

Fig. 3.19. Time responses and phase portraits with three different initial conditions (i, iv) A, (ii, v) B, and (iii, vi) C as key in Fig.3.18 (ii)

It is observed that the amplitude of steady state response obtained by solving the temporal equation (3.11) is same as the response shown in Fig. 3.18 (ii, point B) obtained by using method of normal forms. It is found from Fig. 3.19(iii, vi) that the trajectory, which is initiated from the unstable fixed-point response i.e., point C ($a = 0.0,\ \bar{\omega}_2 = 2.1$ in Fig. 3.18 (ii)), moves towards the stable fixed point response i.e. point C' ($a = 1.41, \bar{\omega}_2 = 2.1$). Hence, these response obtained by solving the temporal equation of motion are in good agreement with those obtained by using the method of normal forms.

Figure 3.20 shows the frequency response curves for two different values of the amplitude of static load $\bar{P}_0$. It is observed that with increase in $\bar{P}_0$, the maximum response amplitude increases and the unstable trivial range between the sub-critical pitchfork (R_1) and super-critical pitchfork (R_2) bifurcation point (R_1R_2) decreases. Here, with increase in $\bar{P}_0$ the jump up phenomenon occurs at the sub-critical pitchfork bifurcation point (R_1) which starts at a higher value of nondimensional frequency $\bar{\omega}_2$.

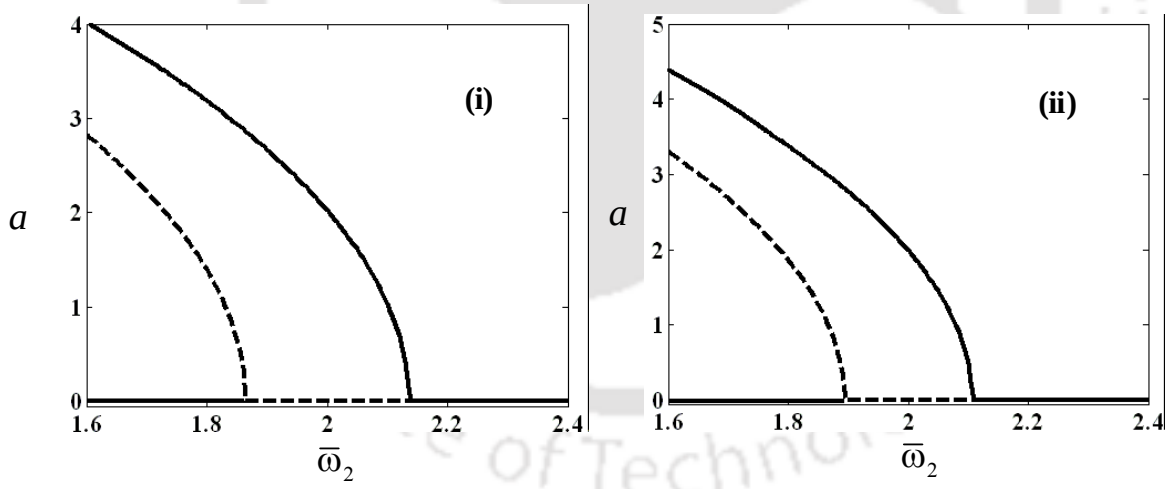

Fig. 3.20. Frequency response curve for $\bar{m}$ =2.0 and $\bar{P}_1 = 0.167$; (i) $\bar{P}_0 = 0.167$ (ii) $\bar{P}_0 = 0.334$.

The frequency response curves for two different values of mass ratio $\bar{m}$ are shown in Fig.3.21. One may note from Fig 3.18 (ii) and Fig. 3.21 that with increase in $\bar{m}$, the response amplitude increases. It may also be observed that with increase in $\bar{m}$, the unstable

trivial range R_1R_2 increases and sub-critical pitchfork bifurcation point occurs at a lower frequency $\overline{\omega}_2$.

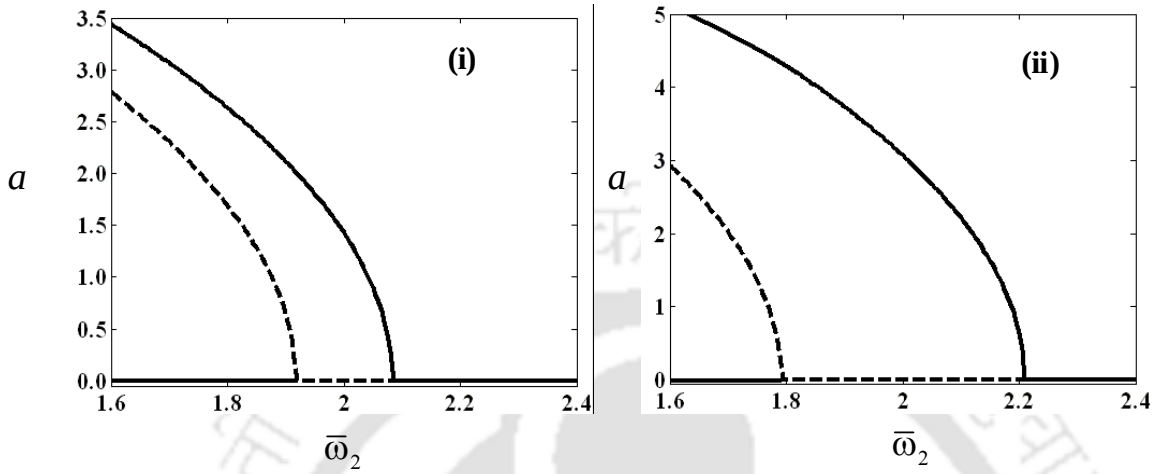

Fig. 3.21. Frequency response curve for $\overline{P}_0 = 0.167$ and $\overline{P}_1 = 0.167$ (i) $\overline{m}$ =1.0 (ii) $\overline{m}$ = 4.0.

3.4.2.3 Simultaneous Resonance Condition ($\overline{\omega}_1 \approx 1$ and $\overline{\omega}_1 \approx 2$)

Here, the roller-supported end of the manipulator is subjected to a harmonic motion with a frequency nearly equal to the first natural frequency of the system and the right end is subjected to an axial force with a frequency nearly equal to twice the natural frequency of the system. One may note from equation (3.59-3.60) that similar to simple resonance case; here also, only nontrivial response exists for the system. In contrast to the simple resonance case, here one more region appears (region S_2 of Fig. 3.22) in the frequency response curve. Instead of bi-stable region as observed in simple resonance case, here one may find tri-stable regions with two saddle-node bifurcation points (C_1, C_2). Figure 3.22 shows the influence of phase angle (ϕ) on the frequency responses for $\overline{m} = 2.0$, $\overline{P}_0 = 0.0$, $\overline{P}_1 = 0.167$ and $\overline{Z} = 0.0298$ for four different values of ϕ (viz., $\phi = 0$, $\pi/6, \pi/2$, and π). It is observed from Fig. 3.22(i) that for this simultaneous resonance case one additional region marked by S_2 in the frequency response curve arises in addition to the region S_1 observed in the case of simple resonance case. With increase in ϕ upto $\pi/2$, this region S_2 gets reduced as the pulsating axial force factor $\alpha_6 \cos(\phi)$ reduces with increase in ϕ upto

$\pi/2$ (Fig. 3.22(iii)). With further increase in ϕ, as the influence of the pulsating force component increases, region S_2 again increases as shown in Fig. 3.22(iv). The region S_1, in the frequency response curves gets reduced with increase in ϕ. It may be noted that, in this frequency response curves only $a \sim \bar{\omega}_1$ is plotted as $\bar{\omega}_2$ can be written in terms of $\bar{\omega}_1$ and ϕ as given in equation (3.59-3.60).

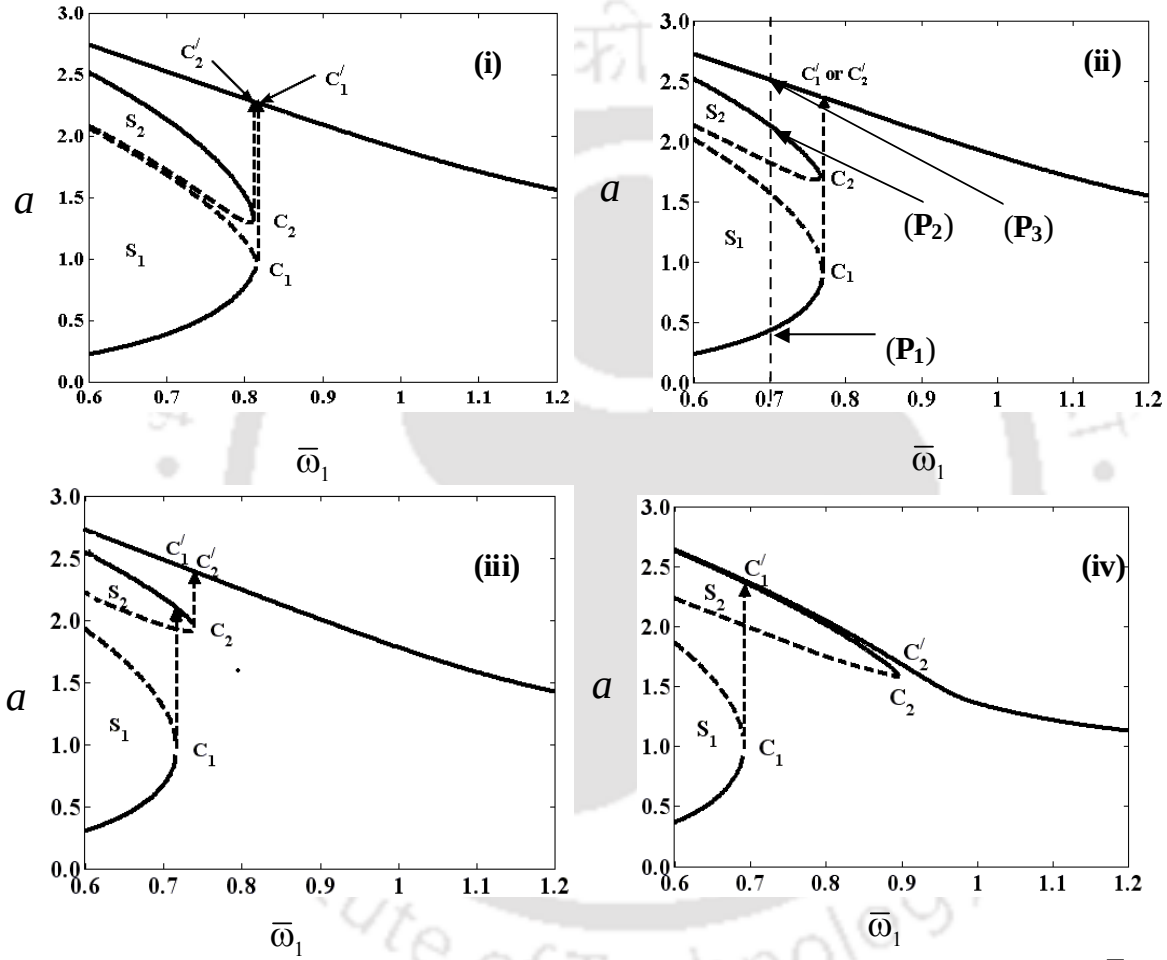

Fig. 3.22. Influence of phase angle (ϕ) on the frequency responses for $\bar{m} = 2.0$, $\bar{P}_0 = 0.0$, $\bar{P}_1 = 0.167$, $\bar{Z} = 0.0298$; (i) $\phi = 0$, (ii) $\phi = \frac{\pi}{6}$, (iii) $\phi = \frac{\pi}{2}$ and (iv) $\phi = \pi$.

Here, one may observe three distinct cases related to saddle-node bifurcations points C_1 and C_2. In the first case, when both the excitations take place simultaneously ($\phi \approx 0$), C_1 follows C_2 as shown in Fig. 3.22(i). With increase in frequency beyond C_1, the system will experience a jump up phenomenon and will jump to the upper most stable nontrivial

state C_1'. In the second case, when C_1 is just below C_2, similar to the first case, the system will jump to the upper most stable nontrivial state (point C_1'). When the excitation frequency at the tip mass is lagged by more than $\pi/6$, bifurcation point C_1 precedes bifurcation point C_2 and hence, if the excitation frequency exceeds the critical point C_1 in the third case, the response may jump to stable nontrivial state in region S_2. With further increase in frequency beyond critical point C_2, the system undergoes a second catastrophic failure due to the sudden jump from C_2 to C_2'. When these two excitations are nearly in opposite phase ($\phi \approx \pi$), upper most stable nontrivial branch and the stable branch in region S_2 gets merged and the system has a bistable region in the lower frequency range. In the above explanation, it is assumed that the system is in the lower region S_1 at the starting of the manipulator. But it may be noted that as three stable nontrivial solutions exist in the lower frequency range, the system will have a particular response depending on the initial condition.

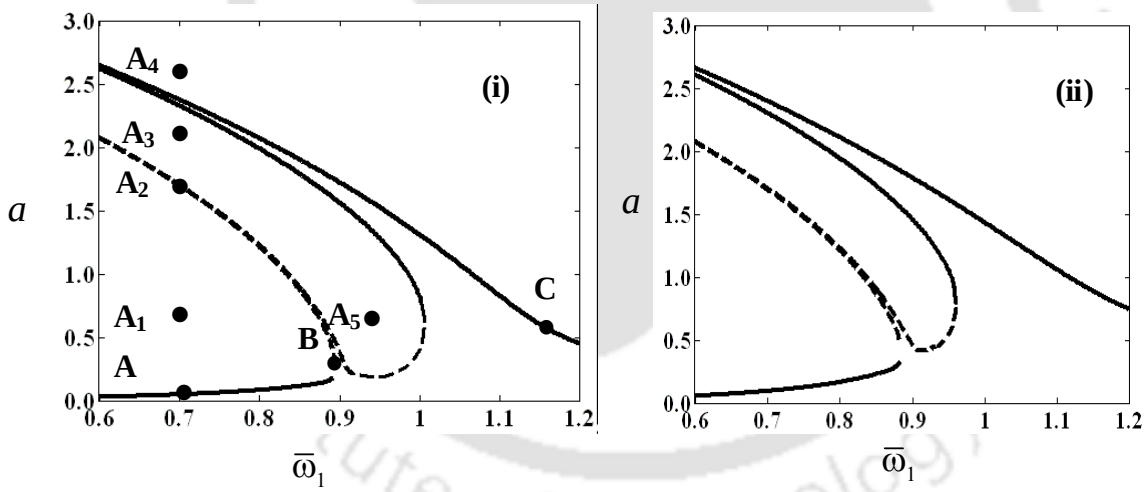

Fig. 3.23. Influence of amplitude of Base excitation ($\bar{Z}$) on the frequency responses for $\bar{m} = 2.0$, $\bar{P}_0 = 0.0$, $\phi = 0$, and $\bar{P}_1 = 0.167$; (i) $\bar{Z} = 0.00372$ (ii) $\bar{Z} = 0.00744$.

From Figs. 3.23 and 3.22(i), one may study the effect of amplitude of base excitation ($\bar{Z}$) on the frequency response curve in case of simultaneous resonance. With increase in $\bar{Z}$, both the regions S_1 and S_2 get decreased and the S-N bifurcation points occur at lower

frequencies. With increase in $\bar{Z}$, it may be observed that the bifurcation point C_1 precedes the bifurcation point C_2. It may also be noted that for a large value of amplitude of base excitation $\bar{Z}$, the critical point C_1 follows point C_2 as shown in Fig. 3.22(i) and hence, with increase in frequency beyond C_1, the system will experience a jump up phenomenon and will jump to the upper most stable nontrivial state C_1'.

To verify the accuracy of the response curves obtained by using the perturbation method in case of simultaneous resonance case, the time responses and phase portraits for three different points (viz., point A, B, C in Fig 3.23(i)) are obtained by solving the temporal equation of motion (3.11), which are shown in Fig. 3.24. From these figures one may note that the steady state results obtained by solving the temporal equation (3.11) are found to be in good agreement with the results obtained by the method of normal forms (Fig . 3.23 (i))).

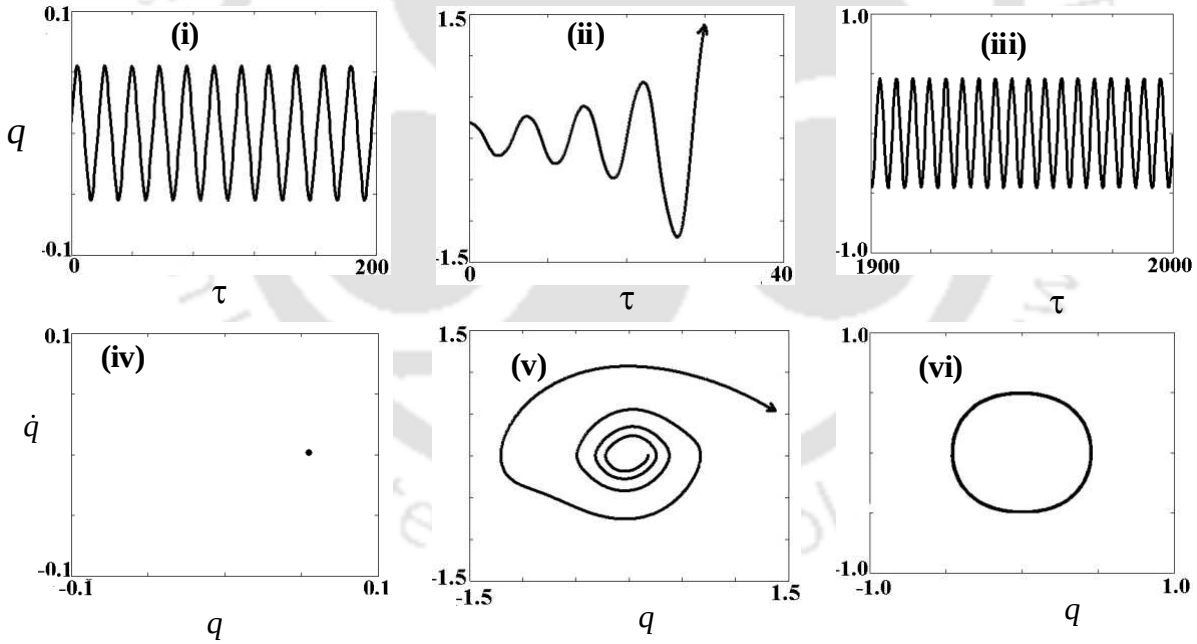

Fig. 3.24. Time response and Poincare's sections corresponding to point A (i, iv); time responses and phase portraits corresponding to points B (ii, v), and C (iii, vi). Key as in Fig. 3.23(i).

As the system has a tri-stable region in the lower frequency range, to know exactly what should be the response of the system, the reduced equations (3.59, 3.60) are numerically solved taking initial conditions corresponding to four points (A_1-A_4) as marked in Fig. 3.23(i). The time response and corresponding state space plots are shown in Fig. 3.25. With initial condition corresponding to point A_1, the response (Fig. 3.25 (i, v)) is found to be in the lower stable branch in region S_1. Similarly, corresponding to initial conditions for points A_2 and A_3, the response of the system has an amplitude of 2.335 (Fig. 3.25 (ii, iii, vi, vii)) which is in the stable branch of region S_2. It is interesting to see that for initial point A_4, the response is found to have an amplitude of 2.375 (Fig. 3.25 (iv, viii)) which is in the upper most stable nontrivial branch as shown in Fig. 3.23 (i).

Due to the presence of tri-stable region before the S-N bifurcation point C_1, the initial condition in this region will play an important role to find the appropriate steady-state response. To illustrate this point, one may plot the basin of attraction by numerically solving the reduced equations (3.59, 3.60) in the a – γ plane as explained in subsection 3.4.2.1. Here, for $\bar{\omega}_1$ equal to 0.7, the basin of attraction is shown in Fig. 3.26, which clearly depicts three stable solutions corresponding to points P_1, P_2 and P_3 as marked in Fig. 3.22(ii).

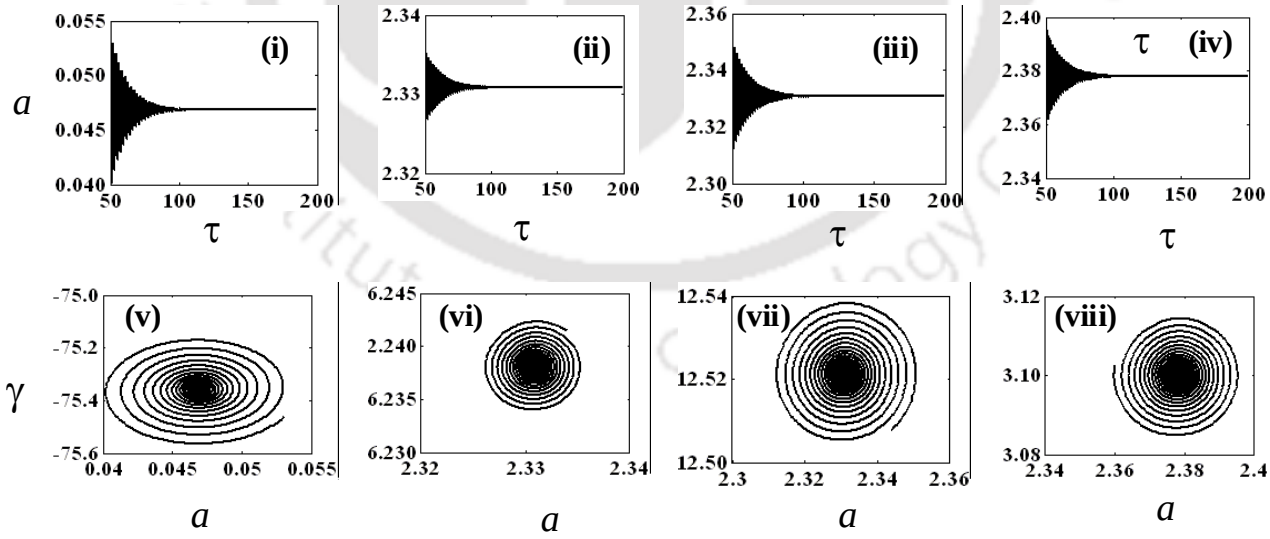

Fig. 3.25. Time responses and phase portraits three different points initial conditions (i, v)A_1, (ii, vi)A_2, (iii, vii)A_3, and (iv, viii)A_4 as key in Fig.13 (i).

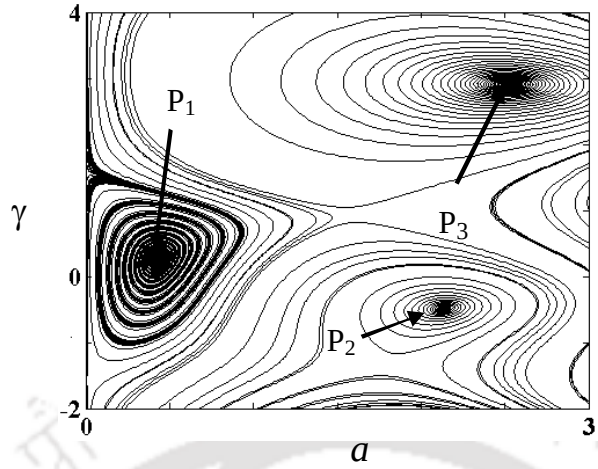

Fig. 3.26. Basins of attraction for $\bar{\omega}_1 = 0.70$, key as in Fig. 3.22(ii).

Figure 3.27 shows the frequency response curves for two different values of $\bar{P}_1$ with amplitude of base excitation equal to 0.0298. One may observe from Fig. 3.22(i) and Fig. 3.27 that with increase in $\bar{P}_1$, the response amplitude increases and the bifurcation point C_1 starts at a lower frequency and C_2 starts at a higher frequency. It may also be observed from these figures that with increase in $\bar{P}_1$, the region S_1 gets decreased and S_2 gets increased. It may be noted that with increase in $\bar{P}_1$, the bifurcation point C_1 always precedes the bifurcation point C_2. In such a case, with further increase in frequency at the critical point C_1, the system will experience a jump up phenomenon similar to that explained in Fig. 3.22(ii).

Figure 3.28 shows the frequency response curves for two different values of amplitude of static load $\bar{P}_0$. One may note that with increase in $\bar{P}_0$, the response amplitude increases and the S-N bifurcation point C_1 occurs at a higher frequency and C_2 occurs at a lower frequency $\bar{\omega}_1$. Unlike the previous case, here, one may observe that with increase in $\bar{P}_0$, region S_2 gets reduced while region S_1 gets increased. With increase in $\bar{P}_0$, it is observed that the critical point C_1 follows C_2 as shown in Figs. 3.28 and 3.22(i). With increase in

frequency beyond C_1, the system will have a jump up phenomenon and may jump to the upper most stable nontrivial state C_1'.

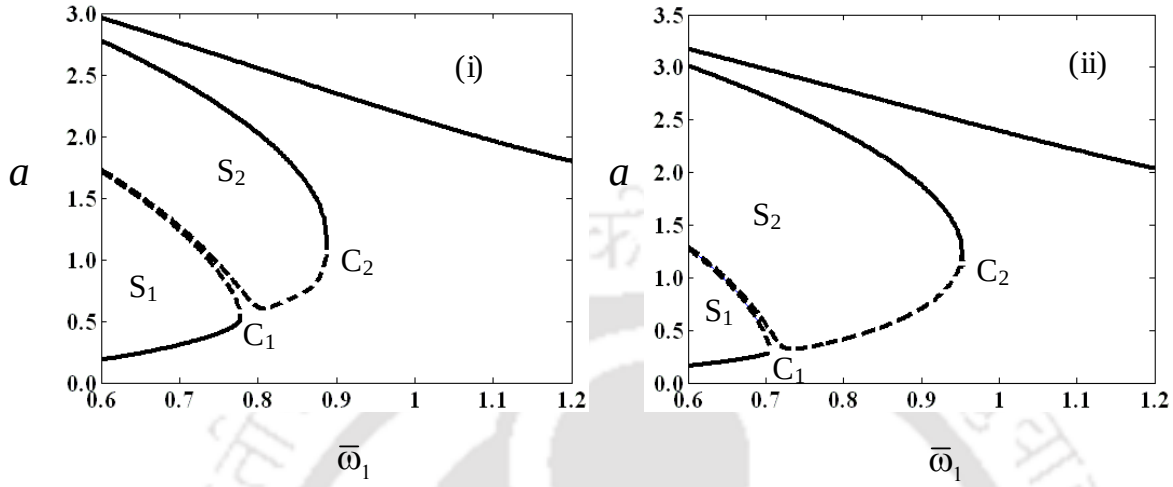

Fig. 3.27. Influence of amplitude of dynamic load $\bar{P}_1$ on the frequency response curve for $\bar{m} = 2.0$, $\bar{P}_0 = 0.0$, $\phi = 0$, $\bar{Z} = 0.0298$; (i) $\bar{P}_1 = 0.333$, (ii) $\bar{P}_1 = 0.499$.

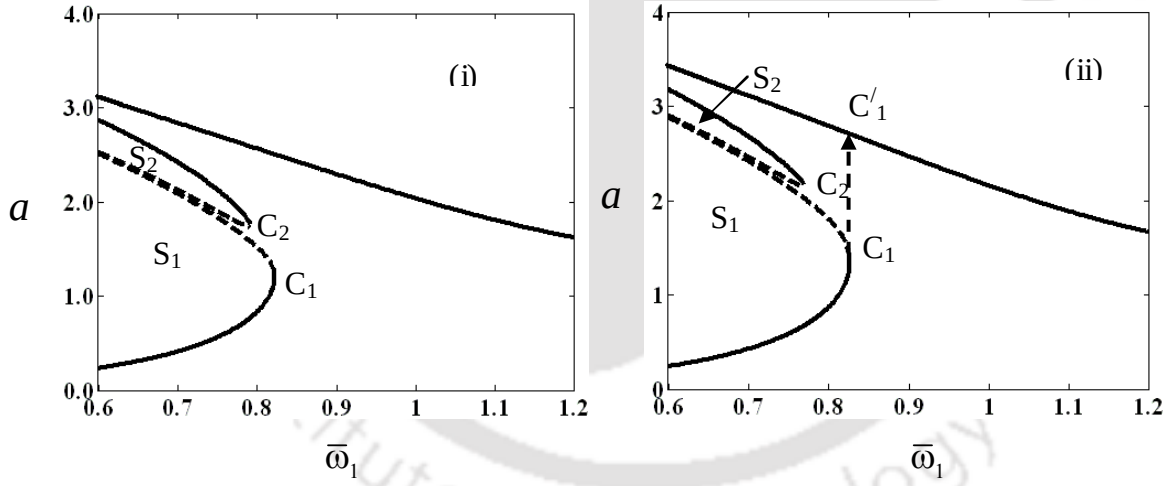

Fig. 3.28. Influence of amplitude of static load $\bar{P}_0$ on the frequency response curve for $\bar{m} = 2.0$, $\bar{Z} = 0.0298$, $\phi = 0$, $\bar{P}_1 = 0.167$; (i) $\bar{P}_0 = 0.167$, (ii) $\bar{P}_0 = 0.334$.

Figure 3.29 shows the frequency response curves for two different values of mass ratio $\bar{m}$. From the Fig. 3.22 (i) and Fig. 3.29, it is observed that with increase in $\bar{m}$, the response amplitude increases and while the region S_1 gets decreased, region S_2 gets increased. Hence, it is observed that while point C_1 moves toward a lower frequency, point C_2 moves

to a higher frequency with increase in $\bar{m}$ and in this case also, one may observe similar jump up phenomenon as explained in Fig. 3.22.

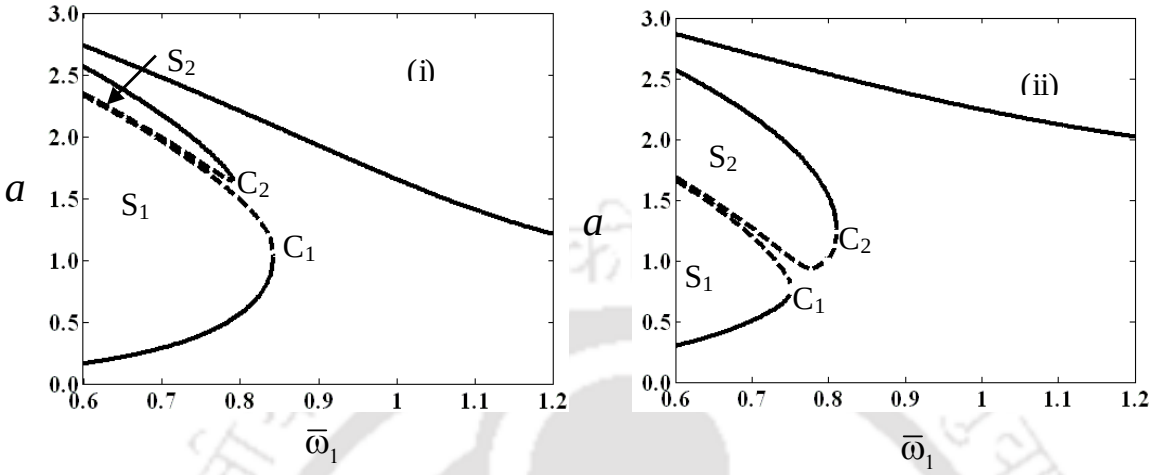

Fig. 3.29. Influence of mass ratio $\bar{m}$ on the frequency response curve for $\bar{Z} = 0.0298$, $\bar{P}_0 = 0.0$, $\phi = 0$, $\bar{P}_1 = 0.167$; (i) $\bar{m} = 1.0$, (ii) $\bar{m} = 4.0$.

3.5 Summary

In the present work, the nonlinear dynamics of flexible Cartesian manipulators with and without harmonically varying axial tip force are carried out. The temporal equation of motion of these systems are obtained by using D' Alembert's principle and generalized Galerkin's method. While the first order method of multiple scales is used to solve the temporal equation of motion for Cartesian manipulator without axial force, method of normal forms is used to solve the temporal equation of motion for the system with harmonically varying axial tip force. The frequency response curves are plotted and their stability and bifurcations are studied for both the systems. Influences of different system parameters on frequency response curves are also observed for different resonance conditions.

The manipulator without axial force has simple and subharmonic resonance conditions. While in simple resonance condition, the system possesses only nontrivial response, in subharmonic resonance condition; both trivial and nontrivial response is observed.

In simple resonance condition, with decrease in amplitude of external excitation, the nontrivial response amplitude remained almost same and system undergoes a catastrophic failure due to jump up phenomenon at saddle-node bifurcation point. Unlike simple resonance case, in subharmonic case where the frequency of the system is nearly three times the natural frequency of the system, along with nontrivial response, stable trivial state response exists for a wide range of system parameters and jump down phenomenon occurs due to the presence of saddle-node bifurcation point. Hence, the system may undergo a catastrophic failure due to the presence of jump down phenomenon. For the system without axial force, it may be concluded that the Cartesian manipulator may be operated at a frequency near the subharmonic resonance zone due to the presence of stable trivial zone. But while sweeping the frequency from simple resonance zone to sub-harmonic resonance zone, the system may fail due to the catastrophic jump up phenomenon. Hence, it is advisable not to operate the manipulator beyond the saddle-node bifurcation point.

Unlike the system without axial force, the system with harmonically varying axial tip force where the manipulator subjected to a harmonic motion at the roller-supported left end and a harmonically varying axial force at the free end has three distinct resonance conditions such as simple, principal parametric and simultaneous resonance conditions.

In simple resonance case for the system with axial force, it is observed that with increase in static force, amplitude of base excitation and mass ratio, system response increases and the system may fail at the saddle-node bifurcation point. Hence, the manipulator should be safely operated at a frequency less than that of the saddle node bifurcation point. Similarly, when the endeffector of the manipulator is subjected to a harmonically varying axial force with a frequency nearly equal to twice the natural frequency of the system, it is recommended to operate the manipulator below the sub-critical pitchfork bifurcation point to avoid excessive vibration. It is observed that in simultaneous resonance case, the system has a tri-stable region while in simple and principal parametric resonances the system has

bi-stable regions. In case of simultaneous resonance condition, the manipulator should be operated at a frequency which is below the saddle-node bifurcation point.

It may be noted that carrying out expensive experiments and computationally solving the temporal equation of motion are tedious and time consuming and hence, one may use the developed simplified mathematical expressions in these work for finding the critical bifurcation points and frequency responses for different resonance conditions. These findings will find extensive applications in the feed-forward control of flexible Cartesian manipulator for precision positioning and constraint motion without any vibration. The present numerical results are compared with previously published experimental results and numerically solving the temporal equation of motion which are found to be in good agreement.

Chapter 4

VISCOELASTIC CARTESIAN MANIPULATOR

4.1 Introduction

In this chapter, the usability of viscoelastic material for manipulator purpose is explored by studying the dynamics of the roller-supported viscoelastic manipulator with and without harmonically varying tip load. Similar to the elastic manipulator, here also D' Alembert's principle and generalized Galerkin's method are used to obtain the temporal equation of motions. Unlike the case of elastic manipulators, here the temporal equation of motion contains terms with complex coefficients and nonlinear damping term originating from the geometry of the large deflection of the manipulator. Method of multiple scales is used to determine the approximate solution of the complex temporal equation of motion and to study the response, stability, and bifurcation of the systems for various system parameters. The response curves obtained using viscoelastic beams is compared with those obtained from a linear Kelvin–Voigt model and also with an equivalent elastic beam.

Similar to the previous chapter, here also two different Cartesian manipulators are studied. While in the first case, the dynamics of viscoelastic Cartesian manipulator without axial force is carried out, in the second case, the viscoelastic Cartesian manipulator with harmonically varying axial load is studied. In section 4.2, the mathematical formulations of the governing equation of motion for both the viscoelastic manipulators are obtained. While in section 4.3, solution of the temporal equation of motion and numerical results for viscoelastic Cartesian manipulator without axial force are discussed, in section 4.4, similar analysis are made for the viscoelastic Cartesian manipulator with harmonically varying axial tip force. In this chapter similar procedures as discussed in the previous chapter are used to find the time and frequency response of the system and to plot the basin of attraction

4.2 Mathematical Formulation

Figure 4.1 shows a viscoelastic single-link flexible Cartesian manipulator with payload mass *M*. Similar to the elastic manipulator, here also the left end is roller-supported and subjected to time varying support motion $Y_b(t) = Z\cos\Omega_1 t$, and the payload end is subjected to harmonically varying axial force $P(t) = P_0 + P_1\cos\Omega_2 t$. Unlike the elastic material of the manipulator in the previous chapter, here, the material of the manipulator is viscoelastic. Using D' Alembert's principle and following similar procedure as discussed in chapter 3, the governing differential equation of motion of the system in terms of transverse deflection *v* is obtained as follows:

$$E^*I\left(v_{ssss} + \frac{1}{2}v_s^2 v_{ssss} + 3v_s v_{ss} v_{sss} + v_{ss}^3\right) + \rho A v_s\left(\int_0^s\left(\dot{v}_\xi^2 + v_\xi \ddot{v}_\xi\right)d\xi\right) + M\left(\ddot{v} + \ddot{Y}_b\right)v_s v_{ss} + v_s v_{ss}$$

$$\left(\rho A\ddot{Y}_b(L-s) + \int_s^L\left(\rho A\ddot{v} + c_d\dot{v}\right)d\eta\right) - v_{ss}\left(\int_s^L \rho A\int_0^\xi\left(\dot{v}_\xi^2 + v_\xi\ddot{v}_\xi\right)d\xi d\eta + M\int_0^s\left(\dot{v}_\xi^2 + v_\xi\ddot{v}_\xi\right)d\xi\right) +$$

$$\left(1 - \frac{1}{2}v_s^2\right)\left(\rho A\left(\ddot{v} + \ddot{Y}_b\right) + c_d\dot{v}\right) + \left(P(t)v_s\right)_s = 0\,. \qquad (4.1)$$

with boundary conditions: at $s = 0$, displacement $v = Y_b$, slope $v_s = 0$; at $s = L$, bending moment $E^*Iv_{ss} = 0$, and shear force $E^*Iv_{sss} = M\left(\ddot{Y}_b + \ddot{v}\right)$.

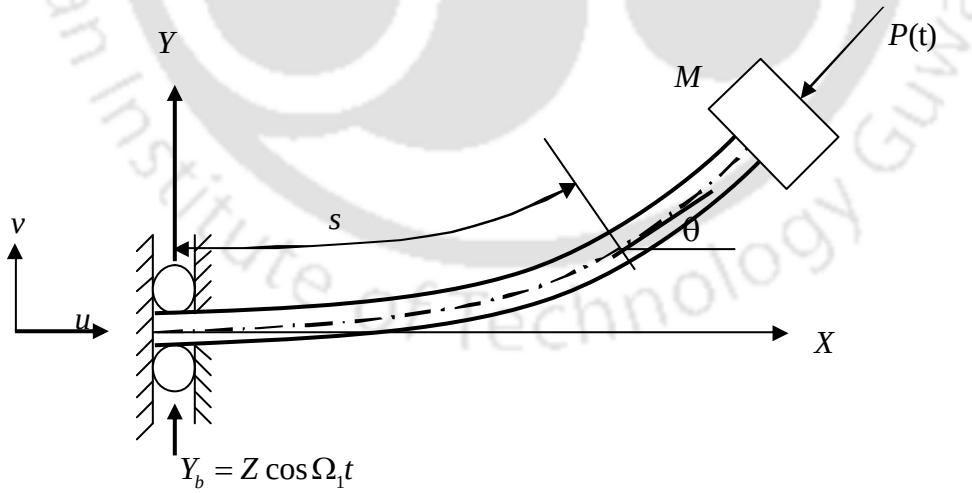

Fig. 4.1. Schematic diagram of a single-link viscoelastic Cartesian manipulator with payload *M* subjected to harmonically varying axial force.

Here, E^* is the Young's modulus of the viscoelastic beam represented by a complex quantity $E_1 + iE_2 = E_1(1+i\delta)$, where the real part of this complex term (storage modulus, E_1) relates to the elastic behavior of the material, and defines the stiffness of the material. The imaginary component (loss modulus, E_2) relates to the material's viscous behavior, and defines the energy dissipative ability of the material and δ is the material loss factor. By replacing E^* with E which is the Young's modulus of the elastic manipulator, equation (4.1) reduces to that of equation (3.6) of the elastic manipulator presented in previous chapter and that of Cuvalci (2000) when the pendulum is considered to be in locked position.

Here, generalized Galerkin's method is used to discretize the equation of motion (4.1) by using the following assumed mode expression.

$$v(s,t) = r\,\psi(s)\,q(t) \tag{4.2}$$

Here, r, $\psi(s)$, *and* $q(t)$ are respectively, the scaling factor, an admissible function and time modulation. Following Gurgoze et al. (2005), the same shape function as used in chapter 3 (equation 3.8) is used in this case. The following non-dimensional parameters are used in the analysis.

$$\bar{x} = \frac{s}{L}, \tau = \omega_s\, t\,,\ \bar{\omega}_1 = \frac{\Omega_1}{\omega_s},\ \bar{\omega}_2 = \frac{\Omega_2}{\omega_s},\ \bar{r} = \frac{r}{L},\ \bar{m} = \frac{M}{\rho AL}, \delta = \frac{E_2}{E_1}$$

$$\bar{P}_0 = \frac{P_0}{P_c},\ \bar{P}_1 = \frac{P_1}{P_c},\ \chi = \frac{EI}{\rho AL^4}, \kappa = \frac{Z}{r}, \text{ and } \bar{Z} = \frac{Z}{L} \tag{4.3}$$

Here, P_c is the critical Euler buckling load for a cantilever beam, which is equal to $(\pi^2 E_1 I)/(4L^2)$ and ω_s is the system fundamental frequency. Substituting equation (4.2) into equation (4.1) and using the generalized Galerkin's method the resulting non-dimensional temporal equation of motion is obtained as:

$$\ddot{q} + q + i\varepsilon\left(2\zeta q + \eta q^3\right) + \varepsilon\left(\alpha_1 q^3 + \alpha_2 q^2 \ddot{q} + \alpha_3 \dot{q}^2 q\right) + \varepsilon\left(\alpha_4 \bar{\omega}_1^2 \cos\bar{\omega}_1 \tau\, q^2 + \alpha_5 \bar{\omega}_1^2 \cos\bar{\omega}_1 \tau + \alpha_6 \cos\bar{\omega}_2 \tau\, q\right) = 0. \tag{4.4}$$

The expression for the coefficients of equation (4.4) is given below.

$$\omega_s = \sqrt{\frac{EI}{\rho A L^4}\left(\frac{h_{14}}{h_2} + \frac{P_0 \pi^2}{4P_c}\frac{h_{21}}{h_2}\right)} = \sqrt{\chi\left(\frac{h_{14}}{h_2} + \bar{P}_0 \frac{\pi^2}{4}\frac{h_{21}}{h_2}\right)}, \quad \zeta = \frac{E_2}{2\varepsilon E_1} = \frac{\delta}{2\varepsilon},$$

$$\eta = \frac{E_2 I}{\varepsilon \rho A L^4}\frac{\bar{r}^2}{\omega_e^2}\left(\frac{h_{19}}{h_2} + \frac{h_{18}}{2h_2} + 3\frac{h_{20}}{h_2}\right) = \frac{\delta}{\varepsilon}\bar{r}^2\left(\frac{h_2}{h_{12}}\right)\left(\frac{h_{19}}{h_2} + \frac{h_{18}}{2h_2} + 3\frac{h_{20}}{h_2}\right)$$

$$\alpha_1 = \frac{\chi \bar{r}^2}{\varepsilon \omega_e^2}\left(\frac{h_{19}}{h_2} + \frac{h_{18}}{2h_2} + 3\frac{h_{20}}{h_2}\right), \; \alpha_2 = \frac{\bar{r}^2}{\varepsilon}\left(\frac{h_3}{h_2} + \frac{h_4}{h_2} + \bar{m}\frac{h_5}{h_2} - \frac{h_6}{h_2} - \bar{m}\frac{h_7}{h_2} - \frac{h_8}{h_2}\right),$$

$$\alpha_3 = \frac{\bar{r}^2}{\varepsilon}\left(\frac{h_{11}}{h_2} - \frac{h_{12}}{h_2} - \bar{m}\frac{h_{13}}{h_2}\right), \alpha_4 = \frac{\overline{Z\lambda}}{\varepsilon}\left(\frac{h_{15}}{h_2} + \bar{m}\frac{h_{16}}{h_2} - \frac{h_{17}}{2h_2}\right),$$

$$\alpha_5 = \frac{\kappa}{\varepsilon}\left(\frac{h_1}{h_2}\right), \text{ and } \alpha_6 = \frac{P_1}{M\,\omega_s^2 L^2}\left(\frac{h_{21}}{h_2}\right).$$

The expressions for $h_1, h_2, \cdots\cdots h_{21}$ are same as those of elastic manipulator and can be found in chapter 3.

In order to make all the coefficients i.e., $\zeta, \alpha_1, \alpha_2 \cdots \alpha_6$ in the same order of unity a book-keeping parameter ε which is less than one is introduced. One may find that the non-dimensional temporal equation (4.4) contains linear damping term ($2i\zeta q$), a nonlinear damping term ($i\eta q^3$), a force term ($\alpha_5 \bar{\omega}_1^2 \cos\bar{\omega}_1\tau$) and a nonlinear parametric excitation term ($\alpha_4 \bar{\omega}_1^2 \cos\bar{\omega}_2\tau\, q^2$) due to the harmonic support motion, a parametric term $\alpha_6 \cos\bar{\omega}_2\tau\, q$ due to the harmonically varying axial force, along with cubic geometric ($\alpha_1 q^3$) and inertia ($\alpha_2 q^2\ddot{q} + \alpha_3 \dot{q}^2 q$) nonlinear terms. It may be noted that the equation of motion (4.4) contains two terms with complex coefficient, viz., $2i\zeta q$, and $i\eta q^3$ which are not present for an elastic manipulator discussed in chapter 3. These two terms arising from the viscoelastic property of the beam material will primarily be responsible for the energy dissipation and hence, vibration suppression in this system.

Similar to the elastic manipulator, here also the studies are carried out for manipulator with and without axial force applied at the tip end. For the system without axial force, one may

obtain the following non-dimensional equation of motion by neglecting the parametric term $\alpha_6 \cos\bar{\omega}_2\tau\ q$ from equation (4.4).

$$\ddot{q}+q+i\varepsilon\left(2\zeta q+\eta q^3\right)+\varepsilon\left(\alpha_1 q^3+\alpha_2 q^2\ddot{q}+\alpha_3\dot{q}^2 q\right)+$$
$$\varepsilon\left(\alpha_4\bar{\omega}^2\cos\bar{\omega}\tau\, q^2+\alpha_5\bar{\omega}^2\cos\bar{\omega}\tau\right)=0. \qquad (4.5)$$

In the above equation as the system subjected only a single harmonic motion at the roller-supported end, for simplicity in representation, $\bar{\omega}_1$ is replaced by $\bar{\omega}$. It may be noted that the temporal equation of motion contains many nonlinear terms and it is very difficult to find the closed form solution or exact solution. Hence, one may go for approximate solution by solving equation (4.4) or equation (4.5) using perturbation methods as described in the following section.

Similar to previous chapter, here also solution and numerical simulations of two different systems are carried out in the next sections. While in section 3.3, the discussions are made for viscoelastic Cartesian manipulator without axial force, in section 3.4, viscoelastic Cartesian manipulator with harmonically varying axial force is studied.

4.3 Viscoelastic Cartesian Manipulator without Axial Force

4.3.1 Analysis

Here, method of multiple scales is used to find the solution of the equation (4.5) where the displacement q can be represented in terms of different time scales (T_0, T_1) and a book-keeping parameter ε, as explained in previous chapter. Following similar procedure as in section 3.3.1, substituting $T_n = \varepsilon^n \tau$, $n = 0, 1, 2\cdots$ and $q(\tau;\varepsilon) = q_0(T_0, T_1) + \varepsilon q_1(T_0, T_1) + O(\varepsilon^2)$ in equation (4.5) and equating the coefficients of like powers of ε, one may obtain the following expressions:

Order ε^0: $D_0^2 q_0 + q_0 = 0$ (4.6)

Order ε^1: $D_0^2 q_1 + q_1 = -2D_0 D_1 q_0 - 2i\zeta q_0 - i\eta q^3 - \alpha_1 q_0^3 - \alpha_2 q_0{}^2 D_0^2 q_0 - \alpha_3 (D_0 q_0)^2 q_0$

$$-\alpha_4 q_0^2 \bar{\omega}^2 \cos(\bar{\omega}\tau) - \alpha_5 \bar{\omega}^2 \cos(\bar{\omega}\tau) \quad (4.7)$$

For simplicity, here $\bar{\omega}_1$ is replaced by $\bar{\omega}$.

General solution of equation (4.6) can be written as

$$q_0 = A(T_1)\exp(iT_0) + \bar{A}(T_1)\exp(-iT_0). \quad (4.8)$$

Substituting equation (4.8) into equation (4.7) leads to

$$D_0{}^2 q_1 + q_1 = -\left(2iD_1 A + 2i\zeta A + 3i\eta A^2 \bar{A} + 3\alpha_1 A^2 \bar{A} - 3\alpha_2 A^2 \bar{A} + \alpha_3 A^2 \bar{A}\right)\exp(iT_0)$$

$$+\left(i\eta - \alpha_1 + \alpha_2 + \alpha_3\right) A^3 \exp(3iT_0) - \frac{1}{2}\alpha_4 \bar{\omega}^2 A^2 \exp i(2+\bar{\omega})T_0$$

$$-\frac{1}{2}\alpha_4 \bar{\omega}^2 \bar{A}^2 \exp i(\bar{\omega}-2)T_0 - \bar{\omega}^2\left(\alpha_4 A\bar{A} + \frac{1}{2}\alpha_5\right)\exp i(\bar{\omega}T_0) + cc. \quad (4.9)$$

Here, *cc* stands for the complex conjugate of the preceding terms. It may be noted from equation (4.9) that it will contain secular or small divisor terms when $\bar{\omega} \approx 1$ or $\bar{\omega} \approx 3$. The resonance condition corresponding to $\bar{\omega} \approx 1$ is known as simple resonance and that

corresponds to $\bar{\omega} \approx 3$, is the subharmonic resonance. These two resonance cases are studied in the following subsections.

4.3.1.1 Simple Resonance Case ($\bar{\omega} \approx 1$)

In the case of simple resonance, one may use the detuning parameter σ to express the nearness of $\bar{\omega}$ to 1 as

$$\bar{\omega} = 1 + \varepsilon\sigma, \qquad \sigma = O(1). \tag{4.10}$$

Substituting equation (4.10) into equation (4.9) and eliminating the secular or small divisor terms one may obtain the following equations.

$$2iA' + 2i\zeta A + 3i\eta A^2\bar{A} + 3\alpha_1 A^2\bar{A} - 3\alpha_2 A^2\bar{A} + \alpha_3 A^2\bar{A} + \frac{1}{2}\bar{\omega}^2\alpha_4 A^2 \exp i(-\sigma T_1) +$$

$$\bar{\omega}^2\left(\alpha_4 A\bar{A} + \frac{1}{2}\alpha_5\right)\exp i(\sigma T_1) = 0. \tag{4.11}$$

Substituting A in the polar form i.e. $A = \frac{1}{2}a(T_1)exp(i\beta T_1)$ and separating the real and imaginary parts yields the following expressions.

$$a' = -\zeta a - \frac{3}{8}\eta a^3 - \bar{\omega}^2\left(\frac{\alpha_4}{8}a^2 + \frac{1}{2}\alpha_5\right)\sin\gamma, \tag{4.12}$$

$$a\gamma' = a\sigma - \frac{3}{8}Ka^3 - \bar{\omega}^2\left(\frac{3\alpha_4}{8}a^2 + \frac{1}{2}\alpha_5\right)\cos\gamma. \tag{4.13}$$

Here, $(\,)' = \frac{\partial}{\partial T_1}$, $K = \alpha_1 - \alpha_2 + \frac{\alpha_3}{3}$ and $\gamma = \sigma T_1 - \beta$. For steady state response (a_0, γ_0), a' and γ' are equal to zero. Eliminating γ from equations (4.12) and (4.13), one may find a fifth order polynomial in a^2, which can be expressed as

$$Q_5 a^{10} + Q_4 a^8 + Q_3 a^6 + Q_2 a^4 + Q_1 a^2 + Q_0 = 0. \tag{4.14}$$

The coefficients of the above fifth order polynomial in a^2 are given by the following expressions

$$Q_0 = -\frac{1}{16}\bar{\omega}^8\alpha_5^4,\ Q_1 = \frac{1}{4}\zeta^2\bar{\omega}^4\alpha_5^2 + \frac{1}{4}\bar{\omega}^4\sigma^2\alpha_5^2 - \frac{1}{8}\bar{\omega}^8\alpha_4\alpha_3^3,$$

$$Q_2 = \frac{3}{8}\zeta^2\bar{\omega}^4\alpha_4\alpha_5 + \frac{1}{8}\bar{\omega}^4\sigma^2\alpha_4\alpha_5 + \frac{3}{16}\bar{\omega}^4\zeta\eta\alpha_5^2 - \frac{3}{16}\bar{\omega}^4 K\sigma\alpha_5^2 - \frac{11}{32}\bar{\omega}^8\alpha_4^2\alpha_5^2,$$

$$Q_3 = \frac{9}{64}\zeta^2\bar{\omega}^4\alpha_4^2 + \frac{1}{64}\bar{\omega}^4\sigma\alpha_4^2 + \frac{9}{256}\bar{\omega}^4 K^2\alpha_5^2 + \frac{9}{256}\bar{\omega}^4\eta^2\alpha_5^2 + \frac{9}{32}\bar{\omega}^4\zeta\eta\alpha_4\alpha_5$$
$$-\frac{3}{32}\bar{\omega}^4\sigma K\alpha_4\alpha_5 - \frac{1}{128}\bar{\omega}^8\alpha_4^3\alpha_5,$$

$$Q_4 = \frac{9}{512}\bar{\omega}^4 K^2\alpha_4\alpha_5 + \frac{27}{256}\bar{\omega}^4\zeta\eta\alpha_4^2 + \frac{27}{512}\bar{\omega}^4\eta^2\alpha_4\alpha_5 - \frac{3}{256}\bar{\omega}^4\sigma K\alpha_4^2 - \frac{9}{4096}\bar{\omega}^8\alpha_4^4,$$

and $Q_5 = \frac{9}{4096}\bar{\omega}^4 K^2\alpha_4^2 + \frac{81}{4096}\bar{\omega}^4\eta^2\alpha_4^2.$ (4.15)

Though the equation (4.14) is similar to equation (3.23) of the elastic manipulator, but the coefficients in both the cases are different. Equation (4.14) is an implicit equation for amplitude of the response as a function of the external detuning parameters σ (i.e. the excitation frequency), material loss factor parameter δ, payload mass M and the amplitude of the base excitation Z. One may note from equation (4.14) that, this resonance condition does not have any trivial state response. The response of the system can be obtained by numerically solving equation (4.14). Following similar procedure as in section 3.3.1, the stability in this resonance condition, can be found by investigating the eigenvalues of the Jacobian matrix (J) which is given by

$$J = \begin{bmatrix} -\zeta - \dfrac{9\eta a_o^2}{8} + \dfrac{\frac{1}{2}\alpha_4 a_0\left(\zeta a_0 + \frac{3}{8}\eta a_0^3\right)}{\frac{1}{8}\alpha_2 a_0^2 + \frac{1}{2}\alpha_5} & -\dfrac{\left(\frac{1}{8}\alpha_4 a_0^2 + \frac{1}{2}\alpha_5\right)\left(\sigma a_0 - \frac{3}{8}Ka_0^3\right)}{\frac{3}{8}\alpha_4 a_0^2 + \frac{1}{2}\alpha_5} \\ -\dfrac{3Ka_0}{4} - \dfrac{3}{4}\dfrac{\alpha_4\left(\sigma a_0 - \frac{3}{8}Ka_0^3\right)}{\frac{3}{8}\alpha_4 a_0^2 + \frac{1}{2}\alpha_5} + & -\dfrac{\left(\frac{3}{8}\alpha_4 a_0^2 + \frac{1}{2}\alpha_5\right)\left(\zeta + \frac{3}{8}\eta a_0^2\right)}{\frac{1}{8}\alpha_4 a_0^2 + \frac{1}{2}\alpha_5} \\ \dfrac{\sigma a_0 - \frac{3}{8}Ka_0^3}{a^2} & \end{bmatrix}. \quad (4.16)$$

From equation (4.8), the first order nontrivial steady state approximate solution can be given by

$$q = a\cos(\bar{\omega}\tau - \gamma) + O(\varepsilon). \tag{4.17}$$

4.3.1.2 Subharmonic Resonance Case ($\bar{\omega} \approx 3$)

In this case, to describe the nearness of $\bar{\omega}$ to 3, here one may use a detuning parameter σ as

$$\bar{\omega} = 3 + \varepsilon\sigma, \qquad \sigma = O(1). \tag{4.18}$$

Substituting equation (4.18) into equation (4.9) and by eliminating the secular or small divisor terms one may obtain the following equation.

$$2iA' + 2i\zeta A + 3i\eta A^2\bar{A} + 3\alpha_1 A^2\bar{A} - 3\alpha_2 A^2\bar{A} + \alpha_3 A^2\bar{A} + \frac{1}{2}\bar{\omega}^2\alpha_4 A^2 \exp i(\sigma T_1) = 0. \tag{4.19}$$

Here also taking $A = \frac{1}{2}a(T_1)exp(i\beta T_1)$, and substituting it in equation (4.19) and separating the real and imaginary parts, one may have the following equations.

$$a' = -\zeta a - \frac{3}{8}\eta a^3 - \bar{\omega}^2\frac{\alpha_4}{8}a^2\sin\gamma \tag{4.20}$$

$$a\gamma' = a\sigma - \frac{9}{8}Ka^3 - \bar{\omega}^2\frac{3\alpha_4}{8}a^2\cos\gamma, \tag{4.21}$$

Here, $K = \alpha_1 - \alpha_2 + \frac{\alpha_3}{3}$ and $\gamma = \sigma T_0 - 3\beta$. For steady state condition, a' and γ' equal to zero. Eliminating γ from equations (4.20) and (4.21), one may find a fourth order polynomial equation in a^2 which is given by

$$a^2\left(Q_1 + Q_2a^2 + Q_3a^4\right) = 0. \tag{4.22}$$

The coefficients of the above polynomial are given below.

$Q_1 = 64\zeta^2\bar{\omega}^4 + \frac{64}{9}\sigma^2\bar{\omega}^4$, $Q_2 = 48\zeta\eta - 16\bar{\omega}^4\sigma K - \bar{\omega}^8\alpha_4^2$, and

$$Q_3 = 9\bar{\omega}^4K^2 + \frac{64}{9}\sigma^2\bar{\omega}^4 + 9\eta^2. \tag{4.23}$$

One may determine the system response by solving numerically the polynomial equation (4.23) for different system parameters. Due to similar reason as mentioned in section 3.3.1.2, here also, the stability of the system can be obtained by using the transformation

$p_s = a\cos\gamma$ and $q_s = a\sin\gamma$ in the reduced equations (4.20) and (4.21) and finding the resulting Cartesian form of modulation equations as follows.

$$p_s' = -\zeta p_s - \sigma q_s + \frac{1}{4}\alpha_4\bar{\omega}^2 p_s q_s - \frac{9}{8}\left(\frac{1}{3}\eta p_s - K q_s\right)(p_s^2 + q_s^2), \qquad (4.24)$$

$$q_s' = -\zeta q_s + \sigma p_s - \frac{1}{8}\alpha_4\bar{\omega}^2\left(3p_s^2 + q_s^2\right) - \frac{9}{8}\left(\frac{1}{3}\eta q_s + K p_s\right)(p_s^2 + q_s^2). \qquad (4.25)$$

Stability of the steady state response (p_0, q_0) can be determined by investigating the eigenvalues of the Jacobian matrix (J) which is obtained by perturbing the equations (4.24) and (4.25). The Jacobian matrix (J) is given by

$$J = \begin{bmatrix} -\zeta + \frac{1}{4}\alpha_4\bar{\omega}^2 q_0 - \frac{3}{8}\eta\left(p_o^2 + q_0^2\right) - \frac{9}{4}\left(\frac{\eta}{3}p_0 - Kq_0\right)p_0 & -\sigma + \frac{1}{4}\alpha_4\bar{\omega}^2 p_0 + \frac{9}{8}K\left(p_o^2 + q_0^2\right) - \frac{9}{4}\left(\frac{\eta}{3}p_0 - Kq_0\right)q_0 \\ \sigma - \frac{3}{4}\alpha_4\bar{\omega}^2 p_0 - \frac{9}{8}K\left(p_o^2 + q_0^2\right) - \frac{9}{4}\left(\frac{\eta}{3}q_0 + Kp_0\right)p_0, & -\eta - \frac{1}{4}\alpha_4\bar{\omega}^2 q_0 - \frac{3}{8}\eta\left(p_o^2 + q_0^2\right) - \frac{9}{4}\left(\frac{\eta}{3}p_0 + Kq_0\right)q_0 \end{bmatrix}. \qquad (4.26).$$

One may write the first order nontrivial steady state response for this resonance condition as

$$q = a\cos\left(\frac{1}{3}\left(\bar{\omega}\tau - \gamma\right)\right) + O(\varepsilon) \qquad (4.27)$$

In the following subsection the above system is modeled as a single degree of freedom linear-Kelvin-Voigt model to find the response of the system.

4.3.1.3 Response of an Equivalent Single-Degree of Freedom Linear Kelvin-Voigt Model

The Cartesian manipulator without axial force can be modeled as a single-degree of freedom spring-mass-damper system with support motion as shown in Fig. 4.2. To model

the viscoelastic beam material, following Gurgoze et al. (2005), a Kelvin-Voigt model is considered which has equivalent spring constant (K) and internal damping (C) as

$$K = \frac{3E_1 I}{L^3}, \quad C = \frac{E_2 I}{L^3}. \tag{4.28}$$

The damping ratio (ζ) and natural frequency (ω_n) for the linear model are given by

$$\zeta = \frac{C}{2m\omega_n}, \quad \omega_n^2 = \frac{K}{m_e}, \tag{4.29}$$

where m_e is the equivalent mass of the system, which for this linear model can be expressed as $m_e = M + \frac{33}{140}(\rho AL)$.

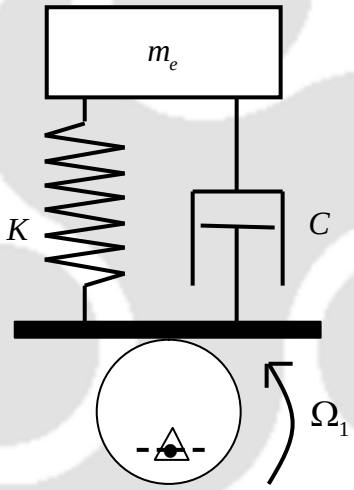

Fig. 4.2. Equivalent spring-mass-damper system with Kelvin -Voigt model.

For the equivalent base excited spring mass damper system as shown in Fig.4.2, the mathematical expression for the deflection (a) of the equivalent mass of the linear Kelvin-Voigt Model can be given by

$$a = Z\left(\frac{1+(2\zeta\bar{\omega})^2}{\left(1-(\bar{\omega})^2\right)^2+(2\zeta\bar{\omega})^2}\right)^{\frac{1}{2}} \tag{4.30}$$

where, $\bar{\omega} = \frac{\Omega_1}{\omega_n}$. It may be noted that same notation (a) for deflection is used for both linear and nonlinear systems as discussed in section 4.3.1.2.

4.3.2 Numerical Results and Discussions

For the numerical analysis, a polymethyl methacrylate (Plexiglass) viscoelastic beam similar to that considered in the work of Shih and Yeh (2005) is taken with length L = 300 mm, width d = 10 mm, height h = 2 mm, and mass density = 1190.2357 kg/m^3. Unlike the work of Shih and Yeh (2005), in this case, as the responses are considered near the resonance conditions for a small frequency range, the complex modulus of elasticity is assumed to remain constant with frequency. Moreover, as in this case nondimensional system parameters are taken, the effect of variation of complex modulus with frequency is not significant and one may take any other viscoelastic material for this study. The book-keeping parameter (ε) and scaling factor ($\bar{r}$) are taken as 0.1 and 0.2, respectively. Similar to the system with elastic manipulator, here also two different resonance conditions are studied. While the simple resonance condition is discussed in section 4.3.2.1, sub-harmonic resonance condition is discussed in section 4.3.2.2.

4.3.2.1 Simple Resonance Case ($\bar{\omega} \approx 1$)

In this resonance condition, the roller-supported end of the manipulator moves harmonically with a frequency nearly equal to the system natural frequency. Figure 4.3 (i) shows the frequency response curves for this system with nondimensional amplitude of base excitation ($\bar{Z}$), mass ratio ($\bar{m}$) and material loss factor (δ) equal to 0.00372, 1.8787 and 0.02 respectively. Keeping all other parameters same, in Fig. 4.3(ii), the material loss factor (δ) is taken to be 0.05. In all frequency response curves, solid lines and dotted lines, respectively represent the stable and unstable response. One may observe from Fig. 4.3 that with increase in frequency of the base excitation $\bar{\omega}$ (e.g., from the point A) the response amplitude increases and it reaches the critical point ($\bar{\omega}$ equal to 0.922), which is a saddle-node bifurcation point. At this bifurcation point with further increase in $\bar{\omega}$, the

system experience a jump up phenomena which results in a sudden jump from the point B to C (indicated by upward dotted arrow in Fig. 4.3(i)). This may lead to catastrophic failure of the system. If the system does not fail, it will vibrate with nontrivial amplitude as shown in Fig. 4.3(i). Now, while switching off the manipulator, for example if it is operating at a frequency marked by point D, it is observed that with decrease in frequency, the response amplitude goes on increasing and finally a sudden catastrophic jump down phenomena may occur at frequency $\overline{\omega}$ equal to 0.75 (point E). This jump down phenomena is indicated by a downward arrow in Fig. 4.3. Hence, it is advised not to operate the manipulator beyond the critical point B. With increase in material loss factor (δ) from 0.02 (Fig. 4.3(i)) to 0.05, one may observe that the maximum response amplitude of the system decreases from 0.9797 to 0.6279 (Fig. 4.3(ii)). The jump up phenomena occurs at $\overline{\omega}$ equal to 0.92 and jump down phenomena occurs at $\overline{\omega}$ equal to 0.896. It is further observed that the jump length during jump up phenomena decreases from 0.3645 (Fig. 4.3(i)) to 0.294 (Fig. 4.3(ii)). The corresponding values for jump down phenomena are 0.896 and 0.4832 respectively. Hence, one may obtain a significant reduction in response amplitude with increase in the value of δ.

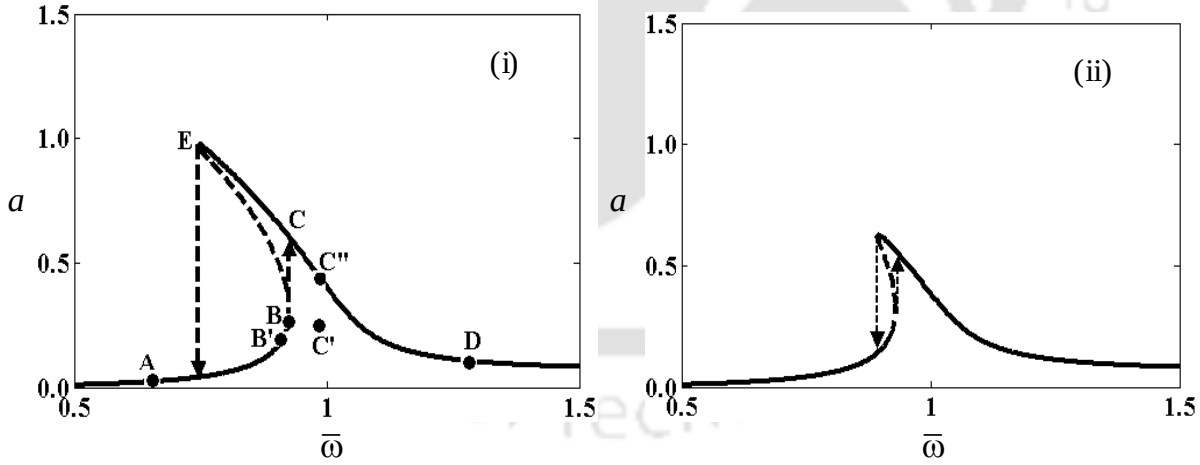

Fig. 4.3. Frequency response curve for viscoelastic manipulator with $\overline{m} = 1.8787$, $\overline{Z} = 0.00372$ (i) $\delta = 0.02$, (ii)) $\delta = 0.05$.

One may validate the results obtained by the perturbation analysis by numerically solving the temporal equation of motion (4.5). Here, the fourth order Runge-Kutta method is used

to solve the temporal equation of motion for finding the time response of the system. Four points viz., A, B′, C′ and D on the frequency response curves shown in Fig.4.3 (i) are considered for the comparison purpose.

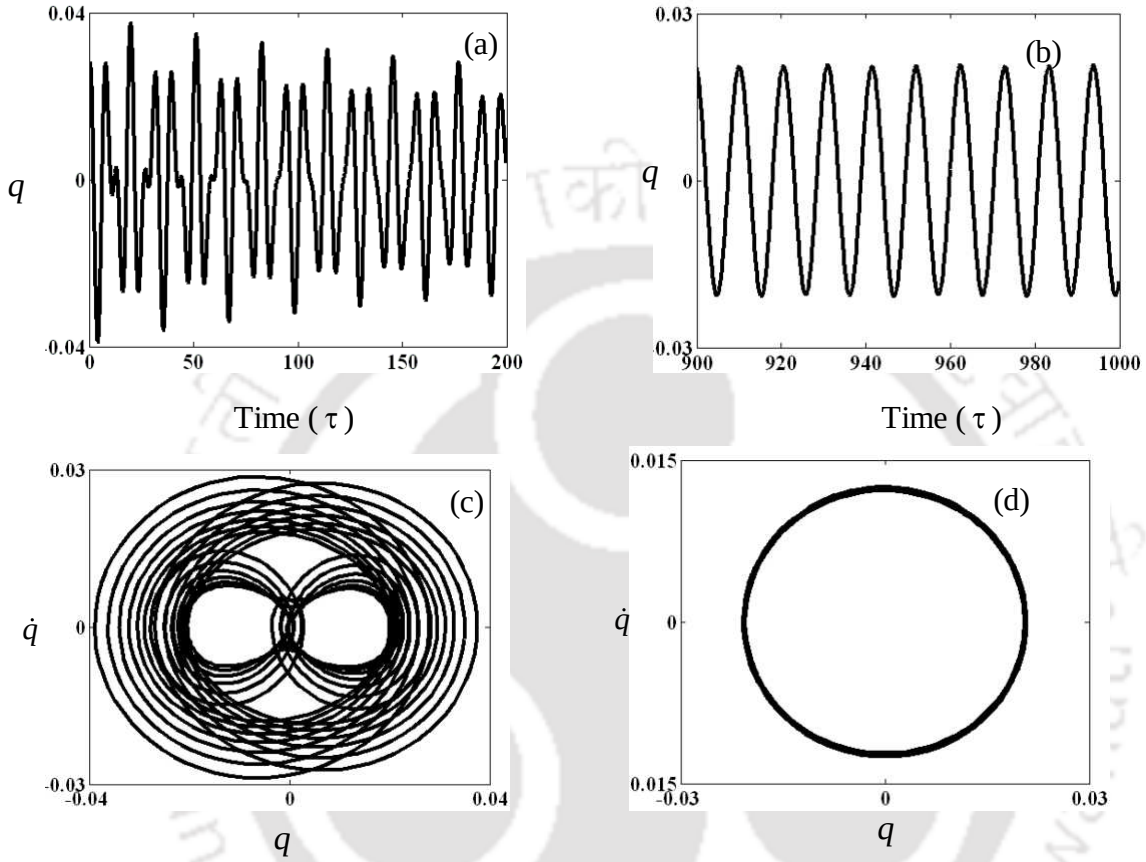

Fig. 4.4. Time response, and phase portrait for the critical points A (key as in Fig. 4.3(i)) where (a, c) are the transient response, and (b, d) are the steady state response.

Fig. 4.4 shows the time response and phase portrait corresponding to point A. The transient response (Fig. 4.4 (a), (c)) shows the quasi-periodic response, which is obtained with initial point (0.021, 0.01). The steady state response is found to be periodic which is clearly depicted in the time response (Fig. 4.4 (b)) and phase portrait (Fig. 4.4(d)). It may clearly be observed that the amplitude of the steady state time response obtained by numerically solving the temporal equation of motion (4.5) (Fig. 4.4) is in good agreement with that obtained by using the perturbation method (Point A of Fig. 4. 3(i)).

Fig. 4.5 shows the time response, phase portrait, and Poincare's section obtained from the temporal equation for a frequency corresponding to point B′ of Fig. 4.3 (i). While the transient response (Fig. 4.5 (a), (c), and (e)) shows a beating type phenomena (obtained with initial point (0.25, 0.01)), the steady state response (Fig. 4.5 (b), (d) and (f)) of the system is found to be periodic. The steady state response amplitude shown in Fig. 4.5 matches well with that shown in Fig. 4.3 (i) point B′.

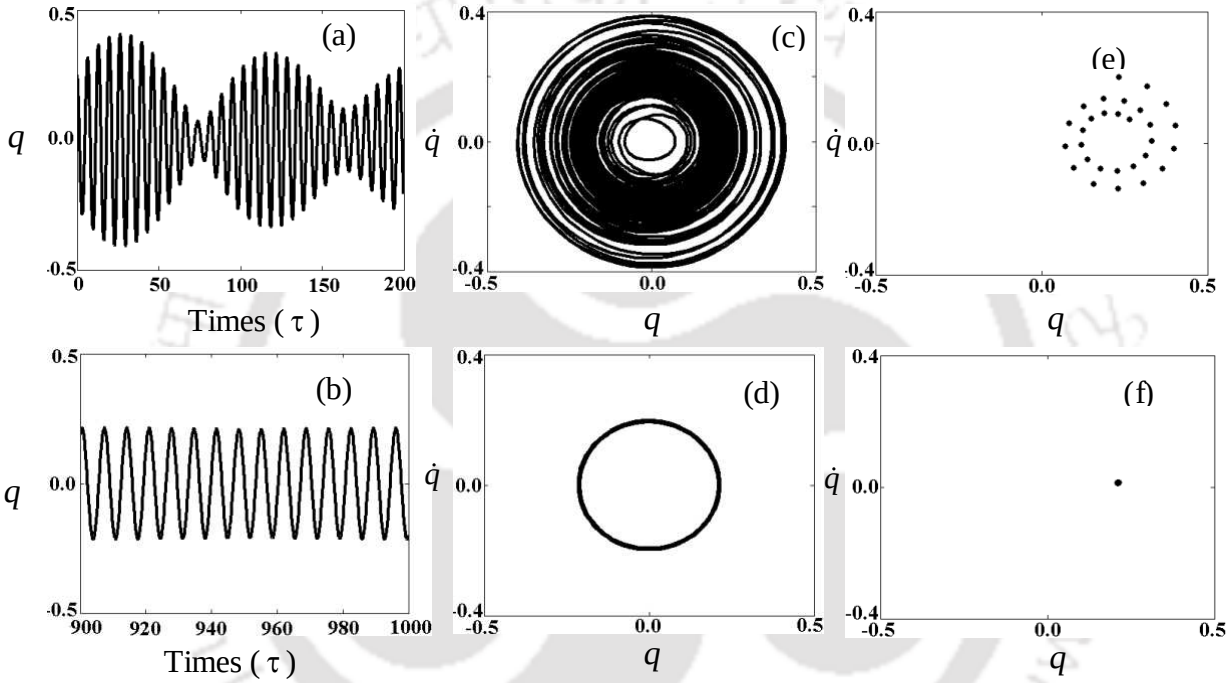

Fig. 4.5. Time response, phase portrait and Poincare's section for the critical points B′ (key as in Fig. 4.3 (i)) where (a, c, e) are the transient response and (b, d, f) are the steady state response.

Figures 4.6 and 4.7 respectively show the steady state time response, and phase portrait corresponding to point C′ and D in Fig. 4.3(i). As the initial point C′ is taken just after the bifurcation point B, the steady state amplitude is found to be matching well with the nontrivial point C''. Clearly it is observed that in all these cases, the steady state response obtained using method of multiple scales are in good agreement with those obtained by numerically solving the temporal equation of motion. Hence, without performing the

tedious and time consuming numerical solution, using equations (4.12 and 4.13) one may obtain the response and stability of the system.

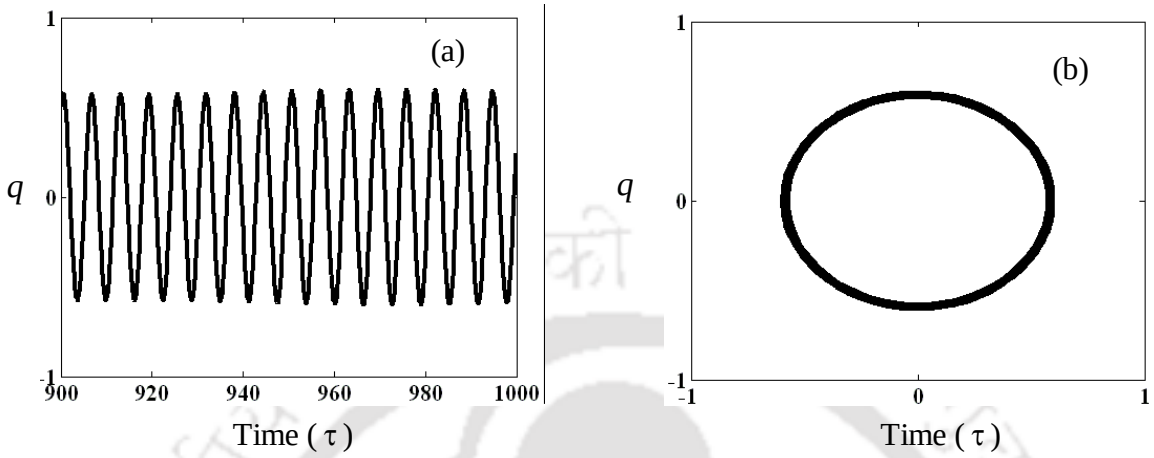

Fig. 4.6. Steady state time response (a) and phase portrait (b) for the critical points C' (key as in Fig. 4.3 (i)).

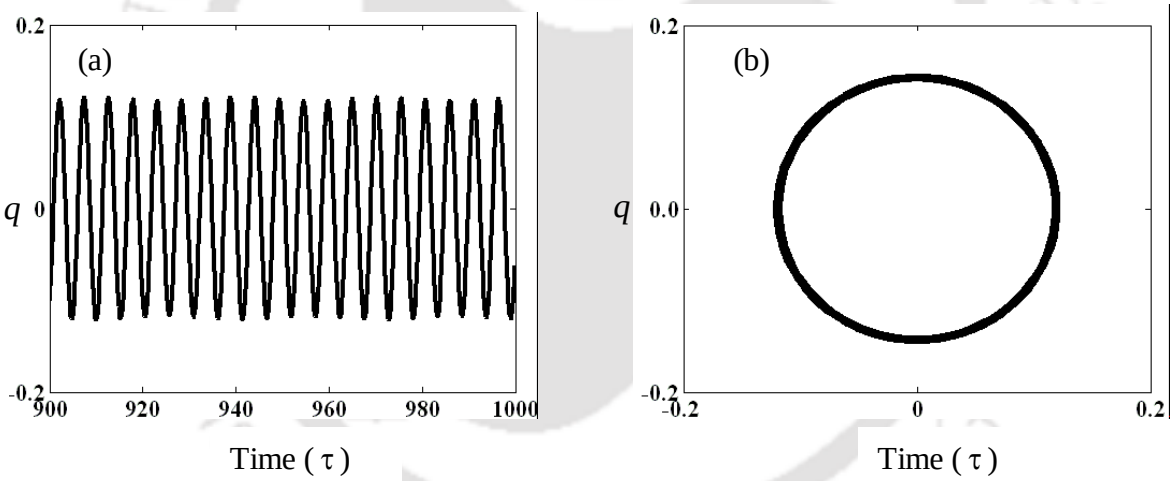

Fig. 4.7. Steady state time response (a) and phase portrait (b) for the critical points D (key as in Fig. 4.3 (i).

Now to study the advantages obtained by using the viscoelastic beam instead of using an elastic beam, the response curve for an elastic beam with same elastic modulus E_1 is plotted as shown in Fig. 4.8. It may be observed from Fig. 4.3 and Fig. 4.8 that in both elastic and viscoelastic manipulator the nature of the response curves remains unchanged. One may observe from Fig. 4.8 that for elastic beam, the jump up and jump down

phenomena occur at the frequency $\overline{\omega}$ equal to 0.92 and 0.5, respectively and corresponding jump lengths are 0.3730 and 1.383, respectively. It is investigated that with a value of damping c_d equal to 0.11 N-s/m, the jump up and jump down phenomenon occur at frequency $\overline{\omega}$ equal to 0.921 and 0.5 and the corresponding jump lengths are 0.3198 and 1.265 as shown in Fig. 3.2 (Chapter 3). One may note that for all the cases, the saddle-node bifurcation point occurs nearly at the same frequency $\overline{\omega}$ equal to 0.92 which is same as that observed in the experimental work of Cuvalci (2000) when the pendulum is in locked position. It may be observed that while the maximum response amplitude for an elastic beam with zero damping is 1.383, with damping factor c_d equal to 0.11 N-s/m, it is 1.265, for the corresponding viscoelastic beam with material loss factor 0.02, it is 0.9797. It shows that the maximum response amplitude in a viscoelastic beam is very less in comparison to that of elastic beam even with higher value of damping.

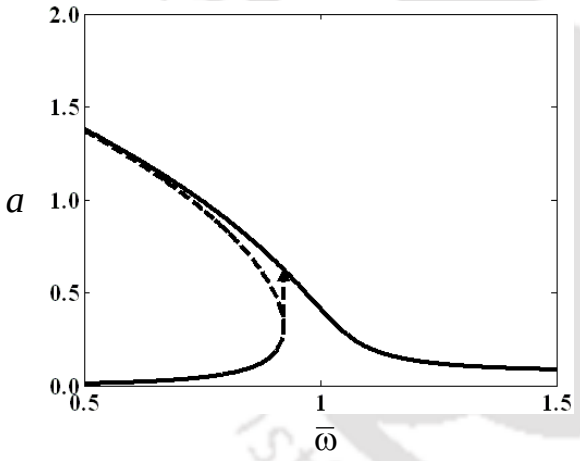

Fig. 4.8. Frequency response curve for elastic beam for $\overline{m} = 1.8787$, $\overline{Z} = 0.00372$.

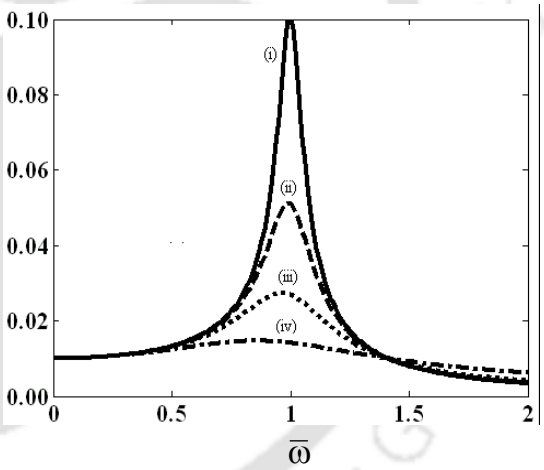

Fig. 4.9. Frequency response for the equivalent spring-mass-damper system (i) $\zeta = 0.05$, ii) $\zeta = 0.1$,(iii) $\zeta = 0.2$ and (iv) $\zeta = 0.5$

To further compare the nonlinear response with that of the linear Kelvin-Voigt model (Gurgoze et al., 2005), the system is reduced to an equivalent base excited single degree of freedom system as shown in Fig. 4.2. The parameters of the equivalent system and the mathematical expression for the frequency response curve are discussed in section 4.3.1.3.

Figure 4.9 shows the frequency response curve obtained for this linear system with different values of internal damping. One may note that in the equivalent Kelvin-Voigt model the maximum amplitude is around 0.1 or less depending on the values of internal damping. These values are very less in comparison to the actual response amplitude obtained using the present nonlinear analysis. As the linear model is giving erroneous result, hence one should go for nonlinear model as suggested in this work.

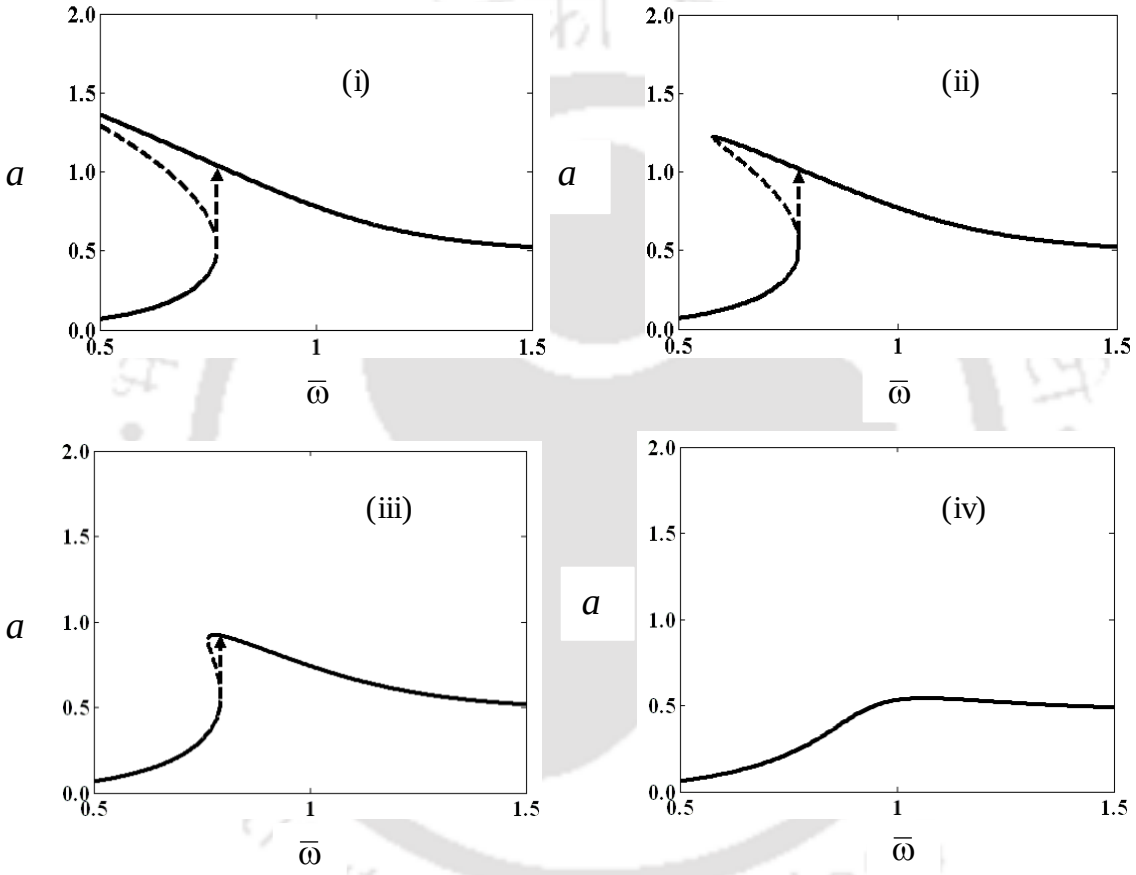

Fig. 4.10. Effect of material loss factor (δ) on the frequency response curve for $\bar{m} = 1.3333$, $\bar{Z} = 0.0333$; (i) $\delta = 0.05$, (ii) $\delta = 0.1$, (iii) $\delta = 0.2$, and (iv) $\delta = 0.5$.

The effect of material loss factor (δ) on the steady state response is studied in Fig. 4.10 where the nondimensional amplitude of base excitation ($\bar{Z}$) and mass ratio ($\bar{m}$) are taken as 0.0333 and 1.3333, respectively. From these figures, it is found that with increase in

material loss factor, the maximum response amplitude reduces and jump length at the critical points decreases.

Also it is seen that for lower value of δ while a bi-stable region exists before the bifurcation point, for higher value of δ the bifurcation point disappears and only a stable nontrivial state with very low response amplitude exists (4.10(iv)). But this response amplitude (Fig. 4.10 (iv)) is still very high in comparison to the value obtained using the linear Kelvin-Voigt model as shown in Fig. 4.9.

Figure 4.11 shows the frequency response curves for two different values of nondimensional amplitude of base excitation $\bar{Z}$ with δ and $\bar{m}$ equal to 0.05 and 1.3333, respectively. One may observe from Fig.4.10 (i) and Fig. 4.11 that with increase in $\bar{Z}$ the maximum response amplitude will increase.

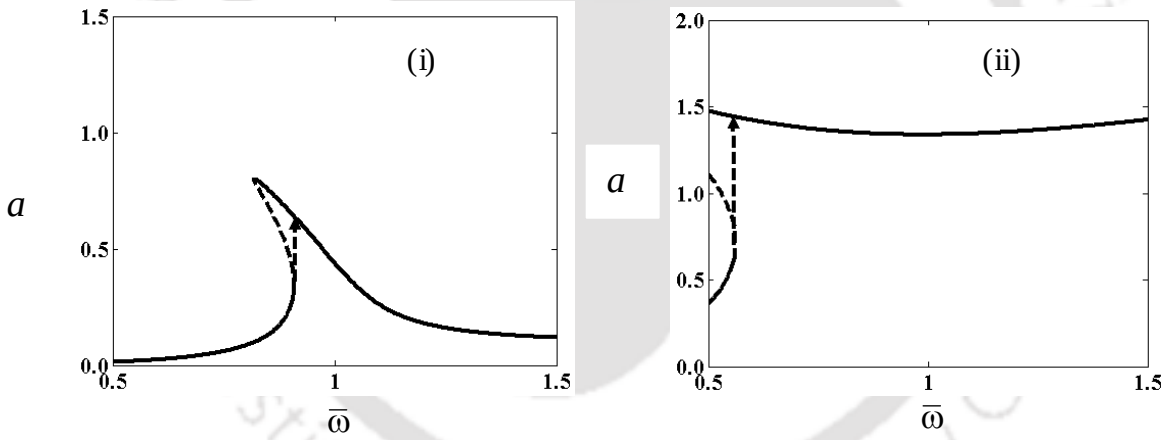

Fig. 4.11. Effect of amplitude of base motion ($\bar{z}$) on the frequency response curve for $\bar{m} = 1.333$, $\delta = 0.05$; (i) $\bar{z} = 0.00667$, (ii) $\bar{z} = 0.1667$.

From Fig. 4.11 and Fig. 4.10 (i), one may find that the saddle-node bifurcation point B occurs at point $\bar{\omega}$ equal to 0.9, 0.77, and 0.56 for $\bar{Z}$ equal to 0.00667, 0.0333 and 0.1667, respectively and the corresponding value of the jump lengths equal to 0.3846, 0.5625 and 0.6533, respectively. Hence, one may note that with increase in $\bar{Z}$, the bifurcation point moves away from $\bar{\omega} = 1.0$ and the jump length will increase. So, the system will be

unstable due to sudden jump up phenomena at a lower value of frequency with increase in $\bar{Z}$.

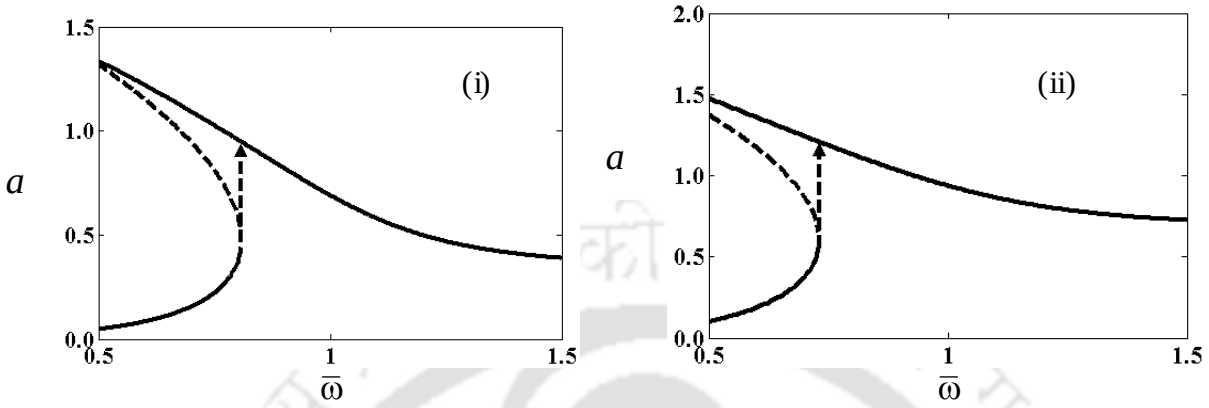

Fig. 4.12. Effect of payload ($\bar{m}$) on the frequency response curve for δ =0.05, $\bar{Z}$ =0.0333; (i) $\bar{m}$ =0.6667, (ii) $\bar{m}$ =2.6667.

The effect of increase in payload $\bar{m}$ on the steady state response is studied in Fig. 4.12. Here, the frequency response curves are plotted with $\bar{Z}$ and δ equal to 0.0333 and 0.05, respectively for $\bar{m}$ equal to 0.6667 (Fig. 4.12 (i)) and 2.6667 (Fig. 4.12 (ii)). One may note from the Fig. 4.10 (i) and Fig. 4.12 that with increase in mass ratio $\bar{m}$ (which may be due to increase in payload mass or decrease in the mass of the beam), the amplitude of the response increases. As the natural frequency of the system decrease with increase in mass ratio, the jump up point is correctly observed to be occurring at a lower frequency $\bar{\omega}$ with increase in $\bar{m}$.

4.3.2.2 Subharmonic Resonance Case ($\bar{\omega} \approx 3$)

Similar to the simple resonance case, here also the influence of material loss factor δ on the steady state response is studied. Fig. 4.13 shows the frequency response curve for four different values of δ (0, 0.01, 0.05, and 0.1) with nondimensional amplitude of base excitation $\bar{Z}$ and mass ratio $\bar{m}$ equal to 0.333 and 0.667, respectively. Similar to that of an elastic beam (Chapter 3), here also the trivial state is stable for a wide range of system parameters. But the perturbation analysis result shows along with this stable trivial

response curve, there also exist nontrivial response curve with saddle-node bifurcation. This bifurcation point occurs at a lower frequency for higher values of δ.

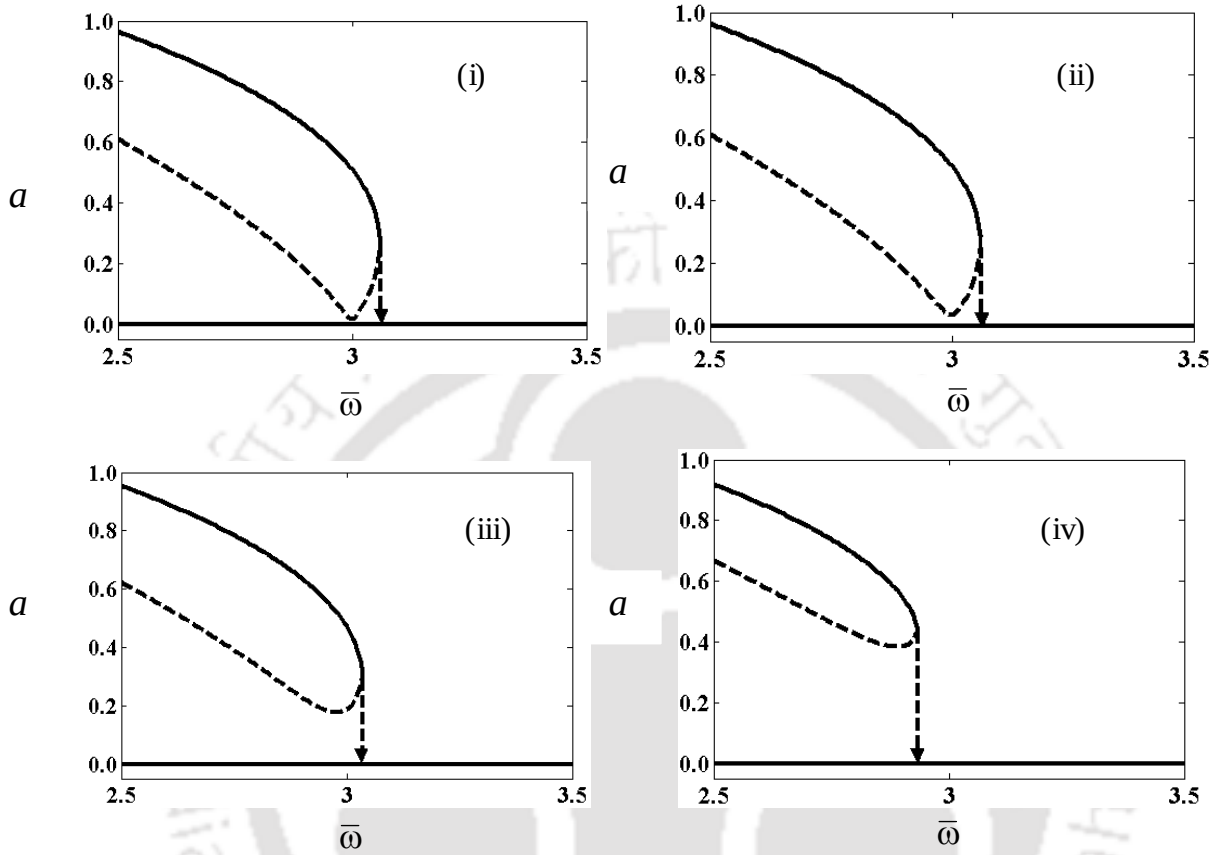

Fig. 4.13. Effect of material loss factor (δ) on the frequency response curve for $\bar{m} = 0.667$, $\bar{Z} = 0.333$ (i) $\delta = 0.0$, (ii) $\delta = 0.01$, (iii) $\delta = 0.05$, and (iv) $\delta = 0.1$.

Figure 4.14 shows the frequency response curves for two different values of $\bar{Z}$ with material loss factor δ and mass ratio $\bar{m}$ equal to 0.05 and 0.6667, respectively. One may observe from Fig. 4.13 (iii) and Fig. 4.14 that with increase in $\bar{Z}$ the maximum response amplitude of the frequency response curve increases. The jump down phenomena starts at the lower values $\bar{\omega}$ with decrease in amplitude ratio $\bar{Z}$.

Figure 4.15 shows the frequency response curve for two different values of mass ratio $\bar{m}$ with δ and $\bar{Z}$ equal to 0.05 and 0.333, respectively. From Fig. 4.15, and Fig. 4.13 (iii)

one may observe that with increase in mass ratio $\bar{m}$, the maximum response decreases. One may also find that with increase in mass ratio, the saddle-node bifurcation point at which the system experiences a jump down phenomena start at a lower frequency.

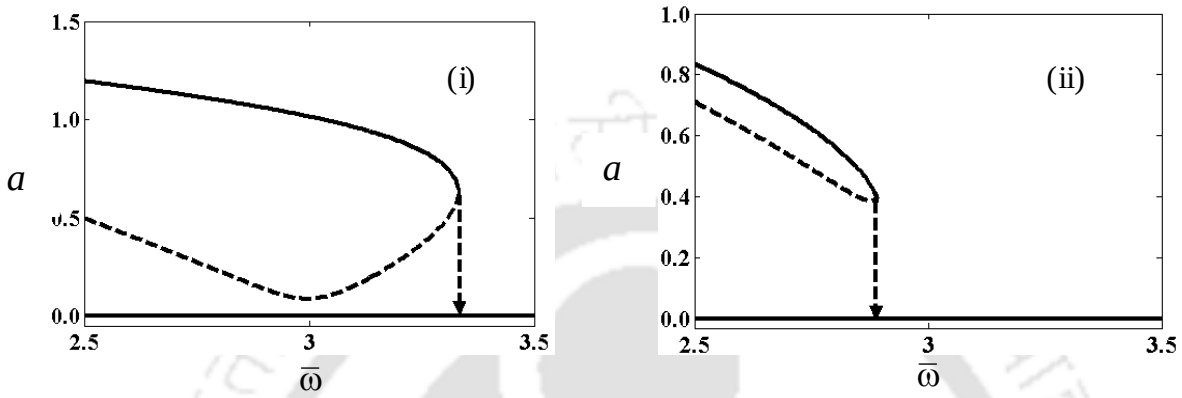

Fig. 4.14.Effect of amplitude of base motion ($\bar{Z}$) on the frequency response curve for $\bar{m} = 0.667$, $\delta = 0.05$; (i) $\bar{Z} = 0.1667$, (ii) $\bar{Z} = 0.6667$.

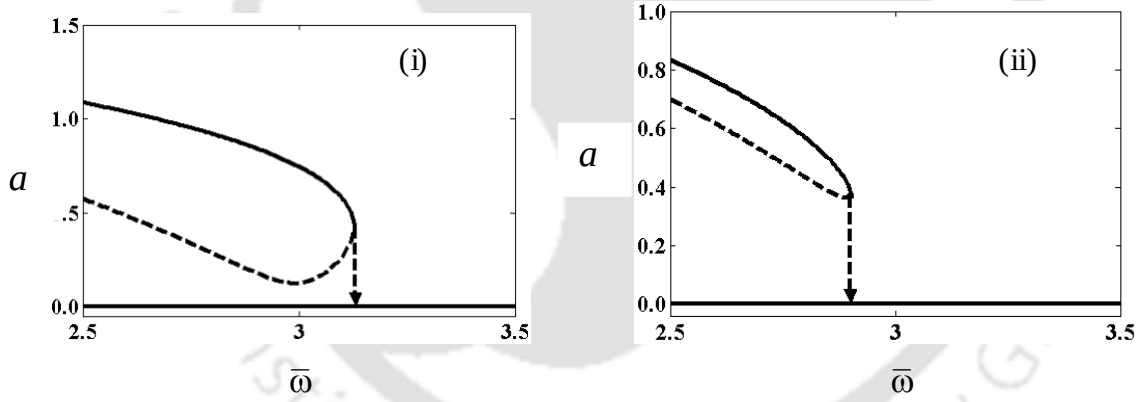

Fig. 4.15.Effect of payload ($\bar{m}$) on the frequency response curve for $\delta = 0.05$, $\bar{Z} = 0.333$; (i) $\bar{m}$ =0.50, (ii) $\bar{m}$ =1.0.

4.4 Viscoelastic Cartesian Manipulator with Sinusoidally Varying Tip Force

4.4.1 Analysis

In this section, the solution of the temporal equation of motion (4.4) of the viscoelastic Cartesian manipulator with harmonically varying axial force is carried out using method of multiple scales. By using similar procedure as explained in sections 3.3.1 and 4.3.1, substituting $T_n = \varepsilon^n \tau$, $n = 0, 1, 2, 3\cdots$ and $q(\tau;\varepsilon) = q_0(T_0, T_1) + \varepsilon q_1(T_0, T_1) + \quad + O(\varepsilon^2)$ in equation (4.4) and equating the coefficients of like powers of ε, one may find the following expressions:

Order $\varepsilon^0 : D_0^2 q_0 + q_0 = 0$, (4.31)

Order $\varepsilon^1 : D_0^2 q_1 + q_1 = -2D_0 D_1 q_0 - 2i\zeta q_0 - \eta q_0^3 - \alpha_1 q_0^3 - \alpha_2 \left(D_0^2 q_0\right) q_0 - \alpha_3 \left(D_0 q_0\right)^2 q_0^2$

$$-\bar{\omega}_1^2 \alpha_4 \cos\left(\bar{\omega}_1 T_0\right) q_0^2 - \bar{\omega}_1^2 \alpha_5 \cos\left(\bar{\omega}_1 T_0\right) + \alpha_6 \cos\left(\bar{\omega}_2 T_0\right) q_0 . \quad (4.32)$$

General solutions of equation (4.30) can be written as

$$q_0 = A(T_1)\exp(iT_0) + \bar{A}(T_1)\exp(-iT_0) . \quad (4.33)$$

Substituting equation (4.33) into equation (4.32) leads to

$$D_0^2 q_1 + q_1 = -\left(2iD_1 A + 2i\zeta A + 3i\eta A^2 \bar{A} + 3\alpha_1 A^2 \bar{A} - 3\alpha_2 A^2 \bar{A} + \alpha_3 A^2 \bar{A}\right)\exp(i\tau)$$

$$+\left(-\alpha_1 + \alpha_2 + \alpha_3\right) A^3 \exp\left(3iT_0\right) - \frac{1}{2}\alpha_4 A^2 \exp i\left(2 + \bar{\omega}_1\right) T_0 - \frac{1}{2}\alpha_4 \bar{A}^2 \exp i\left(\bar{\omega}_1 - 2\right) T_0$$

$$-\left(\alpha_4 A\bar{A} + \frac{1}{2}\alpha_5\right)\exp i\left(\bar{\omega}_1 T_0\right) + \frac{\alpha_6}{2}\left[A\exp i(\bar{\omega}_2 + 1) + \bar{A}\exp i(\bar{\omega}_2 - 1)\right] T_0 + cc . \quad (4.33)$$

Here, *cc* stands for the complex conjugate of the preceding terms. Unlike the previous case of viscoelastic manipulator without axial force, here the system has five different resonance conditions viz., (i) $\bar{\omega}_1 \approx 1$ and $\bar{\omega}_2$ is away from 2; (ii) $\bar{\omega}_2 \approx 2$ and $\bar{\omega}_1$ is away from 1 and 3; (iii) when $\bar{\omega}_1 \approx 1$ and $\bar{\omega}_2 \approx 2$; (iv) $\bar{\omega}_1 \approx 3$ and $\bar{\omega}_2$ is away from 2; (v) $\bar{\omega}_2 \approx 2$ and $\bar{\omega}_1 \approx 3$. Neglecting the last two higher order resonance conditions i.e., the subharmonic

($\bar{\omega}_1 \approx 3$ and $\bar{\omega}_2$ is away from 2) and the simultaneous resonance conditions $\bar{\omega}_1 \approx 3$ and $\bar{\omega}_2 \approx 1$, in the following subsections, three resonance conditions viz., (i) simple resonance ($\bar{\omega}_1 \approx 1$ and $\bar{\omega}_2$ is away from 2), (ii) principal parametric resonance condition ($\bar{\omega}_2 \approx 2$ and $\bar{\omega}_1$ is away from 1 or 3), and (iii) simultaneous resonance conditions ($\bar{\omega}_1 \approx 1$ and $\bar{\omega}_2 \approx 2$) are studied.

4.4.1.1 Simple Resonance Due to Support Motion ($\bar{\omega}_1 \approx 1$ and $\bar{\omega}_2$ is away from 2)

Similar to the previous case, using detuning parameter σ as $\bar{\omega}_1 = 1 + \varepsilon\sigma$ in equation (4.33), one may obtain the following secular or small divisor terms.

$$2iA' + 2i\zeta A + 3i\eta A^2\bar{A} + 3\alpha_1 A^2\bar{A} - 3\alpha_2 A^2\bar{A} + \alpha_3 A^2\bar{A} + \frac{1}{2}\alpha_4 A^2 \exp i\left(-\sigma T_1\right) + \left(\alpha_4 A\bar{A} + \frac{1}{2}\alpha_5\right)\exp i\left(\sigma T_1\right) = 0. \quad (4.34)$$

Putting A equal to $\frac{1}{2}a\left(T_1\right)e^{\left(i\beta T_1\right)}$ and $\gamma = \sigma T_1 - \beta$ into equation (4.34) and separating the real and imaginary terms, one may obtain a set of reduced equations as given below.

$$a' = -\zeta a - \frac{3}{8}\eta a^3 - \bar{\omega}_1^2\left(\frac{\alpha_4}{8}a^2 + \frac{1}{2}\alpha_5\right)\sin\gamma\,, \quad (4.35)$$

$$a\gamma' = a\sigma - \frac{3}{8}\left(\alpha_1 - \alpha_2 + \frac{\alpha_3}{3}\right)a^3 - \bar{\omega}_1^2\left(\frac{3\alpha_4}{8}a^2 + \frac{1}{2}\alpha_5\right)\cos\gamma\,. \quad (4.36)$$

The response of the system can be determined by numerically solving equations (4.35) and (4.36), simultaneously. To find the stability of the steady state responses, one may follow similar procedure as in previous sections and obtain the Jacobian matrix (J) as given below which is similar to the equation 4.16.

$$J=\begin{bmatrix} -\zeta-\dfrac{9\eta a_o^2}{8}+\dfrac{\dfrac{1}{2}\alpha_4 a_0\left(\zeta a_0+\dfrac{3}{8}\eta a_0^3\right)}{\dfrac{1}{8}\alpha_2 a_0^2+\dfrac{1}{2}\alpha_5} & -\dfrac{\left(\dfrac{1}{8}\alpha_4 a_0^2+\dfrac{1}{2}\alpha_5\right)\left(\sigma a_0-\dfrac{3}{8}Ka_0^3\right)}{\dfrac{3}{8}\alpha_4 a_0^2+\dfrac{1}{2}\alpha_5} \\ -\dfrac{3Ka_0}{4}-\dfrac{3}{4}\dfrac{\alpha_4\left(\sigma a_0-\dfrac{3}{8}Ka_0^3\right)}{\dfrac{3}{8}\alpha_4 a_0^2+\dfrac{1}{2}\alpha_5}+ & -\dfrac{\left(\dfrac{3}{8}\alpha_4 a_0^2+\dfrac{1}{2}\alpha_5\right)\left(\zeta+\dfrac{3}{8}\eta a_0^2\right)}{\dfrac{1}{8}\alpha_4 a_0^2+\dfrac{1}{2}\alpha_5} \\ \dfrac{\sigma a_0-\dfrac{3}{8}Ka_0^3}{a^2} & \end{bmatrix}. \quad (4.37)$$

Here, $K=\alpha_1-\alpha_2+\dfrac{\alpha_3}{3}$. It may be noted that the system will be stable if and only if all the real parts of the eigen-values are negative. Now the first order nontrivial steady state response of the cantilever beam with a tip mass can be given by

$$q=a\cos\left(\bar{\omega}_1\tau-\gamma\right). \quad (4.38)$$

4.4.1.2 Principal Parametric Resonance Due to Harmonically Varying Force ($\bar{\omega}_2\approx 2$ and $\bar{\omega}_1$ is away from 1 or 3)

Using $\bar{\omega}_2=2+2\varepsilon\sigma$ where σ is the detuning parameter, in equation (4.33), one may obtain the following secular or small divisor terms.

$$-\left(2iD_1A+2i\zeta A+3i\eta A^2\bar{A}\right)\exp(iT_0)-\left(3\alpha_1-3\alpha_2+\alpha_3\right)A^2\bar{A}\exp(iT_0)+\frac{\alpha_6}{2}\bar{A}\exp\left(2\sigma T_1\right)=0. \quad (4.39)$$

Putting A equal to $\dfrac{1}{2}a\left(T_1\right)e^{\left(i\beta T_1\right)}$ into equation (4.39) and separating the real and imaginary terms, one may find the following reduced equations.

$$\dot{a}=-\zeta a-\frac{3}{8}\eta a^3-\frac{\alpha_6}{4}a\sin\gamma, \quad (4.40)$$

$$a\dot{\gamma}=2a\sigma-\frac{3}{4}\left(\alpha_1-\alpha_2+\frac{\alpha_3}{3}\right)a^3-\frac{\alpha_6}{2}a\cos\gamma. \quad (4.41)$$

Here, $\gamma = \sigma\tau - \beta$. For steady state, $\dot{a} = 0$ and $\dot{\gamma} = 0$. From equations (4.40), and (4.41), one may observe that the system possesses both trivial and nontrivial responses which can be determined by solving these equations, simultaneously. To find the stability of the steady state responses, one may investigate eigen-values of the Jacobian matrix (J) which is given by

$$J = \begin{bmatrix} -\zeta - \frac{9}{8}\eta a_0^2 - \frac{\alpha_6}{4}\sin\gamma_0 & \frac{\alpha_6}{4} a_0 \cos\gamma_0 \\ -\frac{3}{2}\left(\alpha_1 - \alpha_2 + \frac{\alpha_3}{3}\right) a_0 & -\frac{\alpha_6}{2}\sin\gamma_0 \end{bmatrix}. \qquad (4.42)$$

For this case the system will be stable if and only if all the real parts of the eigen-values are negative. Now the first order nontrivial steady state response of the system can be given as

$$q = a\cos\left(\frac{\bar{\omega}_2\tau}{2} - \gamma\right). \qquad (4.43)$$

4.4.1.3 Simultaneous Resonance Case ($\bar{\omega}_1 \approx 1$ and $\bar{\omega}_2 \approx 2$)

Following similar procedure as described in section 3.4.1.3, here one may use the detuning parameter σ and phase angle ϕ to express the nearness of $\bar{\omega}_1$ to 1 and $\bar{\omega}_2$ to 2 as given below.

$$\bar{\omega}_1 = 1 + \varepsilon\sigma, \text{ and } \bar{\omega}_2\tau = 2\bar{\omega}_1\tau + \phi, \ \sigma = O(1). \qquad (4.44)$$

Substituting equation (4.44) into equation (4.33), one may obtain the following equation:

$$2iA' + 2i\zeta A + 3\eta A^2\bar{A} - 3\alpha_1 A^2\bar{A} - 3\alpha_2 A^2\bar{A} + \alpha_3 A^2\bar{A} + \frac{1}{2}\alpha_4 A^2 \exp i\left(-\sigma_1 T_1\right) +$$

$$\left(\alpha_4 A\bar{A} + \frac{1}{2}\alpha_5\right)\exp i\left(\sigma_1 T_1\right) + \frac{\alpha_6}{2}\bar{A}\exp\left(2\sigma_2 T_1\right) = 0. \qquad (4.45)$$

Similar to the previous cases, substituting A equal to $\frac{1}{2}a\left(T_1\right)e^{\left(i\beta T_1\right)}$ in equation (4.45) and separating the real and imaginary parts, yields the following reduced equations:

$$\dot{a} = -\zeta a - \frac{3}{8}\eta a^3 - \left(\frac{\alpha_4}{8}a^2 + \frac{1}{2}\alpha_5\right)\sin\gamma - \frac{1}{4}\alpha_6 a\sin(2\gamma + \phi), \qquad (4.46)$$

$$a\dot{\gamma} = a\sigma_1 - \frac{3}{8}\left(\alpha_1 - \alpha_2 + \frac{\alpha_3}{3}\right)a^3 - \left(\frac{3\alpha_4}{8}a^2 + \frac{1}{2}\alpha_5\right)\cos\gamma - \frac{1}{4}\alpha_6\, a\cos(2\gamma+\phi). \quad (4.47)$$

Here, $\gamma = \sigma_1\tau - \beta$. For steady state response (a_0, γ_0), $\dot{a}$ and $\dot{\gamma}$ equal to zero. One may obtain the response (a,γ) numerically by solving the equations (4.46), and (4.47), simultaneously. The stability of the steady state fixed-point response can be determined by finding the eigen-values of the Jacobean matrix (J). The Jacobian matrix is given below.

$$J = \begin{bmatrix} -\zeta - \frac{9}{8}a_0^2 - \frac{1}{4}\alpha_4 a_0 \sin\gamma_0 - \frac{1}{4}\alpha_6 \sin(2\gamma_0+\phi) & -\left(\frac{1}{8}\alpha_4 a_0^2 + \frac{1}{2}\alpha_5\right)\cos\gamma_0 - \frac{1}{2}\alpha_6 a_0 \cos(2\gamma_0+\phi) \\ -\frac{3}{4}\left(\alpha_1 - \alpha_2 + \frac{\alpha_3}{3}\right)a_0 - \frac{3}{4}\alpha_4\cos\gamma_0 - \frac{3(\alpha_4 a_0^2 + 4\alpha_5)\cos\gamma_0}{8a_0^2} & \frac{3(\alpha_4 a_0^2 + 4\alpha_5)\sin\gamma_0}{8a_0} + \frac{1}{2}\alpha_6 \sin(2\gamma_0+\phi) \end{bmatrix}. \quad (4.48)$$

Thus for this condition, the system is stable if the real part of the all eigenvalues of the Jacobian matrix (J) are negative.

4.4.2 Numerical Results and Discussions

Here, the numerical results of a viscoelastic Cartesian manipulator subjected to harmonically varying tip force are discussed. Same system parameters as in section 4.3.2 are taken for the numerical analysis. Unlike the case of manipulator without axial force as in section 4.3.1, here both book-keeping parameter (ε) and scaling factor ($\bar{r}$) are considered as 0.1. Similar to the system with elastic manipulator subjected to the axial force as discussed in section 3.4.2, here also the system is subjected to two frequency excitations and has three different types of resonance conditions. Theses resonance conditions viz., simple resonance, principal parametric resonance and simultaneous resonance conditions are studied in subsection 4.4.2.1, 4.4.2.2, 4.4.2.3, respectively.

4.4.2.1 Simple Resonance Due to Support Motion ($\bar{\omega}_1 \approx 1$ and $\bar{\omega}_2$ away from 2)

Here, the roller-supported end of the Cartesian manipulator is harmonically excited with a frequency nearly equal to the natural frequency of the system and the frequency of the applied tip load is away from the principal parametric resonance zone. Figure 4.16 shows the influence of material loss factor (δ) on the frequency response curves for $\bar{m} = 1.0$, $\bar{P}_0 = 0.0$, and $\bar{Z} = 0.0166$. From the reduced equations (4.35, 4.36), it is noted that the system does not have any trivial solution ($a = 0$). Therefore, here the manipulator may always resonate with a magnitude equal to the nontrivial response as shown in Fig. 4.16. It is observed from the Fig. 4.16 that while the amplitude (a) of the manipulator with material loss factor δ equal to zero which is similar to an elastic manipulator, is equal to 3.0, the amplitude of the viscoelastic manipulator with $\delta = 0.15$, is equal to 1.7.

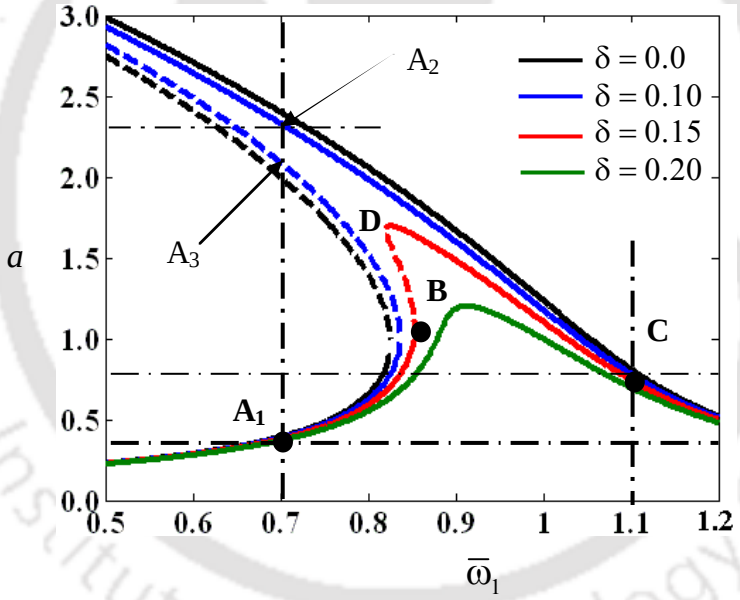

Fig. 4.16. Influence of material loss factor (δ) on the frequency response curves for $\bar{m} = 1.0$, $\bar{P}_0 = 0.0$, and $\bar{Z} = 0.0166$.

With further increase in δ, for example, $\delta = 0.2$, the system behaves similar to a linear single degree freedom system with maximum response amplitude equal to 1.25. Hence, peak amplitude at resonance of the nontrivial response is significantly reduced by increasing material loss factor. Therefore, one may note that by using a manipulator with

loss factor $\delta \geq 0.2$, the system will vibrate sinusoidally with bounded response amplitude. When the manipulator is started with a frequency $\bar{\omega}_1$ equal to 0.6, with increase in frequency the manipulator will attain a critical frequency at saddle-node bifurcation point B (Fig. 4.16). At this point with further increase in frequency, the manipulator will experience jump up phenomenon. Due to this sudden jump, the manipulator may undergo catastrophic failure or oscillate with amplitude corresponding to the stable nontrivial response. For lower value of material loss factor (e. g., $\delta = 0.15$), while switching of the manipulator from a higher frequency (e.g., point C, Fig. 4.16), the system will undergo a second catastrophic failure due to the jump down phenomena at the saddle-node bifurcation point D. It may be noted that irrespective of material loss factor the system response remains unchanged upto a frequency corresponding to point A as marked in Fig. 4.16.

From the figure (Fig. 4.16), one may observe a bistable region between point B and point D where the initial condition determines which steady state solution is physically attainable by the system. To show the importance of initial condition, the basin of attraction in the $a - \gamma$ plane is plotted in Fig. 4.17 corresponding to δ equal to 0.1, and $\bar{\omega}_1$ equal to 0.7 and 1.1. This is obtained by solving the reduced equations (4.35, 4.36). It may clearly be observed from Fig. 4.17 (i) that corresponding $\bar{\omega}_1 = 0.7$, the system has two stable focuses at point A_1 and A_2, and a saddle point at A_3. These points are same as the points marked in Fig. 4.16. Corresponding to $\bar{\omega}_1$ equal to 1.1, the basin of attraction Fig. 4.17 (ii), clearly depicts a single stable focus (point C) which is in good agreement with point shown in Fig. 4.16.

To evaluate the accuracy of the perturbation results, one may compare the response curves obtained by the method of multiple scales with the response obtained numerically by solving the temporal equation of motion (4.4). Figures 4.18 displays the steady state time responses, and phase portraits of the manipulator with system parameters corresponding to

points A, B, and C marked in Fig. 4.16 for δ equal to 0.15 and are found to be in good agreement with those determined by using the method of multiple scales in Fig. 4.16.

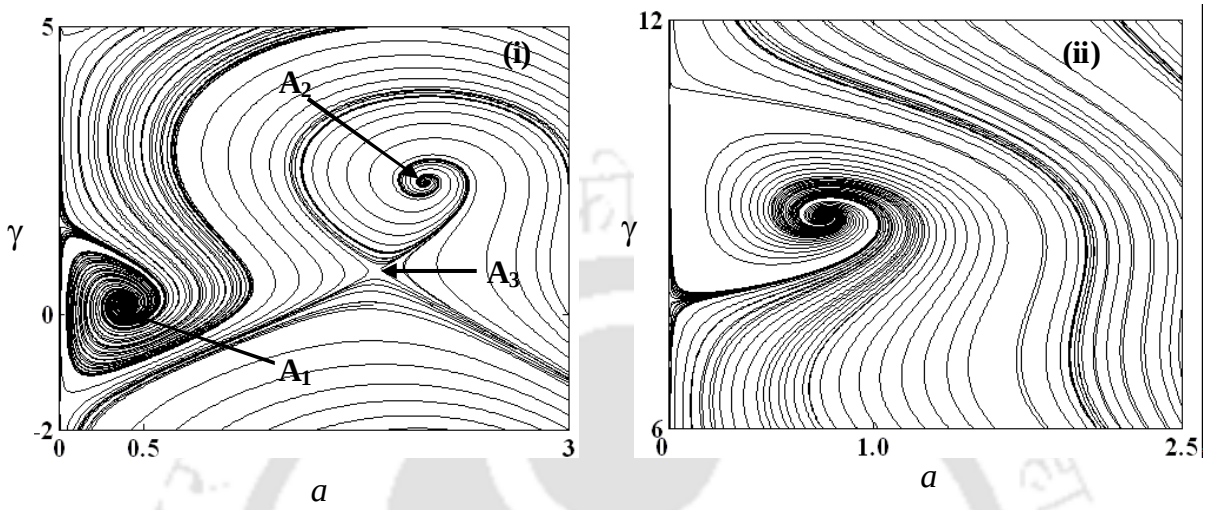

Fig. 4.17. Basin of attraction (i) $\bar{\omega}$ equal to 0.7 (ii) $\bar{\omega}$ equal to 1.1. Key as in Fig. 4.16 for δ equal to 0.1

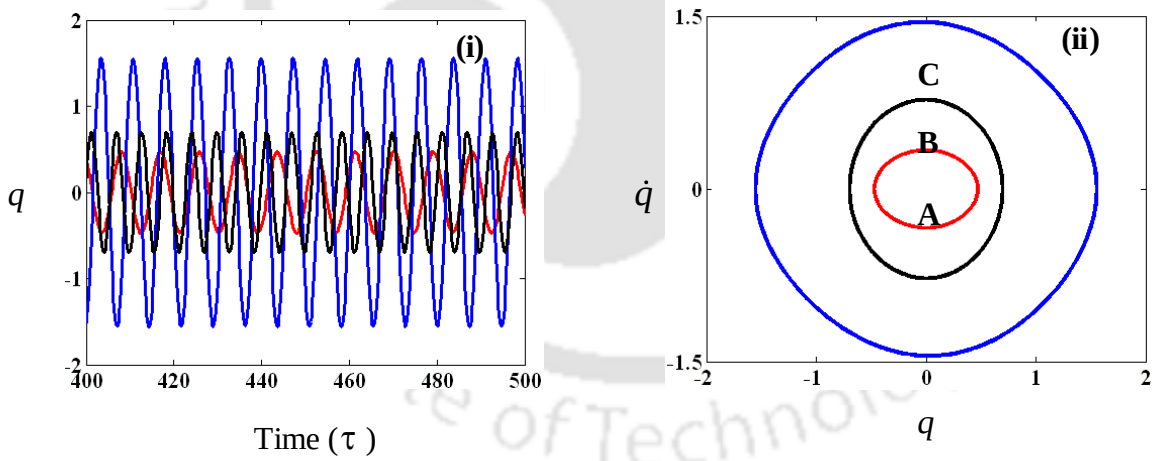

Fig. 4.18. (i) Time responses and (ii) phase portraits for points A, B, and C for δ equal to 0.15. Key as in Fig. 4.16.

Figure 4.19 shows the frequency response curves for two different values of amplitude of support motion $\bar{Z}$, with payload mass $\bar{m}$, material loss factor δ and amplitude of static

loading $\bar{P}_0$ equal to 1.0, 0.15 and 0.0, respectively. With increase in $\bar{Z}$, both the nonlinear response amplitude and jump up length of the system increases. It is observed that for lower value of $\bar{Z}$, the system has stable nontrivial response for the whole range of considered frequency. Hence, it is expected that there may exist a critical value of $\bar{Z}$ below which the system always has a bounded nontrivial response. The saddle-node bifurcation point (B) starts at lower values of frequency $\bar{\omega}_1$ with increase in $\bar{Z}$.

Figure 4.20 shows the frequency response curves for two different values of the amplitude of the static load $\bar{P}_0$. It may be noted from Fig. 4.16 and Fig. 4.20 that unlike the elastic manipulator, here with increase in $\bar{P}_0$, the response amplitude decrease slightly. This is due to the fact that with increase in $\bar{P}_0$, the system fundamental natural frequency increases which decreases both the nonlinear damping term (η) and nonlinear geometric term (α_1). As in the elastic manipulator where the both linear and nonlinear damping terms reduces with increases in $\bar{P}_0$, in viscoelastic manipulator only the nonlinear damping term gets reduced. While with decrease in damping (η), the system response increases, with decrease in geometric nonlinear term (α_1), the response amplitude of the system reduces. Therefore, overall response amplitude reduces with increase in $\bar{P}_0$. With increase in $\bar{P}_0$, the change in the critical value of $\bar{\omega}_1$ at which the bifurcation occurs (i.e., point B) is marginal.

Figure 4.21 shows the effect of payload mass ($\bar{m}$) on the frequency response curves. From Fig 4.21 and Fig. 4.16, one may observe that with increase in $\bar{m}$, the response amplitude increases significantly. It may also be noted that with increase in $\bar{m}$, the critical bifurcation point B starts at a lower frequency $\bar{\omega}_1$.

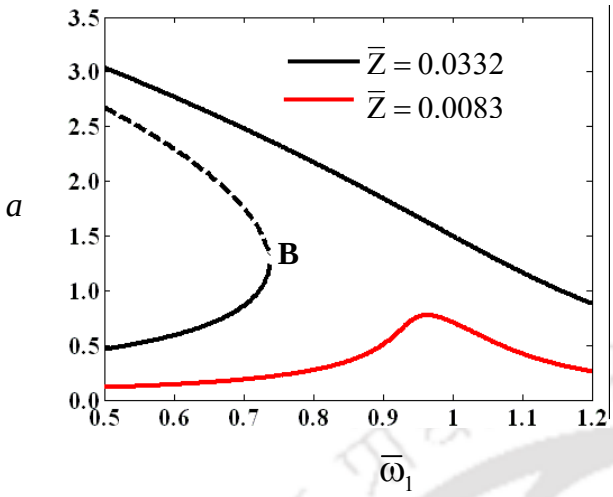

Fig. 4.19. Influence of amplitude of support motion ($\bar{Z}$) on the frequency response curves for $\bar{m} = 1.0$, $\bar{P}_0 = 0.0$, $\bar{Z} = 0.0166$.

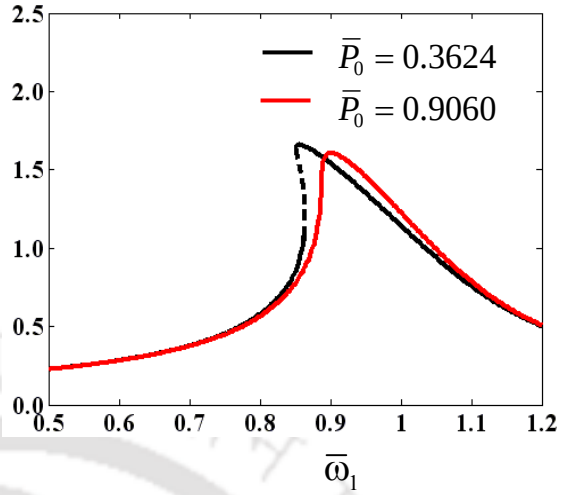

Fig. 4.20. Influence of amplitude of static load ($\bar{P}_0$) on the frequency response curves for $\bar{Z} = 0.0166$, $\bar{m} = 1.0$, $\delta = 0.15$.

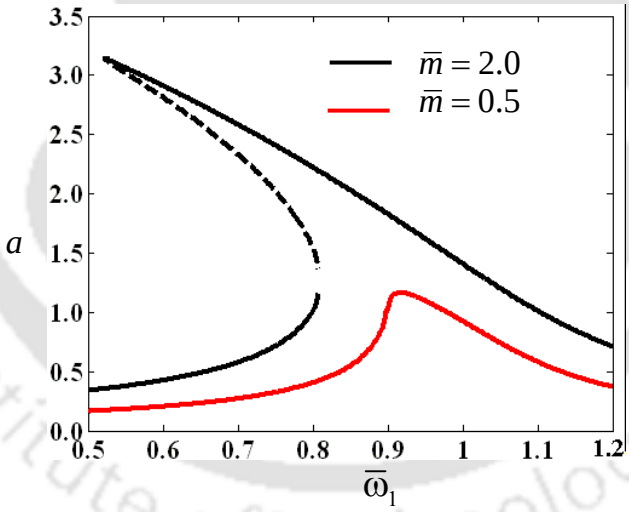

Fig. 4.21. Influence of payload mass ($\bar{m}$) on the frequency response curves for $\bar{Z} = 0.0166$, $\bar{P}_0 = 0.0$, $\delta = 0.15$.

4.4.2.2 Principal Parametric Resonance Due to Tip Loading ($\bar{\omega}_2 \approx 2$ and $\bar{\omega}_1$ away from 1)

In this case, the manipulator is subjected to an axial load at the tip with a frequency nearly equal to twice the natural frequency of the system and the frequency of the support motion at the roller-supported end is away from the natural frequency of the system. In Fig. 4.22 (i), the frequency response curve of the system is plotted for material loss factor δ = 0.2, payload $\bar{m} = 1.0$, amplitude of static loading $\bar{P}_0 = 0.0$ and amplitude of dynamic loading $\bar{P}_1 = 0.3624$.

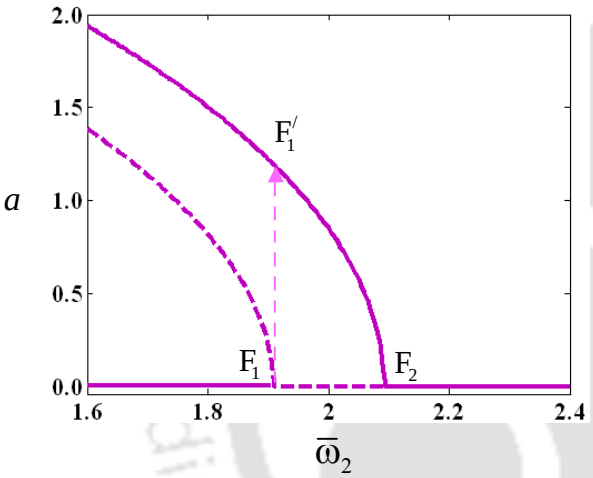

Fig. 4.22. Frequency response curves for material loss factor δ = 0.2, $\bar{m} = 1.0$, $\bar{P}_0 = 0.0$, $\bar{P}_1 = 0.3624$.

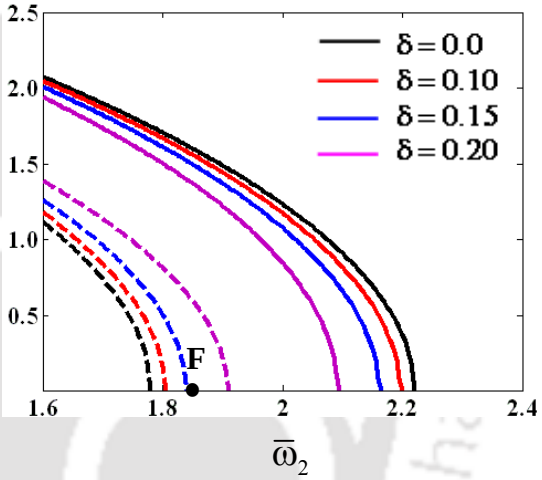

Fig. 4.23. Influence of material loss factor (δ) on the frequency response curves for $\bar{m} = 1.0$, $\bar{P}_0 = 0.0$, $\bar{P}_1 = 0.3624$.

It is found that the system has both trivial and nontrivial responses. In other words, irrespective of the frequency of the base motion at the roller-supported end, the system will not vibrate if the frequency of the dynamic loading is below the sub-critical pitchfork bifurcation point marked by point F_1 or if it operates at a frequency which is above the super-critical pitchfork bifurcation point marked by point F_2. With increase in the frequency $\bar{\omega}_2$ beyond this critical point F_1, the manipulator may fail due to a catastrophic jump up phenomenon or the manipulator may starts vibrating with amplitude equal to that of the nontrivial state marked by point F_1'. In the region F_1F_2, the manipulator will vibrate

with amplitude equal to that of the nontrivial stable state corresponding to $\bar{\omega}_2$. This vibration will continue till it reaches the super-critical pitchfork bifurcation point F_2. It should be noted that the system has a bi-stable region before the sub-critical pitchfork bifurcation point F_1 and hence, depending on the initial conditions, the manipulator may be at stationary position (trivial state) or vibrate with amplitude corresponding to frequency $\bar{\omega}_2$ as marked in Fig. 4.22.

The effect of the material loss factor δ on the frequency response curves is shown in Fig. 4.23. In this figure only the nontrivial state is plotted. As in Fig. 4.22, here also the trivial state is unstable between the sub-and super critical pitchfork bifurcation points from which the nontrivial branch originates. It is found that with increase in δ, both nontrivial response amplitude and trivial unstable region F_1F_2 decreases. For example, while a point F corresponding to $\bar{\omega}_2$ equal to 1.85, is in the unstable trivial region for the value of δ equal to 0.10, it will be in the stable region for δ equal to 0.2. From this observation, it may be noted that the system response can be brought to the stable trivial state by increasing δ. Thus, to control the vibration of the manipulator, it is better to operate the manipulator below its sub-critical pitchfork frequency.

Figure 4.24 shows the influence of dynamic loading ($\bar{P}_1$) on the frequency response curves for $\bar{m} = 1.0$, $\bar{P}_0 = 0.0$, and δ = 0.15. From this figure, one may observe that with increase in the amplitude of the dynamic loading $\bar{P}_1$, the response amplitude of the system increases and the range of unstable trivial state between sub and super critical pitchfork bifurcation points F_1F_2 increases.

Figure 4.25 shows the frequency response curves for two different values of the amplitude of static load $\bar{P}_0$. It is observed that with increase in $\bar{P}_0$, the response amplitude increases and the unstable trivial range between the sub and super critical pitchfork bifurcation point (F_1F_2) decreases. Unlike the case of dynamic loading, here with increase in $\bar{P}_0$, the

unstable trivial range decreases which may be due to fact that the stiffness and hence the natural frequency increases with increase $\bar{P}_0$. Hence, to control the vibration the manipulator may be safely operated upto a higher frequency using a lower value of $\bar{P}_1$ and a higher value of $\bar{P}_0$.

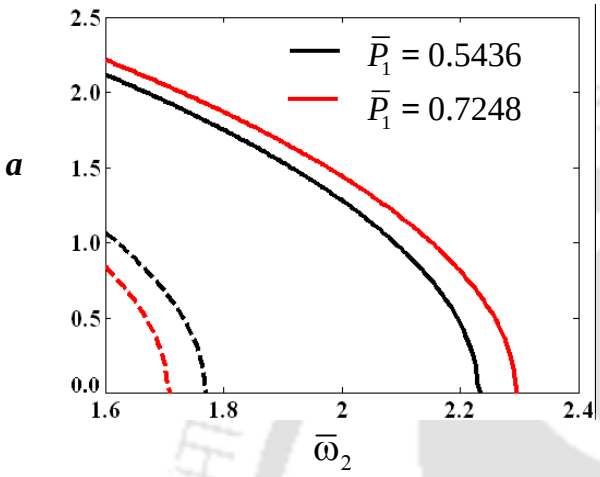

Fig. 4.24. Influence of dynamic loading ($\bar{P}_1$) on the frequency response curves for $\bar{m} = 1.0, \bar{P}_0 = 0.0, \delta = 0.15$.

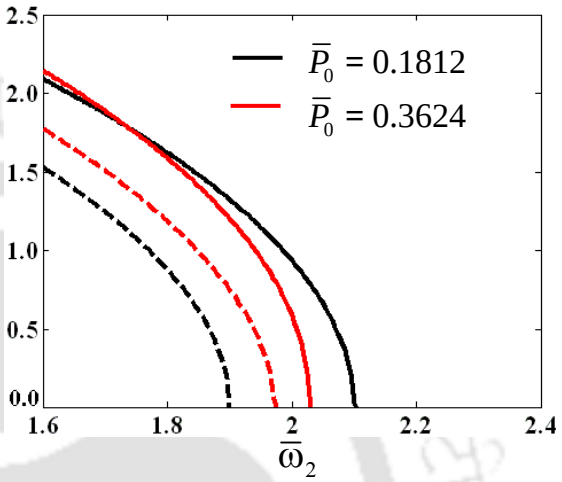

Fig. 4.25. Influence of static loading ($\bar{P}_0$) on the frequency response curves for $\bar{m} = 1.0, \bar{P}_1 = 0.3624, \delta = 0.15$.

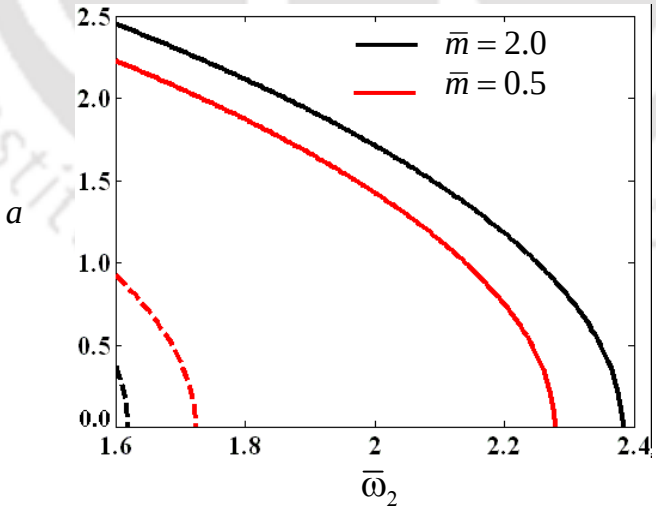

Fig. 4.26. Influence of payload ($\bar{m}$) on the frequency response curves for $\bar{P}_0 = 0.0, \bar{P}_1 = 0.3624, \delta = 0.15$.

The frequency response curves for two different values of mass ratio $\bar{m}$ are shown in Fig. 4.26. One may note from Fig 4.23 and Fig. 4.26 that with increase in $\bar{m}$ both the response amplitude and the unstable trivial range F_1F_2 increases. Similar to the previous cases, the sub-critical pitchfork bifurcation point occurs at a lower frequency $\bar{\omega}_2$.

4.4.2.3 Simultaneous Resonance Condition ($\bar{\omega}_1 \approx 1$ and $\bar{\omega}_2 \approx 2$)

Here, the roller-supported end of the manipulator is excited sinusoidally with a frequency nearly equal to the first natural frequency of the system and also it is subjected to a harmonic tip load with a frequency nearly equal to twice the natural frequency of the system. Like simple resonance case, here also it is observed that the system has only nontrivial response. Similar to the observation made in case of elastic manipulator with simultaneous resonance condition (section 3.4.2.3), here also, in additional to the zones present in simple resonance condition, one may find an additional region in the frequency response curves (region S_2 of Fig. 4.27). The system has tri-stable regions with two saddle-node bifurcation points (C_1, C_2) instead of bi-stable region as found in simple resonance cases.

Figure 4.27 shows the effect of material loss factor δ on the frequency responses for $\bar{m} = 1.0$, $\bar{P}_0 = 0.0$, $\bar{P}_1 = 0.3624$, and $\bar{Z} = 0.0166$ for four different values of material loss factor ($\delta = 0.0, 0.1, 0.15, 0.2$). From the Fig. 4.27, it is observed that with increase in δ, while the region S_1 remains unchanged, the region S_2 gets reduced and with higher value of δ it disappears as shown in Fig. 4.27(iv). For less value of δ (e.g., $\delta \leq 0.125$), the saddle–node bifurcation point C_1 precedes saddle-node bifurcation point C_2 and hence, if the excitation frequency exceeds the critical point C_1, the response may jump to stable nontrivial state in region S_2 (e.g., point C'_1). With further increase in frequency beyond critical point C_2, the system undergoes a second jump up phenomenon from C_2 to point C'_2. Due to the presence of tri-stable region before the saddle-node bifurcation point C_1, the initial condition in this region will play an important role to find the appropriate steady-state response. Hence, in order to know the influence of initial condition, basin of

attraction is plotted in the a – γ plane corresponding to $\bar{\omega}_1$ equal to 0.7 and 0.8 as shown in Fig. 4.28. It is observed that the system has three stable responses (P_1, P_2 and P_3) corresponding to $\bar{\omega}_1$ equal to 0.7 (Fig. 4.27, iii) and two stable responses corresponding to $\bar{\omega}_1$ equal to 0.8. To find the appropriate steady-state solution, proper domain has to be chosen.

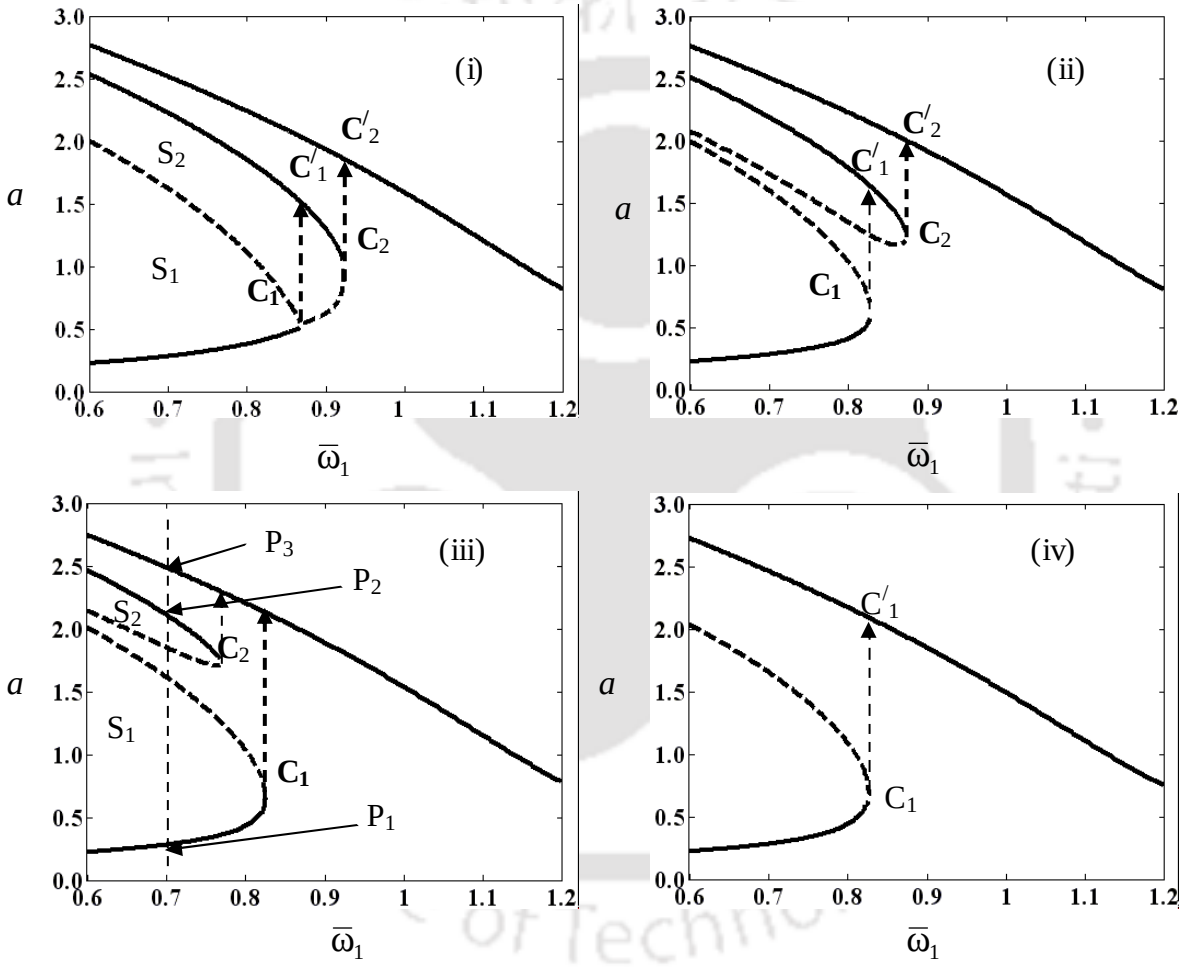

Fig. 4.27. Influence of material loss factor (δ) on the frequency response curves for $\bar{m} = 1.0$, $\bar{P}_0 = 0.0$, $\bar{P}_1 = 0.3624$, $\bar{Z} = 0.0166$; (i) $\delta = 0.0$, (ii) $\delta = 0.1$, (iii) $\delta = 0.15$, (iv) $\delta = 0.2$.

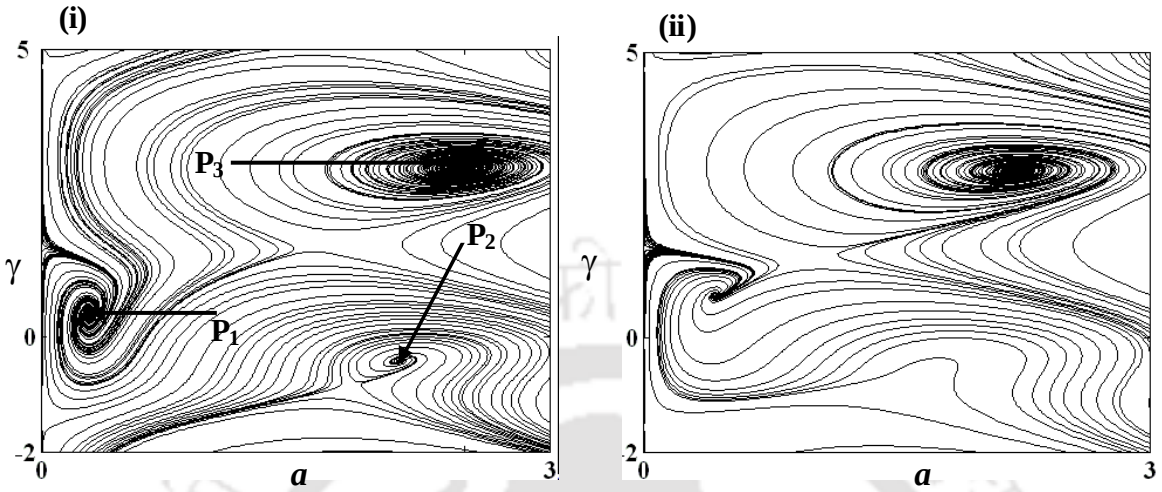

Fig. 4.28. Basins of attraction for (i) $\bar{\omega}_1$ equal to 0.7 (ii) $\bar{\omega}_1$ equal to 0.8. Key as in Fig. 4.27 (iii).

Figure 4.29 shows the influence of phase angle (ϕ) on the frequency responses for four different values of ϕ (viz., $\phi = \pi/4$, $\pi/2$, $3\pi/4$ and π). Similar to the elastic manipulator as discussed in chapter 3, here also with increase in ϕ upto $\pi/2$, this region S_2 gets reduced as the coefficient of parametric term $\alpha_6 \cos(\phi)$ reduces with increase in ϕ upto $\pi/2$ (Fig. 4.31 (iii)). With further increase in ϕ, as the influence of the tip load component increases, region S_2 again increases as shown in Fig. 4.29(iii-iv). But, the region S_1 in the frequency response curves always gets reduced with increase in. While in elastic manipulator for $0 \le \phi \le \pi/4$, C_2 always precedes to C_1, in viscoelastic manipulator C_1 always follows C_2 for $0 \le \phi \le 3\pi/4$ as shown in Fig. 4.29(i-iii). In this case, if the excitation frequency exceeds the critical point C_1, the response may jump to upper most stable nontrivial state C_1'. Similar to the elastic manipulator here also, it is observed that when these two excitations are nearly in opposite phase ($\phi \approx \pi$), C_2 follows C_1 as shown in Fig. 4.29(iv). With increase in frequency beyond C_1, the system will experience a jump up phenomena and will jump to nontrivial state C_1'. With further increases in frequency beyond C_2, a second catastrophic failure is observed due to the sudden jump from saddle-

node point C_2 to point C_2'.From the Fig. 4.29(iii) and Fig. 4.29(iv), it is observed that the there exist a value of ϕ between $\pi/2$ to $5\pi/6$, when C_1 is just below C_2. In this case, the system will jump to the upper most stable nontrivial state (point C_1').

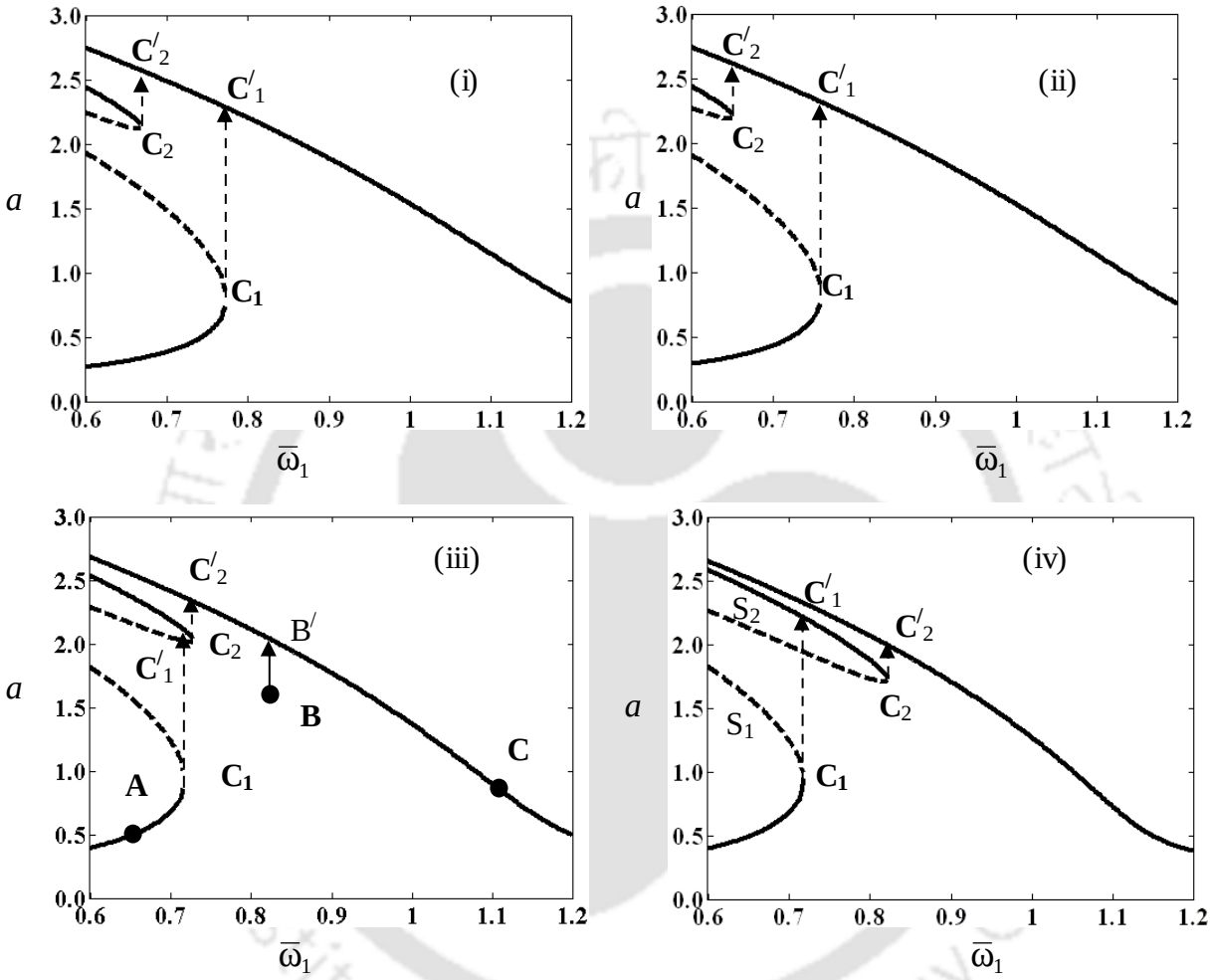

Fig. 4.29. Influence of phase angle (ϕ) on the frequency response curves for $\bar{m}=1.0$, $\bar{P}_0=0.0$, $\bar{P}_1=0.3624$, $\delta=0.15$, $\bar{Z}=0.0166$; (i) $\phi=\pi/4$, (ii) $\phi=\pi/2$, (iii) $\phi=5\pi/6$, (iv) $\phi=\pi$.

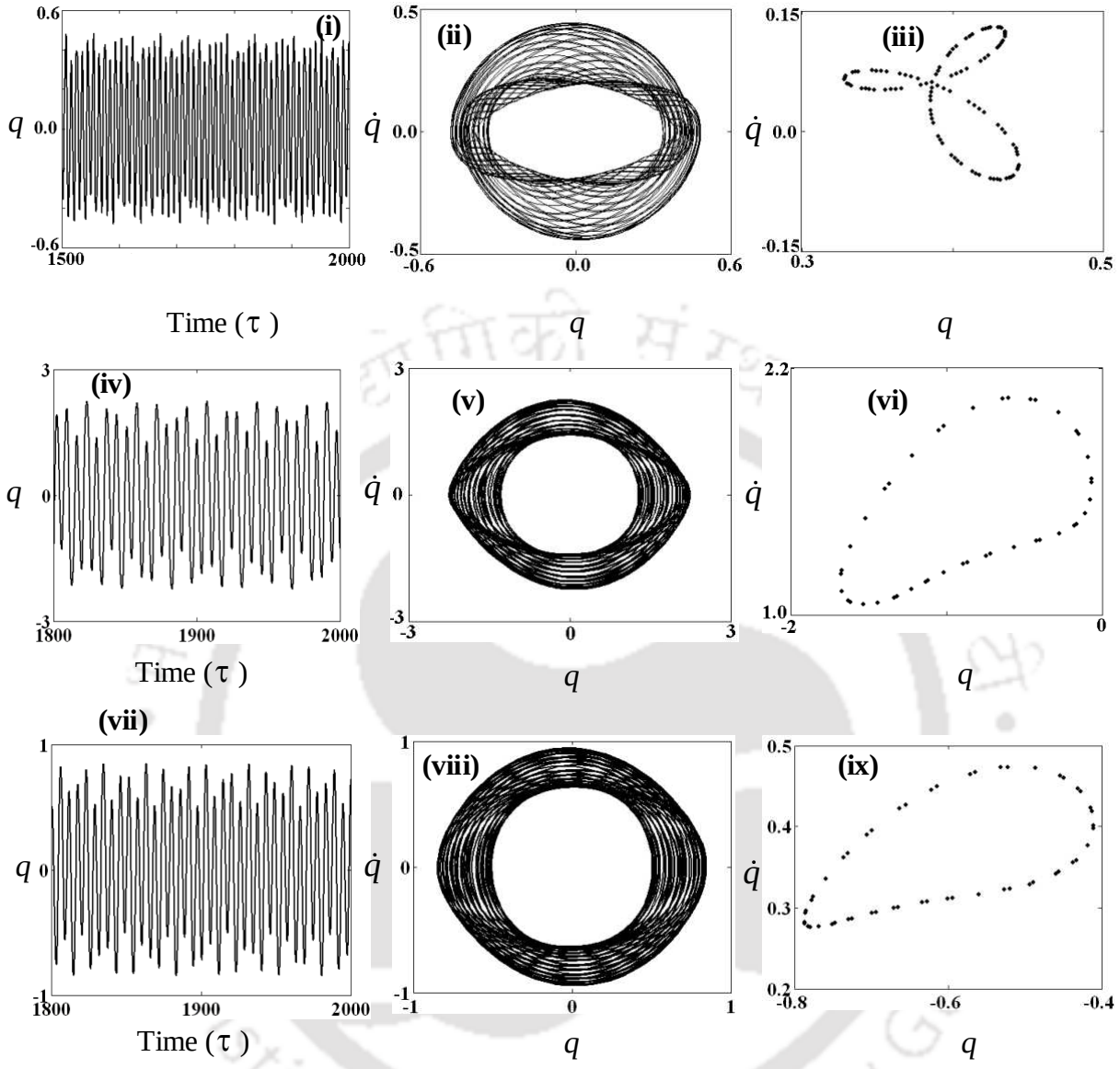

Fig. 4.30. Time response, phase portrait and Poincare's section for the points A, B, and C, key as in Fig. 4.29(iii).

The accuracy of the perturbations results is compared with the results obtained by solving numerically the temporal equation of motion (4.4).The time response, phase portrait and Poincare's section are plotted for the points A, B, and C. The time response, phase portrait and Poincare's section for the point A is shown in Fig. 4.30 (i-iii). It is observed that by solving the temporal equation of motion in point A, the system experience a 3 period-

quasi-periodic response with the stable amplitude equal to A obtained by perturbation method in Fig. 4.29(iii). Figure 4.30 (iv-vi) shows the time response, phase portrait, and Poincare's section for point B and here, the manipulator has a quasi-periodic motion with the amplitude same that obtained for point B' shown in Fig. 4.29 (iii). Similarly, time response, phase portrait, and Poincare's section for point C is also plotted in Fig. 4.30 (vii-ix). Here, also the system will have a quasi-periodic response with steady state amplitude equal to C in Fig. 4.29(iii). Hence, it may be noted that the steady state responses obtained by solving the temporal equation of motion are in good agreement with the results obtained by method of multiple scales.

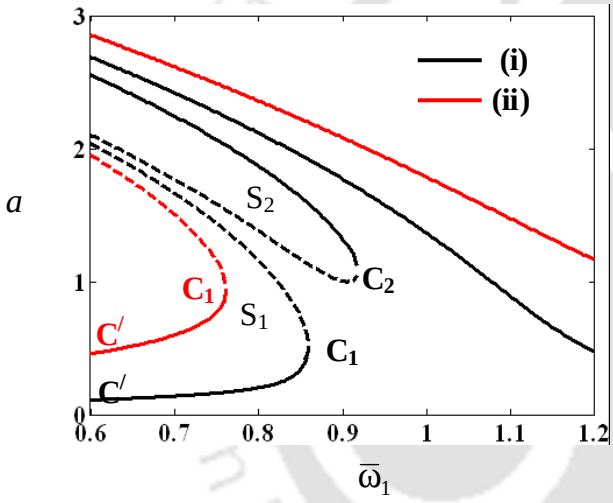

Fig. 4.31. Influence of amplitude of base excitation ($\bar{Z}$) on the frequency response curves for $\bar{m}=1.0$, $\bar{P}_0=0.0$, $\bar{P}_1=0.3624$, $\delta=0.15$; (i) $\bar{Z}=0.0083$, (ii) $\bar{Z}=0.0332$

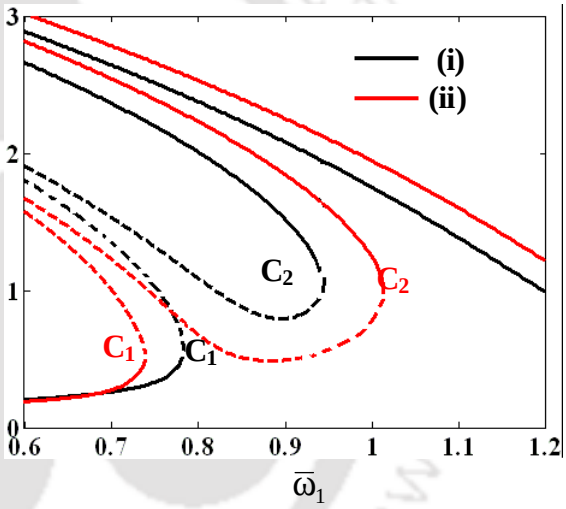

Fig. 4.32. Influence of amplitude of dynamic loading ($\bar{P}_1$) on the frequency response curves for $\bar{m}=1.0, \delta=0.15$, $\bar{P}_0=0.0$, $\bar{Z}=0.0166$; (i) $\bar{P}_1=0.5436$, (ii) $\bar{P}_1=0.7248$.

Figure 4.31 shows the frequency response curves for two different values of amplitude of base excitation $\bar{Z}$. It may also be observed that with increase in $\bar{Z}$, while the response amplitude increases, both regions S_1 and S_2 get decreased. Unlike elastic manipulator, one

may observe that in manipulator with viscoelastic material, for high value of $\bar{Z}$, the regions S_2 disappears from the frequency response curves. Hence, for high value of $\bar{Z}$ the bifurcation point C_1 starts at a lower frequency, and the critical point C_2 will disappear from the response curves. Unlike to elastic manipulator, here it is also observed that with increase in $\bar{Z}$, nontrivial stable branch ($C'C_1$) of region S_1 start at a higher value of amplitude (a) of the response. It may be noted that for less value of $\bar{Z}$ (Fig. 4.31(i)) the bifurcation point C_1 precedes the bifurcation point C_2. In such a case, with further increase in frequency at the critical point C_1, the system will experience a jump up phenomena similar to that explained in Fig. 4.27.

Figure 4.32 shows the frequency response curves for two different values of amplitude of dynamic loading $\bar{P}_1$. A similar observation as explained in elastic manipulator (chapter 3) is made in this case also. It is observed that upto frequency $\bar{\omega}_1$ equal to 0.7, response of the system remain same for all values of $\bar{P}_1$.

Figure 4.33 shows the frequency response curves for two different values of payload $\bar{m}$. From the Fig. 4.31 and Fig. 4.33, it is observed that with increase in $\bar{m}$, the response amplitude increases significantly and while the region S_1 gets decreased, region S_2 gets increased. Unlike in dynamic loading ($\bar{P}_1$), here for low value of $\bar{m}$, region S_2 will disappeared from the response curves. Hence, it is observed that with increase in $\bar{m}$ while point C_1 moves toward a lower frequency, point C_2 moves to a higher frequency and in this case also, one may observe similar jump up phenomena as explained in Fig. 4.27. Like the case of increase in $\bar{Z}$, here also the nontrivial stable branch ($C'C_1$) of region S_1 start at a higher value of amplitude (a) of the response with increase in $\bar{m}$.

Figure 4.34 shows the frequency response curves for two different values of amplitude of static loading $\bar{P}_0$. Similar to the increase in $\bar{Z}$, one may observe that with increase in $\bar{P}_0$, response amplitude increases and for large value of $\bar{P}_0$, region S_2 gets disappeared. But

unlike in cases of $\bar{Z}$, $\bar{P}_1$ and $\bar{m}$, here with increase in $\bar{P}_0$, the critical bifurcation point C_1 starts at a higher frequency. Similar to the case of increase in $\bar{P}_1$, for any value of $\bar{P}_0$, the response amplitude of the manipulator remain same upto frequency $\bar{\omega}_1$ equal to 0.85.

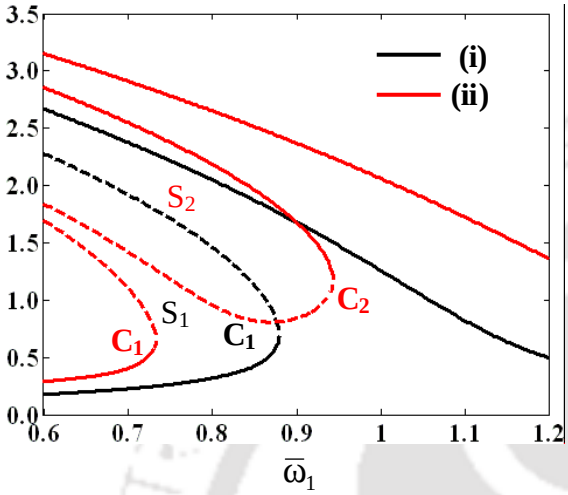

Fig. 4.33. Influence of payload ($\bar{m}$) on the frequency response curves for $\delta = 0.15$, $\bar{P}_0 = 0.0$, $\bar{Z} = 0.0166$, $\bar{P}_0 = 0.0$, $\delta = 0.15$, $\bar{P}_1 = 0.3624$; (i) $\bar{m} = 0.5$, (ii) $\bar{m} = 2.0$.

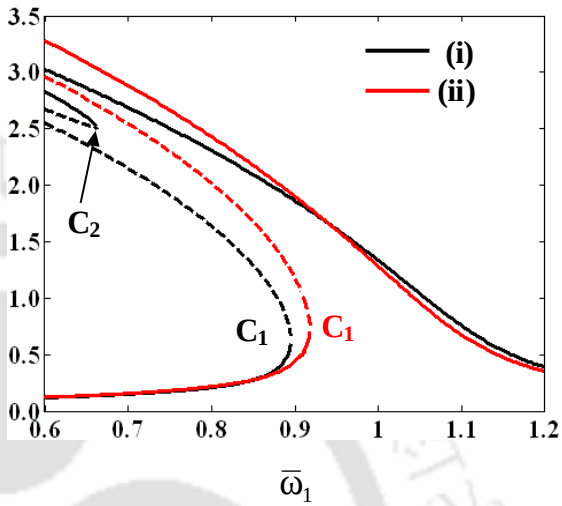

Fig. 4.34. Influence of static force (P_0) on the frequency response curves for, $\bar{m} = 1.0, \delta = 0.15, \bar{P}_1 = 0.3624$, $\bar{Z} = 0.0166$; (i) $\bar{P}_0 = 0.3624$, (ii) $\bar{P}_0 = 0.7248$.

4.5 Summary

In this chapter, nonlinear behavior of flexible viscoelastic Cartesian manipulators with and without harmonically varying axial tip force is studied. The nondimensional temporal equation of motion for both the systems is derived by using D' Alembert's principle and generalized Galerkin's method. First order method of multiple scales is used to solve the temporal equation of motion for both the systems. The frequency response curves are plotted and their stability and bifurcations are studied for both the systems. Influences of different system parameters on frequency response curves are also observed for different resonance conditions.

In case of viscoelastic Cartesian manipulator without axial force, a comparison is made with an equivalent elastic beam and the reduction in maximum amplitude of vibration using a viscoelastic manipulator is found to be very significant. The results are also compared with those obtained by taking a linear Kelvin–Voigt model and it is shown that the linear model gives very erroneous results. In simple resonance case, the nontrivial frequency response curve shows critical saddle-node bifurcation point at which the system may fail due to jump-up phenomena. With increase in material loss factor and decrease in amplitude of base excitation the maximum response amplitude decreases.

Unlike simple resonance case, in sub-harmonic resonance case, the system possesses both trivial and nontrivial response. But for a wide range of system parameters, the trivial state is found to be stable. The effect of material loss factor, amplitude of base excitation and mass ratio is studied for both the resonance conditions and are found to be in the expected lines.

Similar to the elastic manipulator, here also, for the system with harmonically varying axial force, three distinct resonance conditions are studied. In simple resonance condition, when the frequency of the support motion is nearly equal to the natural frequency of the system and frequency of axial loading is away form the principal resonance zone, the resonance amplitude has found to be reduced by increasing the material loss factor. It is observed that the response amplitude increases with increase in amplitude of support motion, and mass ratio. Similar to the previous case, here also, the manipulator should be safely operated at a frequency below the saddle node bifurcation point.

But when the manipulator is subjected to tip load with a frequency nearly equal to twice the natural frequency of the system, catastrophic failure may occur at the sub-critical pitchfork bifurcation point. Irrespective of the frequency of the base motion at the roller-supported end, the system will not vibrate if the frequency of the dynamic loading is below the sub-critical pitchfork bifurcation point or if it operates at a frequency which is above

the super-critical pitchfork bifurcation point. It may be noted that the system response can be brought to the stable trivial state by increasing material loss factor.

One may find that in simultaneous resonance case the system has a similar tri-stable region as in case of elastic manipulator. In this resonance condition, unlike the elastic manipulator, here it is also observed that with increase in amplitude of support motion and mass ratio, nontrivial stable branch of region S_1 start at higher response amplitude (a). It is observed that while for all values of $\bar{P}_1$, the response of the manipulator remains same upto frequency equal to 0.7, response of the manipulator remains same upto frequency equal to 0.85 for all values of $\bar{P}_0$. Basin of attraction is plotted to know the initial condition for particular response of the manipulator.

Similarly, here it can be noted that carrying out expensive experiments and computationally solving the temporal equation of motion are tedious and time consuming and hence, one may use the developed simplified reduced equations in these work for finding the critical bifurcation points and frequency responses for different resonance conditions. These findings will find extensive applications in the feed-forward control of flexible Cartesian manipulator for precision positioning and constraint motion without any vibration.

Chapter 5

MAGNETOELASTIC CARTESIAN MANIPULATOR

5.1 Introduction

In this chapter, the dynamic analysis of a flexible magnetoelastic Cartesian manipulator subjected to sinusoidally varying magnetic field with and without harmonically varying tip force is carried out. First and second order method of multiple scales is used to determine the instability regions and frequency response curves. The region of instability found in this chapter is compared with the experimental findings. The influences of different system parameters on the steady state responses and instability regions for different resonance conditions are investigated.

As mentioned in chapter 2, unlike elastic manipulators, very limited study has been carried out for magnetoelastic manipulators. Hence, in this chapter, the manipulator is modeled either as a cantilever beam or as a roller supported beam, and both small and large elastic deflection problems are considered to access the usability of magnetoelastic beam for manipulator purpose. In section 5.2, mathematical modeling of five different manipulators is carried out by deriving the nonlinear governing equation of motion. While in section 5.3, the beam with small elastic deflection is taken, in sections 5.4-5.7, beams with large elastic deflection are considered. Taking physical system parameters, numerical simulations are carried out in these sections to show the applicability of magnetoelastic manipulators for vibration control purpose of the flexible manipulators. In sections 5.3-5.6, the manipulator is considered as an Euler-Bernoulli cantilever beam with tip mass, and in section 5.7, the manipulator is modeled as a base excited roller-supported beam with tip mass. In this work, the analysis is limited two frequency excitations of the system. As discussed in Chapter 3, here also Newton's method is used for solving the set of nonlinear algebraic equations and RK-4 method is used to solve the temporal and reduced equations. Basin of attraction is also plotted following similar procedure as discussed in Chapter 3.

5.2 Mathematical Modeling

Figure 5.1 shows the schematic diagram of a Cartesian manipulator with payload *M*, which is modeled as an Euler Bernoulli beam with roller supported left end and point mass *M* at the right end. The roller-supported end of the manipulator is subjected to a periodically varying support motion $Y_b(t) = Z\cos\Omega_1 t$. This manipulator is subjected to both sinusoidally varying magnetic transverse field $B_0(t) = B_m\cos\Omega_2 t$ and harmonically varying tip force $P(t) = P_0 + P_1\cos\Omega_3 t$. The governing equation of motion of the cantilever beam is derived by using D' Alembert's principal which can be given by

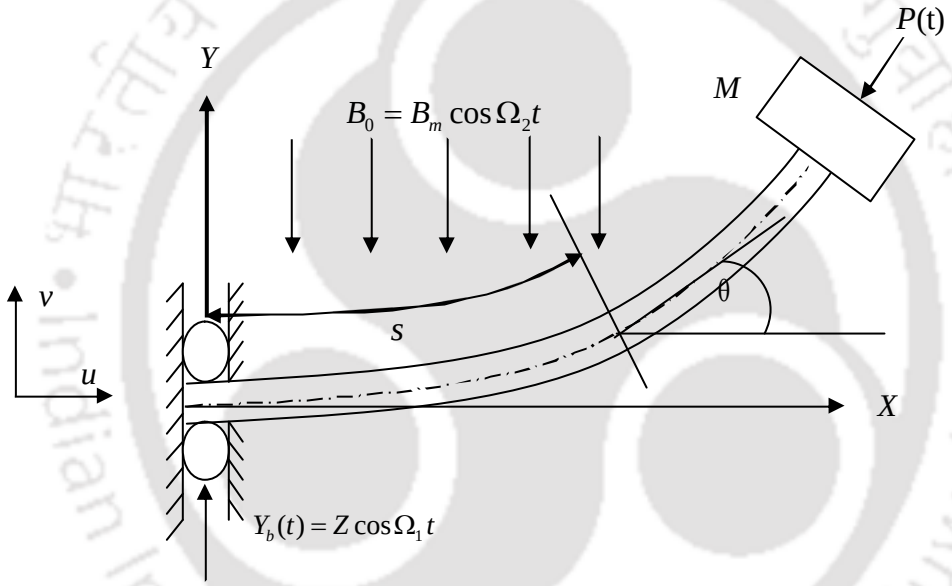

Fig. 5.1. Schematic diagram of a magnetoelastic Cartesian manipulator with payload subjected to harmonically varying axial tip force.

Similar to elastic and viscoelastic manipulators, here also by using D' Alembert's principle, the governing equation of motion of the present system is developed. In the present case, following Wu et al. (2000), Wu (2005) and Liu and Chang (2006), expressions for the moment due to the inertia force at a distance ξ from the roller-supported end $M_\xi(s)$ and the moment due to the inertia force for the payload at the tip of the manipulator $M_L(s)$ can be given as:

$$M_\xi(s) = -\int_s^L \rho A\ddot{u}\int_s^\xi \sin\theta\, d\eta\, d\xi - \int_s^L \rho A\left(\ddot{v}+\ddot{Y}_b\right)\int_s^\xi \cos\theta\, d\eta\, d\xi$$
$$-\int_s^L p_m\, d\xi\int_s^\xi \sin\theta\, d\eta\ - c_m\int_s^\xi \cos\theta\, d\eta. \qquad (5.1)$$

and, $M_L(s) = -M\ddot{u}\int_s^L \sin\theta\, d\xi - M\left(\ddot{v}+\ddot{Y}_b\right)\int_s^L \cos\theta\, d\xi - P(t)\int_s^L \sin\theta\, d\xi$. (5.2)

Here, p_m is the axial body force and c_m is couple acting on the beam which are generated due to the applied magnetic field B_0. The expressions for these two parameters can be given by (Wu et al., 2000; Wu , 2005; and Liu and Chang , 2006)as

$$p_m = -\sigma\ h\ d\ B_0(t)^2\int_0^\xi\left(v_s\dot{v}_s - \frac{1}{2}v_s v_s^2\dot{v}_s\right)d\xi, \text{ and } c_m = \left(\frac{\chi_m}{\mu_0\mu_r}h\ d\ B_0(t)^2\right)v_s. \qquad (5.3)$$

Considering equivalent viscous damping $c_d\dot{v}$ and by applying the Leibniz's rule and binomial expansion, one may obtain the following nonlinear governing differential equation of motion.

$$EI\left(v_{ssss} + \frac{1}{2}v_s^2 v_{ssss} + 3v_s v_{ss} v_{sss} + v_{ss}^3\right) + \rho A v_s\left(\int_0^s\left(\dot{v}_\xi^2 + v_\xi\ddot{v}_\xi\right)d\xi\right) + M\left(\ddot{v}+\ddot{Y}_b\right)v_s v_{ss} + v_s v_{ss}$$
$$\left(\rho A\ddot{Y}_b(L-s) + \int_s^L\left(\rho A\ddot{v} + c_d\dot{v}\right)d\eta\right) - v_{ss}\left(\int_s^L \rho A\int_0^\xi\left(\dot{v}_\xi^2 + v_\xi\ddot{v}_\xi\right)d\xi d\eta + M\int_0^\xi\left(\dot{v}_\xi^2 + v_\xi\ddot{v}_\xi\right)d\xi\right) +$$
$$\left(1-\frac{1}{2}v_s^2\right)\left(\rho A\left(\ddot{v}+\ddot{Y}_b\right) + c_d\dot{v}\right) - \left(v_{ss}\int_s^L\left(p_m d\xi\right) - p_m v_s\right) - \left(\frac{dc_m}{ds}\left(1-\frac{1}{2}v_s^2\right) + v_s v_{ss}\left(1+\frac{1}{2}v_s^2\right)c_m\right) +$$
$$\left(P(t)v_s\right)_s = 0. \qquad (5.4)$$

In absence of magnetic field, this equation reduces to that of equation (3.6) of an elastic Cartesian manipulator discussed in chapter 3. Here, by taking the following assumed mode expression, one may use generalized Galerkin's method to discretize the equation of motion (5.4) to obtain the temporal equation of motion.

$$v(s,t) = r\,\psi(s)\,q(t) \qquad (5.5)$$

Here, r, $\psi(s)$, and $q(t)$ are, respectively the scaling factor, an admissible function and time modulation. Here, the same shape function $\psi(s)$ as used in chapter 3 (equation 3.8) is used. The following non-dimensional parameters are used for further analysis.

$$\bar{x}=\frac{s}{L},\tau=\omega_e t,\bar{\omega}_1=\frac{\Omega_1}{\omega_e},\bar{\omega}_2=\frac{\Omega_2}{\omega_e},\bar{\omega}_3=\frac{\Omega_3}{\omega_e},\ \bar{r}=\frac{r}{L},\ \bar{m}=\frac{M}{\rho AL},\bar{P}_0=\frac{P_0}{P_c},$$

$$\bar{P}_1=\frac{P_1}{P_c},\ \chi=\frac{EI}{\rho AL^4},\kappa=\frac{Z}{r},\text{ and }\bar{Z}=\frac{Z}{L} \tag{5.6}$$

Substituting Equation (5.5) into Equation (5.4) and using the generalized Galerkin's method, one may obtain the following non-dimensional temporal equation of motion.

$$\ddot{q}+2\varepsilon\zeta\dot{q}+q+\varepsilon\left(\alpha_1 q^3+\alpha_2 q^2\ddot{q}+\alpha_3\dot{q}^2 q\right)+\varepsilon\bar{\omega}_1^2 f_1\cos\left(\bar{\omega}_1\tau\right)+\varepsilon\bar{\omega}_1^2 k_1\cos\left(\bar{\omega}_1\tau\right)q^2$$
$$-\varepsilon f_2\cos\left(2\bar{\omega}_2\tau\right)q-\varepsilon k_2\left(1+\cos\left(2\bar{\omega}_2\tau\right)\right)\dot{q}q^2+\varepsilon f_3\cos\left(\bar{\omega}_3\tau\right)q=0. \tag{5.7}$$

The expressions for the coefficients ($\zeta, \alpha_1, \alpha_2, \alpha_3, f_1, f_3$ and k_1) are given in chapters 3 and expressions for remaining coefficients (ω_e, f_2, f_4, k_2, and k_3) are given as:

$$\omega_e^2=\frac{EI}{mL^4}\frac{h_2}{h_{14}}+\frac{P_0}{mL^2}\left(\frac{h_{21}}{h_{14}}\right)-\frac{B_m^2}{2}\frac{\chi_m h d}{\mu_0\mu_r mL^2}\left(\frac{h_{22}}{h_{14}}\right)=\omega_L^2\left(1+\bar{P}_0-\bar{B}_m\right)\text{ or}$$

$$\omega_s^2=\frac{EI}{mL^4}\frac{h_2}{h_{14}}\left(1-\left(B_s^2+\frac{B_d^2}{2}\right)\frac{\chi_m h d L^2}{\mu_0\mu_r EI}\left(\frac{h_{22}}{h_1}\right)\right)=\omega_L^2\left(1-\bar{B}_s-\bar{B}_d\right),$$

$$f_2=\frac{B_r^2}{\omega_e^2 B_c^2}=\left(\frac{f_0}{\delta^2}\right),\qquad \delta=\frac{\omega_L}{\omega_e},\qquad f_0=\frac{B_r^2\delta^2}{\omega_e^2 B_c^2},\qquad k_{0,2}=\left(B_s^2+\frac{B_d^2}{2}\right)\frac{\sigma h d}{m\omega_e}\bar{r}^2\left(-\frac{h_{23}}{h_{14}}+\frac{h_{24}}{h_{14}}\right),$$

$$k_2=-\frac{B_m^2\sigma h d}{2m\omega_e}\bar{r}^2\left(-\frac{h_{23}}{h_{14}}+\frac{h_{24}}{h_{14}}\right),\ f_4=4\frac{B_{rr}^2}{\varepsilon\omega_e^2 B_c^2}=f_{1,0}\left(\frac{\omega_L^2}{\omega_e^2}\right),$$

$$k_3=\frac{2B_s B_d\sigma h d}{m\omega_e}\bar{r}^2\left(-\frac{h_{23}}{h_{14}}+\frac{h_{24}}{h_{14}}\right).$$

Here,

$$\omega_L^2=\frac{EI}{mL^4}\frac{h_2}{h_{14}},B_r^2=\frac{B_m^2}{2},B_c^2=\frac{\mu_0\mu_r EIL^2}{\chi_m h d}\left(\frac{h_2}{h_{14}}\right),\bar{P}_0=\frac{P_0L^2}{mEI}\left(\frac{h_{21}}{h_2}\right),\ B_{rr}^2=\frac{B_s B_d}{2},$$

$$\bar{B}_m = \frac{B_m^2 \chi_m h d L^2}{2\mu_0 \mu_r EI}\left(\frac{h_{22}}{h_2}\right), \bar{B}_s = \frac{B_s^2 \chi_m h d L^2}{\mu_0 \mu_r EI}\left(\frac{h_{22}}{h_2}\right), \bar{B}_d = \frac{B_d^2 \chi_m h d L^2}{2\mu_0 \mu_r EI}\left(\frac{h_{22}}{h_2}\right),$$

$$h_{22} = \int_0^1 \left[\frac{d^2\psi(\bar{x})}{d\bar{x}^2}\psi(\bar{x})\right] d\bar{x}\,, \quad h_{23} = \int_0^1 \frac{d\psi(\bar{x})}{d\bar{x}}\left(\int_0^{\bar{x}} \frac{d\psi(\bar{\xi})}{d\bar{\xi}} d\bar{\xi}\right)\psi(\bar{x}) d\bar{x}\,,$$

And $$h_{24} = \int_0^1 \frac{d^2\psi(\bar{x})}{d\bar{x}^2}\left(\int_{\bar{x}}^1 \int_0^{\bar{\xi}} \frac{d\psi(\bar{\xi})}{d\bar{\xi}} d\bar{\eta} d\bar{\xi}\right)\psi(\bar{x}) d\bar{x}\,. \tag{5.8}$$

The expressions for $h_1, h_2, \cdots\cdots h_{21}$ are same as given in chapters 3 (equation, 3.12) and 4.

Similar to the elastic and viscoelastic manipulators, here one may use a book-keeping parameter ε in order to make all the coefficients i.e., $\zeta, \alpha_1, \alpha_2, \alpha_3, f_1, f_2, f_3, k_1,$ and k_2 in the same order of unity. It is observed from equation (5.7) that the non-dimensional temporal equation of motion has linear damping term ($2\zeta\dot{q}$), a force term ($\alpha_5 \bar{\omega}_1^2 \cos\bar{\omega}_1\tau$), parametric terms $f_2 \cos(2\bar{\omega}_2\tau)q$ and $f_3 \cos(\bar{\omega}_3\tau)q$, a nonlinear parametric excitation term ($k_1\bar{\omega}_1^2 \cos\bar{\omega}_1\tau\, q^2$) and a nonlinear damping term $k_2\left(1+\cos(2\bar{\omega}_2\tau)\right)\dot{q}q^2$ along with cubic geometric ($\alpha_1 q^3$) and inertial ($\alpha_2 q^2\ddot{q} + \alpha_3\dot{q}^2 q$) nonlinear terms. Equation 5.7, containing the above mentioned nonlinear terms is very complex with three frequency excitation terms. To study the usability of magnetic field to control the vibration of the manipulator, the following five different manipulator configurations are considered. The studies are limited to the two frequency excitations.

5.2.1 Roller-Supported Manipulator without Axial Force

Similar to the elastic and viscoelastic manipulator, here also the magnetoelastic manipulator is studied without considering axial force applied at the tip end. These types of systems can be mainly used in many industrial applications for pick and place operations. To control the vibration, by applying sinusoidally varying magnetic field, one may obtain the governing equation of motion of the system by neglecting the parametric

term $f_3 \cos(\bar{\omega}_3 \tau) q$ in equation (5.7). The resulting non-dimensional equation of motion becomes:

$$\ddot{q} + 2\varepsilon\zeta\dot{q} + q + \varepsilon\left(\alpha_1 q^3 + \alpha_2 q^2 \ddot{q} + \alpha_3 \dot{q}^2 q\right) + \varepsilon\bar{\omega}_1^2 f_1 \cos(\bar{\omega}_1 \tau) + \varepsilon\bar{\omega}_1^2 k_1 \cos(\bar{\omega}_1 \tau) q^2 - \varepsilon f_2 \cos(2\bar{\omega}_2 \tau) q - \varepsilon k_2 \left(1 + \cos(2\bar{\omega}_2 \tau)\right) \dot{q} q^2 = 0. \quad (5.9)$$

5.2.2 Cantilevered Manipulator with Harmonically Varying Tip Force

Unlike the previous case, in many applications, when the manipulator reached the work piece for the intended operation, no longer it is required to be in motion. For these applications, the roller supported end of the prismatic manipulator or the rotating end of the revolute manipulator may be replaced by a fixed or clamped end and the manipulator may be modeled as a cantilevered beam with tip mass subjected to axial force from the working environment as shown in Fig. 5.2.

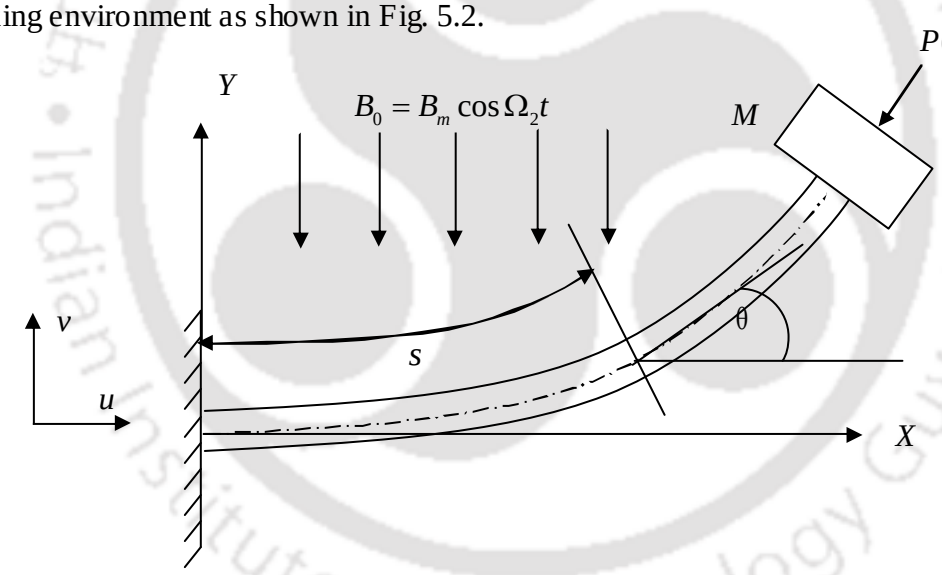

Fig. 5.2. Schematic diagram of magnetoelastic cantilevered manipulator subjected to harmonically varying tip force.

As the link is considered to be flexible, the manipulator may be under vibration due to the axial force. Hence, to control this vibration, if one applies a sinusoidally varying magnetic field, the governing equation of motion of this Cartesian manipulator with axial force, can

be obtained from equation 5.7 by putting $Y_b = 0$, or by neglecting terms $\varepsilon\bar{\omega}_1^2 f_1 \cos(\bar{\omega}_1\tau) + \varepsilon\bar{\omega}_1^2 k_1 \cos(\bar{\omega}_1\tau) q^2$ from the equation (5.7) as follows:

$$\ddot{q} + 2\varepsilon\zeta\dot{q} + q + \varepsilon\left(\alpha_1 q^3 + \alpha_2 q^2\ddot{q} + \alpha_3 \dot{q}^2 q\right) - \varepsilon f_2 \cos(2\bar{\omega}_2\tau) q - \varepsilon k_2 \left(1 + \cos(2\bar{\omega}_2\tau)\right)\dot{q}q^2 + \varepsilon f_3 \cos(\bar{\omega}_3\tau) q = 0. \quad (5.10)$$

5.2.3 Cantilevered Manipulator without Axial Force

If the manipulator discussed in section 5.2.2, is not subjected to any axial force from the environment or work piece, then it will be similar to a flexible cantilever beam with transverse magnetic field as shown in Fig. 5.3. This is a very common system and as pointed out earlier, the large transverse vibration of such systems have not been fully explored. The temporal equation of motion of this type of system can be obtained by neglecting the term $\varepsilon f_3 \cos(\bar{\omega}_3\tau) q$ from the equation (5.10) as follows:

$$\ddot{q} + 2\varepsilon\zeta\dot{q} + q + \varepsilon\left(\alpha_1 q^3 + \alpha_2 q^2\ddot{q} + \alpha_3 \dot{q}^2 q\right) - \varepsilon f_2 \cos(2\bar{\omega}_2\tau) q - \varepsilon k_2 \left(1 + \cos(2\bar{\omega}_2\tau)\right)\dot{q}q^2 = 0. \quad (5.11)$$

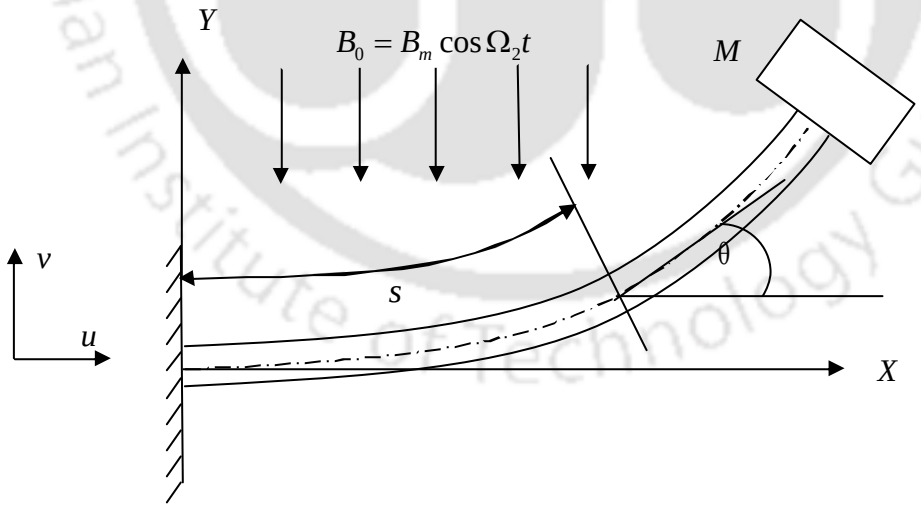

Fig. 5.3. Schematic diagram of magnetoelastic cantilevered manipulator.

5.2.4 Cantilevered Manipulator with Static and Dynamic Magnetic Field

Now, similar manipulator as shown Fig. 5.3 may be subjected to both static and dynamic magnetic fields $B_0(t) = B_s + B_m \cos\Omega_2 t$ as shown in Fig. 5.4. For such systems, temporal equation of motion can be obtained as follows:

$$\ddot{q} + 2\varepsilon\zeta\dot{q} + q + \varepsilon\left(\alpha_1 q^3 + \alpha_2 q^2\ddot{q} + \alpha_3 \dot{q}^2 q\right) - \varepsilon\left(f_4\cos\left(\bar{\omega}_2\tau\right) + f_2\cos\left(2\bar{\omega}_2\tau\right)\right)q$$
$$-\varepsilon\left(k_{0,2} + k_3\cos\bar{\omega}_2\tau + k_2\cos 2\bar{\omega}_2\tau\right)\dot{q}q^2 = 0. \quad (5.12)$$

Where, the expressions for $k_{0,2}, k_3,$ and f_4 can be found from the equation (5.8). It may be noted that the static magnetic field will change the natural frequency of the system.

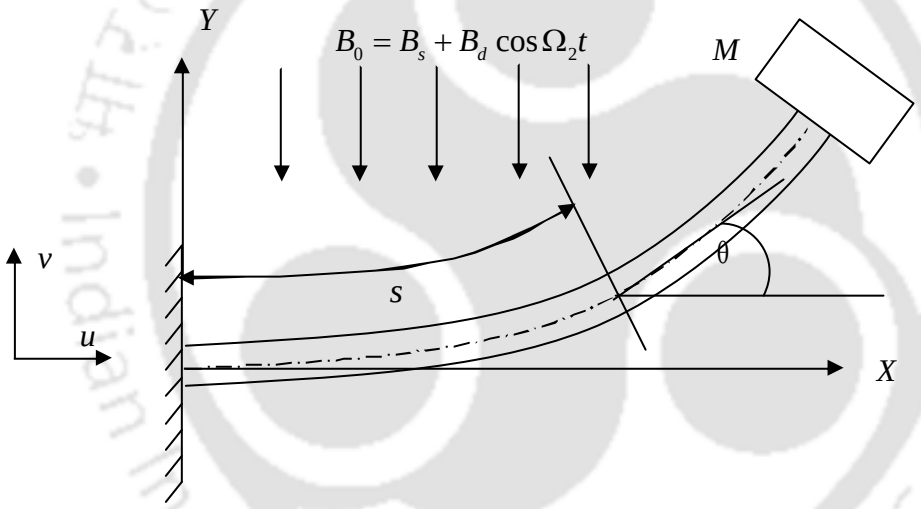

Fig. 5.4. Schematic diagram of magnetoelastic cantilevered manipulator subjected to both static and dynamic magnetic fields.

5.2.5 Cantilevered Manipulator Considering Small Transverse Deflection

While for the systems discussed in sections 5.2.1-5.2.4, large transverse deflection of the flexible manipulator is considered, due to the nonavailability of closed form solution for the systems with small transverse deflection, it was felt to study such a system. In these studies, the parametric instability regions of the trivial state of a manipulator as subjected to both harmonically varying tip force $P = P_0 + P_1\cos\Omega_3 t$ and sinusoidally varying

transverse magnetic field $B_0 = B_m \cos\Omega_1 t$ shown in Fig. 5.5 can be found out. For these systems one may obtain the following temporal equation of motion by neglecting the nonlinear terms from equation (5.7).

$$\ddot{q} + 2\,\varepsilon\,\zeta\,\dot{q} + q + \varepsilon\left(f_3 \cos\bar{\omega}_3\tau - f_2 \cos 2\bar{\omega}_2\tau\right)q = 0. \qquad (5.13)$$

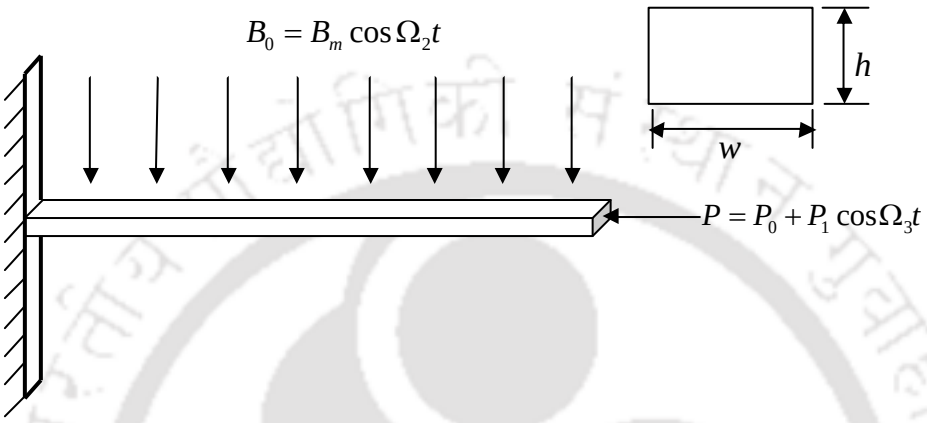

Fig. 5.5. Schematic diagram of a magnetoelastic cantilevered manipulator subjected to harmonically varying tip force considering small transverse deflection.

It can be observed that the temporal equation of motion of the manipulators given by equations (5.7-5.13) contain many nonlinear terms. Hence, finding the closed form expressions of exact solutions is very difficult. Hence, one may go for approximate solution by solving these equations using perturbation methods. Here, the analysis is limited to the study of the systems with two frequency excitations. It may be noted that, as superposition rule is not applicable for nonlinear systems, the solutions of the systems given in equations (5.9-5.13) should be treated separately. This is due to the fact that, these systems will have different resonance conditions which are primarily responsible for the difference in the resulting solutions or response of the systems. Solution and numerical simulations of these five different systems are carried out in the following sections. Unlike the previous two sections, here the discussions are started for a simpler system i.e., the cantilever manipulator with axial load and magnetic field and subsequently more complex system are discussed.

5.3. Cantilevered Manipulator with Axial Force Considering Small Deflection

5.3.1 Analysis

In this case to obtain the solution of the temporal equation of motion (5.13), here second order method of multiple scales is used to find the analytical expressions for the instability regions. In this method, the displacement q can be represented in terms of different times scales (T_0, T_1, T_2) and a book keeping parameter ε as follows.

$$q(\tau;\varepsilon) = q_0(T_0,T_1,T_2) + \varepsilon q_1(T_0,T_1,T_2) + \varepsilon^2 q_2(T_0,T_1,T_2) + O(\varepsilon^3) \ , \qquad (5.14)$$

here $T_n = \varepsilon^n \tau,\ n = 1, 2, 3\cdots$. The transformation of first and second time derivatives are given by

$$\frac{d}{d\tau} = D_0 + \varepsilon D_1 + \varepsilon^2 D_2 + O(\varepsilon^2), \qquad (5.15)$$

$$\frac{d^2}{d\tau^2} = D_0^2 + 2\varepsilon D_0 D_1 + \varepsilon^2 (D_1^2 + 2D_0 D_2) + O(\varepsilon^3), \qquad (5.16)$$

where, $D_0 = \frac{\partial}{\partial T_0}, D_1 = \frac{\partial}{\partial T_1}$ and $D_2 = \frac{\partial}{\partial T_2}$. Substituting equations (5.14-5.16) into equation (5.13) and equating the coefficient of like powers of ε, yields the following equations.

Order ε^0 : $D_0^2 q_0 + q_0 = 0$. (5.17)

Order ε^1 : $D_0^2 q_1 + q_1 = -2D_0 D_1 q_0 - 2\zeta D_0 q_0 - f_3 \cos(\bar{\omega}_3 \tau) q_0 + f_2 \cos(2\bar{\omega}_2 \tau) q_0$. (5.18)

Order ε^2 : $D_0^2 q_2 + q_2 = -2D_0 D_1 q_1 - 2\zeta D_1 q_0 - 2\zeta D_0 q_1 - \left(D_1^2 + 2D_0 D_2\right) q_0$

$$- f_3 \cos(\bar{\omega}_3 \tau) q_1 + f_2 \cos(2\bar{\omega}_2 \tau) q_1 \qquad (5.19)$$

General solutions of equation (5.17) can be written as

$$q_0 = A(T_1, T_2) \exp(iT_0) + \bar{A}(T, T_2) \exp(-iT_0) \ . \qquad (5.20)$$

Substituting equation (5.20) into equation (5.18) leads to

$$D_0^2 q_1 + q_1 = -2iD_1 A\exp(iT_0) - 2i\zeta A\exp(iT_0) - \frac{f_3}{2}\left[A\exp i(1+\bar{\omega}_3)T_0 + \bar{A}\exp i(\bar{\omega}_3 - 1)T_0\right]$$

$$+\frac{f_2}{2}\left[A\exp i(1+2\bar{\omega}_2)T_0 + \bar{A}\exp i(2\bar{\omega}_2 - 1)T_0\right] + cc\ . \qquad (5.21)$$

One may observe that any solution of equation (5.21) will contain secular or small divisor terms when nondimensional frequency of external axial loading ($\bar{\omega}_3$) is nearly equal to 2 and/or nondimensional frequency of magnetic field ($\bar{\omega}_2$) is nearly equal to 1. Hence, one may have three different resonance conditions viz. (i) $\bar{\omega}_3 \approx 2$ and $\bar{\omega}_2$ is away from 1, (ii) $\bar{\omega}_2 \approx 1$ and $\bar{\omega}_3$ is away from 2 and (iii) $\bar{\omega}_3 \approx 2$ and $\bar{\omega}_2 \approx 1$ simultaneously. These three conditions are discussed in the following subsections.

5.3.1.1 Principal Parametric Resonance Case ($\bar{\omega}_3 \approx 2$ and $\bar{\omega}_2$ away from 1)

For this case, to express the nearness of $\bar{\omega}_3$ to 2, one may use the detuning parameter σ as

$$\bar{\omega}_3 = 2 + 2\varepsilon\sigma, \text{ and } \sigma = O(1)\,. \qquad (5.22)$$

Substituting equation (5.22) into equation (5.21) and eliminating the secular or small divisor terms yields

$$2iD_1 A + 2i\zeta A + \frac{f_3}{2}\bar{A}\exp i(2\sigma T_1) = 0\ . \qquad (5.23)$$

One may write the particular solution of equation (5.21) as

$$q_1 = \frac{f_3}{2\left[\left(1+\bar{\omega}_3\right)^2 - 1\right]}\left(A(T_1)\exp i(1+\bar{\omega}_3)\tau\right) - \frac{f_2}{2\left[\left(1+2\bar{\omega}_2\right)^2 - 1\right]}\left(A(T_1)\exp i(1+2\bar{\omega}_2)\tau\right)$$

$$-\frac{f_2}{2\left[\left(1-2\bar{\omega}_2\right)^2 - 1\right]}\left(A(T_1)\exp i(2\bar{\omega}_2 - 1)\tau\right) + cc\,. \qquad (5.24)$$

Substituting equations (5.23) and (5.24) into the equation (5.19) and eliminating the secular or small divisor terms yields

$$2iD_2 A + 2\mu D_1 A + D_1^2 A + \Gamma A = 0\,, \qquad (5.25)$$

where, $\Gamma = \frac{1}{2}\left(\frac{f_3^2}{4\bar{\omega}_3 + 2\bar{\omega}_3^2}\right) + \frac{1}{2}\left(\frac{f_2^2}{8\bar{\omega}_2 + 8\bar{\omega}_2^2}\right) + \frac{1}{2}\left(\frac{f_2^2}{-8\bar{\omega}_2 + 8\bar{\omega}_2^2}\right)$.

From equation (5.23), one may obtain

$$D_1^2 A = \zeta^2 A + \left(\frac{\alpha_1}{4}\right)^2 A - \frac{f_3}{4}\left(2\zeta i + 2\sigma\right)\bar{A}\exp(2i\sigma T_1)\,. \qquad (5.26)$$

Substituting equations (5.23) and (5.26) into equation (5.25), gives

$$2iD_2 A + \left(-\zeta^2 + \left(\frac{f_3}{4}\right)^2 + \Gamma\right)A - \frac{f_3}{2}\sigma\bar{A}\exp(2i\sigma T_1) = 0\,. \qquad (5.27)$$

Substituting equations (5.23) and (5.26) to equation (5.15), one may obtain following equation.

$$2i\frac{dA}{d\tau} + \left(2i\varepsilon\zeta + \varepsilon^2\left[-\zeta^2 + \left(\frac{f_3}{4}\right)^2 + \Gamma\right]\right)A + \frac{f_3}{4}\left(\varepsilon - 2\varepsilon^2\sigma\right)\bar{A}\exp(2i\sigma T_1) = 0\,. \qquad (5.28)$$

Putting $A = (B_r + iB_i)\exp(i\varepsilon\sigma\tau)$), where B_r, and B_i are real and imaginary parts in equation (5.28) and separating the real and imaginary parts yield the following equations.

$$2\frac{dB_r}{d\tau} + 2\varepsilon\zeta B_r + \left[2\varepsilon\sigma + \varepsilon\frac{f_3}{2} - \varepsilon^2\left(\frac{f_3}{2}\sigma\right) - \left(-\zeta^2 + \left(\frac{f_3}{4}\right)^2 + \Gamma\right)\right]B_i = 0\,. \qquad (5.29)$$

$$2\frac{dB_i}{d\tau} + 2\varepsilon\zeta B_i + \left[-2\varepsilon\sigma + \varepsilon\frac{f_3}{2} - \varepsilon^2\left(-\frac{f_3}{2}\sigma\right) + \left(-\zeta^2 + \left(\frac{f_3}{4}\right)^2 + \Gamma\right)\right]B_r = 0\,. \qquad (5.30)$$

Substituting $(B_r, B_i) = (b_r, b_i)\exp(\gamma\tau)$ into the equations (5.29) and (5.30) yields the following equations.

$$2\gamma b_r + 2\varepsilon\zeta b_r + \left[2\varepsilon\sigma + \varepsilon\frac{f_3}{2} - \varepsilon^2\left(\frac{f_3}{2}\sigma\right) - \left(-\zeta^2 + \left(\frac{f_3}{4}\right)^2 + \Gamma\right)\right]b_i = 0, \qquad (5.31)\,.$$

$$2\gamma b_i + 2\varepsilon\mu b_i + \left[-2\varepsilon\sigma + \varepsilon\frac{f_3}{2} - \varepsilon^2\left(-\frac{f_3}{2}\sigma\right) + \left(-\zeta^2 + \left(\frac{f_3}{4}\right)^2 + \Gamma\right)\right]b_r = 0\,. \qquad (5.32)$$

For steady state trivial response, γ is equal to zero. One may obtain the expression for the transition curves by finding the value of σ from the above two equations. Neglecting the terms $O(\varepsilon^3)$, one may write the expression for transition curves of the second order expansion when $\bar{\omega}_3 \approx 2$ as

$$\bar{\omega}_3 = 2 \pm \varepsilon \sqrt{\left(\varepsilon^2 \left(\zeta^2 + 3\left(\frac{f_3}{4} \right)^2 - \Gamma \right)^2 + 4\left(\frac{f_3^2}{16} - \zeta^2 \right) \right)} - \varepsilon^2 \left(\zeta^2 + 3\left(\frac{f_3}{4} \right)^2 - \Gamma \right). \qquad (5.33)$$

5.3.1.2 Simple Resonance Case ($\bar{\omega}_2 \approx 1$ and $\bar{\omega}_3$ away from 2)

Following the method similar to that described in section 5.3.1.1, for this simple resonance case $\bar{\omega}_2 \approx 1$ ($\bar{\omega}_2 = 1 + \varepsilon\sigma$) and $\bar{\omega}_3$ is away from 2, the transition curves emanating from $\bar{\omega}_2 \approx 1$ may be written as

$$\bar{\omega}_2 = 1 \pm \frac{\varepsilon}{2} \sqrt{\left(\varepsilon^2 \left(\zeta^2 + 3\left(\frac{f_2}{4} \right)^2 - \Gamma \right)^2 + 4\left(\frac{f_2^2}{16} - \mu^2 \right) \right)} - \frac{\varepsilon^2}{2} \left(\zeta^2 + 3\left(\frac{f_2}{4} \right)^2 - \Gamma \right). \qquad (5.34)$$

Here, $\Gamma = \frac{1}{2}\left(\frac{f_3^2}{4\bar{\omega}_3 + 2\bar{\omega}_3^2} \right) + \frac{1}{2}\left(\frac{f_3^2}{-4\bar{\omega}_3 + 2\bar{\omega}_3^2} \right) + \frac{1}{2}\left(\frac{f_2^2}{8\bar{\omega}_2 + 8\bar{\omega}_2^2} \right)$

5.3.1.3 Simultaneous Resonance Case ($\bar{\omega}_2 \approx 1$ and $\bar{\omega}_3 \approx 2$)

In this resonance condition when the system is excited simultaneously by the external axial force and the magnetic field the frequency of excitation can be given by $\bar{\omega} = \bar{\omega}_3 = 2\bar{\omega}_2 = 2 + 2\varepsilon\sigma$. Following the method similar to that described in section 5.3.1.1 and 5.3.1.2, the expression for the transition curves can be given by

$$\bar{\omega} = 2 \pm \varepsilon \left(\varepsilon^2 \left(\zeta^2 + 3\left(\frac{\Delta}{4} \right)^2 - \Gamma \right)^2 + 4\left(\frac{(\Delta)^2}{16} - \zeta^2 \right) \right)^{\frac{1}{2}} - \varepsilon^2 \left(\zeta^2 + 3\left(\frac{\Delta}{4} \right)^2 - \Gamma \right). \qquad (5.35)$$

Here, $\Delta = f_3 - f_2$, and

$$\Gamma = -\frac{1}{2}\left(\frac{f_3^2}{4\bar{\omega}_3 + 2\bar{\omega}_3^2} \right) + \frac{1}{2}\left(\frac{f_3 f_2}{4\bar{\omega}_3 + 2\bar{\omega}_3^2} \right) - \frac{1}{2}\left(\frac{f_2^2}{8\bar{\omega}_2 + 8\bar{\omega}_2^2} \right) + \frac{1}{2}\left(\frac{f_3 f_2}{8\bar{\omega}_2 + 8\bar{\omega}_2^2} \right).$$

5.3.2 Numerical Results and Discussions

In all simulations, a steel beam with length L = 0.5 m, width d = 0.001 m, depth h = 0.005 m, Young's modulus $E = 1.94 \times 10^{11}$ N/m^2, mass of the beam m =0.04 kg, the permeability

of the vacuum, $\mu_0 = 1.26 \times 10^{-06}$ Hm^{-1}, and relative permeability $\mu_r = 3000$ are considered. In section 5.3.2.1, the results for the case with nondimensional frequency of magnetic field $\bar{\omega}_2 \approx 1$ and nondimensional frequency of external axial loading $\bar{\omega}_3$ away from 2, in section 5.3.2.2, the results for the case with $\bar{\omega}_3 \approx 2$ and $\bar{\omega}_2$ away from 1 and in section 5.3.2.3, the results for the case with $\bar{\omega}_2 \approx 1$ and $\bar{\omega}_3 \approx 2$ are presented. The instability regions are plotted and the effect of the key parameters like magnetic field B_m, damping constant c_d, static axial force P_0, amplitude of axial periodic load P_1, and tip mass M on the region of instability are investigated. In these plots, the regions bounded by the curves are unstable and regions outside the curves are stable.

5.3.2.1 Simple Resonance Due to Magnetic Field ($\bar{\omega}_2 \approx 1$ and $\bar{\omega}_3$ is away From 2)

In this case, the system is subjected to magnetic field with a frequency nearly equal to the natural frequency of the system and the frequency of external axial loading is away from the principal parametric instability zone. Fig. 5.6 shows the parametric instability region in $(\Omega_2/\omega_L)^2 \sim (B_r/B_c)^2$ plane for a cantilever beam subjected to only the transverse magnetic field. For comparison purpose, the instability region obtained experimentally and numerically by Moon and Pao (1969) has also being plotted. It is observed that the present result and the experimental result of Moon and Pao (1969) are in very good agreement. It may be noted that Wu et al. (2000) also obtained similar result by a different method (i.e., IHB method). But they have not studied the case of cantilever beam with tip-mass. Also the IHB method does not yield any close-form expression as obtained in the present work.

To thoroughly study the instability region for different system parameters, in the following figures, they are plotted either in $P_1 \sim \bar{\omega}_3$ or in $B_m^2 \sim \bar{\omega}_2$ plane. Figs. 5.7 and 5.8 respectively show the influence of static load parameter P_0 and mass ratio $\bar{m}$ on the instability regions.

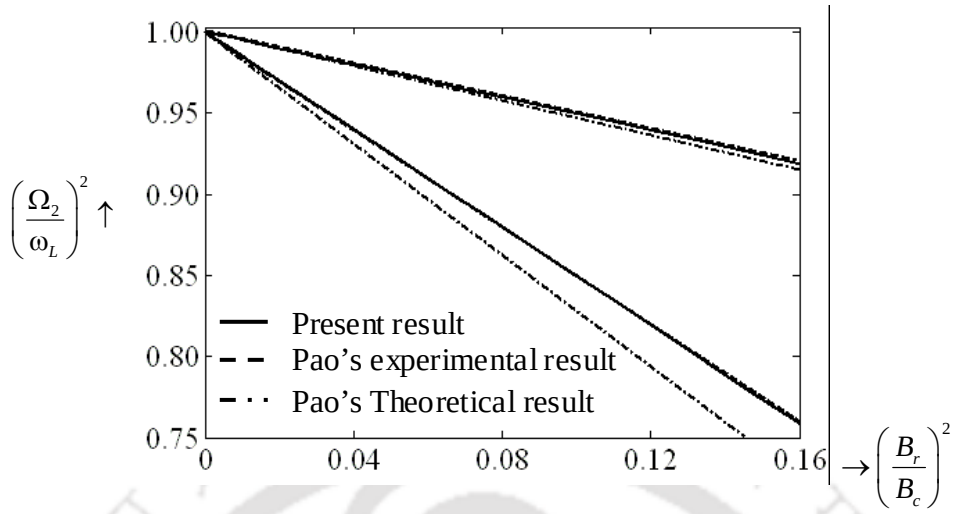

Fig. 5.6. The region of instability in magnetic field for cantilever beam.

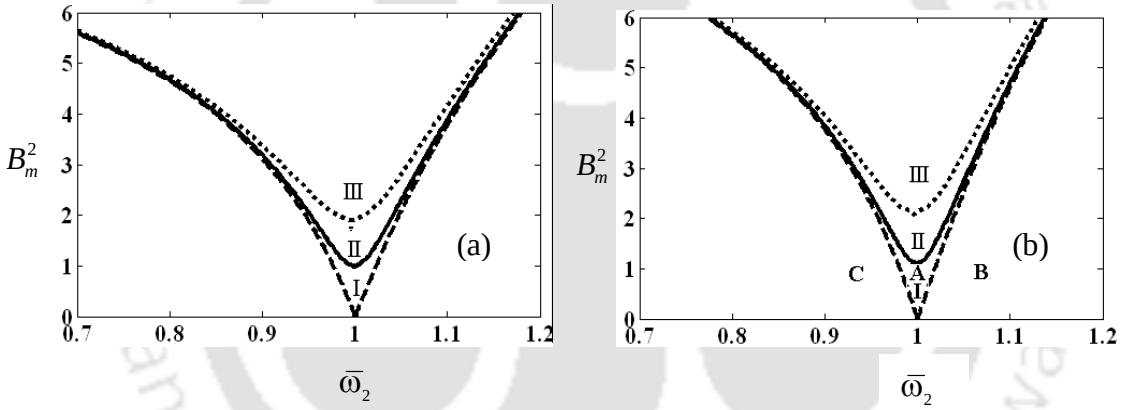

Fig. 5.7. Influence of the static axial force on the transition curves in magnetic field for cantilever beam without tip mass (I) c_d = 0.0 (II) c_d = 0.2 N-s/m, and (III) c_d = 0.4 N-s/m; (a) P_0 = 5 N, and (b) P_0 =10 N.

From Fig. 5.7, one may observe that with increase in static force the parametric instability region is decreased. One may note from Figs. 5.7 and 5.8 that with decrease in tip mass M and with increase in damping c_d the region of instability get decreased. It may be observed that these instability regions are independent of P_1 as the frequency of axial loading is away from the principal parametric zone.

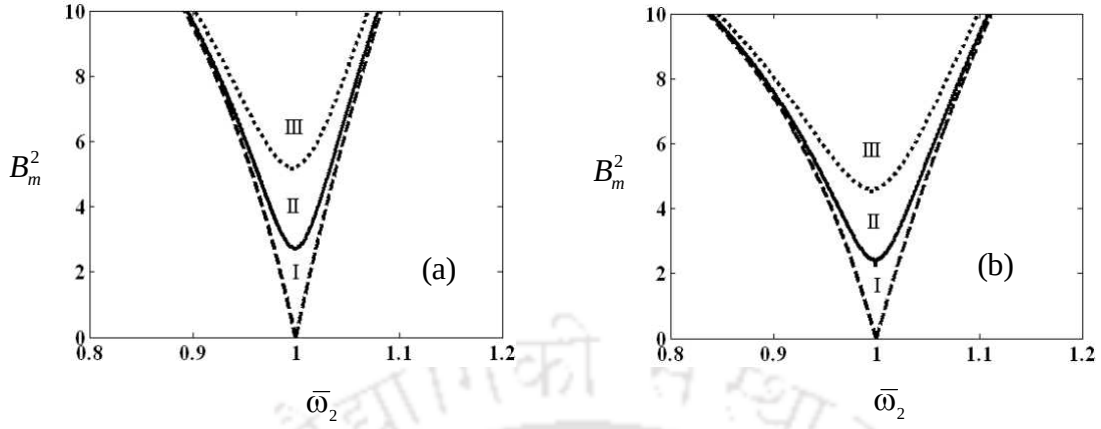

Fig. 5.8. Influence of the mass ratio on the transition curves in magnetic field for cantilever beam with tip mass for $P_0 = 1.0$, (I) c_d = 0.0 (II) c_d = 0.2 N-s/m, and (III) c_d = 0.4 N-s/m; (a) $\bar{m}$ =0.1, and (b) $\bar{m}$ =0.2.

The instability regions obtained in this resonance case are verified by solving the temporal differential equation of motion (5.13). The time responses for three points in the instability regions are determined (points of A, B, and C of Fig. 5.7(b, I)) with damping c_d =0.0 as shown in Figs. 5.9(a, b, c). It may clearly be observed from the time responses that while points B and C are stable trivial state response, point A is unstable, which is in good agreement with the perturbation analysis.

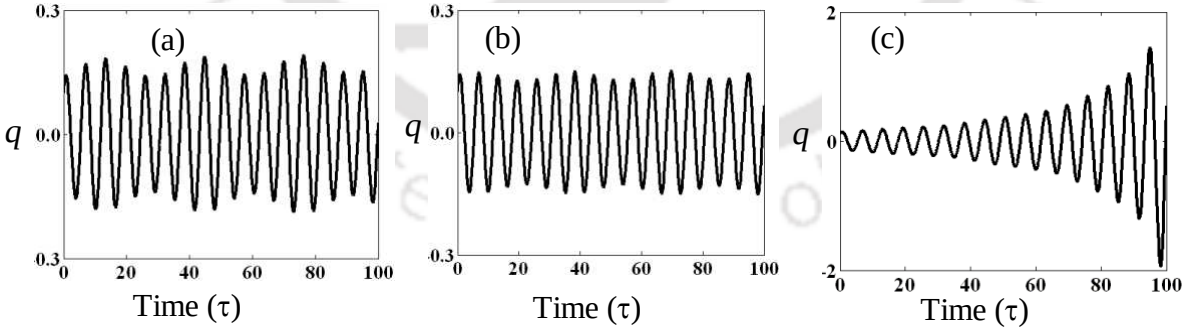

Fig. 5.9. Time response for (a) point C (b) point B and (c) point A; key as in Fig. 5.7(b, I).

5.3.2.2 Principal Parametric Resonance ($\bar{\omega}_3 \approx 2$ and $\bar{\omega}_2$ away from 1)

In this section, effect of damping constant, magnetic field, static axial force, and mass ratio on the parametric instability regions in periodic axial force field are investigated. Figs. 5.10-5.12 show the instability regions when the system is excited at a frequency $\bar{\omega}_3 \approx 2$ (i.e. nearly equal to twice the fundamental frequency) and $\bar{\omega}_2$ is away from 1.

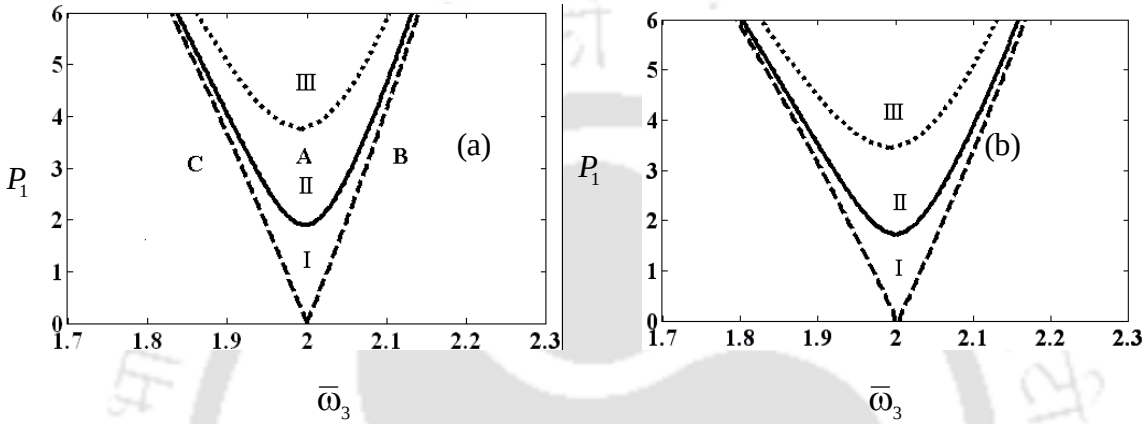

Fig. 5.10. Influence of the magnetic field on the transition curves in periodic axial force field for $P_0 = 1.0$, $\bar{m} = 0$, (I) $c_d = 0.0$ (II) $c_d = 0.2$ N-s/m, and (III) $c_d = 0.4$ N-s/m; (a) $B_m =$ 0.3 T, and (b) $B_m =$1.3 T.

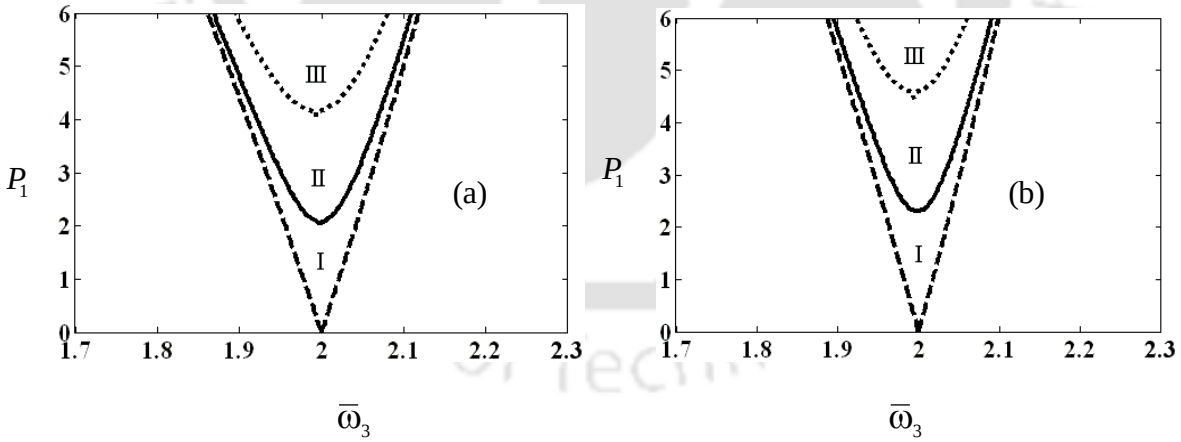

Fig. 5.11. Influence of the static axial force on the transition curves in periodic axial force field for $B_m = 0.3$ T, $M = 0$, (I) $c_d = 0.0$ (II) $c_d = 0.2$ N-s/m, and (III) $c_d = 0.4$ N-s/m; (a) P_0 = 5 N, and (b) $P_0 = 10$ N.

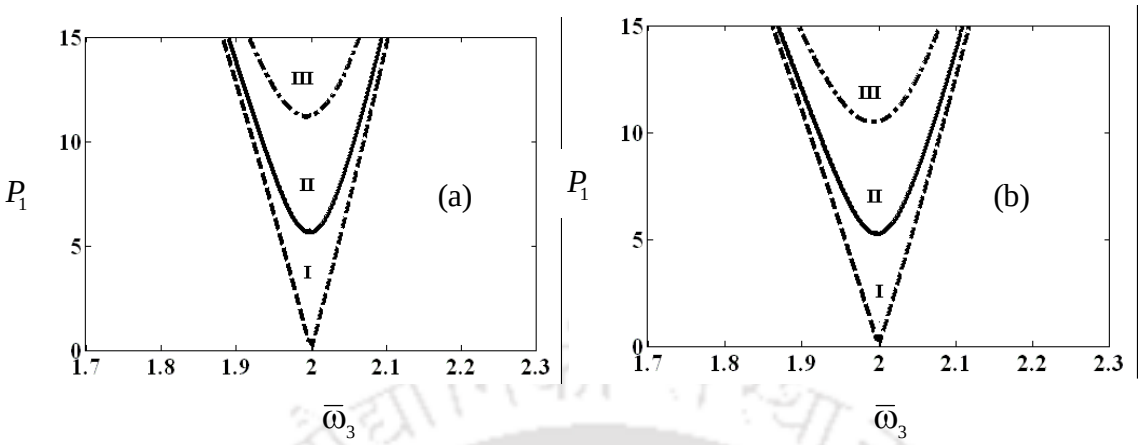

Fig. 5.12. Influence of the mass ratio on the transition curves in periodic axial force field for B_m = 0.3 T and P_0 = 1.0 N, (I) c_d = 0.0 (II) c_d = 0.2 N-s/m, and (III) c_d = 0.4 N-s/m; (a) $\bar{m}$ =0.1, and (b) $\bar{m}$ =0.2.

In Fig. 5.10, the influence of magnetic field and damping on the instability regions for the system shown in Fig. 5.5 is investigated. It is observed that with increase in magnetic field strength B_m, the instability region increases and with increase in damping the system becomes more stable. Fig. 5.11 shows the influence of static load parameter P_0 and damping on the parametric instability regions for the same system. From Figs. 5.10(a) and 5.11, it is apparent that with increase in P_0 the instability regions decreases. This is due to the fact that with increases in P_0 the natural frequency of the system increases, which reduces the range of instability regions. Fig. 5.12 shows the influence of tip mass ratio $\bar{m}$ (ratio of the tip mass to the mass of the beam) on the instability regions for the system shown in Fig. 5.5. As with increase in mass ratio, the natural frequency ω_L decreases, $\bar{\omega}_3$ increases. This causes the increase in the instability region, which may be noted from Figs. 5.10-5.12. From all these figures, it is observed that damping improves the stability of the system.

Similar to the previous case, here also for the principal parametric resonance case i.e., $\bar{\omega}_3 \approx 2$, one may verify the instability regions obtained using the perturbation analysis by

plotting the time response which are determined numerically by solving the temporal equation (5.13). Figs. 5.13(a, b, c) show the time responses for three points A, B, and C which are marked in Fig. 5.10 (a, II) with c_d =0.2. In Fig. 5.10, it is shown that while point B and C are in stable region point A is in the unstable regions, which are in good agreement with the time response obtained from the temporal equation.

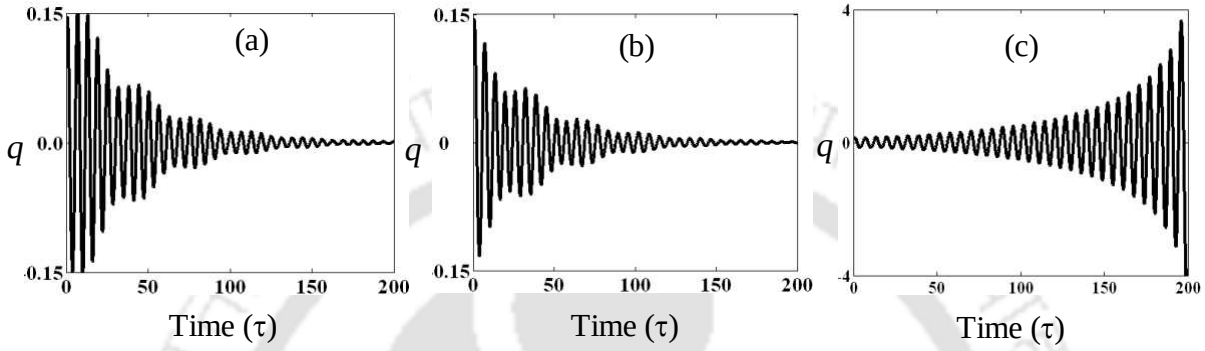

Fig. 5.13. Time response for (a) point C (b) point B and (c) point A; key as in Fig. 5.10(a, II).

5.3.2.3 Simultaneous Principal Parametric and Simple Resonance ($\bar{\omega}_2 \approx 1$ and $\bar{\omega}_3 \approx 2$)

In this case, the system is subjected to magnetic field with a frequency nearly equal to the natural frequency of the system and an external axial loading with a frequency nearly equal to twice the fundamental frequency. Hence the system is subjected to simultaneous principal parametric resonance due to external axial loading and simple resonance due to magnetic field. In this case, Fig. 5.14 shows the influence of magnetic field and damping on the transition curves for the system shown in Fig. 5.5. It is observed that with increase in magnetic field and damping the stability of the system improves. One may find a critical value P_1 below which the system is always stable. For example, from Fig. 5.14(b) for the system with c_d =0.2 the critical value P_1 is 5.05 N. These values will be very much useful for designing the flexible manipulators.

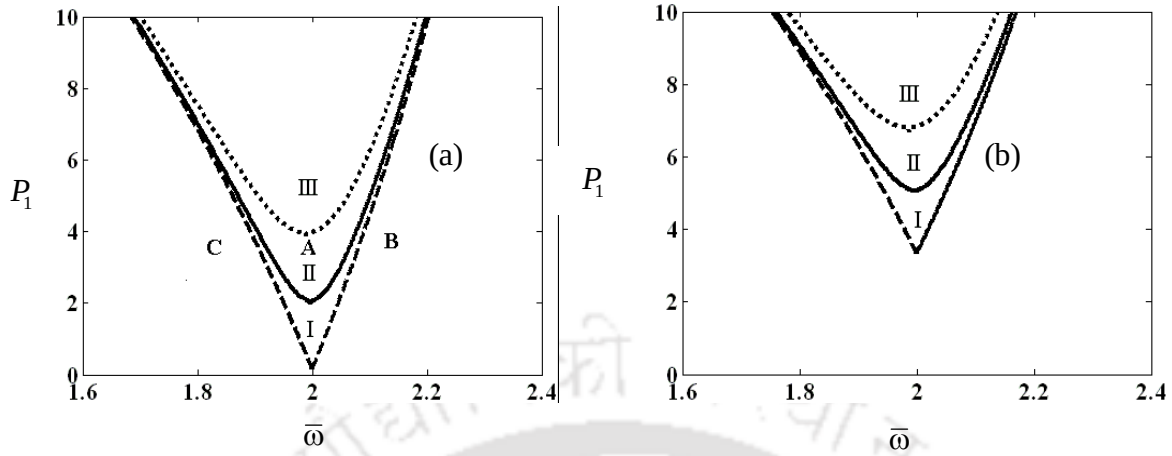

Fig.5.14. Influence of the magnetic field on the transition curves for $P_0 = 1.0$ N, $M = 0$, (I) $c_d = 0$ (II) $c_d = 0.2$ N-s/m, and (III) $c_d = 0.4$ N-s/m; (a) $B_m = 0.3$ T, and (b) $B_m = 1.3$ T.

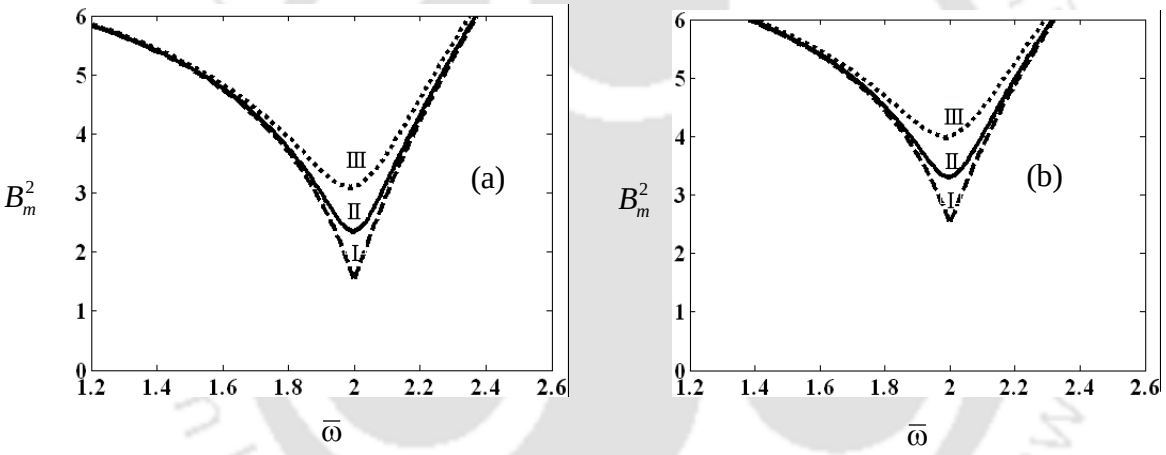

Fig. 5.15. Influence of the periodic axial force on the transition curves for $P_1 = 1.0$ N, $M = 0$, (I) $c_d = 0.0$ (II) $c_d = 0.2$ N-s/m, and (III) $c_d = 0.4$ N-s/m; (a) $P_0 = 5$ N, and (b) $P_0 = 10$ N.

The influence of static load P_0 on the instability regions B_m^2 □ Ω is shown in Fig. 5.15 (a, b) and it is observed that with increase in P_0, the instability region decreases. For example, from Fig. 5.15 (a, III) the system is always stable for a magnetic field of B_m^2 less than 3.1 and with increase of P_0 to 5 this critical value of B_m^2 increases to 3.95.

Figures 5.16 and 5.17 show the influence of mass ratio $\overline{m}$ on the parametric instability regions in $P_1 - \Omega$ and $B_m^2 - \Omega$ planes, respectively. One may observe that similar to the previous cases, here also with increase in $\overline{m}$ the region of instability increases.

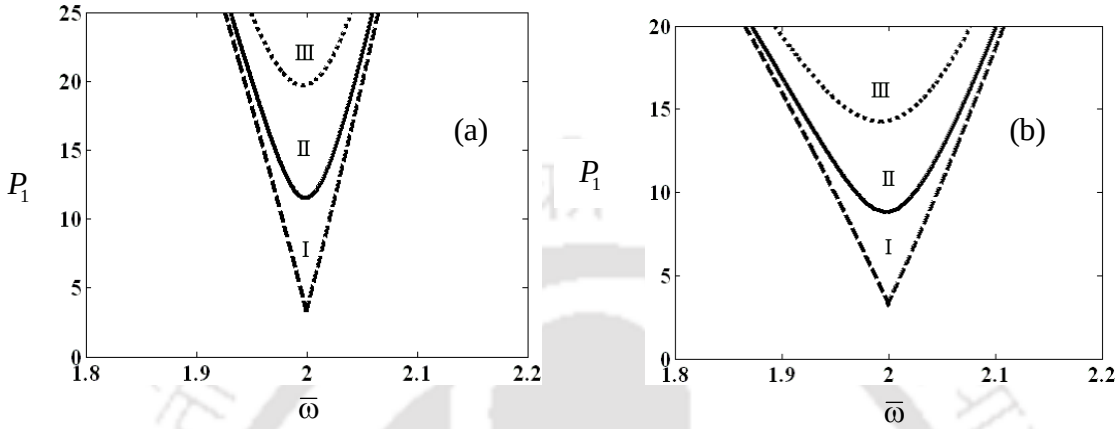

Fig. 5.16. Influence of the mass ratio in periodic axial force on the transition curves for $P_0 = 1.0$ N, B_m = 0.3 T, (I) c_d = 0.0 (II) c_d = 0.2 N-s/m, and (III) c_d = 0.4 N-s/m; (a) $\overline{m}$ =0.1, and (b) $\overline{m}$ =0.2.

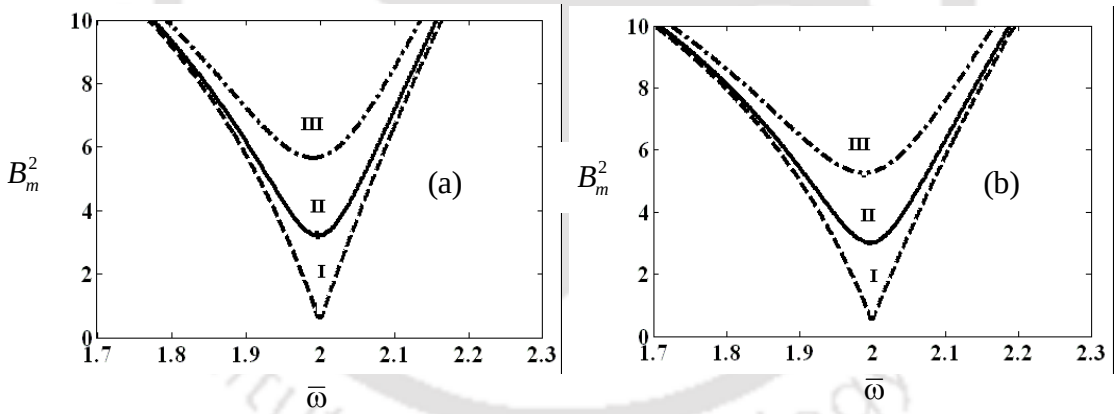

Fig. 5.17. Influence of the mass ratio in magnetic field on the transition curves for $P_1 = 1.0$ N, $P_0 = 1.0$ N, (I) c_d = 0.0 (II) c_d = 0.2 N-s/m, and (III) c_d = 0.4 N-s/m; (a) $\overline{m}$ =0.1, and (b) $\overline{m}$ =0.2.

Similar to previous cases, here the results from the perturbation analysis are compared by plotting the time response, which are obtained by numerically solving the temporal

equation of motion (5.13). Fig. 5.18 (a, b, c) correspond respectively to the point A, B, C of Fig. 5.14 (a, II). They are found to be in good agreement.

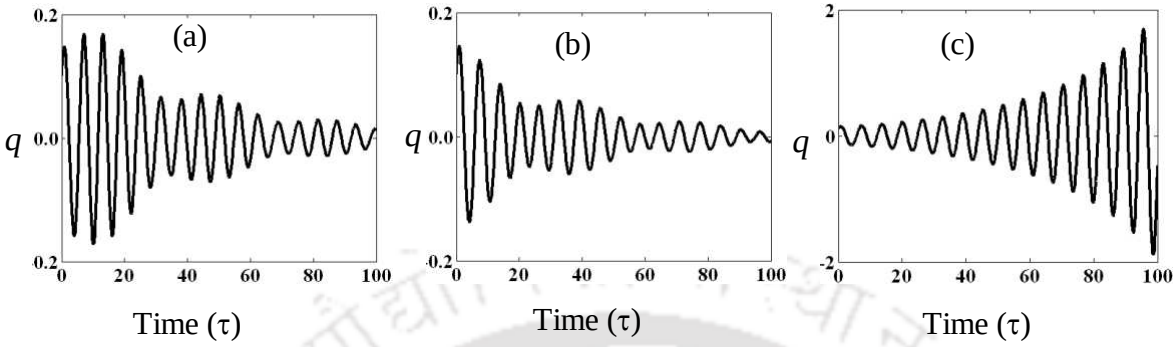

Fig. 5.18. Time response for (a) point C (b) point B and (c) point A; key as in Fig. 5.10(a, II).

5.4 Cantilevered Manipulator with both Static and Dynamic Magnetic Field

5.4.1 Analysis

Unlike the previous cases, where the manipulator is subjected to a dynamic magnetic field only, here the manipulator is subjected to both static and dynamic magnetic field as shown in Fig. 5.4. Following similar procedure of method of multiple scales as explained in section 3.3.1(Chapter 3), here also the solution of the equation (5.12) can be obtained by representing the displacement q in terms of different time scales (T_0, T_1) and a book-keeping parameter ε. Following similar procedure as in section 3.3.1, substituting $T_n = \varepsilon^n \tau$, $n = 0, 1, 2\cdots$ and $q(\tau;\varepsilon) = q_0(T_0, T_1) + \varepsilon q_1(T_0, T_1) + O(\varepsilon^2)$ in equation (5.12) and equating the coefficients of like powers of ε, one may obtain the following expressions:

Order ε^0 : $D_0^2 q_0 + q_0 = 0$, (5.36)

Order ε^1 : $D_0^2 q_1 + q_1 = -2D_0 D_1 q_0 - 2\zeta D_0 q_0 - \alpha_1 q_0^3 - \alpha_2 (D_0^2 q_0) q_0 - \alpha_3 (D_0 q_0)^2 q_0^2$

$$+ f_4 \cos(\bar{\omega}_2 T_0) q_0 + f_2 \cos(2\bar{\omega}_2 T_0) q_0 + k_{0,2} (D_0 q_0) q_0^2$$

$$+ (k_3 \cos\bar{\omega}_2 \tau + k_2 \cos 2\bar{\omega}_2 \tau)(D_0 q_0) q_0^2 . \quad (5.37)$$

In this case,

General solutions of equation (5.36) can be written as

$$q_0 = A(T_1, T_2)\exp(iT_0) + \bar{A}(T, T_2)\exp(-iT_0) . \quad (5.38)$$

Substituting equation (5.38) into equation (5.37) leads to

$$D_0^2 q_1 + q_1 = -2i D_1 A \exp(iT_0) - 2i\zeta A \exp(iT_0) - (3\alpha_1 - 3\alpha_2 + \alpha_3 - ik_{0,2}) A^2 \bar{A} \exp(iT_0)$$

$$+ (-\alpha_1 + \alpha_2 + \alpha_3 + ik_{0,2}) A^3 \exp(3iT_0) + \frac{f_4}{2}\left[A \exp i(\bar{\omega}_2 + 1)T_0 + \bar{A} \exp i(\bar{\omega}_2 - 1)T_0\right]$$

$$+ \frac{ik_3}{2} A^3 \exp i(\bar{\omega}_2 + 3)T_0 + \frac{ik_3}{2} A^2 \bar{A} \exp i(\bar{\omega}_2 + 1)T_0 - \frac{ik_3}{2} A\bar{A}^2 \exp i(\bar{\omega}_2 - 1)T_0$$

$$+ \frac{ik_3}{2} A^3 \exp i(3 - \bar{\omega}_2)T_0 + \frac{f_2}{2}\left[A \exp i(2\bar{\omega}_2 + 1) + \bar{A} \exp i(2\bar{\omega}_2 - 1)\right]T_0$$

$$+\frac{ik_2}{2}A^3\exp i(2\bar{\omega}_2+3)T_0+\frac{ik_2}{2}A^2\bar{A}\exp i(2\bar{\omega}_2+1)T_0-\frac{ik_2}{2}\bar{A}^2A\exp i(2\bar{\omega}_2-1)T_0$$

$$+\frac{ik_2}{2}A^3\exp i(3-2\bar{\omega}_2)T_0+cc\,. \tag{5.39}$$

In is observed that equation (5.39) contain many secular or small divisor terms when non-dimensional frequency ($\bar{\omega}_2$) of magnetic field strength is nearly equal to 1 or 2. Hence, in the following subsections, these two cases are studied.

5.4.1.1 Simple Resonance Case ($\bar{\omega}_2 \approx 1$)

By using similar procedure as described in subsection 3.3.1.1 (Chapter 3), one may obtain the following reduced equations:

$$\dot{a}=-\zeta a+\frac{k_{0,2}}{8}a^3+\frac{f_2}{4}a\sin\gamma\,, \tag{5.40}$$

$$a\dot{\gamma}=2a\left(\frac{\bar{\omega}-1}{\varepsilon}\right)-\frac{3}{4}\left(\alpha_1-\alpha_2+\frac{\alpha_3}{3}\right)a^3+\frac{1}{4}a^3k_2\sin\gamma+\frac{f_2}{2}a\cos\gamma\,. \tag{5.41}$$

Both trivial and nontrivial responses can be determined by solving the above reduced equations, simultaneously. Similarly, to find the stability of the steady state responses, one may investigate the eigen-values of the resulting Jacobian matrix (J). The Jacobian matrix (J) is given by

$$J=\begin{bmatrix} -\zeta+\frac{3k_{0,2}}{8}a_0^2+\frac{f_2}{4}\sin\gamma_0 & \frac{f_2}{4}a_0\cos\gamma_0 \\ -\frac{3}{2}\left(\alpha_1-\alpha_2+\frac{\alpha_3}{3}\right)a_0+\frac{1}{2}a_0k_2\sin\gamma_0 & \frac{1}{4}a_0^2k_2\cos\gamma_0-\frac{f_2}{2}\sin\gamma_0 \end{bmatrix}. \tag{5.42}$$

The first order nontrivial steady state response of the system can be given as follows.

$$q=a\cos\left(\bar{\omega}_2\tau-\gamma\right). \tag{5.43}$$

In this resonance condition, one may obtain the following expression for finding the trivial state instability regions.

$$\bar{\Omega} = \bar{\omega}_2 = \frac{\Omega_2}{\omega_L} = \delta \pm \frac{\varepsilon}{2\delta}\left(\frac{f_0^2}{4} - 4\bar{\mu}^2\right) + O\left(\varepsilon^2\right). \tag{5.44}$$

5.4.1.2 Principal Parametric Resonance Case ($\bar{\omega}_2 \approx 2$)

Here, also, by using similar procedure as explained in previous chapter (subsection 3.4.1.2 and 4.4.1.2), one may obtain the following reduced equations.

$$\dot{a} = -\zeta a + \frac{k_{0,2}}{8}a^3 + \frac{f_4}{4}a\sin\gamma, \tag{5.45}$$

$$a\dot{\gamma} = a\left(\frac{\bar{\omega} - 2}{\varepsilon}\right) - \frac{3}{4}\left(\alpha_1 - \alpha_2 + \frac{\alpha_3}{3}\right)a^3 + \frac{1}{4}a^3 k_3 \sin\gamma + \frac{f_4}{2}a\cos\gamma. \tag{5.46}$$

Similarly, in this condition, one may find the response of the system by solving equations (5.45, 5.46) simultaneously. Also, the stability of the steady state responses can be obtained by investigating the eigenvalues of the Jacobian matrix (J) which is given by

$$J = \begin{bmatrix} -\zeta + \frac{3k_{0,2}}{8}a_0^2 + \frac{f_4}{4}\sin\gamma_0 & \frac{f_4}{4}a_0\cos\gamma_0 \\ -\frac{3}{2}\left(\alpha_1 - \alpha_2 + \frac{\alpha_3}{3}\right)a_0 + \frac{1}{2}a_0 k_3 \sin\gamma_0 & \frac{1}{4}a_0^2 k_3\cos\gamma_0 - \frac{f_4}{2}\sin\gamma_0 \end{bmatrix}. \tag{5.47}$$

For this case the system will be stable if and only if all the real parts of the eigen-values are negative. Now the first order nontrivial steady state response of the system can be given by

$$q = a\cos\left(\frac{1}{2}\left(\bar{\omega}_2\tau - \gamma\right)\right). \tag{5.48}$$

From equation (5.47), the expression for the transition curve (i.e., the trivial state stability region) may be expressed as follows.

$$\bar{\omega}_2 = \frac{\Omega_2}{\omega_L} = 2\delta \pm \frac{\varepsilon}{\delta}\left(\frac{f_{1,0}^2}{4} - 4\bar{\mu}^2\right) + O\left(\varepsilon^2\right). \tag{5.49}$$

5.4.2 Numerical Results and Discussions

Here, in all simulations, a beam made of ferrite material (e.g., $MnZnFe_3O_2$) with length L = 0.5 m, width d = 0.005 m, depth h = 0.001 m, Young's Modulus $E = 2.0\times10^{11}$ N/m^2, mass of the beam per unit length m = 0.0235 kg, the permeability of the vacuum, $\mu_0 = 1.26\times10^{-6}$ Hm^{-1}, material conductivity σ = 100 Vm^{-1}, and relative permeability $\mu_r = 2500$ are considered here. The instability regions and the frequency response curves are plotted and the effect of the key parameters like damping c_d, amplitude of static (B_s) and dynamic (B_d) magnetic field strength, and tip mass (M) on the region of instability and frequency response curves are studied. In region of instability plots, the regions bounded by the curves are unstable and regions outside the curves are stable. In the frequency response curves, the dotted and solid lines represent, respectively the unstable and stable response of the system. In this work, B_m is replaced by B_d.

5.4.2.1 Simple Resonance Case ($\bar{\omega}_2 \approx 1$)

In this resonance case, the beam is subjected to a transverse magnetic field with a frequency nearly equal to the natural frequency of the system and the frequency is away from the principal parametric instability region($\bar{\omega}_2 \approx 2$). Similar to the work of Moon and Pao (1969), and Wu et al. (1997), here, also the regions of instability are plotted in $\left(\Omega_2/\omega_L\right)^2$ □ $\left(B_r/B_c\right)^2$ plane. The experimental and theoretical results of Moon and Pao (1969) are also being plotted in Fig. 5.19 to compare with the present results. It can be observed that the result obtained in the present work is in good agreement with the experimental finding by Moon and Pao (1969). Similar result was obtained by Wu *et al.* (1997) using an incremental harmonic balance (IHB) method for a cantilever beam. From the expression of the natural frequency of the system, one may note that the natural frequency varies with both the static and dynamic amplitude of the magnetic field strength. It may also be noted that the system has a critical values of B_s, B_d beyond which the system will be unstable. From the expression of natural frequency equation (5.8), the

critical value of B_s, B_d can be obtained by equating $\left(1-\bar{B}_s-\bar{B}_d\right)$ to zero. Hence, for a higher value of B_s one should take a lower value of B_d and vise versa. For the present system parameters, the critical value of B_d is found to be 0.57549335 when the static magnetic field strength B_s is equal to zero. In the present work, all B_s and B_d values are considered within the limiting range.

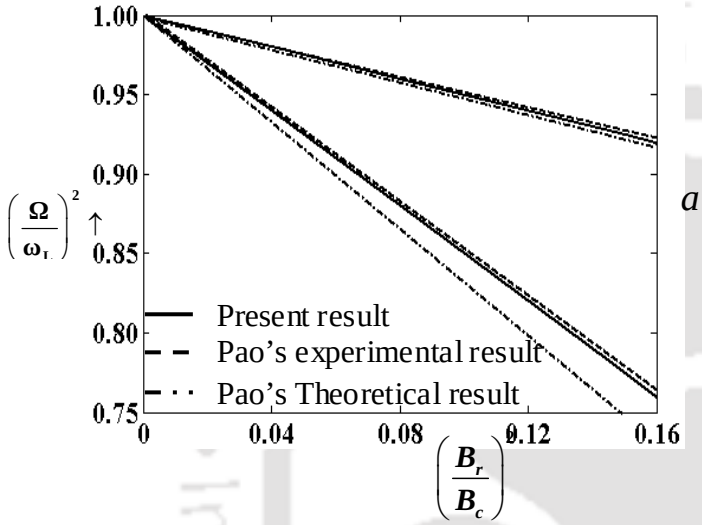

Fig. 5.19. Region of instability in the presence of magnetic field for $M=0.0$, $c_d=0.0$

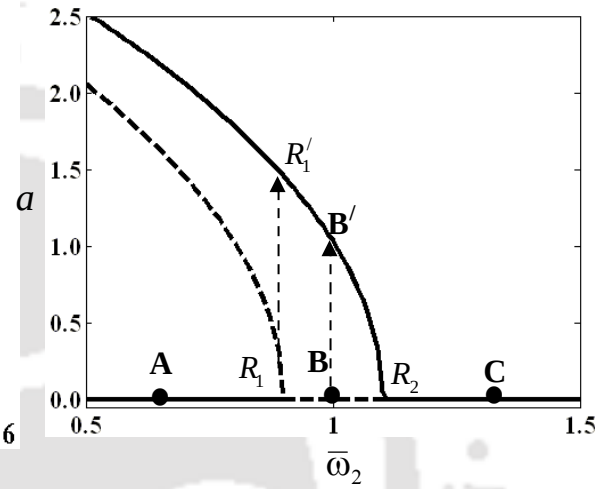

Fig. 5.20. Frequency response curves for $M=0.02$ kg, $c_d=0.01$ N-s/m, $B_s=0.1$ T, $B_d=0.3$ T, and $\sigma=10^2$ Vm^{-1}.

Though the instability region predicts whether the trivial state response is stable or not, one may not know the actual system response which may also be stable or unstable nontrivial response. To study the nontrivial responses along with trivial state responses, the frequency response curves are plotted by using the reduced equations. (5.69, 5.70). Figure 5.20 shows the frequency response curve for B_d and B_s equal to 0.3 T and 0.1 T, respectively. One may observe that the system possesses both nontrivial and trivial state responses. The trivial state becomes unstable by the sub-critical pitchfork bifurcation point R_1 which ends with a super-critical pitchfork bifurcation at R_2. Also, the system has experienced a jump up phenomena at the sub-critical pitchfork bifurcation point R_1, where

it jumps to $R_1^{/}$ with a jump length equal to 1.490. After super-critical pitchfork bifurcation point R_2, the system has a wide range of stable trivial state. If the system is operating at a frequency which is in the unstable trivial state range (e.g., point B), the system will vibrate with amplitude equal to the nontrivial solution (point B') as shown in Fig. 5.20. The system has a bistable region upto R_1. In this region, the initial condition will play the crucial role to find the system response.

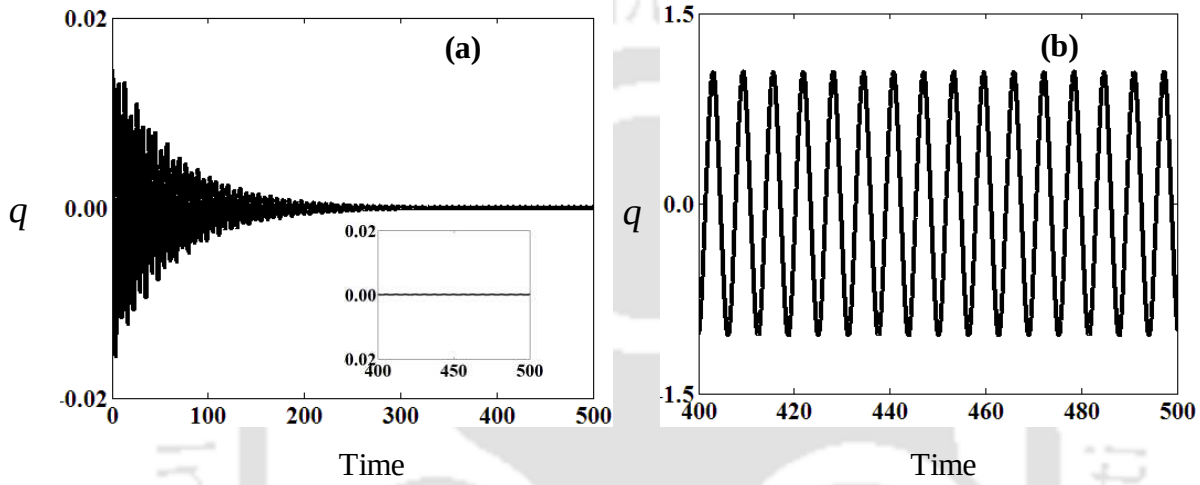

Fig. 5.21. (a) Time response for the point A and (b) time response for the point B as marked in Fig. 5.20.

One may verify the accuracy of the perturbation results by solving the temporal equation of motion (5.12). Figures 5.21 and 5.22 show the time responses of the system with parameters same as the points A. B and C marked in Fig. 5.20. While Figs. 5.21(a) and 5.21(b), show that the time responses for point A and B, Fig. 5.22 shows the time response for the point C. These responses clearly depict that point A and C are stable and point B is unstable trivial state response which are in good agreement with the results obtained by using method of multiple scales (Fig. 5.20). Effect of magnetic field strength on the transient and steady state response is also shown in Fig. 5.22. While solid line represents the response of the manipulator with magnetic field, the dotted line represents the response of the manipulator without magnetic field. It is shown that by using magnetic field, the system response can be reduced significantly.

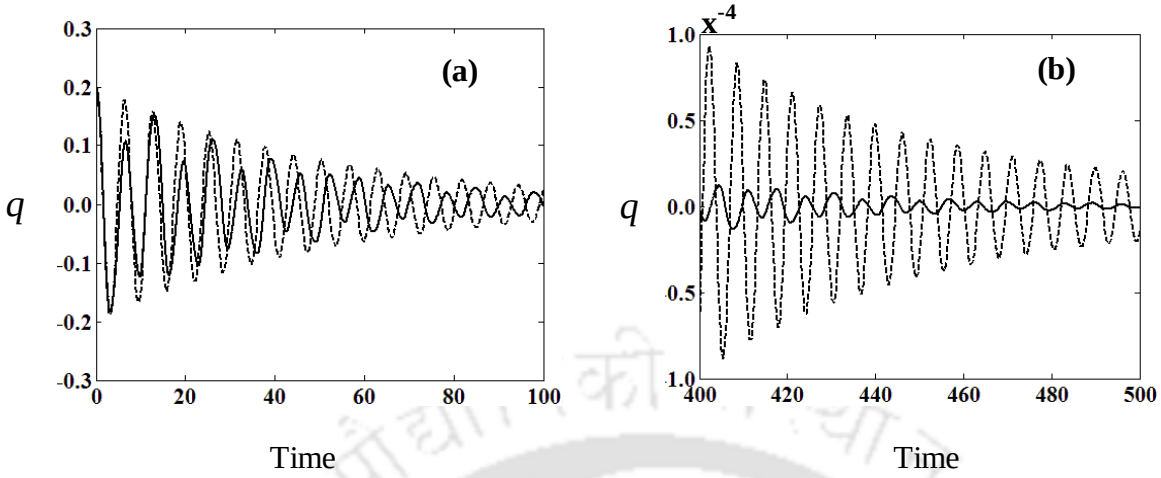

Fig. 5.22. (a) Transient response and (b) steady state time response for the point C.

Figure 5.23 shows the frequency response curve for three different values of amplitude of magnetic field strength (B_d) keeping the value of B_s equal to 0.1 T. It is observed that with increase in B_d, while the response amplitude decreases, the unstable region of the trivial state increases which is similar to that shown in Fig. 5.19. The jump up length $R_1R_1^{/}$ gets increased with increase in B_d. The sub-critical pitchfork bifurcation starts at a lower value of $\bar{\omega}_2$. Hence, for this resonance condition, to control the vibration of the system, the operating frequency Ω_2 should be less than and close to the frequency at the sub-critical pitchfork bifurcation point R_1 and the magnitude of the dynamic magnetic field strength should be as low as possible.

The effect of tip mass (M) on the frequency response curve is shown in Fig. 5.24. It is observed that with increase in tip mass M, the response amplitude decreases and unstable trivial range increases. The bifurcation point R_1 starts at a lower value of $\bar{\omega}$ with increase in M. But the jump length from the critical point R_1 to $R_1^{/}$ increases with increase in M or decrease in m_b (mass of the beam i.e. ρAL).

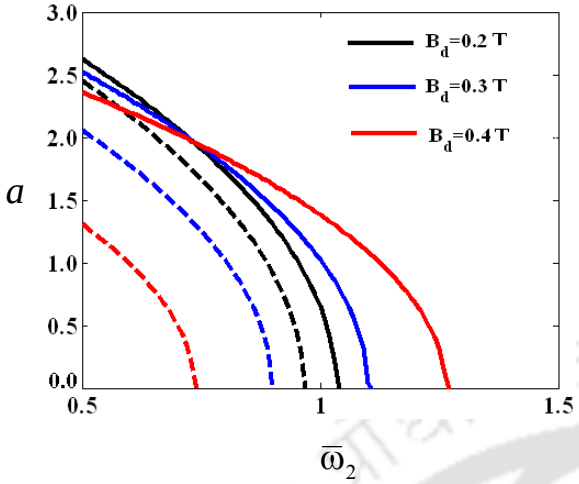

Fig. 5.23. Influences of B_d on the frequency response curves for $M = 0.02$ kg, $c_d = 0.01$ N-s/m, $B_s = 0.1$ T, and $\sigma = 10^2$ Vm^{-1}.

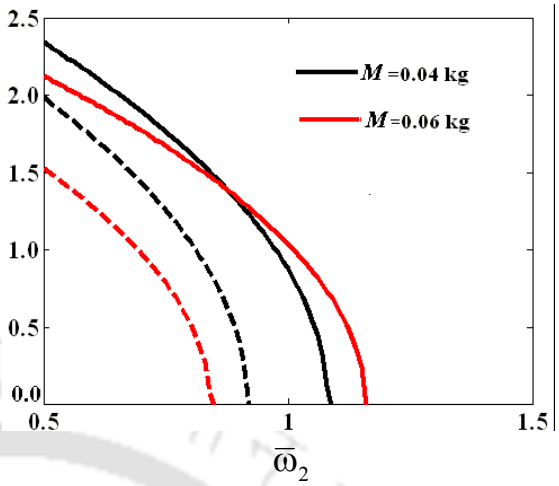

Fig. 5.24. Influences of M on the frequency response curves for $M = 0.02$ kg, $c_d = 0.01$ N-s/m, $B_s = 0.1$ T, and $\sigma = 10^2$ Vm^{-1}.

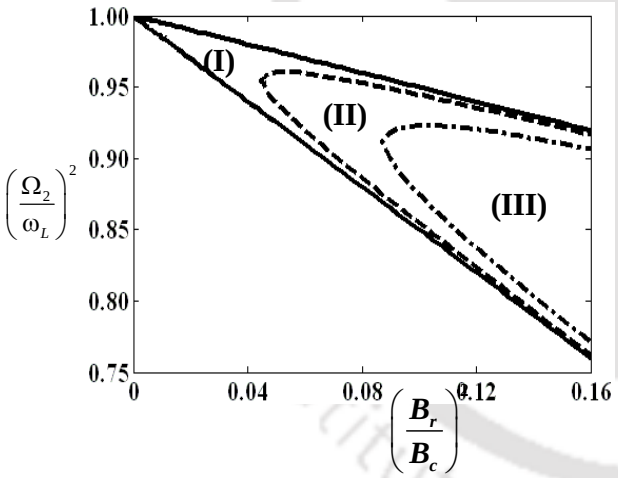

Fig. 5.25. Influence of c_d on instability region for $M = 0.0$, (I) $c_d = 0.0$ N-s/m, (II) $c_d = 0.02$ N-s/m, (III) $c_d = 0.03$ N-s/m.

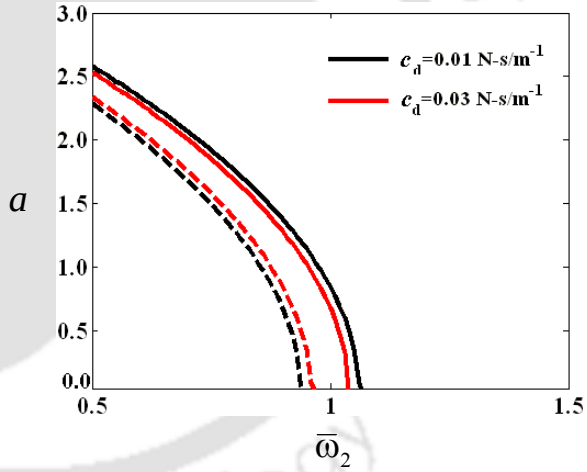

Fig. 5.26. Influences of c_d on the frequency response curves for $M = 0.02$ kg, $B_s = 0.1$ T, and $\sigma = 10^2$ Vm^{-1}.

Figure 5.25 shows the influence of damping c_d on the instability region and it is found that with increase in c_d, the instability region decreases. Similarly, the effect of damping on

nontrivial responses is studied by plotting the frequency response as shown in Fig. 3.26. It is observed that with increase in c_d, both the response amplitude and unstable trivial range get decreased which is similar to that shown in Fig. 5.25.

The effect of static magnetic field strength B_s on the region of instability is shown in Fig. 5.27. One may note that with B_s equal to zero, the transition curves start at a frequency Ω_2 equal to the linear natural frequency (ω_L). But with increase in B_s, the transition curves start at a frequency (Ω_2) which is lower than ω_L. It is also observed that for a particular value of B_d, the range of instability (R_1R_2) remain unchanged with increase in B_s. Figure 5.28 shows the frequency response curves for two different values of B_s.

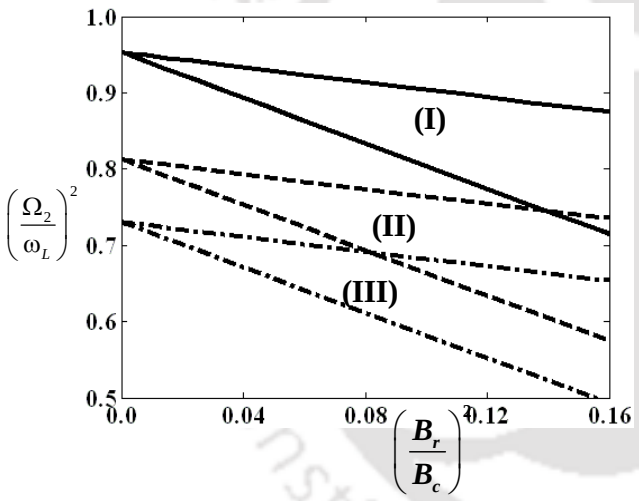

Fig. 5.27. Influence of B_s on instability region for $M = 0.0$ kg, $c_d = 0.0$, (I) $B_s = 0.05$ T, (II) $B_s = 0.1$ T (III) $B_s = 0.2$ T.

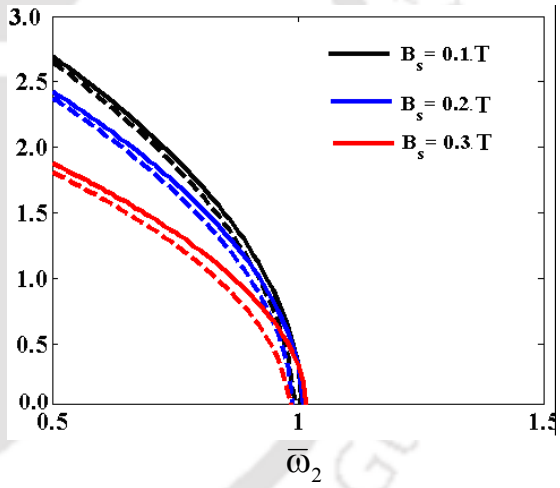

Fig. 5.28. Influence of B_s on the frequency response curves for $M = 0.02$ kg, $c_d = 0.01$ N-s/m, $B_d = 0.1$ T, and $\sigma = 10^2$ Vm^{-1}.

One may observe that with increase in B_s, the response amplitude decreases significantly, while the unstable trivial range remains almost same. Hence, to control the vibration of the system one should properly choose the amplitude (B_s, B_d) and frequency of the magnetic

field (Ω_2). It is observed from Figs. 5.23 and 5.28 that to reduce the amplitude of vibration significantly, one should increase B_s and for minor or precise control of vibration amplitude, B_d may be increased. But these values should be within their critical limits.

5.4.2.2 Principal Parametric Resonance Case ($\bar{\omega}_2 \approx 2$)

In this case, the beam is subjected to a transverse magnetic field with a frequency nearly equal to twice the natural frequency of the system. From the temporal equation of motion (equation 5.12), it may be observed that while f_2 which is the amplitude for simple resonance case is a function of dynamic field strength B_d only, the coefficient of parametric excitation term f_4 is a function of both static and dynamic amplitude of the magnetic field strength. Hence, unlike the previous case, here the instability region is plotted in $(B_{rr}/B_c)^2 \sim (\Omega/\omega_L)$ plane instead of $(B_r/B_c)^2 \sim (\Omega/\omega_L)^2$ plane. Figure 5.29 shows the instability region for three different values of the amplitude of dynamic magnetic field strength B_d. Unlike the simple resonance case, here it is observed that with increase in B_d, the instability region gets increased. But with increase in B_d, the transition curves start at a frequency (Ω_2) which is lower than twice the linear natural frequency (ω_L). As $B_{rr}^2 = \frac{B_s B_d}{2}$, one may get similar curves by keeping B_d constant and changing the parameter B_s.The influence of B_s on the frequency response curves is shown in Fig. 5.30. The influence of B_s on the frequency response curves is shown in Fig.5.30 One may note that with increase in B_s, both the nontrivial response amplitude and instability region increases. The sub-critical pitchfork bifurcation point occurs at a lower value of $\bar{\omega}$ with increase in B_s. The jump length $R_1 R_1'$ increases with increase in B_s. Hence, unlike the simple resonance condition, here, it is observed that the magnetic field has a destabilizing effect. As the effects of tip mass and damping are observed to be similar as in the previous case, these results have not been shown here. Hence, from the numerical results of simple

and principal parametric resonance cases, it is observed that use of a magnetic field with a frequency close to the linear natural frequency will significantly reduce the amplitude of vibration rather than applying a magnetic field with a frequency twice the linear natural frequency.

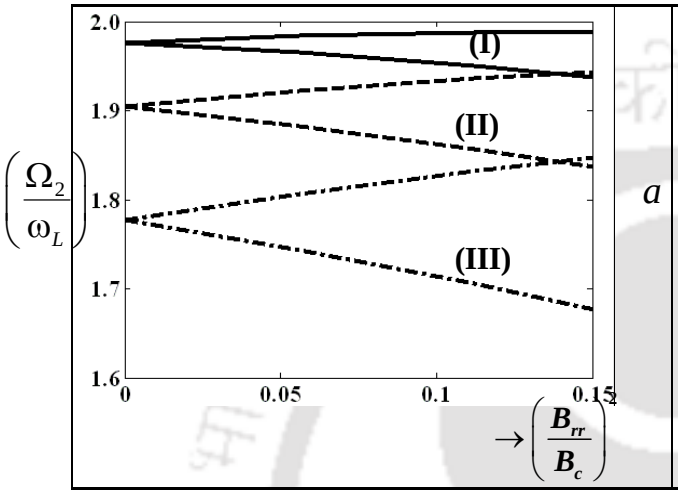

Fig. 5.29. Influence of B_d for $M = 0.02$ kg, $c_d = 0.0$, $B_s = 0.2$ T, $\sigma = 10^2$ Vm^{-1}, (I) $B_d = 0.05$ T (II) $B_d = 0.1$ T (III) $B_d = 0.2$ T.

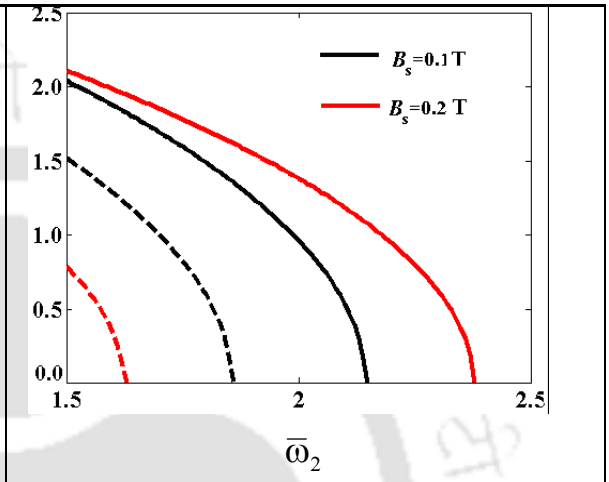

Fig. 5.30. Influence of B_S on frequency response curve for $B_d = 0.2$ T, $M = 0.02$ Kg, $\sigma = 10^2$ Vm^{-1}, $c_d = 0.01$ N-s/m.

5.5 Magnetoelastic Cantilevered Manipulator without Axial Force

5.5.1 Analysis

As mentioned in section 5.4.1, in this case, as the manipulator is modeled as a simple cantilever beam subjected to magnetic field and its equation of motion is given by equation (5.11). To obtain the solution of this equation, by using method of multiple scales, one may use $T_n = \varepsilon^n \tau$, $n = 0, 1, 2\cdots$ and $q(\tau;\varepsilon) = q_0(T_0, T_1) + \varepsilon q_1(T_0, T_1) + O(\varepsilon^2)$ in equation (5.11) and equate the coefficient of like powers of ε, which will yields the following equations.

$$\text{Order}\,\varepsilon^0: \quad D_0^2 q_0 + q_0 = 0, \tag{5.50}$$

$$\text{Order}\ \varepsilon^1: D_0^2 q_1 + q_1 = -2D_0 D_1 q_0 - 2\zeta D_0 q_0 - \alpha_1 q_0^3 - \alpha_2 \left(D_0^2 q_0\right) q_0 - \alpha_3 \left(D_0 q_0\right)^2 q_0^2 + f_2 \cos\left(2\bar{\omega} T_0\right) q_0 + k_2 \left(1 + \cos\left(2\bar{\omega} T_0\right)\right)\left(D_0 q_0\right) q_0^2 . \tag{5.51}$$

General solution of Equation (5.50) can be written as

$$q_0 = A(T_1, T_2)\exp(iT_0) + \bar{A}(T_1, T_2)\exp(-iT_0) . \tag{5.52}$$

Here, $\bar{A}(T_1, T_2)$ is the complex conjugate of $A(T_1, T_2)$.

Substituting Equation (5.52) into Equation (5.51) leads to

$$D_0^2 q_1 + q_1 = -2i A' \exp(iT_0) - 2i\zeta A \exp(iT_0) - \left(3\alpha_1 - 3\alpha_2 + \alpha_3 - ik_2\right) A^2 \bar{A} \exp(iT_0) +$$

$$\left(-\alpha_1 + \alpha_2 + \alpha_3\right) A^3 \exp\left(3iT_0\right) + ik_2 A^3 \exp\left(3iT_0\right) + \frac{f_2}{2}\left[A \exp i(2\bar{\omega}_2 - 1) + \bar{A} \exp i(2\bar{\omega}_2 - 1)\right] T_0$$

$$+ \frac{ik_2}{2} A^3 \exp i(2\bar{\omega}_2 + 3) T_0 + \frac{ik_2}{2} A^2 \bar{A} \exp i(2\bar{\omega}_2 + 1) T_0 - \frac{ik_2}{2} \bar{A}^2 A \exp i(2\bar{\omega}_2 - 1) T_0$$

$$+ \frac{ik_2}{2} A^3 \exp i(3 - 2\bar{\omega}_2) T_0 + cc . \tag{5.53}$$

In this case, one may observe that the solution of equation (5.53) contains secular or small divisor terms when the non-dimensional frequency of magnetic field strength ($\bar{\omega}_2$) is

nearly equal to 1. This will lead to a simple resonance condition. In this case, one may use detuning parameter σ to express the nearness of $\bar{\omega}$ to 1, as

$$\bar{\omega} = 1 + \varepsilon\sigma, \quad \text{and} \quad \sigma = O(1). \tag{5.54}$$

Substituting equation (5.54) into equation (5.53), and equating the secular and small-divisor terms to zero will yield the following equation.

$$-2iA'\exp(iT_0) - 2i\zeta A\exp(iT_0) - (3\alpha_1 - 3\alpha_2 + \alpha_3 - ik_2)A^2\bar{A}\exp(iT_0)$$
$$+\frac{f_2}{2}\bar{A}\exp(2\sigma T_1) + i\frac{k_2}{2}A^3\exp(-2\sigma T_1) - i\frac{k_2}{2}\bar{A}^2A\exp(2\sigma T_1) = 0. \tag{5.55}$$

Putting A equal to $\frac{1}{2}a(T_1)e^{(i\beta T_1)}$ and $\gamma = 2\sigma T_1 - 2\beta$ into equation (5.55) and separating the real and imaginary terms, one may obtain a set of reduced equations as given below.

$$\dot{a} = -\zeta a + \frac{k_2}{8}a^3 + \frac{f_2}{4}a\sin\gamma, \tag{5.56}$$

$$a\dot{\gamma} = 2a\left(\frac{\bar{\omega}-1}{\varepsilon}\right) - \frac{3}{4}\left(\alpha_1 - \alpha_2 + \frac{\alpha_3}{3}\right)a^3 + \frac{1}{4}a^3k_2\sin\gamma + \frac{f_2}{2}a\cos\gamma. \tag{5.57}$$

One may determine both the trivial and nontrivial responses by solving equation (5.56) and (5.57), simultaneously. To find the stability of the steady state responses, one may investigate the eigenvalues of the Jacobian matrix (J) which is given by

$$J = \begin{bmatrix} -\zeta + \frac{3k_2}{8}a_0^2 + \frac{f_2}{4}\sin\gamma_0 & \frac{f_2}{4}a_0\cos\gamma_0 \\ -\frac{3}{2}\left(\alpha_1 - \alpha_2 + \frac{\alpha_3}{3}\right)a_0 + \frac{1}{2}a_0k_2\sin\gamma_0 & \frac{1}{4}a_0^2k_2\cos\gamma_0 - \frac{f_2}{2}\sin\gamma_0 \end{bmatrix}. \tag{5.58}$$

It may be noted that the system will be stable if and only if all the real parts of the eigen-values are negative. By finding the eigenvalues of the Jacobian matrix (J) given in equation (5.58), for the trivial state instability region, one may obtain the following closed form expression.

$$\bar{\Omega} = \bar{\omega}_2 = \frac{\Omega_2}{\omega_L} = \delta \pm \frac{\varepsilon}{2\delta}\left(\frac{f_0^2}{4} - 4\bar{\mu}^2\right) + O(\varepsilon^2). \tag{5.59}$$

It may be noted that this simple expression is obtained by using the first order method of multiple scales. The first order nontrivial steady state response of the cantilever beam with a tip mass can be given as:

$$q = a\cos\left(\frac{1}{2}\left(\bar{\omega}_2\tau - \gamma\right)\right). \tag{5.60}$$

5.5.2 Numerical Results and Discussions

In this work, a magnetoelastic beam is taken with length L = 0.5 m, width d = 0.005 m, depth h = 0.001 m, Young's Modulus $E = 1.94\times10^{11}$ N/m^2, mass of the beam per unit length m = 0.03965 kg, and the permeability of the vacuum, $\mu_0 = 1.26\times10^{-6}$ Hm^{-1}. Using these parameters, the reduced equations. (5.56) and (5.57) are solved numerically to obtain the instability regions and the frequency response curves. The effect of the amplitude of magnetic field strength (B_m), damping (c_d), tip mass (M), material conductivity (σ), and relative permeability of the material (μ_r) on the frequency response curves are investigated. It pointed out in section 5.5.1, in this case, the system undergo only simple resonance when the beam is subjected to a transverse magnetic field with a frequency nearly equal to the natural frequency of the system. Here, the instability regions are plotted in $\left(\Omega_2/\omega_L\right)^2$ ⊔ $\left(B_r/B_c\right)^2$ plane similar to the work of Moon and Pao (1969), and Wu (2000, 2007). The experimental and theoretical results of Moon and Pao (1969) are also being plotted in Fig. 5.31 for comparison with the present result. It is found from Fig. 5.31 that the result obtained in the present work is in good agreement with the experimental results of Moon and Pao (1969). Similar results are also obtained by Wu (2005) using an incremental harmonic balance method for a cantilever beam. From the expression for the natural frequency of the system (ω_e), one may note that the natural frequency varies with the amplitude of the magnetic field strength B_m. Hence, there exists a critical limit ($\bar{B}_m = 1$) of B_m above which the system will be unstable as ω_e^2 term becomes negative. In the present analysis, B_m values are taken below this critical limit.

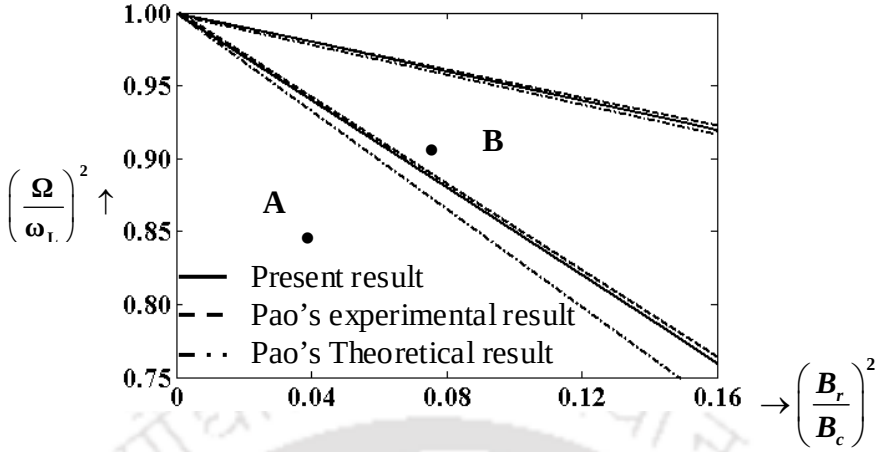

Fig. 5.31. The region of instability of a cantilever beam in magnetic field.

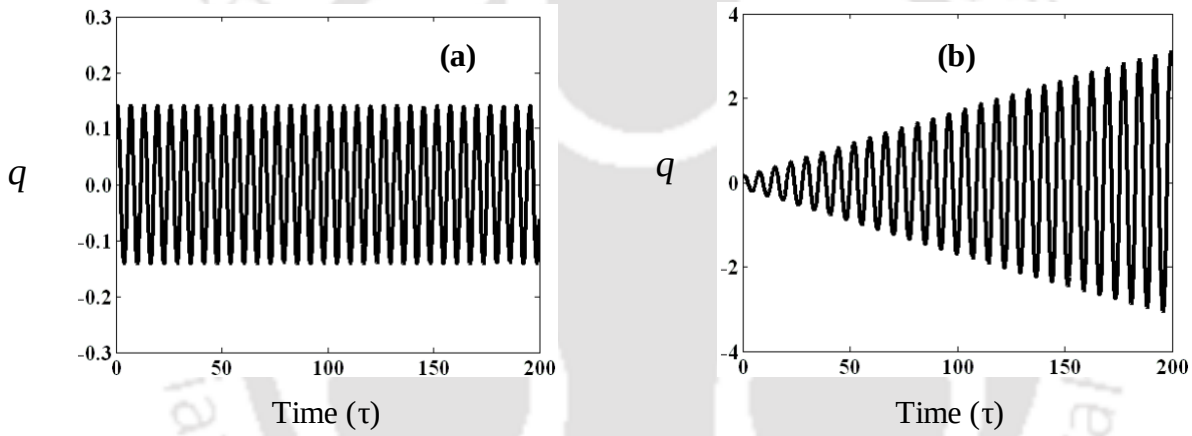

Fig. 5.32. (a) Time response for the point A and (b) time response for the point B (points A and B are marked in Fig. 5.31).

The accuracy of the instability region obtained by using the first order method of multiple scales can be verified by numerically solving the temporal equation of motion (5.11) and plotting the time response (Fig. 5.32) for two different points A and B as marked in Fig. 5.31. Figure 5.32 (i) clearly shows that the response is stable and Fig. 5.32(ii) shows that the response is unstable which are in good agreement with the result shown in Fig. 5.31. Hence, one may use the first order closed form solution (equation 5.59) for finding the instability region.

As shown in Fig. 5.31 and Fig. 5.32, though the instability region will predict the trivial state response of the system, but the actual response of the system may be nontrivial fixed point, periodic, quasi-periodic, or it may be chaotic. To study these fixed point responses the frequency response curves are plotted using the reduced equations (5.56, 5.57). Figure 5.33 shows the frequency response curve for four different values of amplitude of magnetic field strength B_m.

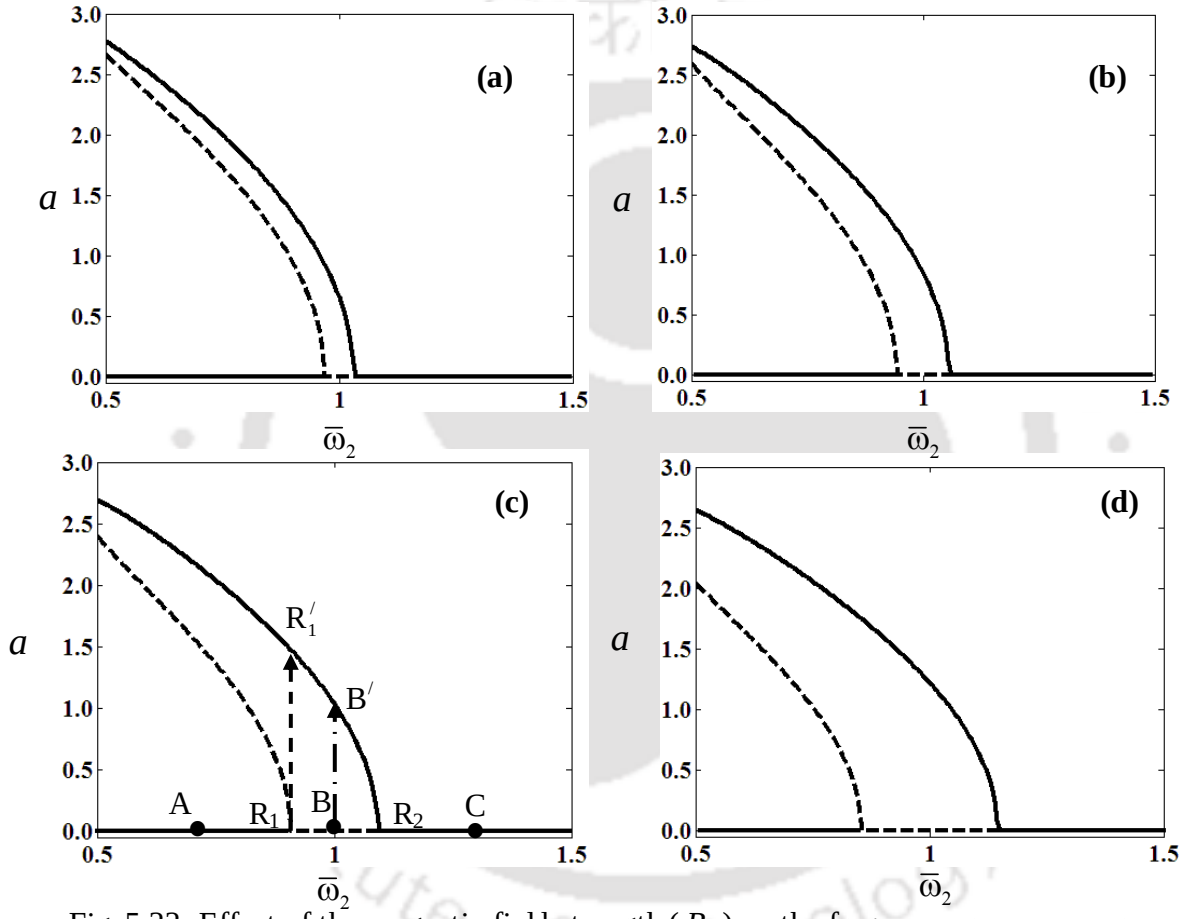

Fig. 5.33. Effect of the magnetic field strength (B_m) on the frequency response curves for $M = 0.02$ kg , $c_d = 0.01$ N-s/m , $\mu_r = 3000$, $\sigma = 10^7$ Vm^{-1} ; (a) $B_m = 0.20$ T , (b) $B_m = 0.25$ T , (c) $B_m = 0.30$ T , (d) $B_m = 0.35$ T.

From Fig. 5.33, it may be noted that with increase in B_m, though the maximum response amplitude remains unchanged, the trivial state becomes unstable which is similar to that

shown in Fig. 5.33. The trivial state becomes unstable by the sub-critical pitchfork bifurcation at R_1, which ends with a super-critical pitchfork bifurcation at R_2. Here, one may observe that the system has a tendency to jump up from the unstable trivial state at R_1 to the stable nontrivial state at R_1'. This jump up length R_1R_1' gets increased with increase in B_m. From Fig.5.33 (a), one may find that for very low value of B_m, the system has a wide range of stable trivial state. If the system is operating at a frequency which is in unstable trivial state range (R_1-R_2), the system will vibrate with an amplitude equal to the nontrivial solution as shown in Fig. 5.33(c).

The obtained perturbation results are verified by numerically solving the temporal equation of motion equation (4.11). Time responses are plotted for the three points A, B and C marked in Fig.5.33 (c). Figure 5.34(a) clearly shows the steady state response as a stable trivial state response and Fig. 5.34(b) shows the steady state response to be periodic with amplitude of 0.8812, which is same as that shown in Fig. 5.33(c) at point B'.

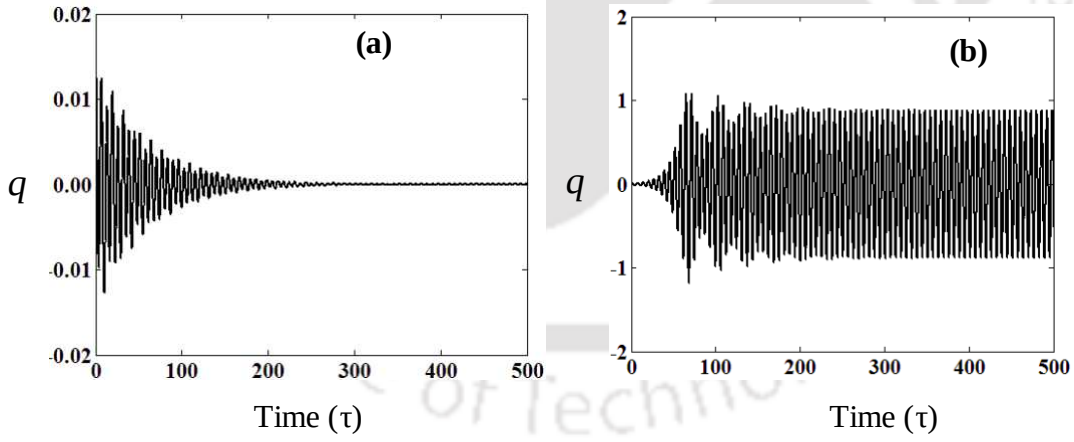

Fig. 5.34. (a) Time response for the point A and (b) time response for the point B (A and B points are marked in Fig. 5.33(c)).

Figures 5.35(a) and 5.35 (b) show the transient and steady state response for point C. In Fig. 5.35 the solid line and dotted line, respectively represent the response of the system

with and without magnetic field. In the presence of magnetic field, it is observed that the steady state response has zero amplitude. Hence, from Fig. 5.34 and Fig. 5.35, it may be noted that the perturbation results obtained by using first order method of multiple scales are in very good agreement with the results obtained by solving the temporal equation motion. Also, it may be noted that the free vibration response of the beam which is shown as dotted line in Fig. 5.35, can be significantly reduced by applying the magnetic field.

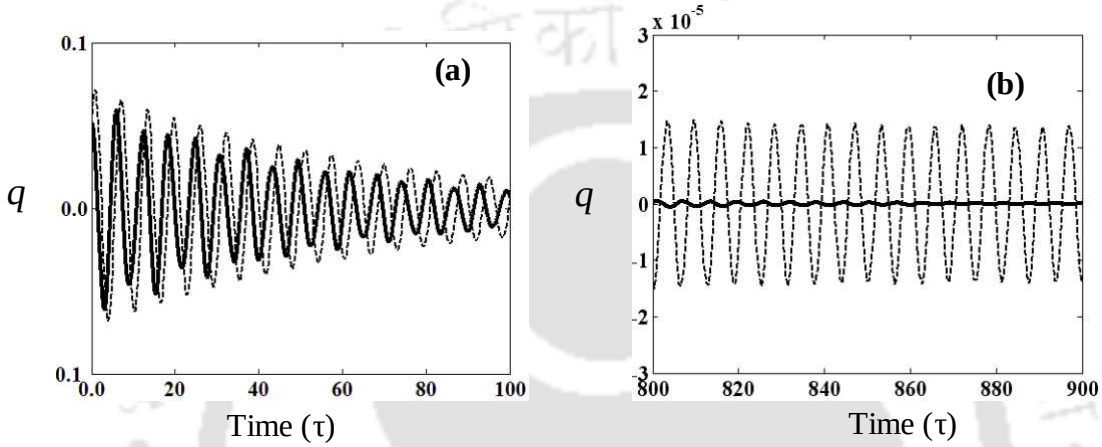

Fig. 5.35. (a) Transient response and (b) steady state time response for the point C with magnetic field (solid line) and without magnetic field (dotted line).

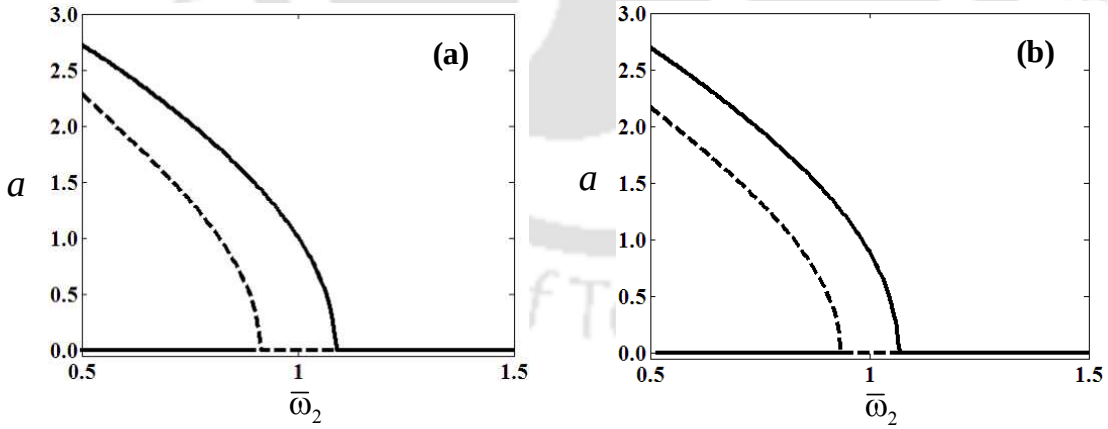

Fig. 5.36. Influence of damping on frequency response curve for $M = 0.02$ kg, $\mu_r = 3000$, $\sigma = 10^7$ Vm^{-1}, $B_m = 0.30$ T; (a) $c_d = 0.02$ N-s/m, (b) $c_d = 0.03$ N-s/m.

The effect of damping c_d on the response curves is shown in Fig. 5.36 and it is observed that with increase in c_d, while the nontrivial response amplitude remains unchanged the trivial state unstable region decreases, the sub-critical pitchfork bifurcation point R_1 occurs at a higher value of $\bar{\omega}_2$ and the corresponding jump length decreases. With increase in tip mass *M*, from Fig. 5.37(a, b) and 5.33(c), one may observe that the response amplitude increases and the bifurcation point R_1 starts at a lower value of $\bar{\omega}_2$.

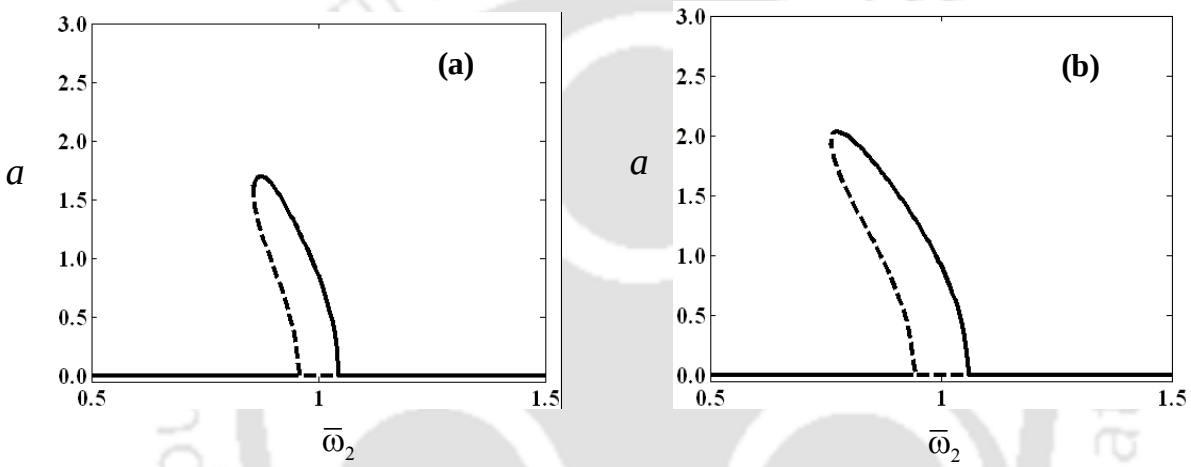

Fig. 5.37. Influence of mass ratio ($\bar{m}$) on frequency response curve for $c_d = 0.01$ N-s/m, $\mu_r = 3000$, $\sigma = 10^7$ Vm^{-1}, $B_m = 0.30$ T; (a) $M = 0.01$ kg, (b) $M = 0.015$ kg.

Keeping the material conductivity (σ) and other system parameters constant, the effect of relative permeability (μ_r) on the frequency response curves is shown in Fig. 5.38. It may be noted that the paramagnetic materials have low relative permeability ($\mu_r > 1$) with high material conductivity (σ). For example armco iron, which is a paramagnetic material, has an μ_r equal to 7.0 and conductivity σ equal to 0.99×10^7 Vm^{-1}. From Fig. 5.33(c) and Fig. 5.38, one may note that with decrease in μ_r, both the response amplitude (*a*) and unstable trivial region R_1R_2 decreases. For very less value of μ_r, a wide range of stable trivial state is observed. From the expression of natural frequency (ω_e) and coefficient of parametric

excitation term (f_2), it may be observed that decrease in μ_r, the natural frequency ω_e increases, and f_2 decreases. Due to increase in ω_e and with decrease in f_2, one may expect the decrease in the range of trivial unstable state and the response amplitudes which are similar to those observed in Figs. 5.33(c) and 5.38.

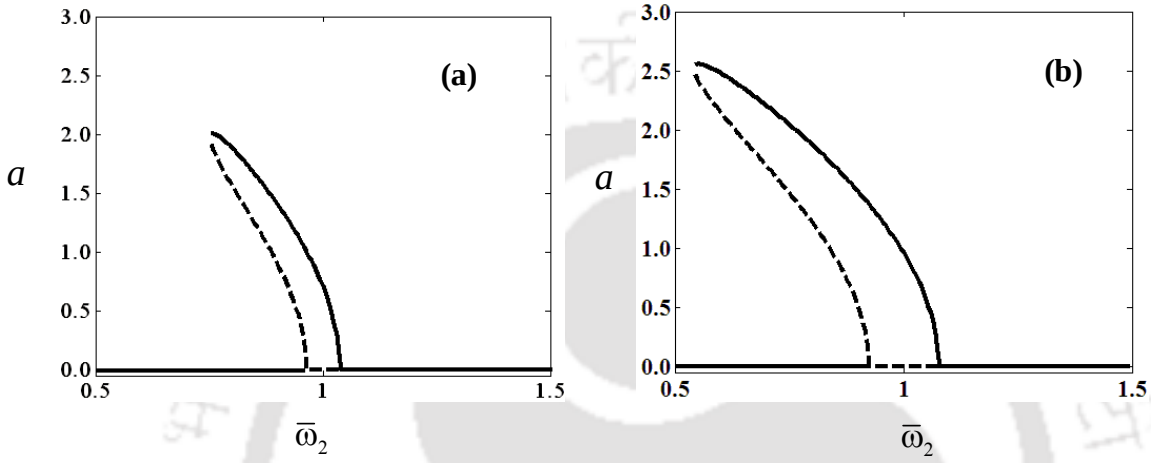

Fig. 5.38. Effect of relative permeability (μ_r) of the material on the frequency response curve $M = 0.02$ kg , $c_d = 0.01$ N-s/m , $\sigma = 10^7$ Vm^{-1}, $B_m = 0.30$ T ; (a) $\mu_r = 2.0$, (b) $\mu_r = 7.0$.

Keeping the values of the relative permeability (μ_r) and other system parameters same as that in Fig. 5.33(c), the influence of material conductively (σ) on the nonlinear frequency response curves is shown in Fig. 5.39. For ferrimagnetic materials, one may observe that their relative permeability is nearly same as that of the ferromagnetic material but their material conductivity is very low as compared to the ferromagnetic materials. For example, while $MnFe_2O_4$ a ferrimagnetic material has very low value of σ (equal to 100 Vm^{-1}), iron (95% pure), which is a ferro-magnetic material, has an σ equal to 1.01×10^7 Vm^{-1}. In both cases, the relative permeability μ_r is equal to 2500. From Figs. 5.33(c) and Fig.5.39(a, b), it is observed that with decrease in material conductively (σ), while the trivial state unstable region remains unchanged, the response amplitude marginally decreases. This may be

explained by examining the expression of k_2, which is a function of σ. With increase in σ, while the coefficient of nonlinear damping term k_2 is increasing; the overall damping is marginally decreased, as the damping factor ζ is very large in comparison to k_2 even with a very high value of σ. Hence, for accurate calculation of the system response while one may consider k_2, this term may be neglected for most of the practical design purposes.

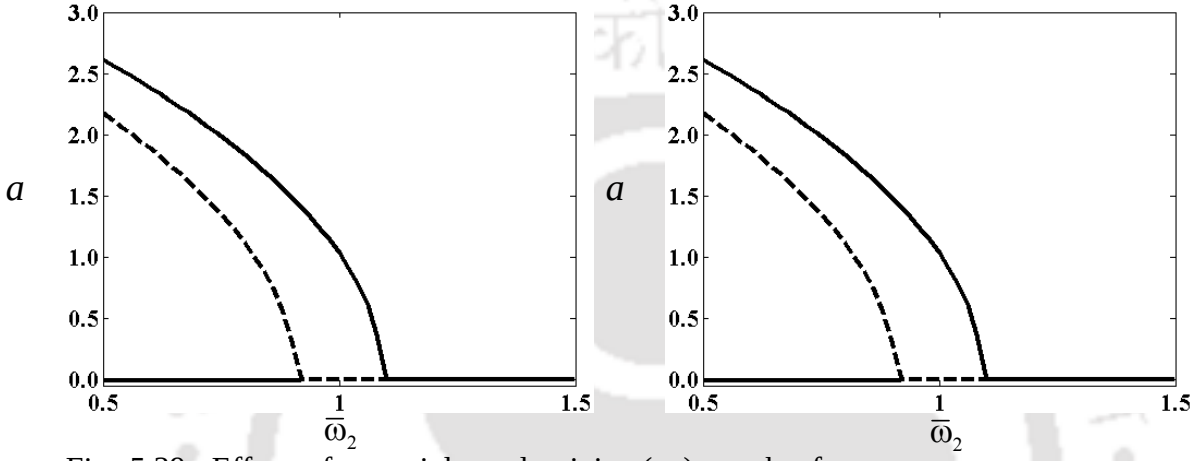

Fig. 5.39. Effect of material conductivity (σ) on the frequency response curve for $M = 0.02$ kg, $c_d = 0.01$ N-s/m, $\mu_r = 2500$, $B_m = 0.30$ T; (a) $\sigma = 10^2$ Vm^{-1}, (b) $\sigma = 10^6$ Vm^{-1}.

5.6 Magnetoelastic Cantilevered Manipulator with Periodically Varying Axial Tip Force

5.6.1 Analysis

In this section, the solution of the equation motion (5.10) for the cantilevered manipulator discussed in section 5.3.1.2 is carried out using first order method of multiple scales. Following similar procedure as explained in previous sections, substituting $T_n = \varepsilon^n \tau$, $n = 0, 1, 2\cdots$ and $q(\tau;\varepsilon) = q_0(T_0, T_1) + \varepsilon q_1(T_0, T_1) + O(\varepsilon^2)$ in equation (5.10) and equating coefficients of like powers of ε, one may find the following expressions.

Order ε^0 : $D_0^2 q_0 + q_0 = 0$, (5.61)

Order ε^1 : $D_0^2 q_1 + q_1 = -2 D_0 D_1 q_0 - 2\zeta D_0 q_0 - \alpha_1 q_0^3 - \alpha_2 (D_0^2 q_0) q_0 - \alpha_3 (D_0 q_0)^2 q_0^2 +$

$k_2 (D_0 q_0) q_0^2 + f_2 \cos(2\bar{\omega}_2 T_0) q_0 + k_2 \cos(2\bar{\omega}_2 T_0)(D_0 q_0) q_0^2 - f_3 \cos(\bar{\omega}_3 T_0) q_0$. (5.62)

General solutions of Equation (5.61) can be written as

$$q_0 = A(T_1, T_2)\exp(iT_0) + \bar{A}(T_1, T_2)\exp(-iT_0) \ . \tag{5.63}$$

Here, $\bar{A}(T_1, T_2)$ is the complex conjugate of $A(T_1, T_2)$.

Substituting equation (5.63) into equation (5.62) leads to the following expression

$$D_0^2 q_1 + q_1 = -2i A' \exp(iT_0) - 2i\zeta A \exp(iT_0) - (3\alpha_1 - 3\alpha_2 + \alpha_3 - ik_2) A^2 \bar{A} \exp(iT_0)$$

$$+ \vartheta A^3 \exp(3iT_0) + ik_2 A^3 \exp(3iT_0) + \frac{f_2}{2}\left[A \exp i(2\bar{\omega}_2 + 1) + \bar{A} \exp i(2\bar{\omega}_2 - 1)\right] T_0$$

$$- \frac{f_3}{2}\left[A \exp i(\bar{\omega}_3 - 1) + \bar{A} \exp i(\bar{\omega}_3 - 1)\right] T_0 + \frac{ik_2}{2} A^3 \exp i(2\bar{\omega}_2 + 3) T_0 +$$

$$\frac{ik_2}{2} A^2 \bar{A} \exp i(2\bar{\omega}_2 + 1) T_0 - \frac{ik_2}{2} \bar{A}^2 A \exp i(2\bar{\omega}_2 - 1) T_0 + \frac{ik_2}{2} A^3 \exp i(3 - 2\bar{\omega}_2) T_0 + cc. \tag{5.64}$$

Here, $\vartheta = -\alpha_1 + \alpha_2 + \alpha_3$ and *cc* stands for the complex conjugate of the preceding terms. It may be noted that any solution of equation (5.64) will contain secular or small divisor terms when non-dimensional frequency of magnetic field strength ($\bar{\omega}_2$) is nearly equal to

1, and/or non-dimensional frequency of axial load ($\bar{\omega}_3$) is nearly equal to 2. Unlike the previous case, here one may obtain three different resonance conditions viz. (i) $\bar{\omega}_2 \approx 1$ and $\bar{\omega}_3$ is away from 2, (ii) $\bar{\omega}_3 \approx 2$ and $\bar{\omega}_2$ is away from 1, and (iii) $\bar{\omega}_2 \approx 1$ and $\bar{\omega}_3 \approx 2$, simultaneously. In the following subsections, these resonance cases are discussed.

5.6.1.1 Simple Resonance Case Due to Magnetic Field ($\bar{\omega}_2 \approx 1$ and $\bar{\omega}_3$ away from 2)

Similar to the previous case, here also one may use a detuning parameter σ as $\bar{\omega} = 1 + \varepsilon\sigma$ to express the nearness of $\bar{\omega}$ to 1 and substituting it into equation (5.64), and eliminating the secular or small divisor terms one may obtain the following equation.

$$-2iA'\exp(iT_0) - 2i\zeta A\exp(iT_0) - \left(3\alpha_1 - 3\alpha_2 + \alpha_3 - ik_2\right)A^2\bar{A}\exp(iT_0)$$
$$+\frac{f_2}{2}\bar{A}\exp\left(2\sigma T_1\right) + i\frac{k_2}{2}A^3\exp\left(-2\sigma T_1\right) - i\frac{k_2}{2}\bar{A}^2A\exp\left(2\sigma T_1\right) = 0. \qquad (5.65)$$

Substituting A equal to $\frac{1}{2}a(T_1)e^{(i\beta(T_1))}$ in equation (5.65) and separating the real and imaginary terms, one may find the reduced equations as given below.

$$\dot{a} = -\zeta a + \frac{k_2}{8}a^3 + \frac{f_2}{4}a\sin\gamma, \qquad (5.66)$$

$$a\dot{\gamma} = 2a\sigma - \frac{3}{4}\left(\alpha_1 - \alpha_2 + \frac{\alpha_3}{3}\right)a^3 + \frac{1}{4}a^3k_2\sin\gamma + \frac{f_2}{2}a\cos\gamma. \qquad (5.67)$$

One may observe from equation (5.66, 5.67) that the system possesses both trivial and nontrivial responses. Hence, one may determine the nontrivial responses by solving equations (5.66, 5.67), simultaneously. Similarly, to find the stability of the steady state response, one may investigate the eigenvalues of the Jacobian matrix (J), which is given below.

$$J = \begin{bmatrix} -\zeta + \frac{3k_2}{8}a_0^2 + \frac{f_2}{4}\sin\gamma_0 & \frac{f_2}{4}a_0\cos\gamma_0 \\ -\frac{3}{2}\left(\alpha_1 - \alpha_2 + \frac{\alpha_3}{3}\right)a_0 + \frac{1}{2}a_0k_2\sin\gamma_0 & \frac{1}{4}a_0^2k_2\cos\gamma_0 - \frac{f_2}{2}\sin\gamma_0 \end{bmatrix}. \qquad (5.68)$$

It may be noted that the system will be stable if and only if all the real parts of the eigen-values are negative. Now, the first order nontrivial steady state response of the system can be given by

$$q = a\cos\left(\frac{\bar{\omega}_2\tau}{2} - \gamma\right) \tag{5.69}$$

5.6.1.2 Principle Parametric Resonance Due to Axial Tip Load ($\bar{\omega}_3 \approx 2$ and $\bar{\omega}_2$ away from 1)

Using, $\bar{\omega}_3 = 2 + 2\varepsilon\sigma$, where σ is the detuning parameter in equation (5.64), one may obtain the following secular or small divisor terms.

$$-\left(2iA' + 2i\zeta A\right)\exp(iT_0) - \left(3\alpha_1 - 3\alpha_2 + \alpha_3 - ik_2\right)A^2\bar{A}\exp(iT_0) - \frac{f_3\bar{A}}{2}\exp\left(2\sigma T_1\right) = 0. \tag{5.70}$$

Substituting A equal to $\frac{1}{2}a\left(T_1\right)e^{(i\beta(T_1))}$ into equation (5.70) and separating the real and imaginary terms, one may obtain the following reduced equations.

$$\dot{a} = -\zeta a + \frac{k_2}{8}a^3 - \frac{f_3}{4}a\sin\gamma, \tag{5.71}$$

$$a\dot{\gamma} = a\sigma - \frac{3}{4}\left(\alpha_1 - \alpha_2 + \frac{\alpha_3}{3}\right)a^3 - \frac{f_3}{2}a\cos\gamma. \tag{5.72}$$

Here also, the response of the system can be determined by numerically solving equations (5.71, 5.72), simultaneously. Similar to the previous cases, here also, to determine the stability of the system, one may investigate the eigenvalues of the Jacobian matrix (J) which is given below.

$$J = \begin{bmatrix} -\zeta + \frac{3k_2}{8}a_0^2 - \frac{f_3}{4}\sin\gamma_0 & -\frac{f_3}{4}a_0\cos\gamma_0 \\ -\frac{3}{2}\left(\alpha_1 - \alpha_2 + \frac{\alpha_3}{3}\right)a_0 & \frac{f_3}{2}\sin\gamma_0 \end{bmatrix}. \tag{5.73}$$

For this case the system will be stable if and only if all the real parts of the eigen-values are negative and the steady state response of the system in this resonance condition can be given by

$$q = a\cos\left(\frac{1}{2}\left(\bar{\omega}_3\tau - \gamma\right)\right). \tag{5.74}$$

5.6.1.3 Simultaneous Resonance Due to Magnetic Field and Axial Load ($\bar{\omega}_2 \approx 1$ and $\bar{\omega}_3 \approx 2$)

For this resonance condition, when the frequency of the axial load is nearly equal to the natural frequency of the system and the frequency of the magnetic field is nearly equal to twice the natural frequency, one may use the detuning parameters σ_1 and σ_2 to express the nearness of $\bar{\omega}_2$ to 1 and $\bar{\omega}_3$ to 2 as given below.

$$\bar{\omega}_2 = 1 + \varepsilon\sigma_1, \quad \bar{\omega}_3 = 2 + 2\varepsilon\sigma_2, \text{ and } \quad \sigma_1, \sigma_2 = O(1). \tag{5.75}$$

Substituting equation (5.75) into equation (5.64), one may obtain the following secular or small divisor terms which is eliminated by equating these terms to zero.

$$-2iA'\exp(iT_0) - 2i\zeta A\exp(iT_0) - \left(3\alpha_1 - 3\alpha_2 + \alpha_3 - ik_2\right)A^2\bar{A}\exp(iT_0) + \frac{f_2}{2}\bar{A}\exp\left(2\sigma_1 T_1\right)$$

$$+i\frac{k_2}{2}A^3\exp\left(-2\sigma_1 T_1\right) - i\frac{k_2}{2}\bar{A}^2 A\exp\left(2\sigma_1 T_1\right) - \frac{f_3}{2}\bar{A}\exp\left(2\sigma_2 T_1\right) = 0. \tag{5.76}$$

Similar to previous cases, substituting A equal to $\frac{1}{2}a(T_1)e^{(i\beta(T_1))}$ into equation (5.76) and separating the real and imaginary terms, one may obtain the following reduced equations.

$$\dot{a} = -\zeta a + \frac{k_2}{8}a^3 + \frac{f_2}{4}a\sin\gamma - \frac{f_3}{4}a\sin\left(2\gamma + \phi\right), \tag{5.77}$$

$$a\dot{\gamma} = 2a\sigma - \frac{3}{4}\left(\alpha_1 - \alpha_2 + \frac{\alpha_3}{3} - \frac{1}{4}k_2\sin\gamma\right)a^3 + \frac{f_2}{2}a\cos\gamma - \frac{f_3}{2}a\cos\left(2\gamma + \phi\right). \tag{5.78}$$

Here, $\gamma = \sigma_1\tau - \beta$, and $\phi = 2\left(\sigma_2 - \sigma_1\right)T_1$. It may be noted that ϕ is a measure of the phase difference between the application of the axial load and the magnetic field. In this

resonance condition, the responses of the system can be found by numerically solving equations (5.77, 5.78), simultaneously. Following similar procedure as in previous sections, the Jacobian matrix (J) can be given by

$$J=\begin{bmatrix} -\zeta+\frac{3k_2}{8}a_0^2+\frac{f_2}{4}\sin\gamma_0- & \frac{f_2}{4}a_0\cos\gamma_0 \\ \frac{f_3}{4}\sin\left(2\gamma_0+\phi_0\right) & -\frac{f_3}{2}a_0\cos\left(2\gamma_0+\phi_0\right) \\ -\frac{3}{2}\left(\alpha_1-\alpha_2+\frac{\alpha_3}{3}\right)a_0+\frac{1}{2}a_0k_2\sin\gamma_0 & -\frac{f_2}{2}\sin\gamma_0+f_3\sin\left(2\gamma_0+\phi_0\right) \end{bmatrix}. \quad (5.79)$$

5.6.2 Numerical Results and Discussions

For numerical simulation, a steel beam is taken similar to that considered in the work of Wu [2005, 2007] with length L = 0.5 m, width d = 0.005 m, depth h = 0.001 m, Young's Modulus $E = 1.94\times10^{11}$ N/m^2, mass of the beam per unit length m = 0.03965 kg, damping constant $c_d = 0.01$ N-s/m, relative permeability $\mu_r = 3000$, material 2conductivity $\sigma = 10^7$ Vm^{-1}, and the permeability of the vacuum, $\mu_0 = 1.26\times10^{-6}$ Hm^{-1}. Numerically solving the reduced equations for different resonance conditions the frequency response curves are plotted for different system parameters such as amplitude of magnetic field strength (B_m), tip mass (M), static (P_0) and dynamic (P_1) amplitude of axial load. In the frequency response curves dotted and solid lines represent, respectively the unstable and stable responses of the system. In the following subsections the results obtained for different resonance conditions are critically analyzed.

5.6.2.1 Simple Resonance Due to Magnetic Field ($\bar{\omega}_2 \approx 1$ and $\bar{\omega}_3$ away From 2)

In this case, the cantilever beam is subjected to the transverse magnetic field with a frequency closely equal to the first natural frequency of the system and the frequency of the applied axial load is away from twice the natural frequency of the system. In Fig. 5.41,

the frequency response curve of the system is plotted with amplitude of magnetic field strength equal to 0.30 T for $M = 0.02$ kg , $P_0 = 0.2$ N.

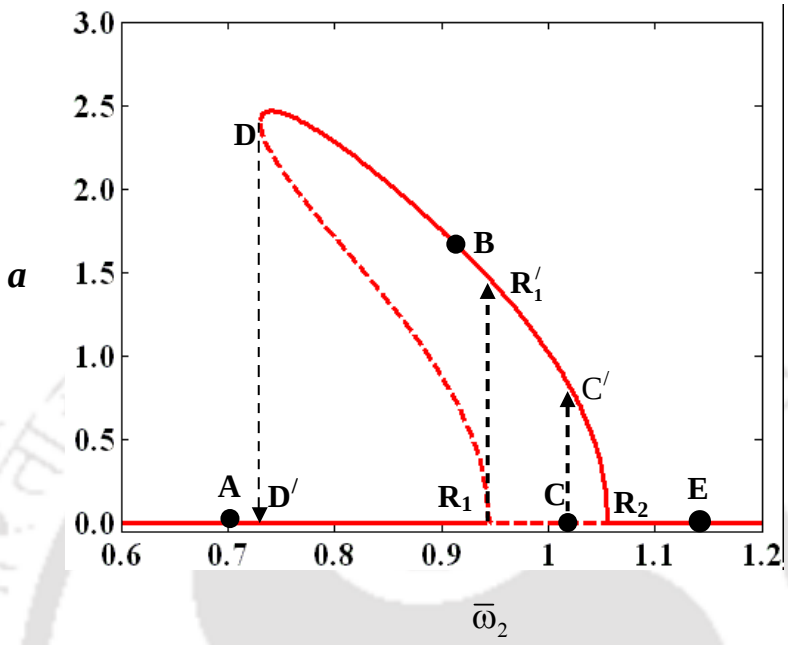

Fig. 5.40. Frequency response curves for $M = 0.02$ kg , $P_0 = 0.2$ N, $B_m = 0.30$T .

It is observed that the system has both trivial response and nontrivial responses. In other words, irrespective of the frequency of the applied axial load, the system will not vibrate if the frequency of the magnetic field is below a frequency marked by point R_1 or if it operates at a frequency which is above the point marked by R_2. With increase in the frequency of the magnetic field, at the sub-critical pitchfork bifurcation point R_1 the cantilever beam suddenly experience a jump up phenomena which may lead to the catastrophic failure of the system or the cantilever beam may start vibrating with amplitude equal to that of the nontrivial state marked by point R_1'. With further increase in the frequency of the magnetic field, the beam will vibrate with amplitude equal to that of the nontrivial stable state corresponding to $\bar{\omega}_2$. This vibration will continue till it reaches the super critical pitchfork bifurcation point R_2. Again, at this stage, if one decreases the frequency of the magnetic field, the system response will go on increasing and follow the path R_2 R_1'BD. At D which is a saddle node (S-N) bifurcation point, with further decrease

in the frequency $\bar{\omega}_1$, the system will experience a jump down phenomena. Similar to the previous jump up phenomena, here also, either the system will fail or the vibration of the system will reduce to zero. Also, it should be noted that the system has a bistable region between frequency ranges $D'R_1$ and hence, depending on the initial conditions, the beam may be at stationary position (trivial state) or vibrates with amplitude equal to that of the nontrivial state corresponding to frequency $\bar{\omega}_2$. Hence to completely suppress the vibration in this resonance condition, it is recommended that one should apply a magnetic field with a frequency which is well below D' or above R_2.

To check the accuracy of the perturbation results, one may compare these results by numerically solving the temporal equation of motion (equation, 5.10). Here, Fig. 5.41(a) shows the time responses and Fig. 5.41(b) shows the phase portraits obtained numerically by solving Equation (5.10) corresponding to three distinct points viz., A, B, and C marked in Fig.5.40. While the dotted line represents the steady state time response and phase portrait for point B, solid and solid-dash lines, respectively represent the steady state responses for point C and A.

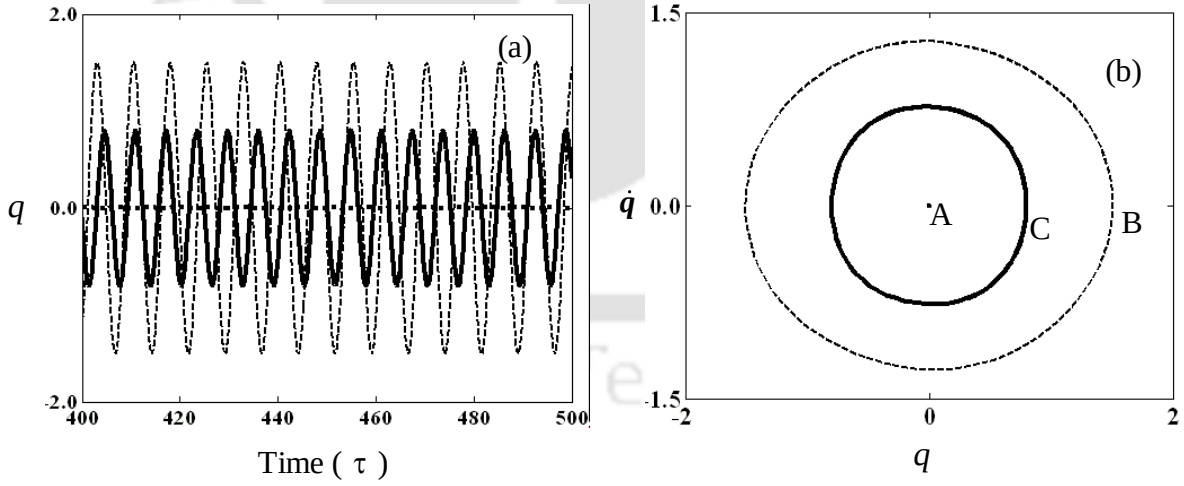

Fig. 5.41. (a) Time responses (b) phase portraits corresponding to the points A, B and C. Key same as in Fig. 5.40.

Clearly, the response curve corresponding to point A shows to have zero amplitude of oscillation and points B and C has amplitude of 1.75 and 0.79 respectively. It is interesting

to see that the steady state trajectory for point C which is initiated from unstable trivial state has amplitude equal to the value corresponding to its stable nontrivial state C/ as shown in Fig. 5.40. Hence, the results obtained by the perturbation method are in good agreement with those obtained by solving the temporal equation of motion.

The influence of magnetic field strength on the reduction of vibration of the system is also illustrated in Fig. 5.42. While Fig. 5.42(a) represents the transient part of the response, Fig. 5.42(b) shows the steady state part of the response corresponding to point E as marked in Fig. 5.40. These figures clearly illustrate the vibration reduction with proper application of magnetic field.

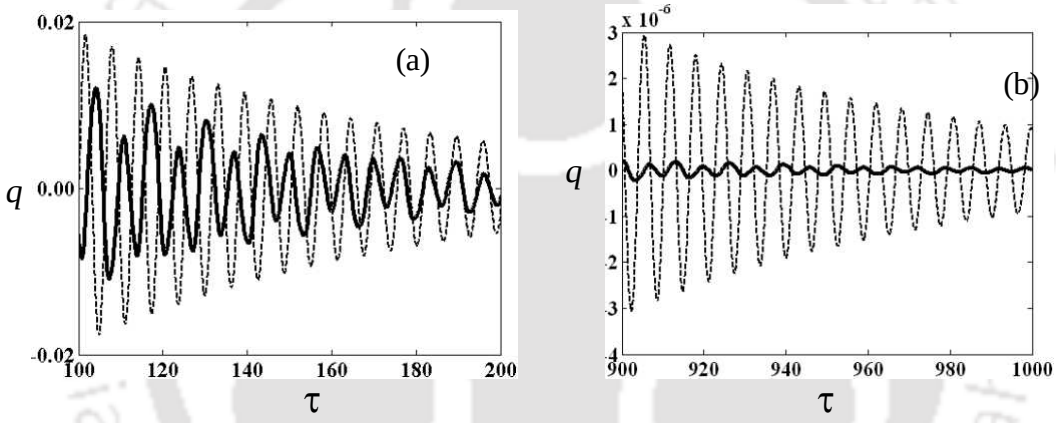

Fig. 5.42. (a) Transient time responses and (b) steady state time responses corresponding to point E as marked in Fig. 5.40. Dotted line represents the response without magnetic field and solid line represents the response with magnetic field. Key same as in Fig. 5.40.

In Figs 5.43-5.45, only the nontrivial states are plotted and one should note that though the trivial state has not been plotted it exists and is unstable only between the sub and super critical pitchfork bifurcation points as discussed in Fig. 5.40. The effect of the amplitude of magnetic field strength B_m on the frequency response is shown in Fig. 5.43. It is observed that with increase in B_m, the trivial unstable region R_1R_2 increases and in this region, the nontrivial response amplitude marginally increases. For example, from Fig. 5.43, it may be observed that a point P/ corresponding to $\bar{\omega}_2$ equal to 0.95 which is in stable trivial

region for the value of B_m equal to 0.20 T will be in the unstable region for B_m equal to 0 .35 T. Also, it is observed that the response amplitude which corresponds to the S-N bifurcation point decreases with increase in B_m and for higher values of B_m (e.g., B_m =0.3 T, 0.35T), this amplitude remains almost constant. Similarly, the frequency $\bar{\omega}_1$ corresponding to this S-N bifurcation point which gives the lower limit of the frequency of the magnetic field above which the system may vibrate, increases with increase in B_m and almost remains unchanged for higher values B_m.

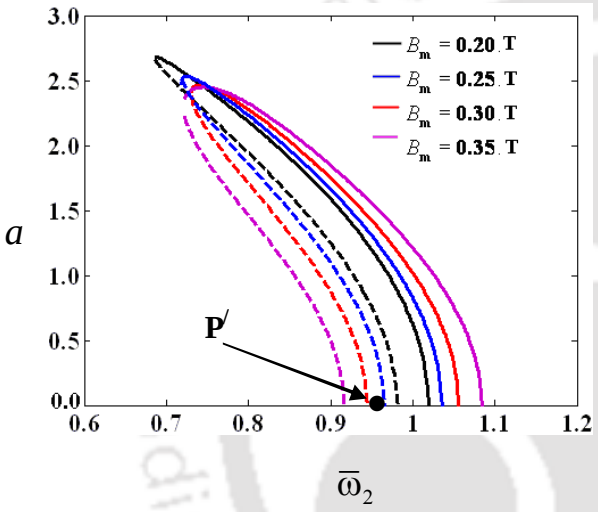

Fig. 5.43. Effect of the B_m on the frequency response curves for $M = 0.02$ kg, and $P_0 = 0.2$ N.

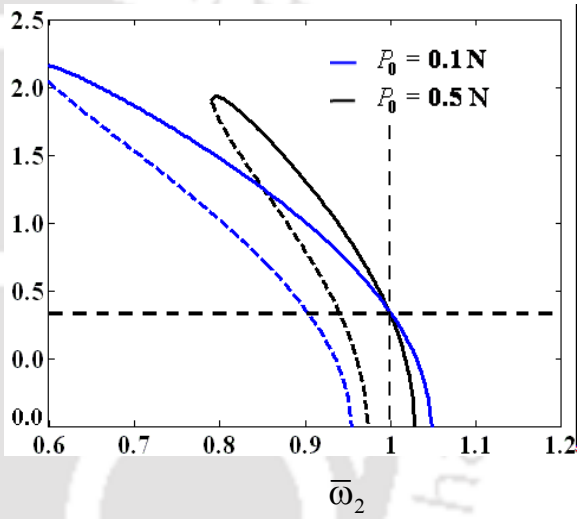

Fig. 5.44. Effect of the amplitude of static axial load (P_0) on the frequency response curves for $M = 0.02$ kg, $B_m = 0.25$ T.

Hence, to control the vibration of the cantilever beam it is advisable to apply lower amplitude of magnetic field strength with a frequency higher than the supercritical pitchfork bifurcation point. Also, one may control the vibration by applying a higher value of amplitude of magnetic field strength with a frequency lower than the frequency corresponding to the S-N bifurcation point. Further, it may be noted from the expression of the natural frequency ω_e that there exist a critical value of B_m ($\bar{B}_m = 1 + \bar{P}_0$) beyond which the system is unstable as ω_e^2 will be negative. Hence, while operating at a lower frequency,

one should not increase the B_m value arbitrarily and should operate within this critical limit. In the present work, all B_m values are taken below the critical limit.

Figure 5.44 shows the effect of the amplitude of the static axial force on the frequency response curves for two different values of P_0. With increase in P_0, the unstable trivial range decreases and the frequency corresponding to the S-N bifurcation point occurs at a higher frequency. Hence, the system response may be brought to the stable trivial state by increasing P_0. It is observed that with increase in P_0, the response amplitude increases for a frequency $\bar{\omega}_2$ less than 1 and decreases for $\bar{\omega}_2$ greater than 1. Hence, P_0 has a stabilizing effect for $\bar{\omega}_2$ greater than 1 and has a destabilizing effect for $\bar{\omega}_2$ less than 1.

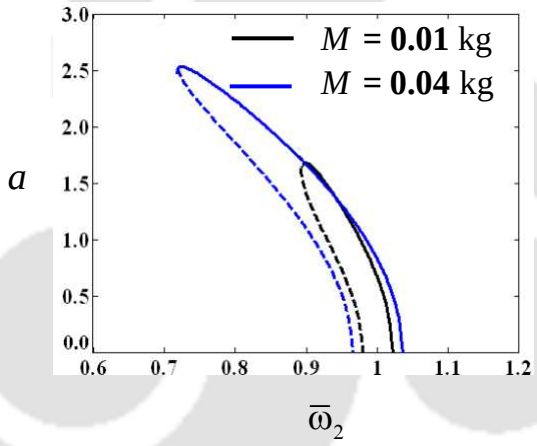

Fig. 5.45. Influence of M on the frequency response curves for $P_0 = 0.2$ N, $B_m = 0.30$ T.

From Fig. 5.45, one may note that with increase in tip mass (M), both the response amplitude and unstable trivial region increases. Therefore, one may control the vibration of the system by decreasing the tip mass.

5.6.2.2 Principle Parametric Resonance Case ($\bar{\omega}_3 \approx 2$ and $\bar{\omega}_2$ away From 1)

In this resonance condition, the cantilever beam with tip mass is subjected to an axial load with a frequency nearly equal to twice the natural frequency of the system and the frequency of the magnetic field is away from the natural frequency of the system. Without

considering magnetic field ($B_m = 0$), the frequency response plot of the system for tip mass $M = 0.02$ kg , $P_1 = 0.2$ N and $P_0 = 0.2$ N is shown in Fig. 5.46.

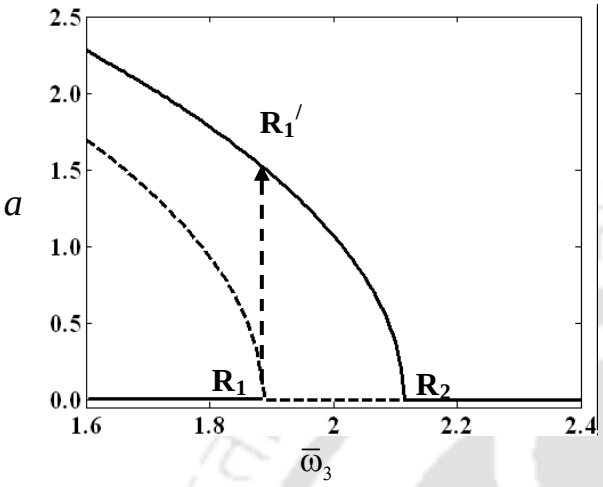

Fig. 5.46. Frequency response curves for $M = 0.02$ kg , $P_0 = 0.2$ N, $P_1 = 0.2$ N, $B_m = 0.0$.

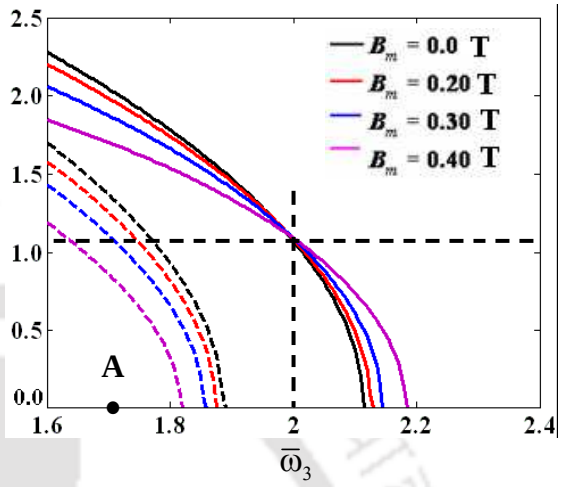

Fig. 5.47. Effect of B_m on the frequency response curves for $M = 0.02$ kg , $P_0 = 0.2$ N, $P_1 = 0.2$ N.

Similar to the previous case, here also the system has both trivial and nontrivial responses. But, in this case, when the frequency of the axial load is nearly equal to twice the natural frequency, the system starts vibrating. Like the previous case, in this case also the system experiences a jump up phenomena at the sub-critical pitchfork bifurcation point R_1 and may fail or may vibrate with amplitude equal to that of the nontrivial steady state response. The system has an unstable trivial state between the sub-critical and super-critical pitchfork bifurcation points and in this range R_1R_2 it may vibrate with amplitude equal to that of the stable nontrivial state. Though, the trivial state exists similar to that shown in Fig. 5.46, in the frequency response curves shown in Fig. 5.47 and Figs. 5.48-5.50, only the nontrivial states are plotted to avoid repeatability.

The effect of the amplitude of magnetic field strength (B_m) on this system is shown in Fig. 5.47. It may be observed that with increase in B_m, the response amplitude decreases

significantly for a frequency $\bar{\omega}_3$ less than 2 and increases marginally for $\bar{\omega}_3$ greater than 2. For example, with $\bar{\omega}_3$ equal to 1.6, when the magnetic field is equal to zero, the response amplitude is equal to 2.3 and for B_m equal to 0.40 T the response amplitude decreases significantly to 1.8. Here, the decrease in the response amplitude is about 21.7%. Hence, unlike in the simple resonance case, here the system can be stabilized with increase in B_m for $\bar{\omega}_3$ less than 2. But for $\bar{\omega}_3$ greater than 2, the magnetic field has a destabilizing effect as the response amplitude increases with increase in B_m. Further, it may be noted that the trivial state unstable range increases with increase in B_m. Hence, it may be observed that if the system is vibrating with a frequency $\bar{\omega}_3$ in between R_1 and R_2, it is difficult to bring the response to its trivial state only by changing the amplitude of the magnetic field.

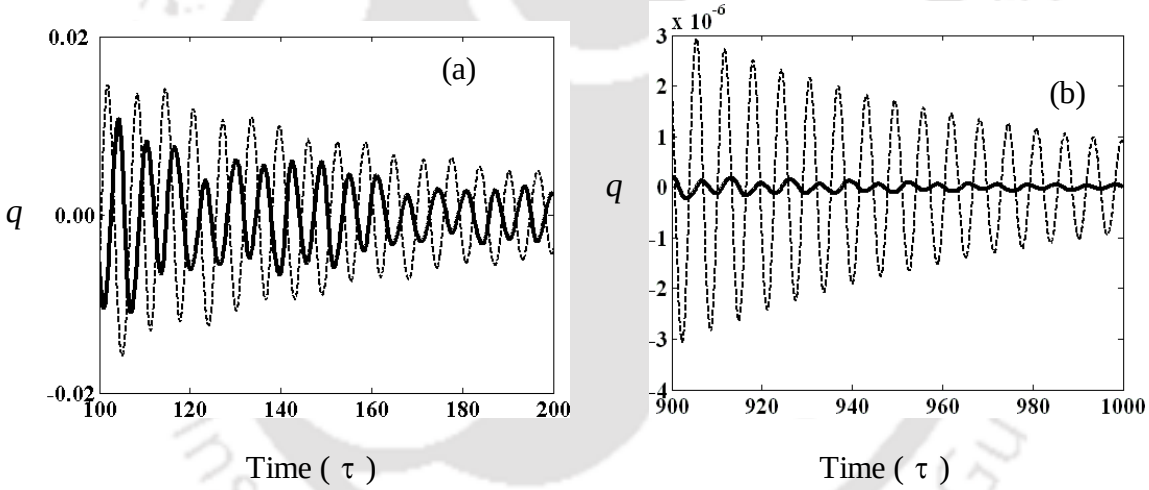

Fig. 5.48. (a) Transient time responses and (b) steady state time responses for point A marked in Fig. 5.47 with B_m equal to 0.30 T. Dotted line represents the response without magnetic field and solid represent the response with magnetic field.

Similar to the simple resonance case, here also the influence of magnetic field strength on the reduction of vibration of the system is depicted in Fig. 5.48 by solving the temporal equation (5.10) numerically. While Fig. 5.48(a) represents the transient part of the response, Fig. 5.48(b) shows the steady state part of the response corresponding to point A

as marked in Fig. 5.47 with B_m equal to 0.3 T. From these figures, it is observed that the vibration can be reduced with proper application of magnetic field.

Figure 5.49 displays the effect of amplitude of dynamic loading (P_1) on the frequency response curve and it is observed that with increase in P_1, both the response amplitude and unstable trivial region gets increased. The influence of static axial load on the frequency response curves is shown in Fig. 5.50. It is found that with increase in P_0, the response amplitude increases for a frequency $\bar{\omega}_3$ less than 2 and decreases for $\bar{\omega}_3$ greater than 2. Hence, P_0 has a stabilizing effect for $\bar{\omega}_3$ greater than 2 and has a destabilizing effect for $\bar{\omega}_3$ less than 2. Unlike in the case of B_m (Fig. 5.47), here with increase in P_0 as the unstable trivial range decreases, there is a possibility that the system response can be brought to the stable trivial state by increasing P_0.

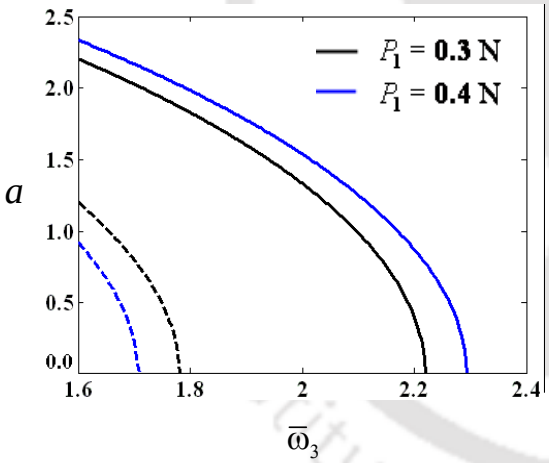

Fig. 5.49. Effect of P_1 on the frequency response curves for $M = 0.02$ kg, $P_0 = 0.2$ N, $B_m = 0.3$ T.

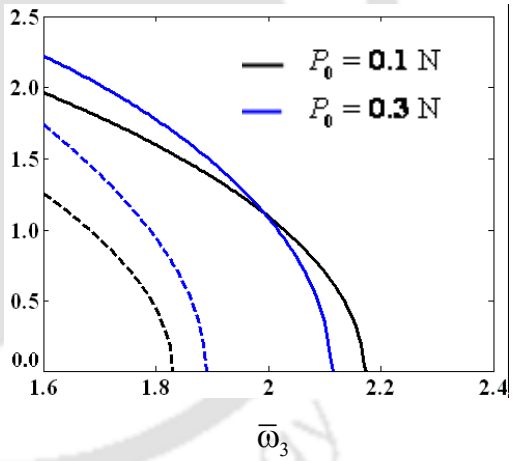

Fig. 5.50. Effect of P_0 on the frequency response curves for $M = 0.02$ kg, $P_1 = 0.2$ N, $B_m = 0.30$ T.

Fig. 5.51 shows the effect of tip mass *M* on the frequency response curve and it is observed that with increase in tip mass (*M*), both the response amplitude and unstable trivial region increases. Similar to simple resonance case, here for a lower value of *M*, the sub and super-

critical pitchfork along with S-N bifurcation points are clearly observed. One may observe similar jump up, jump down phenomena as discussed in Fig. 5.40.

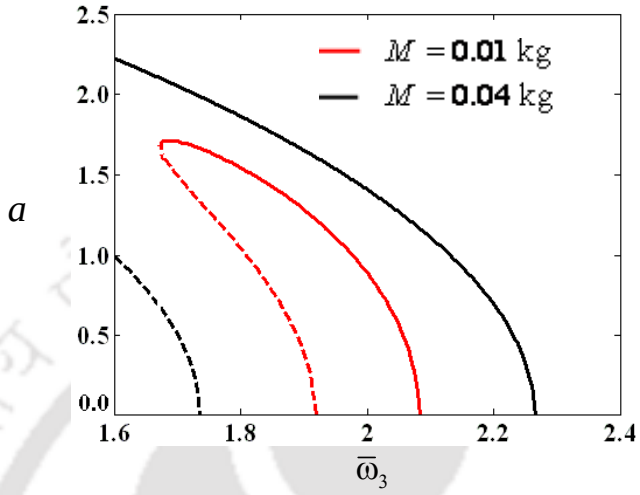

Fig. 5.51. Influence of M on the frequency response curves for $P_0 = 0.2$ N, $P_1 = 0.2$ N, $B_m = 0.30$ T.

5.6.2.3 Simultaneous Resonance Case ($\bar{\omega}_2 \approx 1$ and $\bar{\omega}_3 \approx 2$)

This is the most interesting resonance condition where the system is subjected to a magnetic field with a frequency equal to the natural frequency of the system and also to an axial loading with a frequency nearly equal to twice the natural frequency of the system. Figure 5.52 shows a typical frequency response curve corresponding to $M = 0.02$ kg, $P_0 = 0.2$ N, $P_1 = 0.2$ N, $B_m = 0.25$ T and $\phi = 0$. This curve is similar to that discussed in Fig. 5.40 of the simple resonance condition with three critical bifurcation points, viz., sub-critical pitchfork (R_1), super-critical pitchfork (R_2) and saddle-node (D) bifurcation points. Hence, similar to the simple resonance case, here the system will not vibrate if the frequency $\bar{\omega}_2$ is either less than the frequency corresponding to the point D or more than the frequency corresponding to the point R_2.

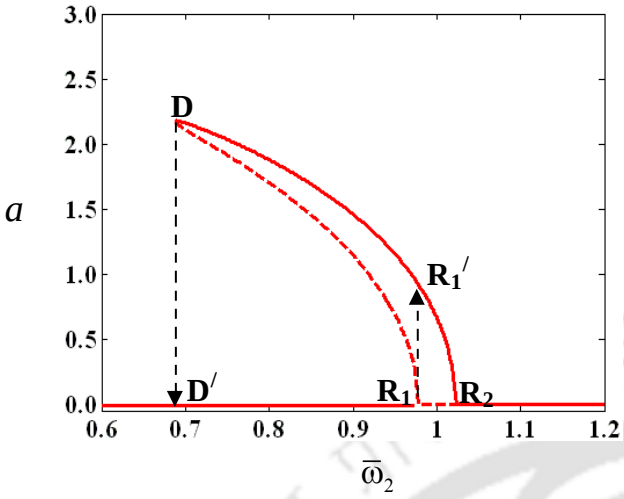

Fig. 5.52. Frequency response curves for $M = 0.02$ kg, $P_0 = 0.2$ N, $P_1 = 0.2$ N, $\phi = 0$, $B_m = 0.25$ T.

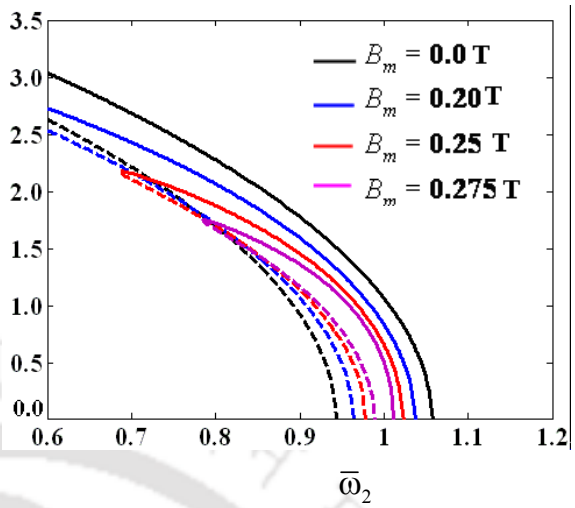

Fig. 5.53. Effect of (B_m) on the frequency response curves for $M = 0.02$ kg, $P_0 = 0.2$ N, $P_1 = 0.2$ N, $\phi = 0$.

Figure 5.53 illustrates the effect of magnetic field strength where the response curves for four different values of the amplitude of magnetic field strength B_m are plotted. Unlike the simple and principal parametric resonance cases, here the unstable trivial region and amplitude of the stable nontrivial state response of the system decreases with increase in B_m. Hence, in this case, the vibration of the system can be reduced completely (i.e., the response can be brought to the stable trivial state) with increase in B_m.

Like the principal parametric resonance, similar effects are observed in this case (Fig. 5.54) by increasing P_1 where both the response amplitude and unstable trivial range increases with increase in P_1.

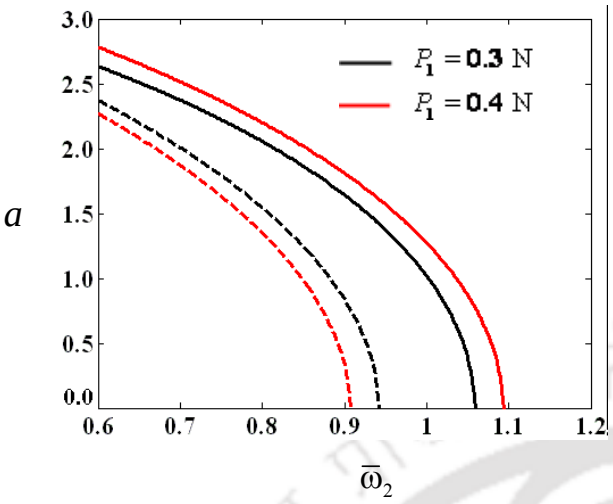

Fig. 5.54. Effect of P_1 on the frequency response curves for $M = 0.02$ kg, $P_0 = 0.2$ N, $B_m = 0.25$ T, $\phi = 0$.

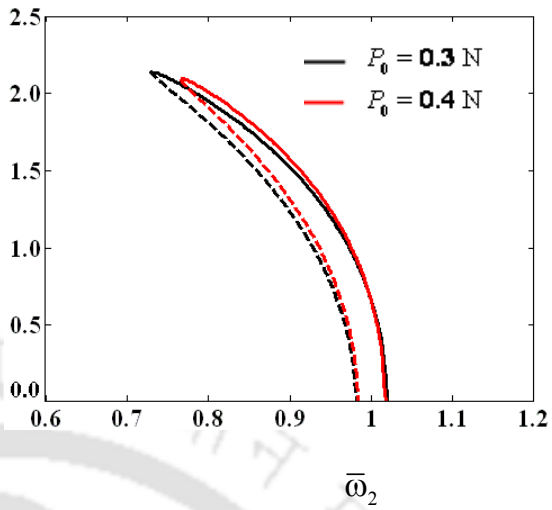

Fig. 5.55. Effect of P_0 on the frequency response curves for $M = 0.02$ kg, $P_1 = 0.2$ N, $B_m = 0.25$ T, $\phi = 0$.

Figures 5.55 and 5.56 show respectively, the effect of amplitude of static load P_0 and tip mass *M*. In this resonance condition, both response amplitude and unstable trivial range decreases marginally with increase in P_0 and increase significantly with increase in *M*. In all these above cases, the frequency of the axial load was considered to be exactly twice the frequency of the magnetic field.

Considering a phase change ϕ between these two frequencies, the response curves are plotted as shown in Fig. 5.57 which shows similar effects that described in Fig. 5.54. It may be observed from Figs. 5.53 and 5.57 that with B_m equal to 0.25 T, while the response amplitude *a* equals to 0.6654 for ϕ equal to zero, with increase in ϕ to $\pi/4$, the amplitude increases to 1.0. In other words, the phase will have a destabilizing effect and both the excitations should be applied simultaneously to have better vibration control.

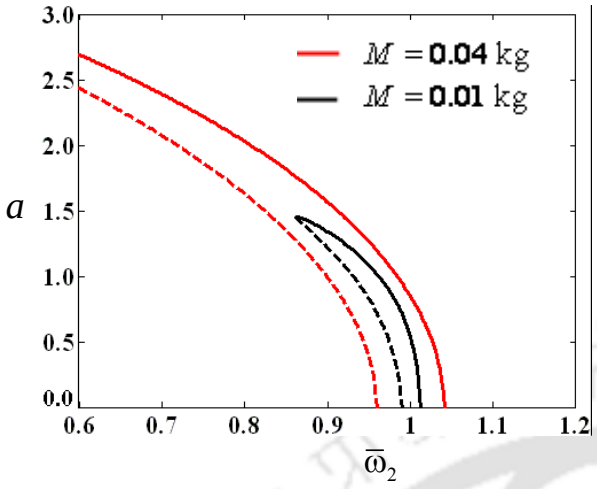

Fig. 5.56. Influence of M on the frequency response curves for $P_0 = 0.0$ N, $P_1 = 0.2$ N, $B_m = 0.25$ T, $\phi = 0$.

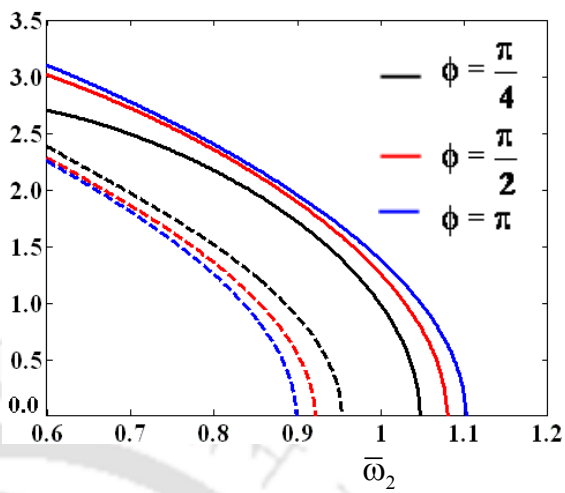

Fig. 5.57. Effect of ϕ on the frequency response curves for $M = 0.02$ kg, $P_0 = 0.2$ N, $P_1 = 0.2$ N, $B_m = 0.25$ T.

5.7 Magnetoelastic Cartesian manipulator

5.7.1 Analysis

Following similar procedure of method of multiple scales as explained in the previous sections, here also the solution of the equation (5.9) can be obtained by representing the displacement q in terms of different time scales (T_0, T_1) and a book-keeping parameter ε. Following similar procedure as in section 3.3.1, substituting $T_n = \varepsilon^n \tau$, $n = 0, 1, 2\cdots$ and $q(\tau;\varepsilon) = q_0(T_0, T_1) + \varepsilon q_1(T_0, T_1) + O(\varepsilon^2)$ in equation (5.9) and equating the coefficients of like powers of ε, one may obtain the following expressions:

Order ε^0 : $D_0^2 q_0 + q_0 = 0$, (5.80)

Order ε^1 : $D_0^2 q_1 + q_1 = -2 D_0 D_1 q_0 - 2\zeta D_0 q_0 - \alpha_1 q_0^3 - \alpha_2 (D_0^2 q_0) q_0 - \alpha_3 (D_0 q_0)^2 q_0^2 +$

$$k_2 (D_0 q_0) q_0^2 + \bar{\omega}_1^2 f_1 \cos(\bar{\omega}_1 \tau) + \bar{\omega}_1^2 k_1 \cos(\bar{\omega}_1 \tau) q_0^2 + f_2 \cos(2\bar{\omega}_2 T_0) q_0 +$$

$$k_2 \cos(2\bar{\omega}_2 T_0)(D_0 q_0) q_0^2 . \quad (5.81)$$

General solution of equation (5.80) can be written as

$$q_0 = A(T_1, T_2)\exp(iT_0) + \bar{A}(T_1, T_2)\exp(-iT_0) . \quad (5.82)$$

Here, $\bar{A}(T_1, T_2)$ is the complex conjugate of $A(T_1, T_2)$.

Substituting equation (5.82) into equation (5.81) leads to the following equation.

$$D_0^2 q_1 + q_1 = -2i A' \exp(iT_0) - 2i\zeta A \exp(iT_0) - (3\alpha_1 - 3\alpha_2 + \alpha_3 - ik_2) A^2 \bar{A} \exp(iT_0)$$

$$+ 9A^3 \exp(3iT_0) + ik_2 A^3 \exp(3iT_0) + \frac{f_2}{2}\left[A \exp i(2\bar{\omega}_2 - 1)T_0 + \bar{A} \exp i(2\bar{\omega}_2 - 1)T_0\right]$$

$$+ \frac{ik_2}{2} A^3 \exp i(2\bar{\omega}_2 + 3)T_0 - \frac{1}{2} k_1 \bar{\omega}_1^2 A^2 \exp i(2 + \bar{\omega}_1)T_0 - \frac{1}{2} k_1 \bar{\omega}_1^2 \bar{A}^2 \exp i(\bar{\omega}_1 - 2)T_0$$

$$- \left(k_1 A\bar{A} + \frac{1}{2} f_1\right) \exp i(\bar{\omega}_1 T_0) + \frac{ik_2}{2} A^2 \bar{A} \exp i(2\bar{\omega}_2 + 1)T_0 - \frac{ik_2}{2} \bar{A}^2 A \exp i(2\bar{\omega}_2 - 1)T_0$$

$$+ \frac{ik_2}{2} A^3 \exp i(3 - 2\bar{\omega}_2)T_0 + cc . \quad (5.83)$$

Here, $\vartheta = -\alpha_1 + \alpha_2 + \alpha_3$ and *cc* stands for the complex conjugate of preceding terms. It is observed form the equation (5.83) that the system has different resonance conditions viz., (i) $\bar{\omega}_1 \approx 1$ and $\bar{\omega}_2$ is away from 1; (ii) $\bar{\omega}_2 \approx 1$ and $\bar{\omega}_1$ is away from 1 and 3; (iii) $\bar{\omega}_1 \approx 1$ and $\bar{\omega}_2 \approx 1$; (iv) $\bar{\omega}_1 \approx 3$ and $\bar{\omega}_2$ is away from 1; (v) $\bar{\omega}_2 \approx 1$ and $\bar{\omega}_1 \approx 3$. Neglecting the last two higher order resonance conditions i.e., the subharmonic ($\bar{\omega}_1 \approx 3$ and $\bar{\omega}_2$ is away from 1) and the simultaneous resonance conditions $\bar{\omega}_1 \approx 3$ and $\bar{\omega}_2 \approx 1$, in the following subsections, three different resonance conditions viz., (i) simple resonance ($\bar{\omega}_1 \approx 1$ and $\bar{\omega}_2$ is away from 1), (ii) principal parametric resonance condition ($\bar{\omega}_2 \approx 1$ and $\bar{\omega}_1$ is away from 1 or 3), and (iii) simultaneous conditions ($\bar{\omega}_1 \approx 1$ and $\bar{\omega}_2 \approx 1$) are studied.

5.7.1.1 Simple Resonance Due to Support motion ($\bar{\omega}_1 \approx 1$ and $\bar{\omega}_2$ is away from 1)

Similar to the previous cases discussed in chapters 3 and 4, using detuning parameter σ as $\bar{\omega}_1 = 1 + \varepsilon\sigma$ in equation (5.83), one may obtain the following equation to eliminate the secular or small divisor terms.

$$-2iA'\exp(iT_0) - 2i\zeta A\exp(iT_0) - \left(3\alpha_1 - 3\alpha_2 + \alpha_3 - ik_2\right)A^2\bar{A}\exp(iT_0)$$
$$-\frac{1}{2}k_1A^2\exp i\left(-\sigma T_1\right) - \left(k_1A\bar{A} + \frac{1}{2}f_1\right)\exp i\left(\sigma T_1\right) = 0 \qquad (5.84)$$

Putting A equal to $\frac{1}{2}a(T_1)e^{(i\beta T_1)}$ and $\gamma = \sigma T_1 - \beta$ into equation (5.84) and separating the real and imaginary terms, one may obtain a set of reduced equations as given below.

$$a' = -\zeta a + \frac{k_2}{8}a^3 - \left(\frac{k_1}{8}a^2 + \frac{1}{2}f_1\right)\sin\gamma\ , \qquad (5.85)$$

$$a\gamma' = a\sigma - \frac{3}{8}\left(\alpha_1 - \alpha_2 + \frac{\alpha_3}{3}\right)a^3 - \left(\frac{3k_1}{8}a^2 + \frac{1}{2}f_1\right)\cos\gamma\ . \qquad (5.86)$$

The response of the system can be determined by numerically solving equations (5.85) and (5.86), simultaneously. To find the stability of the steady state responses, one may follow

similar procedure as in previous sections and obtain the Jacobian matrix (J) as given below.

$$J=\begin{bmatrix} -\zeta-\frac{3}{8}k_2a_o^2+\frac{\frac{1}{2}k_1a_0\left(\zeta a_0+\frac{k_2}{8}a_0^3\right)}{\frac{1}{8}k_1a_0^2+\frac{1}{2}f_1} & -\frac{\left(\frac{1}{8}k_1a_0^2+\frac{1}{2}\alpha_5\right)\left(\sigma a_0-\frac{3}{8}Ka_0^3\right)}{\frac{3}{8}k_1a_0^2+\frac{1}{2}f_1} \\ -\frac{3}{4}Ka_0-\frac{3}{4}\frac{k_1\left(\sigma a_0-\frac{3}{8}Ka_0^3\right)}{\frac{3}{8}k_1a_0^2+\frac{1}{2}f_1}+\frac{\sigma a_0-\frac{3}{8}Ka_0^3}{a^2} & -\frac{\left(\frac{3}{8}k_1a_0^2+\frac{1}{2}\alpha_5\right)\left(\zeta+\frac{k_2}{8}a_0^2\right)}{\frac{1}{8}k_1a_0^2+\frac{1}{2}f_1} \end{bmatrix}. \quad (5.87)$$

Here, $K=\left(\alpha_1-\alpha_2+\frac{\alpha_3}{3}\right)$. It may be noted that the system will be stable if and only if all the real parts of the eigen-values are negative. Now, the first order nontrivial steady state response of the Cartesian manipulator can be given by

$$q=a\cos\left(\bar{\omega}_1\tau-\gamma\right). \quad (5.88)$$

5.7.1.2 Simple Resonance Due to Magnetic Field ($\bar{\omega}_2\approx 1$ and $\bar{\omega}_1$ is away from 1)

In this resonance condition, using $\bar{\omega}_2=1+\varepsilon\sigma$, where σ is the detuning parameter, in equation (5.83), one may obtain the following equation to eliminate the secular or small divisor terms.

$$-2iA'\exp(iT_0)-2i\zeta A\exp(iT_0)-\left(3\alpha_1-3\alpha_2+\alpha_3-ik_1\right)A^2\bar{A}\exp(iT_0)$$
$$+\frac{f_2}{2}\bar{A}\exp\left(2\sigma T_1\right)+i\frac{k_2}{2}A^3\exp\left(-2\sigma T_1\right)-i\frac{k_2}{2}\bar{A}^2A\exp\left(2\sigma T_1\right)=0. \quad (5.89)$$

Putting A equal to $\frac{1}{2}a\left(T_1\right)e^{\left(i\beta T_1\right)}$ into equation (5.89) and separating the real and imaginary terms, one may find the following reduced equations.

$$\dot{a}=-\zeta a+\frac{k_2}{8}a^3+\frac{f_2}{4}a\sin\gamma, \quad (5.90)$$

$$a\dot{\gamma}=2a\sigma-\frac{3}{4}\left(\alpha_1-\alpha_2+\frac{\alpha_3}{3}\right)a^3+\frac{1}{4}a^3k_2\sin\gamma+\frac{f_2}{2}a\cos\gamma. \quad (5.91)$$

Here, $\gamma = \sigma T_1 - \beta$. For steady state, $\dot{a} = 0$ and $\dot{\gamma} = 0$. From equations (5.90), and (5.91), one may observe that the system possesses both trivial and nontrivial responses which can be determined by solving these equations, simultaneously. To find the stability of the steady state responses, one may investigate eigen values of the Jacobian matrix (J) which is given by

$$J = \begin{bmatrix} -\zeta + \frac{3k_2}{8}a_0^2 + \frac{f_2}{4}\sin\gamma_0 & \frac{f_2}{4}a_0\cos\gamma_0 \\ -\frac{3}{2}\left(\alpha_1 - \alpha_2 + \frac{\alpha_3}{3}\right)a_0 + \frac{1}{2}a_0 k_2 \sin\gamma_0 & \frac{1}{4}a_0^2 k_2\cos\gamma_0 - \frac{f_2}{2}\sin\gamma_0 \end{bmatrix}. \quad (5.93)$$

For this case the system will be stable if and only if all the real parts of the eigen-values are negative. Now the first order nontrivial steady state response of the system can be given as

$$q = a\cos\left(\bar{\omega}_2\tau - \gamma\right). \quad (5.94)$$

5.7.2.3 Simultaneous Resonance Case ($\bar{\omega}_1 \approx 1$ and $\bar{\omega}_2 \approx 1$)

Following similar procedure as described in subsections 3.4.1.3 and 4.4.1.3, here one may use the detuning parameter σ and phase angle ϕ to express the nearness of $\bar{\omega}_1$ to 1 and $\bar{\omega}_2$ to 1 as given below.

$$\bar{\omega}_1 = 1 + \varepsilon\sigma, \text{ and } \bar{\omega}_2\tau = \bar{\omega}_1\tau + \phi,\ \sigma = O(1). \quad (5.95)$$

Substituting equation (5.95) into equation (5.93), one may obtain the following secular or small divisor terms which is eliminated by equating these terms to zero.

$$-2iA'\exp(iT_0) - 2i\zeta A\exp(iT_0) - \left(3\alpha_1 - 3\alpha_2 + \alpha_3 - ik_1\right)A^2\bar{A}\exp(iT_0) - \frac{1}{2}k_1A^2\exp i\left(-\sigma T_1\right)$$

$$-\left(k_1A\bar{A} + \frac{1}{2}f_1\right)\exp i\left(\sigma T_1\right) + i\frac{k_2}{2}A^3\exp\left(-2\sigma T_1 - 2\phi\right) - i\frac{k_2}{2}\bar{A}^2A\exp\left(2\sigma T + 2\phi_1\right)$$

$$-\frac{f_2}{2}\bar{A}\exp\left(2\sigma T_1 + 2\phi\right) = 0. \quad (5.96)$$

Similar to previous cases, substituting A equal to $\frac{1}{2}a(T_1)e^{(i\beta(T_1))}$ into equation (5.96) and separating the real and imaginary terms, one may obtain the following reduced equations.

$$\dot{a} = -\zeta a + \frac{k_1}{8}a^3 + \frac{f_1}{4}a\sin\varphi - \left(\frac{k_1}{8}a^2 + \frac{1}{2}f_1\right)\sin\gamma, \tag{5.97}$$

$$a\dot{\gamma} = 2a\sigma - \frac{3}{4}\left(K - k_2\sin\varphi\right)a^3 + \frac{f_2 a}{2}\cos\varphi - \left(\frac{3k_1a^2}{8} + \frac{f_1}{2}\right)\cos\gamma\ . \tag{5.98}$$

Here, $K = \left(\alpha_1 - \alpha_2 + \frac{\alpha_3}{3}\right)$, and $\varphi = 2\gamma + 2\phi$. For steady state response (a_0, γ_0), $\dot{a}$ and $\dot{\gamma}$ equal to zero. One may obtain the response (a, γ) by numerically solving equations (5.97), and (5.98), simultaneously. It may be noted from the equations (5.97), and (5.98) that the system does not have any trivial response.

The stability of the steady state fixed-point response (a_0, γ_0) can be determined by superposing a perturbation (a_1, γ_1) on the singular points by substituting $a = a_0 + a_1$, and $\gamma = \gamma_0 + \gamma_1$, in equations (5.97), and (5.98)and finding the eigen-values of the resulting Jacobean matrix (J). The Jacobian matrix (J) is given below.

$$J = \begin{bmatrix} -\zeta + \frac{3k_1}{8}a_0^2 + \frac{f_1}{4}\sin\varphi_0 & \frac{f_1}{2}a_0\cos\varphi_0 - \left(\frac{k_1}{8}a_0^2 + \frac{1}{2}f_1\right)\cos\gamma_0 \\ -\frac{k_1}{4}a_0\sin\gamma_0, & \\ -\frac{3}{2}\left(K - k_2\sin\varphi_0\right)a_0 - \frac{3}{4}k_1\cos\gamma_0 & \frac{\left(\frac{3}{8}k_1a_0^2 + \frac{1}{2}f_1\right)\cos\gamma_0}{a_0} - f_2\sin\varphi_0 \\ + \frac{\left(\frac{3}{8}k_1a_0^2 + \frac{1}{2}f_1\right)\cos\gamma_0}{a_0^2} & + \frac{3}{4}k_2a_0^2\cos\varphi_0 \end{bmatrix}. \tag{5.99}$$

Thus for this condition, the system is stable if the real part of all the eigen-values of the Jacobian matrix (J) are negative.

$$q = a\cos\left(\bar{\omega}_1\tau - \frac{\varphi}{2} + \phi\right). \tag{5.100}$$

5.7.2 Numerical Results and Discussions

In this work, a magnetic beam with properties length L = 0.5 m, width d = 0.005 m, depth h = 0.001 m, Young's Modulus $E = 1.95\times10^{11}$ N/m^2, mass of the beam per unit length m = 0.04 kg, the permeability of the vacuum, $\mu_0 = 1.26\times10^{-6}$ Hm^{-1}, material conductivity σ = 100 Vm^{-1}, and relative permeability $\mu_r = 2500$ is considered. Both the bookkeeping parameter ε and scaling factor $\bar{r}$ are assumed to be 0.1. The nonlinear response of the Cartesian manipulator is investigated for different values amplitude of support motion Z, damping c_d, mass of the payload M and amplitude of the magnetic field strength B_m. In all frequency response curves, the stable and unstable responses of the system are represented by solid and dotted line, respectively. In the following subsections the responses of the system for different resonance conditions are determined.

5.7.2.1 Simple Resonance Due to Support Motion ($\bar{\omega}_1 \approx 1$ and $\bar{\omega}_2$ away From 1)

In this condition, the roller-supported end of the Cartesian manipulator is excited with a frequency nearly equal to the natural frequency of the system and the frequency of the applied magnetic field is away from the simple resonance zone. The frequency response curves for $M = 0.02$ kg, $B_m = 0.30$ T, $c_d = 0.01$ N-s/m, and $Z = 0.0025$ m is shown in Fig. 5.58. From the reduced equations (5.85, 5.86) and Fig. 5.58, it is observed that the system has no trivial response ($a = 0$) and only nontrivial solution exists. Hence, the manipulator will always vibrate with amplitude equal to the nontrivial response as shown in Fig. 5.58. With increase in the frequency (e.g., from point A), the manipulator has experienced a jump up phenomena at the saddle-node (S-N) bifurcation point B which may cause the manipulator to fail. If the manipulator doesn't fail, it will vibrate with amplitude corresponding to the point D (Fig. 5.58) and with further increase in frequency, the response amplitude decreases. For example, at frequency equal to 1.1, the response amplitude will be same as that marked at point C. At this instance, if the manipulator is switched off then with decrease in frequency the response amplitude goes on increasing

along the line CDE and at E, it suffers a jump down phenomena which may leads to the failure of the manipulator

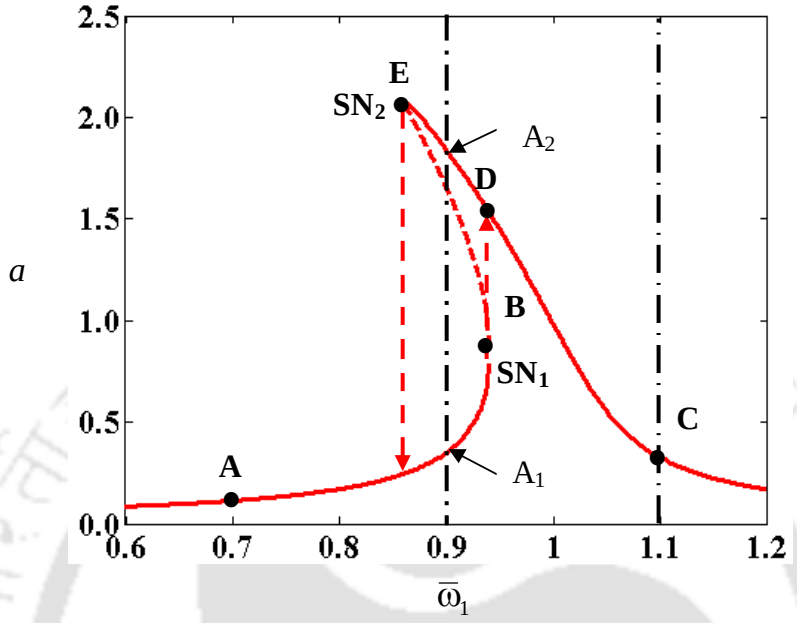

Fig. 5.58. Frequency response curve for $M = 0.02$ kg $B_m = 0.30$ T, $c_d = 0.01$ N-s/m^2, $Z = 0.0025$ m.

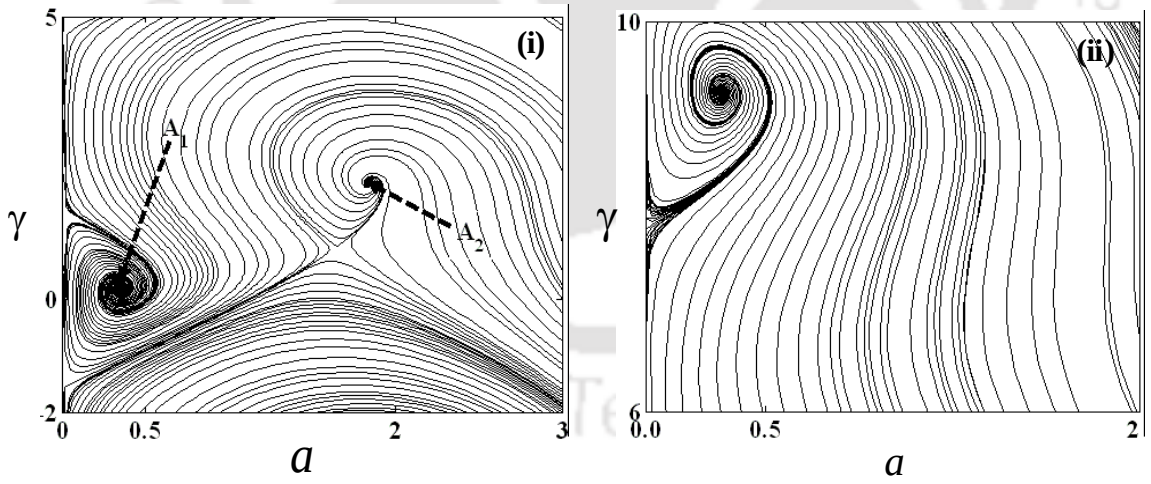

Fig. 5.59. Basin of attraction (i) for $\bar{\omega}_1 = 0.9$ and (ii) $\bar{\omega}_1 = 1.1$. Key as in Fig. 5.58.

As the manipulator has bi-stable region between frequencies E-B, the initial condition determines which steady- state solution is physically realized by the system. This is

illustrated by plotting the basin of attraction (Fig. 5.59) in a – γ plane which is obtained by numerically solving the reduced equations (5.85, 5.86). It is observed from Fig. 5.59 that the system has two stable solutions (A_1 and A_2) in this region (corresponding $\bar{\omega}_1 = 0.9$). From Fig. 5.59, it may be observed that, small change in initial condition may result in a response with higher amplitude.

Further, it may be observed from the expression of the system natural frequency ω_e that there exists a critical value of B_m ($\bar{B}_m = 1$) above which the system is unstable as ω_e^2 term becomes negative. Hence, one should not operate the system above this critical value of B_m. Figure 5.60 displays the critical value of amplitude of magnetic field strength B_m for different tip mass and it is observed that both the fundamental system frequency and the critical value of amplitude of magnetic field B_m increases with decrease in M. In the present work, all B_m values are taken below the critical limit.

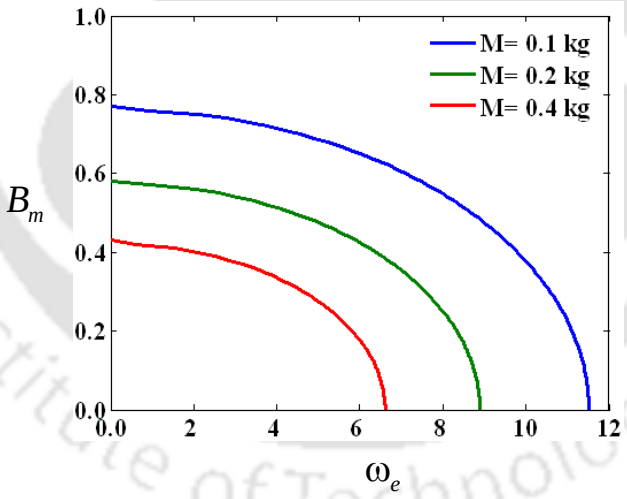

Fig. 5.60. Influence of payload on the critical value of B_m.

To assess the accuracy of the perturbation results, one may compare the response curves obtained by method of multiple scales with the response obtained by numerically solving the temporal equation of motion (5.9). Figures 5.61 (i, ii, iii) show the steady state time response, phase portrait and Poincare's map corresponding to the points A, B, and C marked in Fig. 5.58. One may observe that the steady state responses obtained by

numerically solving the temporal equation of motion (equation 5.9) are in good agreement with those determined by using the method of multiple scales.

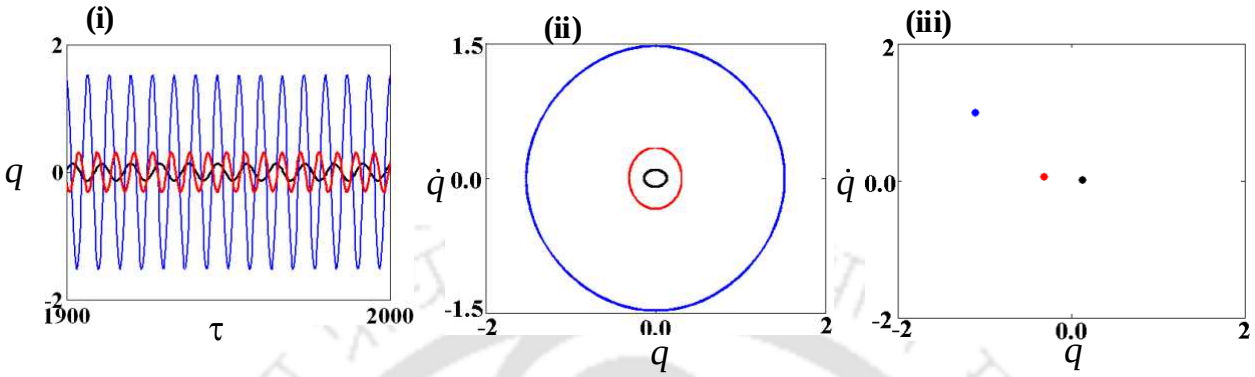

Fig. 5.61. (i) Time response , (ii) phase portrait and (iii) Poincare's map for the points A, B, C key as in Fig. 5.58.

Fig. 5.62 shows the influence of magnetic field on the frequency response curves. From Fig. 5.62, it is observed that the maximum response amplitude of the manipulator is approximately equal to 2.5 when the magnetic field is not applied to the system. But this response amplitude reduced to 0.7 by applying a magnetic field with B_m is equal to 0.55 T. Hence, the vibration of the manipulator can be significantly reduced (70 %) by incorporating the magnetic field to the system. With increase in B_m, the jump up and jump down phenomena occur at lower frequencies SN_1 and SN_2. It can also be observed that both jump up and jump down lengths decrease significantly with increase in B_m. Hence, possibility of catastrophic failure of the system due to the presence of jump phenomena is reduced with increase in B_m. With B_m equal to zero, the present system is similar to that of Cartesian manipulator without axial force (chapter 3) and Cuvalci (2000) when the pendulum is in locked position. Hence, the nonlinear response amplitude obtained in Cartesian manipulator without axial force (chapter 3) and Cuvalci (2000) can be significantly attenuated by using magnetoelastic beam instead of elastic beam. Also, it can be noted that 60 % reduction of vibration was observed in a viscoelastic manipulator (Cuvalci (2000), Fig. 10) by increasing the material loss factor (δ) from 0.05 to 0.5. But, to change the material loss factor one has to change the system completely. But in this

case, without changing the system one may get 70 % or more reduction in the vibration amplitude by using magnetic field. Hence, to reduce large amount of vibration of the manipulator actively, one can use magneto-elastic beam instead of using viscoelastic beam.

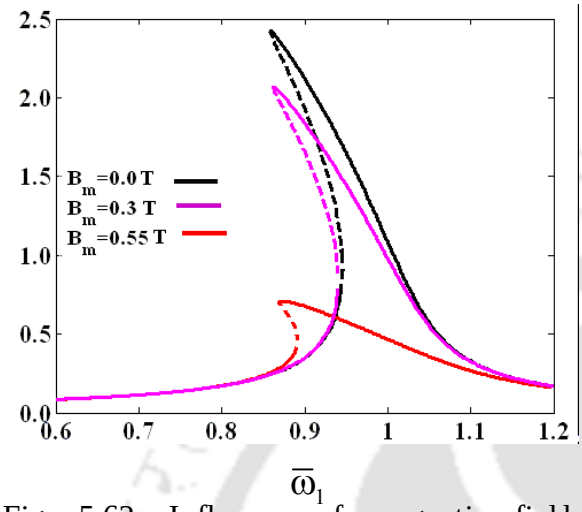

Fig. 5.62. Influence of magnetic field strength (B_m) on the frequency response curves for $M = 0.02$ kg, $c_d = 0.01$ N-s/m, $Z = 0.0025$ m.

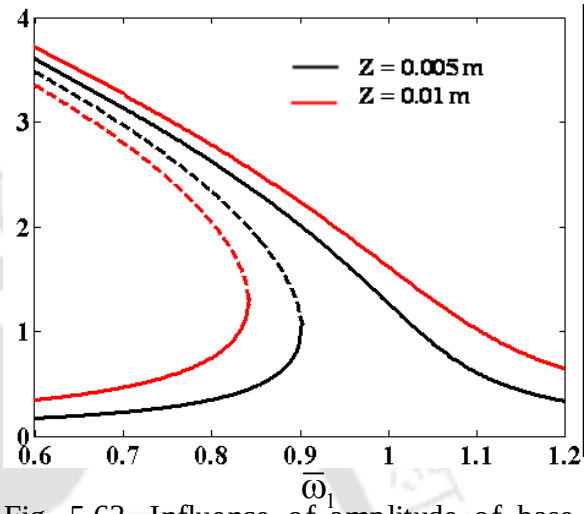

Fig. 5.63. Influence of amplitude of base motion (Z) on the frequency response curves for $M = 0.02$ kg, $c_d = 0.01$ N-s/m, $B_m = 0.30$ T.

Figure 5.63 shows the frequency response curves for two different values of amplitude of support motion Z with payload mass M, damping c_d and amplitude of magnetic field strength B_m equal to 0.02 kg, 0.01 N-s/m and 0.3 T, respectively. With increase in amplitude of base excitation Z, the response amplitude and jump up length of the system increases. Also, the S-N bifurcation point SN_1 starts at lower values of frequency $\bar{\omega}_1$ with increase in Z.

The effect of damping c_d on the frequency response curves is depicted in Fig. 5.64. From Fig. 5.58 and Fig. 5.64, it is observed that with increase in c_d, both the system response amplitude and the jump length get decreased. For c_d equal to 0.03 N-s/m the system behavior is similar to that of a linear single DOF system where the manipulator response is

stable through out the frequency range. Hence; the system vibration can also be reduced with increases in c_d.

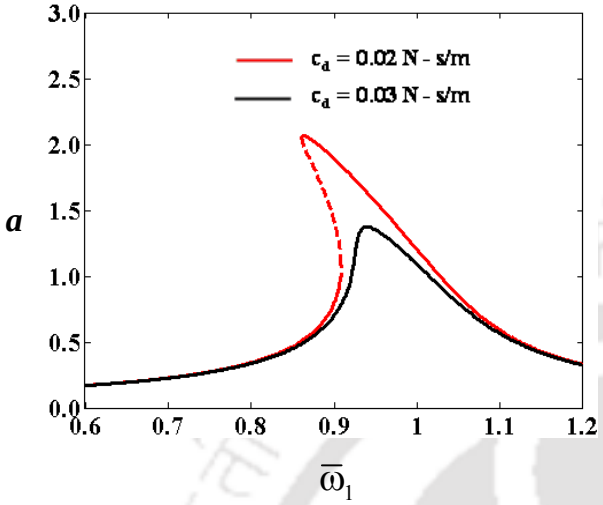

Fig. 5.64. Influence of damping (c_d) on the frequency response curves for $B_m = 0.30$ T, $Z = 0.005$ m, $M = 0.02$ kg.

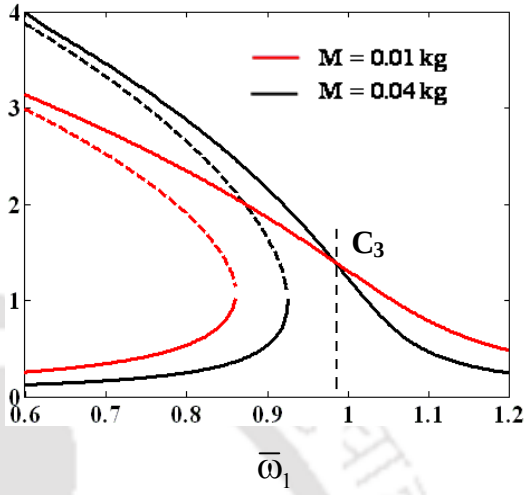

Fig. 5.65. Influence of tip mass (M) on the frequency response curves for $B_m = 0.30$ T, $c_d = 0.01$ N-s/m, $Z = 0.005$ m.

Figure 5.65 shows the effect of payload (M) on the frequency response curves for $B_m = 0.30$ T, $c_d = 0.01$ N-s/m, $Z = 0.005$ m. From Fig 5.62 and Fig. 5.65, one may observe that with increase in M, the response amplitude increases significantly. It may be noted that with increase in M, the manipulator will experience the jump up phenomena at a higher value of nondimensional frequency $\bar{\omega}_1$. Further it may be observed that, the response amplitude is less for a manipulator with higher payload if it is operated at a frequency before the critical point SN_1 or after the frequency corresponding to point C_3 as shown in Fig. 5.62.

5.7.2.2 Simple Resonance Due to Magnetic Field ($\bar{\omega}_2 \approx 1$ and $\bar{\omega}_1$ away From 1)

In this case, the manipulator is subjected to a transverse magnetic field with a frequency closely equal to the first mode natural frequency of the system and the frequency of the support motion is away from the natural frequency of the system. In Fig. 5.66(i), the

frequency response curve of the system is plotted with amplitude of magnetic field strength equal to 0.30 T for $M = 0.02$ kg, and $c_d = 0.01$ N-s/m.

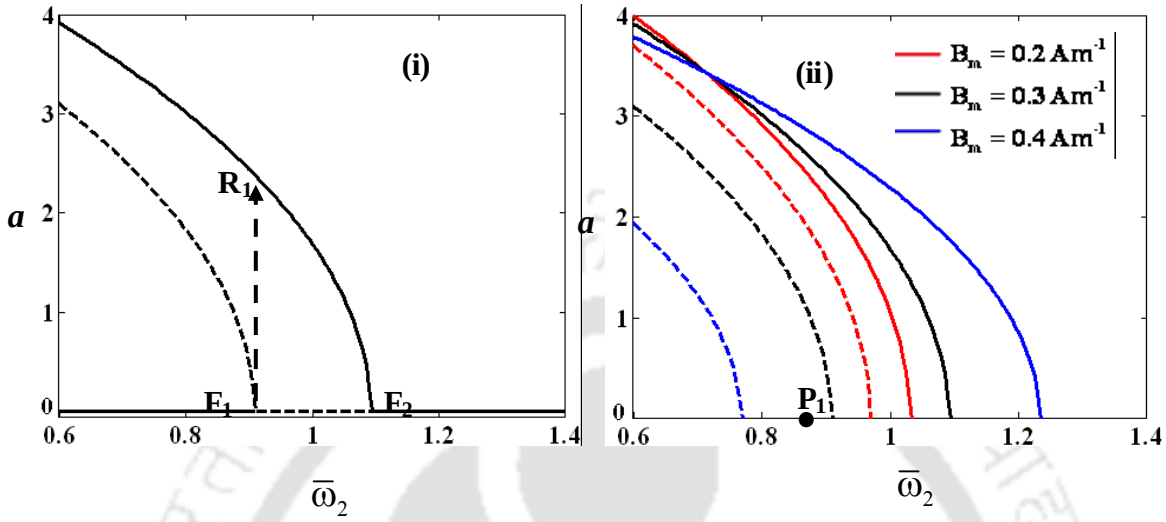

Fig. 5.66. The influence of magnetic field strength (B_m) on frequency response curves for $M = 0.02$ kg, $c_d = 0.01$ N-s/m.

It is found that the system has both trivial and nontrivial responses. In other words, if the frequency of the support motion is not close to 1, for any other values of $\bar{\omega}_1$, the system will not vibrate if the frequency of the magnetic field $\bar{\omega}_2$ is below a frequency marked by point F_1 or if it is operated at a frequency above the point marked by point F_2 in Fig. 5.66. With increase in the frequency of the magnetic field, the manipulator suddenly experience a jump up phenomena due to the presence of sub-critical pitchfork bifurcation point (F_1) which may lead to catastrophic failure of the system or the manipulator may start vibrating with amplitude equal to that of the nontrivial state marked by point R_1. In the region F_1F_2 (region between the sub-critical and super critical pitchfork bifurcation points) the manipulator will vibrate with amplitude equal to that of the nontrivial stable state corresponding to $\bar{\omega}_2$. This vibration will continue till it reaches the super-critical pitchfork bifurcation point F_2. It should be noted that the system has a bistable region before the sub-critical pitchfork bifurcation point F_1 and hence, depending on the initial conditions, the

manipulator may be at stationary position (trivial state) or vibrate with amplitude corresponding to frequency $\bar{\omega}_1$ as shown Fig. 5.66(i).

The effect of the amplitude of magnetic field strength B_m on the frequency response curves is shown in Fig. 5.66(ii). It is found that with increase in B_m, while the nontrivial response amplitude decreases, the trivial unstable region F_1F_2 increases. Hence, it may be noted that increase in magnetic field has a destabilizing effect as the trivial state unstable state start at a lower frequency and unstable trivial state increases with increase in B_m. Thus, to control the vibration of the manipulator, one has to use lower amplitude of magnetic field strength with a frequency less than the sub-critical pitchfork bifurcation point.

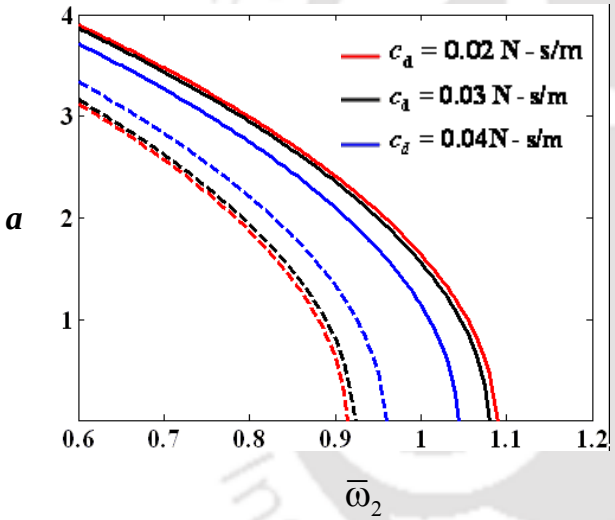

Fig. 5.67. Influence of damping (c_d) on the frequency response curves for $M = 0.02$ kg, $B_m = 0.3$ T.

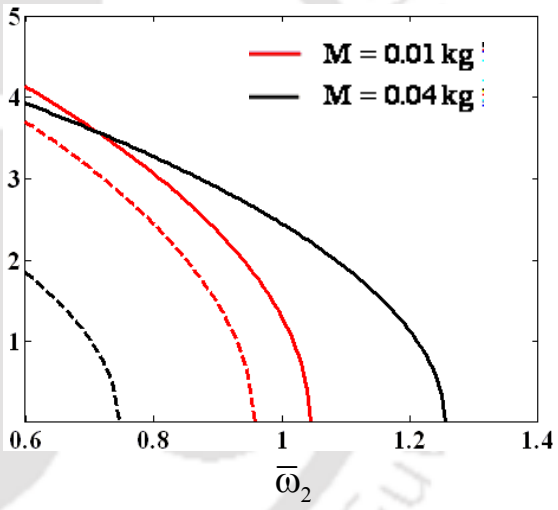

Fig. 5.68. Influence of tip mass (M) on the frequency response curves for $B_m = 0.30$ T, $c_d = 0.01$ N-s/m, $Z = 0.005$ m.

Figure 5.67 shows the effect of the damping on the frequency response curves for two different values of c_d. With increase in c_d, the unstable trivial range as well as response amplitude gets decreased. Hence, damping will help to stabilize the manipulator by reducing the vibration of the system. From Fig. 5.68, one may observe that the nontrivial response amplitude gets decreased with increase in payload M. It is also observed that the

system unstable range increases with increase in *M*. Thus, to control the vibration of the manipulator, one may use a lower payload mass with a frequency lower than the sub-critical pitchfork bifurcation point.

As the frequency of the magnetic field can be independently changed without affecting any physical property of the Cartesian manipulator, from these figures, it may be observed that the large vibration of the manipulator can be actively controlled by applying a magnetic field with a frequency higher than that of the supercritical pitchfork bifurcation point. It should be noted that, unlike the bi-stable region before the sub critical pitchfork bifurcation point, beyond the supercritical pitchfork bifurcation point, as the system has only stable trivial state, the vibration can be completely attenuated if the manipulator is operated beyond this frequency.

5.7.2.3 Simultaneous Resonance Condition ($\bar{\omega}_1 \approx 1$ and $\bar{\omega}_2 \approx 1$)

In this resonance condition, both the frequency of the applied magnetic field, and the harmonic motion of the roller-supported end are nearly equal to the first natural frequency of the system. Similar to the simple resonance case, here also it can be observed that the manipulator will always vibrate with amplitude equal to the nontrivial response as shown in Fig. 5.69. In comparison to the simple resonance case, in this resonance case, one may observe the presence of an additional region (region S_2 of Fig. 5.69) in the frequency response curve. Hence, in this resonance condition, one may have tri-stable regions with two saddle-node bifurcation points (N_1, N_2) instead of a bi-stable region as observed in simple resonance case. One can divide the frequency response curves in three different regions (shown in Fig. 5.69). While in region I, three stable states exists, in regions II and III, two and a single stable state exist, respectively.

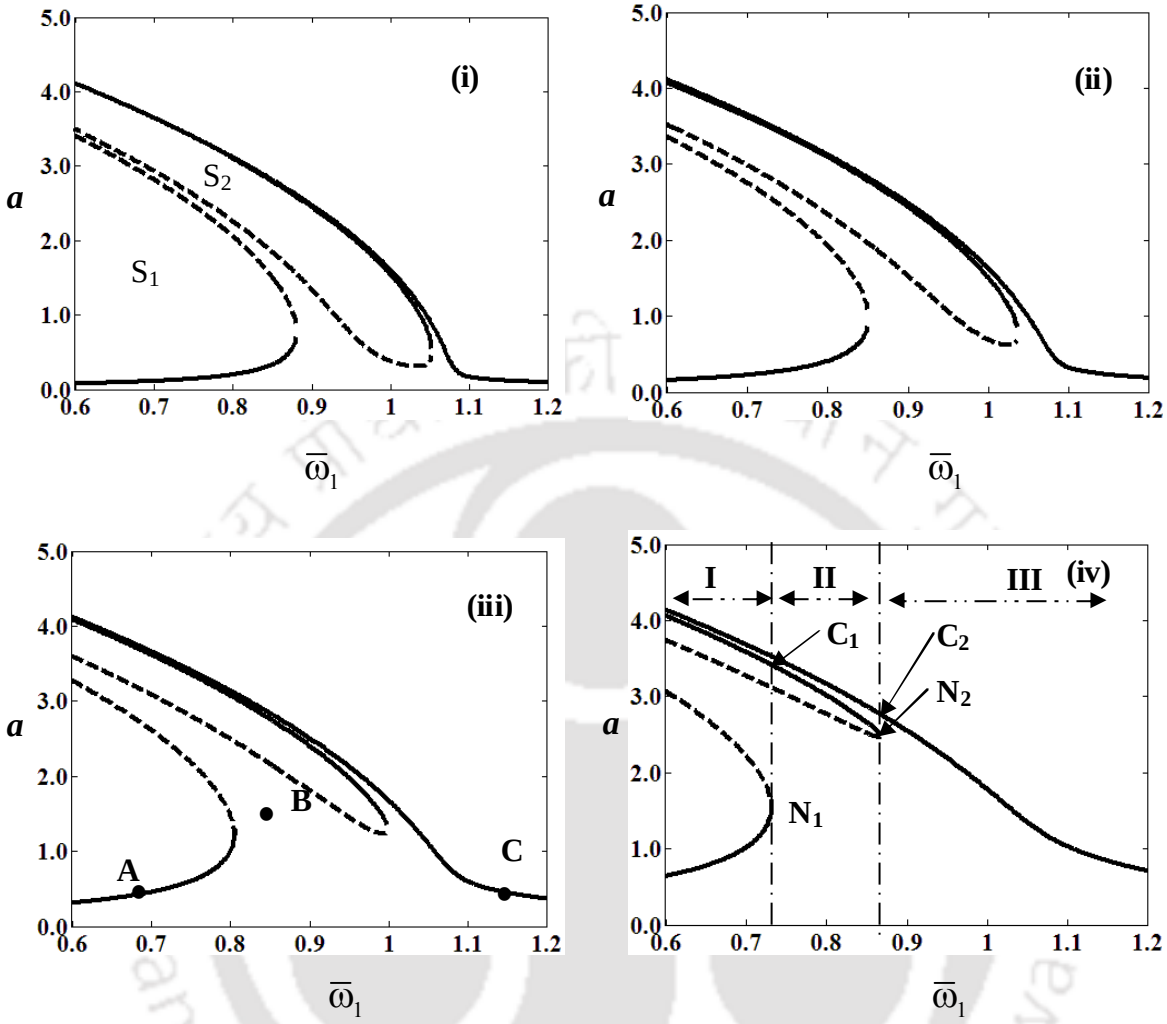

Fig. 5.69. Influence of base excitation (Z) on the frequency response curves for $M = 0.04$ kg, $c_d = 0.01$ N-s/m, $B_m = 0.20$ T; (i) $Z = 0.00125$ m, (ii) $Z = 0.0025$ m, (iii) $Z = 0.005$ m, (iv) $Z = 0.01$ m.

The influence of amplitude of support motion (Z) on the frequency responses for $M = 0.04$ kg, $B_m = 0.20$ T and $c_d = 0.01$ N-s/m for four different values of Z (viz., Z = 0.00125 m, 0.0025 m, 0.005 m, and 0.01 m) is shown in Fig. 5.69. Here, the frequency of the support motion and that of the magnetic field is considered to be same and ϕ equal to zero. From Fig. 5.69, it is observed that with increase in Z, both the regions S_1 and S_2 get reduced and whereas the response amplitude remains almost same in upper stable branch

in zone I and II, in the lower stable branch in zone I and II and the only branch in zone III it marginally increases. It is noted that with increase in Z, both the S-N bifurcation points N_1 and N_2 start at the lower value of frequency $\bar{\omega}_1$. For all values of Z, it is observed that the S-N bifurcation point N_1 always precedes S-N bifurcation point N_2 and hence, if the excitation frequency exceeds the critical point N_1, the response may jump to stable nontrivial state in region S_2 (e.g., point C_1, Fig. 5.69(iv)) .With further increase in frequency beyond critical point N_2, the system undergoes a second catastrophic failure due to the sudden jump from N_2 to point C_2. Hence, due to the early catastrophic failure of the manipulator, the amplitude of the support motion *Z* has a destabilizing effect. Hence, it is advisable to operate the manipulator with a lower amplitude *Z* in frequency zone III. Though the frequency of the magnetic field can be actively changed to this frequency zone, one has to device a mechanism to sweep up the frequency of support motion through zone II and III.

To check the accuracy of the obtained perturbation results, one may compare these results with those obtained by numerically solving the temporal equation of motion (5.9).The time response, phase portrait and Poincare's map for the point A, is shown in Fig. 5.70 (i, ii, iii). It is observed that by solving temporal equation of motion for $\bar{\omega}_1$ corresponding to point A, the system response is similar to a two torus quasiperiodic response with amplitude equal to that observed at point A obtained by perturbation method. Figure 5.70 (iv, v, vi) show the time response, phase portrait, and Poincare's section for point B and it is found that the system is in unstable region. Similarly, the time response, phase portrait, and Poincare's map corresponding to point C is plotted in Fig. 5.70 (vii, viii, ix). In Fig. 5.70 (vii-ix), the response is observed to be that of a 3-torus quasiperiodic response and the steady state response has amplitude equal to the amplitude of C in Fig. 5.70 (iii). Hence, it may be noted that the steady state responses obtained by numerically solving the temporal equation are in good agreement with the results obtained by method of multiple scales.

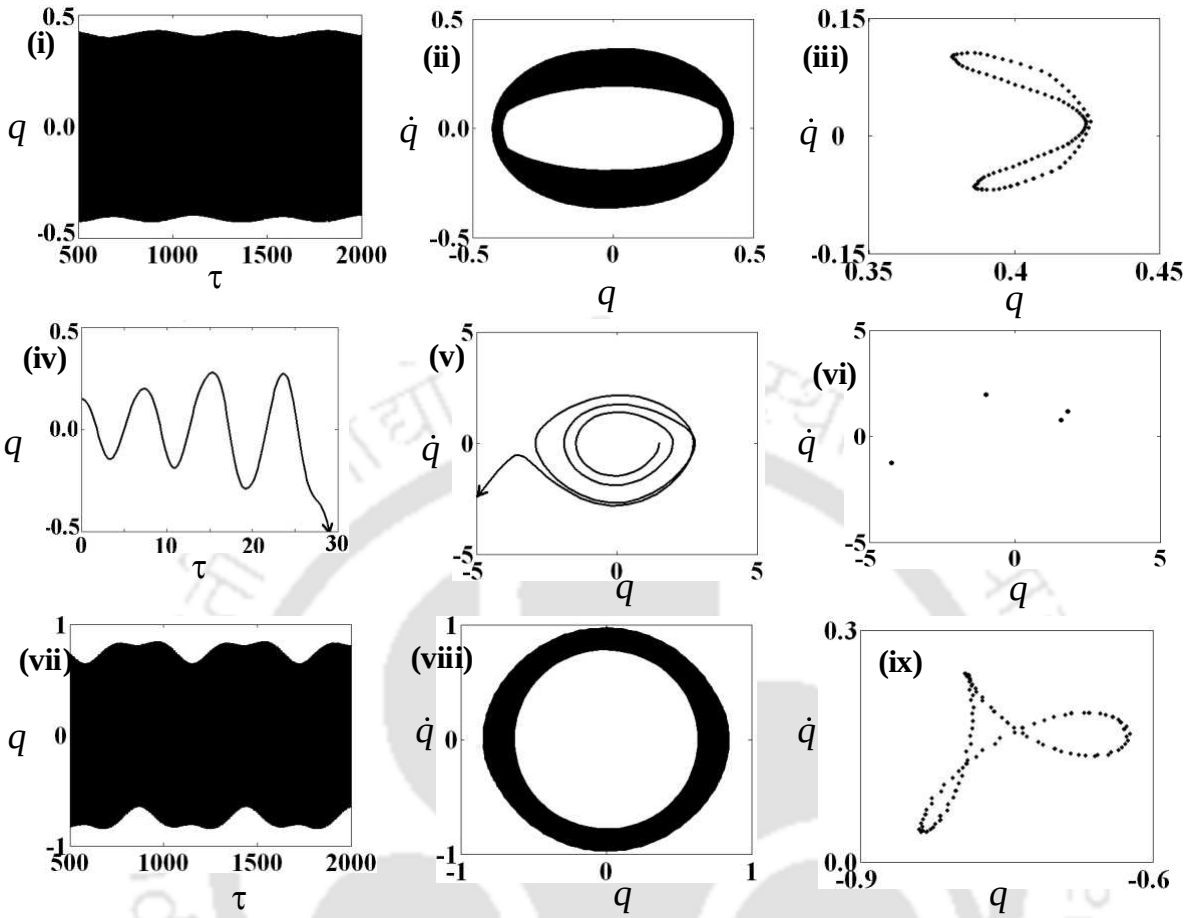

Fig. 5.70. Time response (i, iv, vii), phase portrait (ii, v, viii), and Poincare's map (iii, vi, ix) for points A, B and C key as Fig. 5.69(iii).

Figure 5.71 shows the influence of phase angle ($\phi = 2(\bar{\omega}_1 - \bar{\omega}_2)\tau = 2\varepsilon(\sigma_1 - \sigma_2)\tau$) which is the angle between the frequency of support motion and frequency of magnetic field strength on the frequency response curves for four different values of ϕ (viz., $\phi = \pi/6$, $\pi/3$, $\pi/2$, and π). It may be noted from equation (5.9) that, in this resonance condition, the force due to the magnetic field has a frequency twice that of the frequency of support motion. Here, phase angle ϕ in physical sense implies that the magnetic field is applied after a time interval of $\tau = \phi/(4\pi\bar{\omega}_1)$ after the support is given a harmonic motion.

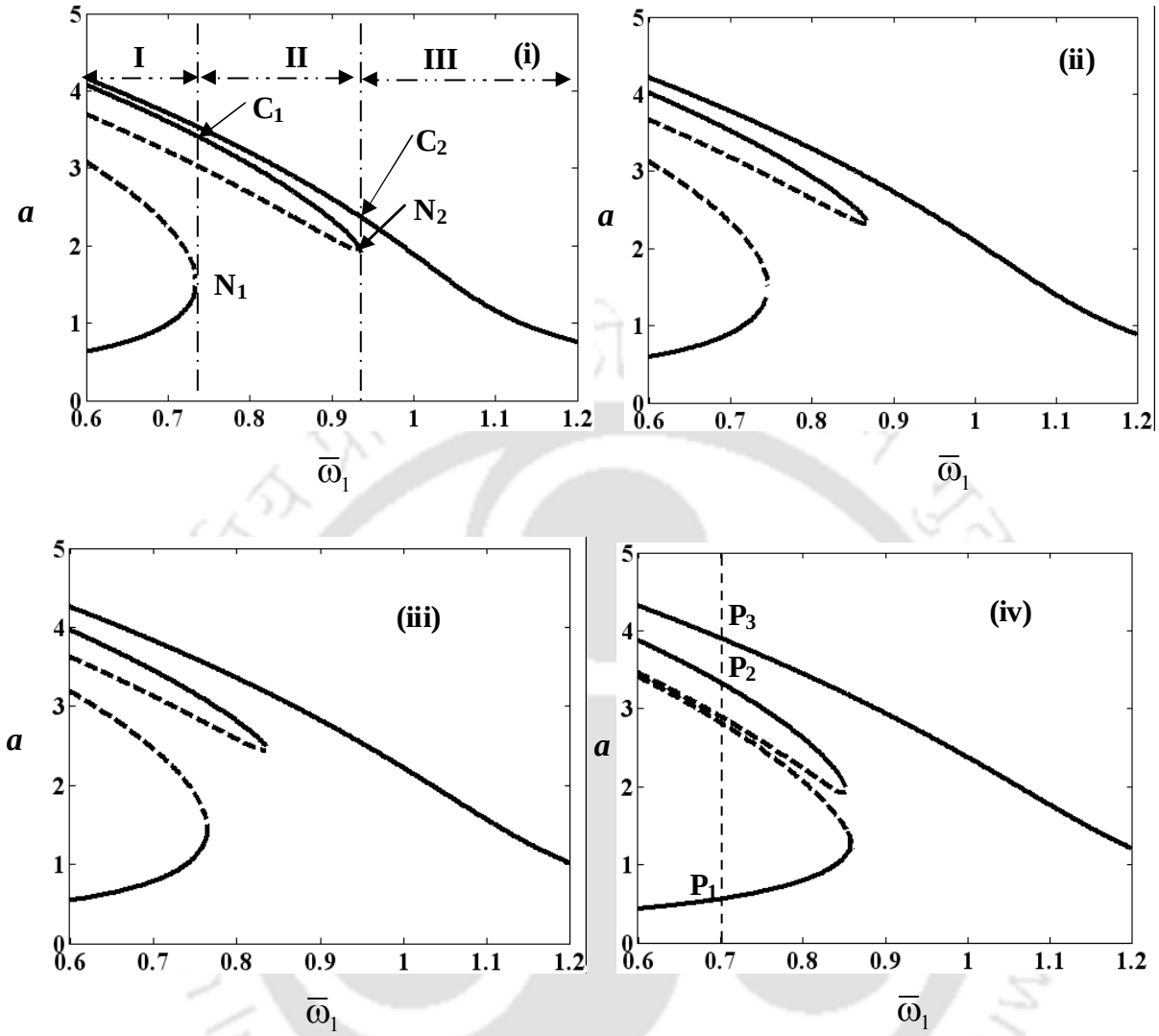

Fig. 5.71. Influence of phase angle (ϕ) on the frequency response curves for $M = 0.04$ kg, $B_m = 0.20$ T, $c_d = 0.01$ N-s/m, $Z = 0.005$ m; (i) $\phi = \pi/6$ (ii) $\phi = \pi/3$, (iii) $\phi = \pi/2$, (iv) $\phi = \pi$.

From Fig. 5.71, it is observed that with increase in ϕ upto $\pi/4$, while the jump up phenomena of the manipulator due to the presence of the S-N bifurcation point N_1 starts at same frequency $\bar{\omega}_1$ (Fig 5.69 (iii) and Fig. 5.71(i)), S-N bifurcation point N_2 starts at higher frequency $\bar{\omega}_1$. Hence, for $\phi < \pi/4$, with increase in ϕ, the region S_2 increases and region S_1

remains same. In this case, if the excitation frequency exceeds the critical point N_1, the response may jump to stable nontrivial state in region S_2 (e.g., C_1). With further increase in frequency beyond critical point N_2, the system undergoes a second catastrophic failure due to the sudden jump from N_2 to C_2. But, with further increase in ϕ upto π, one may observe that while the region S_2 decreases, the region S_1 increases. In this case, when the phase angle ϕ is nearly equal to π i.e., these two excitations are nearly in opposite phase, N_2 precedes N_1 as shown in Fig. 5.71(iv). With increase in frequency beyond N_1, the system will experience a jump up phenomena and will jump to the upper most stable nontrivial state C_1. It may be noted that, in this frequency response curves only $a \sim \bar{\omega}_1$ is plotted as $\bar{\omega}_2$ can be written in terms of $\bar{\omega}_1$ and ϕ as given in the reduced equations (5.97, 5.98). Due to the presence of tri-stable region before the S-N bifurcation point N_1, the initial condition in this region will play an important role to find the appropriate steady-state response. To illustrate this point, one may plot the basin of attraction by numerically solving the reduced equations (5.97, 5.98) in the a – γ plane. Here, for $\bar{\omega}_1$ equal to 0.7, the basin of attraction is shown in Fig. 5.72. It is observed that the system has three stable solutions corresponding to points P_1, P_2 and P_3 as marked in Fig. 5.71(iii).

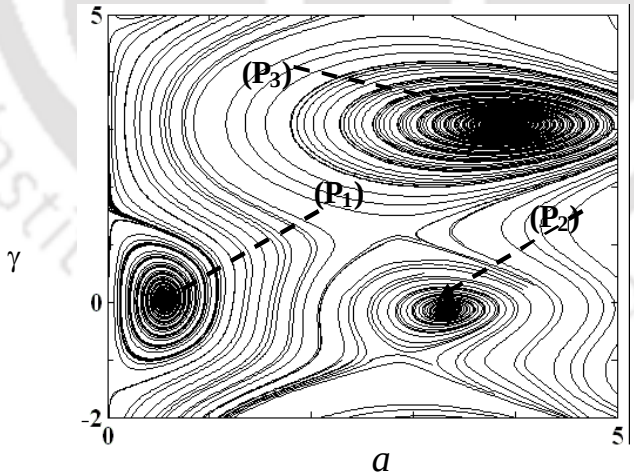

Fig. 5.72. Basin of attraction for $\bar{\omega}_1 = 0.7$. Key as in Fig. 5.71 (iv).

Figure 5.73 shows the frequency response curves for two different values of amplitude of magnetic field strength B_m. One may observe from Fig. 5.69(iii) and Fig. 5.73 that with

increase in B_m, the response amplitude increases and the bifurcation point N_1 starts at a lower frequency and N_2 starts at a higher frequency. It may also be observed from these figures that with increase in B_m, the region S_1 gets decreased and region S_2 gets increased. For low value of magnetic field strength B_m, the region S_2 will disappear from the response curves (Fig. 5.73(i)). It may be noted that with increase in B_m, the bifurcation point N_1 always precedes the bifurcation point N_2. In such a case, with further increase in frequency at the critical point N_1, the system will experience a jump up phenomena similar to that explained in Fig. 5.69.

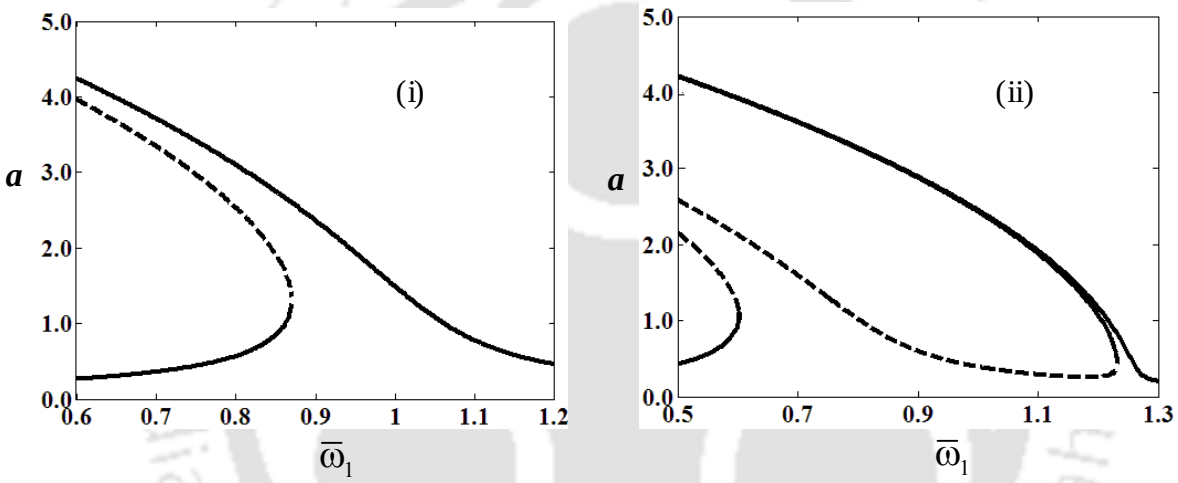

Fig. 5.73. Influence of magnetic field strength (B_m) on the frequency response curves for $M = 0.04$ kg, $c_d = 0.01$ N-s/m, $Z = 0.005$ m;(i) $B_m = 0.10$ T, (ii) $B_m = 0.30$ T.

Figure 5.74 shows the frequency response curves for two different values of payload mass *M*. From Fig. 5.69(iii) and Fig. 5.74 it is observed that with increase in *M*, the response amplitude increases and while the region S_1 gets decreased, region S_2 gets increased. Hence, it is observed that while point N_1 moves toward a lower frequency, point N_2 moves to a higher frequency with increase in *M*. Based on the above observations, to control the vibration of the manipulator in a particular application, the designer should take appropriate system parameters based on this analysis.

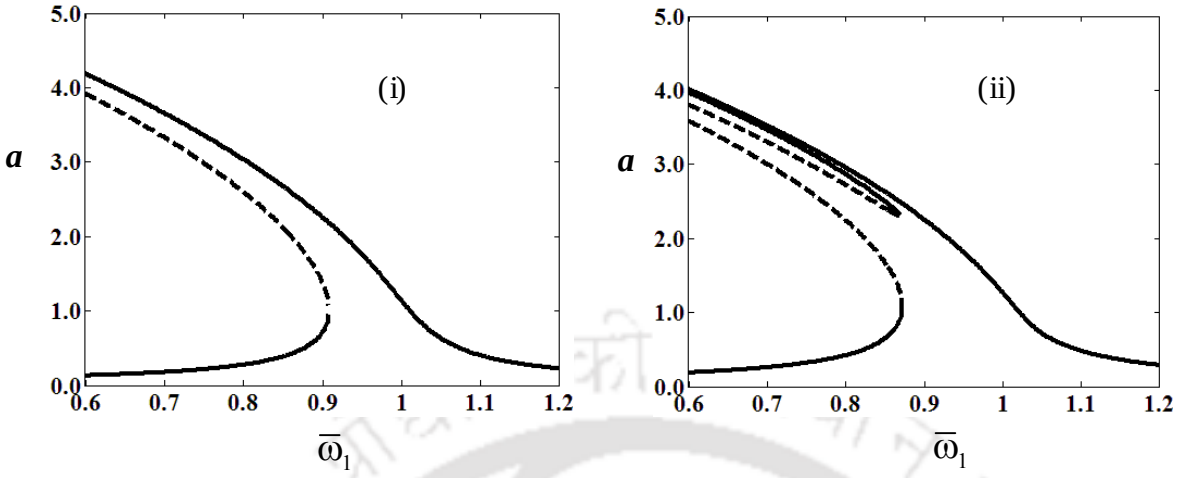

Fig. 5.74. Influence of tip mass (M) on the frequency response curves for $B_m = 0.20$ T, $Z = 0.005$ m, $c_d = 0.01$ N-s/m ; (i) $M = 0.01$ kg , (ii) $M = 0.02$ kg .

5.7 Summary

In this chapter, dynamic analyses of five different magnetoelastic Cartesian manipulators subjected to sinusoidally varying magnetic field with and without harmonically varying tip force are studied. Here, the manipulator is modeled either as a cantilever beam or as a roller-supported beam. While the manipulator with large transverse deflection, first order method of multiple scales is used to determine the instability regions and frequency response curves, the second order method of multiple scales is used to find region of instability for the manipulator with small transverse deflection. As a detail summary about these manipulators will be presented chapter 6, here the results are briefly summarized in the following paragraph.

For the case of magnetoelastic cantilevered manipulator with small transverse deflection, system has three different resonance conditions viz., simple resonance, principal parametric resonance and simultaneous principal parametric and simple resonance. In case of simple resonance, the instability region is compared with the experimental work and has found to be in good agreement. One may use the closed form mathematical expression for determining the parametric instability regions for different resonance conditions for any

similar physical system. For the magnetoelastic cantilevered manipulator with both static and dynamic magnetic field, system has two different types of resonance conditions viz., simple resonance, and principal parametric resonance. Expressions for the critical values of the static and dynamic amplitude of the magnetic field strength are developed which has significant implication in the control of a system using magnetic field. In this case, to reduce the amplitude of vibration significantly, one should increase the static amplitude of magnetic field strength and for minor or precise control of vibration amplitude; the dynamic amplitude of magnetic field strength should be increased.

In case of magnetoelastic cantilevered manipulator without axial force, system has only simple resonance condition. Within the critical magnetic field strength, with increase in magnetic field strength, while the response of the system remains practically unchanged, the unstable trivial region increases. The effects of material conductivity on system response and unstable trivial state region are found to be very negligible. For the magnetoelastic cantilevered manipulator with harmonically varying axial force, three different resonance conditions viz., simple resonance, principal parametric resonance and simultaneous principal parametric and simple resonance are observed and one may utilize the findings of these resonance conditions to effectively control the vibration of the cantilever beam with tip mass by applying appropriate axial load and magnetic field.

Lastly, the magnetoelastic Cartesian manipulator is modeled as a base excited roller-supported beam with tip mass subjected to transverse magnetic field. Here also three resonance conditions viz., simple resonance due to support motion, simple resonance due to magnetic field, and simultaneous resonance condition are observed. In simple resonance condition, the resonance peak is found to be significantly reduced by increasing the amplitude of the magnetic field. From the above discussions, it may be concluded that the magnetoelastic beam can be used as a flexible manipulator and by applying appropriate magnetic field and operating it in safer zone as discussed in this chapter, the vibration of the manipulator can be actively controlled.

Chapter 6

CONCLUSIONS, LIMITATIONS AND SCOPES FOR FUTURE WORK

6.1 General Conclusions

In the present work, nonlinear dynamics of elastic, viscoelastic and magnetoelastic single link flexible Cartesian manipulators with nine different models have been studied. While for all these three types of manipulators, harmonically moving roller supported prismatic joint has been considered, in case of magnetoelastic manipulator, additional models of cantilevered type manipulators have been considered. The manipulator has been modeled as an Euler-Bernoulli beam with large transverse deflection. Taking into account different operations of the endeffector, the free end of the manipulator has been modeled as an attached mass with and without harmonically varying axial load. The following nine different Cartesian manipulator models have been studied

- Harmonically varying roller supported elastic beam
  - without tip load
  - with harmonically varying tip load
- Harmonically varying roller-supported viscoelastic manipulator
  - without tip load
  - with harmonically varying tip load
- Magnetoelastic Cartesian manipulators modeled as
  - Magnetoelastic cantilever beam with small elastic deflection, and periodic tip load
  - Soft magnetoelastic cantilevered beam with both static and dynamic magnetic field.
  - Magnetoelastic cantilever beam dynamic magnetic field
  - Magnetoelastic cantilever beam subjected to harmonically varying tip force
  - Harmonically varying roller-supported beam and periodic magnetic field

For all these three types of manipulators, the governing equation of motion has been developed by using D' Alembert's principle and then the nonlinear temporal equation of motion has been obtained by using generalized Galerkin's method. The temporal equation of motion contains linear forcing term, parametric terms, nonlinear damping terms and nonlinear parametric term along with cubic geometric and inertial terms. While linear forcing term is due to the support motion of manipulator, the parametric terms are due to the harmonically varying axial tip force and periodically varying transverse magnetic field. The nonlinear damping term exists due to the electromagnetic axial force in case of magnetoelastic manipulator and in case of viscoelastic manipulator it is due to the material loss factor. While nonlinear parametric term occurs due to the support motion of the manipulator, nonlinear cubic geometric and inertial terms arise due to the large transverse deflection of the beam.

To solve these temporal equations of motions, first and second order method of multiple scales and method of normal forms have been used. Influences of different system parameters on the instability regions and frequency response curves have been observed for different resonance conditions. The present numerical results have been compared with the previously published experimental results and numerically solving the temporal equation of motion which are found to be in good agreement.

It may be noted that carrying out expensive experiments and numerically solving the highly complex nonlinear temporal equation of motion are tedious and time consuming and hence, one may use the developed simplified mathematical expressions and the reduced equations in this work for finding the parametric instability regions, frequency response and critical bifurcation points for different resonance conditions. These equations will find extensive applications in the feed-forward control of flexible Cartesian manipulator for precision positioning and constraint motion without any vibration.

In most of the manipulators, when the frequency of the support motion is nearly equal to the natural frequency of the system, the system undergoes simple resonance condition and

in this resonance condition, the system may fail due to sudden jump at the saddle node bifurcation point. It has been observed that with increase in amplitude of support motion, and payload mass, system response increases while with increase in damping, the system responses decreases and the system may fail at the saddle-node bifurcation point. Hence, the manipulator should be safely operated at a frequency less than that of the saddle node bifurcation point.

Specific conclusions for different manipulators are given in the following subsections.

6.2 Specific Conclusions

6.2.1 Elastic Cartesian manipulator without tip force

In this case, the nonlinear response of a flexible single link roller-supported Cartesian manipulator with payload subjected to a harmonic base excitation has been investigated. Such types of system can be used for pick and place type of operations. Here, two different resonance conditions viz., simple and subharmonic resonance conditions have been observed. With increase in amplitude of base excitation and payload the response amplitude of the system increases for both the resonance conditions.

In simple resonance case, i.e., when the frequency of the support motion is nearly equal to the natural frequency of the system, the system does not posses any trivial state response and hence, always vibrates with amplitude equal to that of the nontrivial state determined in this work. With decrease in amplitude of external excitation, the maximum value of nontrivial response amplitude remained almost same and system undergoes a catastrophic failure due to jump up phenomena at saddle-node bifurcation point.

Unlike simple resonance case, in subharmonic case where the frequency of the system is nearly three times the natural frequency of the system, along with nontrivial response, stable trivial state response exists for a wide range of system parameters and jump down

phenomena occurs due to the presence of saddle-node bifurcation point. Hence, the system may undergo a catastrophic failure due to the presence of jump down phenomena.

From this study, it may be concluded that the Cartesian manipulator may be operated at a frequency near the sub-harmonic resonance zone due to the presence of stable trivial zone. But while sweeping the frequency from simple resonance zone to sub-harmonic resonance zone, the system may fail due to the catastrophic jump up phenomena. To prevent the failure of the manipulator, there is a need to further investigate such systems by using active and passive control strategies. For this purpose, manipulators with visco-elastic and magneto-elastic materials have been investigated.

6.2. 2. Elastic Cartesian manipulator with harmonically varying tip force

In this work, the nonlinear response of a single-link flexible manipulator subjected to a harmonic motion at the roller supported left end and a pulsating axial force at the free end has been determined. Such systems can be used in the applications when the endeffector is in contact with the environment while doing specific operations like welding, painting, cutting etc. In this case three different resonance conditions such as simple resonance, principal parametric resonance and simultaneous resonance conditions have been investigated for different system parameters.

In simple resonance case, it has been observed that with increase in static force, amplitude of base excitation and mass ratio, nontrivial system response increases and the system may fail at the saddle-node bifurcation point. Hence, the manipulator should be safely operated at a frequency less than that of the saddle node bifurcation point.

Similarly, for principal parametric resonance case, i.e., when the end-effector of the manipulator is subjected to a pulsating constrained force with a frequency nearly equal to twice the natural frequency of the system, it is recommended to operate the manipulator below the sub-critical pitchfork bifurcation point to avoid excessive vibration.

One may note that in simultaneous resonance case the system has a tri-stable region while in simple and principal parametric resonances the system has bi-stable regions. In case of simultaneous resonance condition, the manipulator should be operated at a frequency which is below the saddle-node bifurcation point.

6.2.3 Visco-elastic Cartesian manipulator without axial tip force

In case of viscoelastic Cartesian manipulator, a comparison has been made with an equivalent elastic beam and the reduction in maximum amplitude of vibration using a viscoelastic manipulator is found to be very significant. Hence, one may use a viscoelastic manipulator for vibration control purpose.

The nonlinear response obtained by using perturbation method have bee compared with the results obtained by solving the temporal equation of motion and have been found to be in good agreement. These results have also been compared by modeling the manipulator as a linear Kelvin–Voigt model and it is shown that the linear model gives very erroneous results.

Similar to elastic manipulator here also, the system has simple resonance when the frequency of support motion is nearly equal to the natural frequency of the system and in this case, the non-trivial frequency response curve shows critical saddle-node bifurcation point at which the system may fail due to jump-up phenomena. With increase in material loss factor and decrease in amplitude of base excitation the maximum response amplitude decreases.

Unlike simple resonance case, in sub-harmonic resonance case, the system possesses both trivial and non-trivial response. But for a wide range of system parameters, the trivial state is found to be stable. The effect of material loss factor, amplitude of base excitation and mass ratio are studied for both the resonance conditions and are found to be in the expected lines. These results will be very useful for the design of flexible manipulators to reduce vibration using viscoelastic materials.

6.2.4 Viscoelastic Cartesian manipulator with periodically varying tip force

Here, the nonlinear response of a visco-elastic Cartesian manipulator subjected to tip load has been determined. Similar to elastic manipulator, here also, the stability and bifurcation analyses of the steady state response have been carried out for three different resonance conditions.

In simple resonance condition, the maximum resonate amplitude has been reduced by increasing the material loss factor. It has been observed that the response amplitude increases with increase in amplitude of support motion, and mass ratio. Similar to the previous case, here also, the manipulator should be safely operated at a frequency below the saddle node bifurcation point.

But when the manipulator is subjected to tip load with a frequency nearly equal to twice the natural frequency of the system, catastrophic failure may occur at the sub-critical pitchfork bifurcation point. One may find that in simultaneous resonance case the system has a similar tri-stable region as in case of elastic manipulator. Depending on the application of the manipulator, using the developed results one may safely operate the manipulator by properly choosing the material and other system parameters of the manipulator.

6.2.5 Magnetoelastic cantilever beam subjected to axial force considering small transverse deformation

In this work the stability boundaries of a cantilever beam with and without tip mass subjected to time varying transverse magnetic field and axial periodic load are studied. Instability regions are found by using second order method of multiple scales for three different resonance conditions. In simple resonance case, unlike the previous analytical studies, the instability regions are found to be in good agreement with the experimental findings. Hence, one may use the developed expressions for instability regions to

determine the parametric instability regions for different resonance conditions for any similar physical systems. In all the cases, it is observed that with increase in damping, static axial load and mass ratio the instability region decreases and one may control the vibration of a system using required magnetic field as shown in the figures with parametric instability regions.

6.2.6 Soft magnetoelastic cantilever beam with static and dynamic magnetic field

In this work, the usability of soft magnetoelastic beam for manipulator purpose has been explored. Considering large deflection, study has been carried out to control the transverse vibration of the manipulator actively by applying static and time varying magnetic field. The system is found to have simple and principal parametric resonance conditions and here, the first order closed form expressions for finding the instability regions have been developed which are found to be better than the previously published theoretical and is in good agreement with experimental results. Expressions for the critical values of the static and dynamic amplitude of the magnetic field strength have been developed which will have significant implication in the control of a system using magnetic field.

When a vibrating manipulator is subjected to a magnetic field with a frequency equal to the natural frequency of the system (simple resonance case), it has been observed that with increase in damping or decrease in static magnetic field and tip mass, the instability region decreases. The response amplitude also decreases with increase in damping, tip mass and the amplitude of static and dynamic magnetic field strength. When the system is subjected to a magnetic field with a frequency equal to twice the natural frequency (principal parametric resonance), it has been observed that with increase in the static and dynamic amplitude of magnetic strength, the nontrivial response and the instability region increases. This indicates a destabilizing effect of the magnetic field. Hence, it has been suggested to use the simple resonance condition to control the large amplitude vibration of a system by using magnetic field. To reduce the amplitude of vibration significantly, one should increase the static amplitude of magnetic field strength and for minor or precise control of vibration amplitude; the dynamic amplitude of magnetic field strength should be increased.

Therefore, instead of arbitrarily using the magnetic field, the operator should apply appropriate magnetic field as suggested in this work.

6.2.7 Magnetoelastic cantilever beam with harmonically varying tip force

In this work, an extensive study has been carried out on the nonlinear vibration of a magneto-elastic manipulator subjected to harmonic axial load and time varying magnetic field. Three different resonance conditions have been observed and one may utilize the findings of these resonance conditions to effectively control the vibration of the manipulator by applying appropriate axial load and magnetic field. In all the resonance conditions, with increase in tip mass and amplitude of dynamic loading, the unstable trivial range and the amplitude of stable nontrivial response increases.

For simple resonance condition, it has been observed that lower amplitude of magnetic field strength with a frequency higher than the supercritical pitchfork bifurcation point or a higher value of magnetic field strength with a frequency lower than the frequency corresponding to the saddle-node bifurcation point will be more useful to control the vibration. The amplitude of static loading has a stabilizing effect for frequency of magnetic field greater than the natural frequency and has a destabilizing effect when the corresponding frequency is less than the natural frequency of the system.

In case of principal parametric resonance condition, it may be noted that with increase in magnetic field strength, the response amplitude decreases significantly. Unlike the simple and principal parametric resonance cases, in the case of simultaneous resonance, the unstable trivial region and amplitude of the stable nontrivial state response of the system decreases significantly with increase in magnetic field strength.

6.2.8 Magnetoelastic cantilever beam without tip force

Unlike a soft magnetoelastic beam considered in section 6.2.6, here, a magnetoelastic beam is taken considering large transverse vibration and attempt has been made to study its

dynamics under dynamic magnetic field. It has been observed that there exists a critical value of amplitude of magnetic field strength above which the system becomes unstable. Within this limit with increase in magnetic field strength, while the response of the system remains practically unchanged, the unstable trivial region increases. The response amplitude decreases with increase in damping, decrease in tip mass and relative permeability of the system. The effects of material conductivity on system response and unstable trivial state region have been found to be very negligible. The results obtained in this present work will find application in determining the critical amplitude and frequency of the magnetic field to be used to control the vibration of the manipulator. It may be used to choose proper beam material and system dimensions so as to have very less vibration.

6.2.9 Magnetoelastic Cartesian manipulator

To limit the analysis, within two frequency excitations, in this work, similar to the elastic and viscoelastic manipulators, a harmonically moving roller supported magnetoelastic Cartesian manipulator with moderately large transverse vibration, subjected to time varying magnetic filed has been considered. In this case, simple resonance occurs when the frequency of either the roller support or the magnetic field is nearly equal to the natural frequency of the system and simultaneous resonance occurs when both these excitations have frequencies nearly equal to the natural frequency.

In simple resonance condition, when the roller supported end has a frequency nearly equal to the natural frequency of the system, it has been shown that the resonance peak can be significantly reduced actively by increasing the amplitude of the magnetic field. But it may be noted that depending on the payload mass and material properties of the manipulator, the magnetic field strength has a limit beyond which increase in magnetic field will have a destabilizing effect. In this case the system has two critical saddle-node bifurcation points and hence, the frequency of the roller supported end should be properly chosen so as not to exceed the lower critical saddle-node bifurcation point to avoid catastrophic failure and operate it with minimum vibration.

In the other simple resonance case due to magnetic field, i.e., when the manipulator has been subjected to a magnetic field with a frequency nearly equal to the natural frequency of the system, the operation of the manipulator should be limited to that of the sub-critical pitchfork bifurcation point after which it may suffer a catastrophic failure.

Similarly when both these frequencies are nearly equal to the natural frequencies of the system, i.e., in case of simultaneous resonance condition, as the system does not have a trivial response, it will always vibrate with an amplitude equal to that of the nontrivial state determined by the frequency response curve. But one may keep the vibration minimum by operating the manipulator at a frequency lower than first saddle-node bifurcation point marked in the frequency response curve.

Due to the presence of tristable region in the zone III and bistable region in zone II, it is advisable to operate the manipulator with lower amplitude of support motion in the frequency zone III. Though the frequency of the magnetic field can be actively changed to this frequency zone, one has to device a mechanism to sweep up the frequency of support motion through zone II and III. Also it is observed that increase of magnetic field strength in this resonance condition has a destabilizing effect.

It has been shown that to reduce large amount of vibration of the manipulator actively, one may go for magneto-elastic beam and operate it away from the resonance zones and for passive vibration control viscoelastic beam may be used. Hence, the operator or designer has to take appropriate system parameters based on this analysis to control the vibration of a flexible Cartesian manipulator.

6.3 SCOPES FOR FUTURE WORK

In the present work the nonlinear dynamics of a single link flexible Cartesian manipulator considering elastic, viscoelastic and magnetoelastic materials have been studied. The manipulator has been modeled either as a roller supported or cantilevered Euler Bernoulli beam with moderately large deflection. One may consider many other parameters to improve this model. The following extensions may be carried out.

- Here the analysis has been limited to the fundamental frequency of the system. Multimode analysis may be carried out to study the effect of different system parameters when the system operates at higher frequencies.
- The three frequency excitations observed for the magnetoelastic manipulator with harmonically varying axial load and roller support motion may be explored.
- The higher order super harmonics and simultaneous resonance conditions observed in elastic and viscoelastic beams should be investigated.
- Here the analyses have been carried out considering single frequency excitation for the roller supported end and for the axial load applied at the endeffector. But one may take a more realistic multi-frequency excitation to analyze the system.

- Internal resonance conditions may be considered when the frequencies of different modes are commensurate.
- The planar vibration of the system may be extended further to consider nonplanar motion of the end effector.
- One may consider Rayleigh and Timoshenko beam when the manipulator is no longer slender by considering shear deformation and the rotary inertia effects.
- Instead of considering payload as point mass, one may consider it as an extended payload mass.
- Experiments should be conducted to verify the results obtained in these numerical simulations.
- For passively control the vibration of the manipulator, one may use sandwich structure and shunted piezoceramics dampers.
- To actively reduce the vibration of the manipulator one may use magnetorheological elastomer where, the present analysis can be easily extended.
- The present analyses may be extended for micro and nano manipulator systems which find extensive applications in microsurgery and many precision industrial applications.

REFERENCES

1. Abdelhafez, H.M., 2004, Resonance of a nonlinear forced system with two-frequency parametric and self-excitations, Mathematics and Computers in Simulation 66, 69–83.
2. Abd El-Latif, G.M., 2004, Parametric excitation for forcing van der Pol oscillator, Applied Mathematics and Computation 147, 255–265.
3. Ahmad, M. A., 2008, Vibration and input tracking control of flexible manipulator using LQR with noncontroller, Computer Modeling and Simulation, EMS '08 Second UKSIM European Symposium on 8-10 September, 40 – 45.
4. Ahmad, M.A., Mohamed, Z., and Hambali, N., 2008a, Dynamic modeling of a two-link flexible manipulator system incorporating payload, 3rd IEEE Conference on Industrial Electronics and Applications, 96-101.
5. Ahmad, M.A., Mohamed, Z., Ishak, H., and Nasir, A.N.K., 2008b, Vibration suppression techniques in feedback control of a very flexible robot manipulator, Modeling & Simulation, AICMS 08. Second Asia International Conference on 13-15 May, 469 – 474.
6. Alam, M.S., and Tokhi, M.O., 2008, Hybrid fuzzy logic control with genetic optimization for a single-link flexible manipulator, Engineering Applications of Artificial Intelligence 21, 858–873.
7. Al-bedoor, B. O., and Khulief, Y.A., 1996, An approximate analytical solution of beam vibrations during axial motion, Journal of Sound and Vibration 192,159-171.
8. Al-bedoor, B. O., and Khulief, Y.A., 1996, Finite element dynamic modeling of a translating and rotating flexible link, Computer Methods in Applied Mechanics and Engineering 131,173-189.

9. Alberts, T.E., Xia, H., and Chen, Y., 1992, Dynamic analysis to evaluate viscoelastic passive damping augmentation for the space shuttle remote manipulator system, ASME Journal of Dynamic Systems, Measurement, and Control 114, 468–474.
10. Alexander, N. A., 1998, Evaluating basins of attraction in non-linear dynamical systems using an improve recursive boundary enhancement, Journal of Sound and Vibration 209, 443-472.
11. Alhazza, K, A., Daqaq, M. F., Nayfeh, A.H., and Inman, D.J., 2008, Non-linear vibrations of parametrically excited cantilever beams subjected to non-linear delayed-feedback control, International Journal of Non-Linear Mechanics 43, 801-812.
12. Anderson, T. J., Balachandran, B., Nayfeh, A. H., 1994, Nonlinear responses in a flexible cantilever beam, Journal of Vibration and Acoustics 116, 480-484.
13. Ankarali, A. and Diken, H., 1997, Vibration control of an elastic manipulator link, Journal of Sound and Vibration 204, 162–170.
14. Arafat, H. N., Nayfeh, A. H., and Chin, C. M., 1998, Nonlinear nonplanar dynamics of parametrically excited cantilever beam, Nonlinear Dynamics 15, 31-61
15. Argyris, J., Belubekian, V., Ovakimyan, N., and Minasyan, M., 1996, Chaotic vibrations of a nonlinear viscoelastic beam, Chaos, Solitons & Fractals 7, 151-163.
16. Arteaga, M., 1998, On the properties of a dynamic model of flexible robot manipulators, ASME Journal of Dynamic Systems, Measurement, and Control 120, 8–14.
17. Asada, H., Park, J.H., and Rai, S., 1991, A control-configured flexible arm: integrated structure/control design, Proceedings of the IEEE International Conference on Robotics and Automation 3, 2356–2362.

18. Ashworth, R. P., and Barr, A. D. S., 1987, The responses of structures with quadratic inertial nonlinearity under direct and parametric harmonic excitation, Journal of Sound and Vibration 118, 47-68.
19. Azad, A.K.M., and Tokhi, M.O., 2003, An interactive environment for simulation and control of flexible manipulator systems, Emerging Technologies and Factory Automation, Proceedings. ETFA '03. IEEE Conference **2,** 524- 529.
20. Bahrami, M., and Rahi, A., 2003, Tip dynamic response of elastic joint manipulators subjected to a stochastic base excitation, JSME, Series C 46,1502–1508.
21. Bakri, T., Nabergoj, R., Tondl, A., and Verhulst, F., 2004, Parametric excitation in non-linear dynamics, International Journal of Non-Linear Mechanics 39, 311 – 329.
22. Barbieri, E., Özguner, Ü., 1988, Unconstrained mode expansion for a flexible slewing link, ASME Journal of Dynamic Systems, Measurement, and Control 110, 416–421.
23. Barr, A. D. S., 1980, Some developments in parametric stability and nonlinear vibration (Recent Advances in Structural Dynamics, Vol II. Edited by M. Petyt), Institute of Sound and Vibration Research. England.
24. Barr, A D. S., and McWhannel, D. C., 1971, Parametric instability in structures under support motion, Journal of Sound and Vibration 14, 491—509.
25. Baruh, H., and Tadikonda, S.S.K., 1989, Issues in the dynamics and control of flexible robot manipulators, AIAA Journal of Guidance, Control and Dynamics 12, 659–671.
26. Basher, H. A.M., 2000, Dynamic behavior of a translating flexible beam with a prismatic joint**,** Proceedings of the IEEE, SoutheastCon 7, 31-38.
27. Basher, H. A.M, 2007, Modeling and simulation of flexible robot manipulator with a prismatic joint, Proceedings of IEEE, SoutheastCon, 255-260.

28. Bayo, E., 1988, Computed torque for the position control of open-chain flexible robots, Proceeding of IEEE, International conference on Robotics and Automation 1, 316-321.
29. Bayo, E., and Moulin, H., 1989, An efficient computation of inverse dynamics of flexible manipulator in time the domain, Proceeding of IEEE, International conference on Robotics and Automation 2, 710-715.
30. Belhaq, M., and Sah, S.M., 2008, Fast parametrically excited van der Pol oscillator with time delay state feedback, International Journal of Non-Linear Mechanics 43, 124 – 130.
31. Benamar, R., Bennona, M.M., and White, R. G., 1991, The effect of large vibration amplitudes on the mode shapes and natural frequencies of thin elastic structures part i: Simply supported and clamped-clamped beams, Journal of Sound and Vibration 149, 179-195.
32. Benosman, M., Boyer, F., Vey, G. L., and Primautt, D., 2002, Flexible links manipulators: from modeling to control, Journal of Intelligent and Robotic Systems 34, 381–414.
33. Benosman, M. and Vey, G.L., 2004, Control of flexible manipulators: a survey, Robotica 22, 533–545.
34. Bishop, R. E. D., Cannon, S. M., and Miao, S., 1989, On coupled bending and torsional vibration of uniform beams, Journal of Sound and Vibration 131, 457-464.
35. Bolotin, V. V., 1964, The Dynamic Stability of Elastic Systems, Holden-Day, Inc.
36. Book, W.J., 1984, Recursive Lagrangian dynamics of flexible manipulator arms, The International Journal of Robotics Research 3, 87–101.
37. Book, W.J., 1990, Modeling, design, and control of flexible manipulator arms: a tutorial review, Proceedings of the IEEE Conference on Decision and Control, 500–506.

38. Boyer, F., and Coiffet, P., 1996, Symbolic modeling of a flexible manipulator via assembling of its generalized Newton–Euler model, Journal of Mechanism and Machine Theory 31, 45–56.
39. Dubowsky, S.,1994, Dealing with vibrations in the deployment structures of space robotic systems, in: Fifth International Conference on Adaptive Structures, Sendai International Center, Sendai, Japan, 5–7.
40. Buffinton, K.W., 1992, Dynamics of elastic manipulators with prismatic joints, ASME Journal of Dynamic Systems, Measurement, and Control 114, 41–49.
41. Buffinton, K.W., and Kane, T.R., 1985, Dynamics of beam moving over supports, International Journal of Solids and Structures 21, 617– 643.
42. Burney, S.Z.H., and Jager, L.G., 1971, A method of determining the regions of instability of a column by a numerical approach, Journal of Sound and Vibration 15, 75–91.
43. Burton, T. D., and Kolowith, M., 1988, Non-linear resonances with chaotic motion in a flexible parametrically excited beam, Proceedings of the Second Conference on Non-linear Vibration, Stability, and Dynamics of Structures and Mechanisms. Blacksburg, VA, June 1-3.
44. Cannon, R.H., and Schmitz, E., 1984, Initial experiments on end-point control of a flexible one-link robot, The International Journal of Robotics Research 3, 62–75.
45. Cao, X.T., and Li, Y. C., 2008, Robust RBF neural network force/position control of time varying constrained flexible manipulator, Control and Decision 22, 977-982.
46. Cao, D.X. and Zhang, W., 2008, Global bifurcations and chaotic dynamics for a string-beam coupled system, Chaos, Solitons & Fractals 37, 858–875.
47. Carlson, R. L., Lo, H. C. T., and Briley, R. P., 1980, On the parametric excitation of a tensioned bar with initial curvature, International Journal of Mechanical Sciences 22, 59-65.

48. Cartmell, M.P., 1990, Introduction to Linear, Parametric and Nonlinear Vibrations, Chapman & Hall, London, 1990.
49. Cartmell, M.P., 1990, The equations of motion for a parametrically excited cantilever beam, Journal of Sound and Vibration 143, 395-405.
50. Cederbaum, G., and Mond, M., 1992, Stability properties of a viscoelastic column under a periodic force, Transactions of the ASME. Journal of Applied Mechanics 59, 16-19.
51. Celep, Z.,1985, Dynamic stability of pretwisted columns under periodic axial loads, Journal of Sound and Vibration 103, 35-42
52. Cepon, G., and Boltežar, M., 2007, Computing the dynamic response of an axially moving continuum, Journal of Sound and Vibration 300, 316–329.
53. Chakraborty, G., and Mallik, A.K., 1998, Parametrically excited non-linear traveling beams with and without external forcing, Nonlinear Dynamics 17, 301–324.
54. Chakraborty, G., Mallik, A.K., and Hatwal, H., 1999, Non-linear vibration of a traveling beam. International Journal of Non-Linear Mechanics 34, 655–670.
55. Chalhoub, N.G., and Ulsoy, A.G., 1987, Control of a flexible robot arm: experimental and theoretical results, Trans. ASME, Journal of Dynamic Systems, Measurement, and Control 109, 299–309.
56. Chalhoub, N.G., Foury, G.A.K., and Bazzi, B.A., 2006, Design of robust controllers and a non-linear observer for the control of a single-link flexible robotic manipulator, Journal of Sound and Vibration 291, 437–461.
57. Chang, L.W., and Gannon, K.P., 1990, A dynamic model on a single link flexible manipulator, ASME Journal of Vibration and Acoustics 112,138–143.
58. Chapnik, B.V., Heppler, G.R., and Aplevich, J.D., 1991, Modelling impact on a one link-flexible robotic arm, IEEE Transactions on Robotics and Automation 7, 479–488.

59. Chatjigeorgiou, I. K., 2004, On the parametric excitation of vertical elastic slender structures and the effect of damping in marine applications, Applied Ocean Research 26, 23–33.

60. Chedmail, P., Aoustin, Y., and Chevallereau, Ch., 1991, Modelling and control of flexible robots, International Journal of Numerical Methods in Engineering 32, 1595–1619.

61. Chen, Li. Q., and Yang, X.D., 2005, Stability in parametric resonance of axially moving viscoelastic beams with time-dependent speed, Journal of Sound and Vibration 284, 879–891.

62. Chen, L.Q., and Yang, X.D., 2005, Steady-state response of axially moving viscoelastic beams with pulsating speed: comparison of two nonlinear models, International Journal of Solids and Structures 42, 37–50.

63. Chen, L.Q., and Yang, X.D., 2006, Vibration and stability of an axially moving viscoelastic beam with hybrid supports, European Journal of Mechanics A Solids 25, 996–1008.

64. Chen, L.Q., and Yang, X.D., 2006, Transverse nonlinear dynamics of axially accelerating viscoelastic beams based on 4-term Galerkin's truncation, Chaos, Solitons & Fractals 27, 748–757.

65. Chen, Li. Q., Yang, X.D., and Cheng, C.J., 2004, Dynamic stability of an axially accelerating viscoelastic beam, European Journal of Mechanics. A. Solids 23, 659–666.

66. Chen, C. C., and Yeh, M. K., 1995, Parametric instability of a cantilevered column under periodic loads in the direction of the tangency coefficient, Journal of Sound and Vibration 183, 253-267.

67. Chen, C. C., and Yeh, M. K., 1999, Parametric instability of a column with axially oscillating mass, Journal of Sound and Vibration 224, 643–664.

68. Chen, C. C., and Yeh, M. K., 2001, Parametric instability of a beam under electromagnetic excitation, Journal of Sound and Vibration 240, 747–764.

69. Cheng, X. Z., and Yue, Q. Y., 2004, Dynamic analysis of planar cooperative manipulators with link flexibility, Transactions of the ASME. Journal of Mechanical Design 126, 442-448.
70. Chung J., and Yoo, H.H., 2002, Dynamic analysis of a rotating cantilever beam by using the finite element method, Journal of Sound and Vibration 249,147–164.
71. Chung, J., Jung, D., and Yoo, H.H., 2004, Stability analysis for the flap wise motions of cantilever beam with rotary oscillation, Journal of Sound and Vibration 273, 1047–1062.
72. Choura, S., and Yigit, A.S., 2001, Control of a two-link rigid-flexible manipulator with a moving payload mass, Journal of Sound and Vibration 243, 883–897.
73. Coleman, M.P., 1998, Vibration eigenfrequency analysis of a single-link flexible manipulator, Journal of Sound and Vibration 212, 107–120.
74. Coleman, M.P., McSweeney, L.A., 2004, Analysis and computation of the vibration spectrum of Cartesian flexible manipulator, Journal of Sound and Vibration 274, 445–454.
75. Cuvalci, O., 2000, The effect of detuning parameters on the absorption region for a coupled system: a numerical and experimental study, Journal of Sound and Vibration 229, 837–857.
76. Cuvalci, O., and Ertas, A., 1996, Pendulum as vibration absorber for flexible structures: experiments and theory, Journal of Vibration and Acoustics: Trans. of ASME, 118, 558-566.
77. Cyril, X., Jarr, G.J., and Mishra, A.K., 1995, Dynamical modeling and control of a spacecraft-mounted manipulator capturing a spinning satellite, Acta Astronautica 35, 167–174.
78. Diken, H., 2000, Frequency–response characteristics of a single-link flexible joint manipulator and possible trajectory tracking, Journal of Sound and Vibration 223, 179–194.

79. Ding, H., and Chen, L. Q., 2008, Stability of axially accelerating viscoelastic beams: multi-scale analysis with numerical confirmations, European Journal of Mechanics A/Solids, doi:10.1016/j.euromechsol.2007.11.014.

80. Ding, X., and Selig, J.M., 2004, Lumped parameter dynamic modeling for the flexible manipulator, Fifth World Congress on Intelligent Control and Automation (IEEE Cat. No.04EX788) 1, 280-284.

81. Dixit, U.S., Kumar, R., and Dwivedy, S.K., 2006, Shape optimization of flexible robotic manipulators, ASME, J. Mech. Des. 128, 559–565.

82. Dogan, A. I., 1998, Modeling and control of a two-link flexible robot manipulator, Proceedings of the IEEE International Conference on Control Applications 2, 761–765.

83. Dohnal, F., Verhulst, F., 2008, Averaging in vibration suppression by parametric stiffness excitation, Nonlinear Dynamics, Doi: 10.1007/s11071-007-9325-z.

84. Doren, R.V., 1997, Comments on “zones of chaotic behaviour in the parametrically excited pendulum”, Journal of Sound and Vibration 200, 105-109.

85. Dost, S., and Glockner, P. G., 1982, On the dynamic stability of viscoelastic perfect columns, International Journal of Solids and Structures 18, 587-596.

86. Du, Z., Yu, Y., and Zhang, X., 2007, Dynamic modeling of planar flexible parallel manipulators, Chinese Journal of Mechanical Engineering 43, 96-101.

87. Du Z.C., Yu, Y.G., and Zhang, X. P., 2008, Dynamics modeling and simulation for planar flexible-link parallel robots, Journal of System Simulation 20,1094-1098.

88. Dubowsky, S., 1994, Dealing with vibrations in the deployment structures of space robotic systems, in: Fifth International Conference on Adaptive Structures, Sendai International Center, Sendai, Japan, 5–7.

89. Dwivedy, S.K., and Eberdhard, P., 2006, Dynamic analysis of flexible manipulators, a literature review, Mechanism and Machine Theory 41, 749–777.

90. Dwivedy, S.K., and Kar, R.C., 1999, Nonlinear response of a parametrically excited system using higher order method of multiple scales, Nonlinear Dynamics 20, 115–130.

91. Eissa, M., and Amer, Y.A., 2004, Vibration control of a cantilever beam subject to both external and parametric excitation, Applied Mathematics and Computation 152, 611–619.

92. El-Bassiouny, A. F., 2002, Parametrically excited non-linear systems: a comparison of two methods, Applied Mathematics and Computation 132, 385–410.

93. El-Bassiouny, A.F., 2005, Principal parametric resonances of non-linear mechanical system with two-frequency and self-excitations, Mechanics Research Communications 32, 337–350.

94. El-Bassiouny, A.F., 2006, Single-mode control and chaos of cantilever beam under primary and principal parametric excitations, Chaos, Solitons & Fractals 30, 1098–1121.

95. Elmaraghy, R., and Tabarrok, B., On the dynamic stability of an axially oscillating beam, Journal of the Franklin Institute 299, 14-28.

96. Emam, S.A., and Nayfeh, A.H., 2004, Nonlinear response of buckled beams to subharmonic-resonance excitations, Nonlinear Dynamics 35,105–122.

97. Eriksson , T., Hansen, H. N., and Gegeckaite, A., On the use of industrial robots in microfactories, International Journal of Advanced Manufacturing Technology, DOI 10.1007/s00170-007-1116-7

98. Eringen, C., 1987, Theory of electromagnetic elastic plates, Journal of engineering Science 27, 422-428.

99. Esmailzadeh, E., and Jazar, G.N., 1998, Periodic behavior of a cantilever beam with end mass subjected to harmonic base excitation, International Journal of Non-Linear Mechanics 33, 567–577.

100. Evan-Iwanowski, R. M., 1976, Resonance Oscillations in Mechanical Systems, Elsevier, Amsterdam.
101. Evensen, H. A., and Evan-Iwanowski, R. M., 1996, Effects of longitudinal inertia upon the parametric response of elastic columns, ASME Journal of Applied Mechanics 33,141-148.
102. Everett, L.J., Jennchen, T., and Compere, M., 1999, Designing flexible manipulators with the lowest natural frequency nearly independent of position, IEEE Transactions on Robotics and Automation 15, 605–611.
103. Feliu, V., and Ramos, F., 2005, Strain gauge based control of single-link very lightweight flexible robots to payload changes, Mechatronics 15, 547–571
104. Feliu, V., Rattan, K.S., and Brown, H.B., 1992, Modeling and control of single-link flexible arms with lumped masses, Trans. ASME, Journal of Dynamic Systems, Measurement, and Control 114, 59–69.
105. Feng, Z.H., Lan, X.J., and Zhu, X.D., 2007, Principal parametric resonances of a slender cantilever beam subject to axial narrow-band random excitation of its base, International Journal of Non-Linear Mechanics 42, 1170 – 1185.
106. Fertis, D. G., and Lee, C.T., 1993, Non-linear vibration and instabilities of elastically supported beams with axial restraints, Journal of Sound and Vibration 165,123-135.
107. Forehand, D.I.M., and Cartmell, M.P., 2001, On the derivation of the equation of motion for a parametrically excited cantilever beam, Journal of Sound and Vibration 245, 165–177.
108. Fraser, A. R., and Daniel, R. W., 1991, Perturbation Techniques for Flexible Manipulators. Norwell, MA: Kluwer.
109. Fukuda, T., 1985, Flexibility control of elastic robot arms, Journal of Robotic Systems 2, 73–88.
110. Fung, R.F., and Chang, H. C., 1998a, Dynamic modeling of a non-linearly constrained flexible manipulator with a tip mass by Hamilton's principle, Journal of Sound and Vibration 216, 640–658.

111. Fung, R.F., Huang, J. S., and Chen, W. H., 1998b, Dynamic stability of a viscoelastic beam subjected to harmonic and parametric excitations simultaneously, Journal of Sound and Vibration 198, 1-16.
112. Fung, R. F., Lu, P. Y., and Tseng, C. C., 1998c, Non-linear dynamic modeling of an axially moving beam with a tip mass, Journal of Sound and Vibration 218, 559–571.
113. Fung, E. H. K., and Shi, Z. X., 1997, Vibration frequencies of a constrained flexible arm carrying an end mass, Journal of Sound and Vibration 204, 259-269.
114. Gaultier, P.E., and Cleghorn, W.L., 1989, modeling of flexible manipulator dynamics: a literature survey, in: Proceedings of First National Applied Mechanism and Robot Conference, Cincinnati, 1–10.
115. Geniele, H., Patel, R.V., and Khorasani, K., 1997, End-point control of a flexible manipulator: theory and experiments, IEEE Transactions on Control Systems Technology 5, 556–570.
116. George, L.E., and Book, W.J., 2003, Inertial vibration damping of a flexible base manipulator, IEEE/ASME Transactions on Mechatronics 8, 268–271.
117. Guang, Li., and Min, W., 2005a, Singular perturbation approach for control of hydraulically driven flexible manipulator, Journal of Central South University of Technology 12 (1), 238-242.
118. Guang, Li., and Min, W., 2005b, Singular perturbation approach for control of hydraulically driven flexible manipulator, Journal of Central South University of Technology 12 (5), 578-583.
119. Gurgoze, M., 1986, Parametric vibrations of a restrained beam with an end mass under displacement excitation, Journal of Sound and Vibration 108, 73-84.
120. Gurgoze, M., 1987, Parametric vibrations of a viscoelastic beam (Maxwell model) under steady axial load and transverse displacement excitation at one end, Journal of Sound and Vibration 115, 329–338.

121. Gurgoze, M., Dogruoglu, A.N., and Zeren, S., 2007, On the eigencharacteristics of a cantilevered visco-elastic beam carrying a tip mass and its representation by a spring-damper-mass system, Journal of Sound and Vibration 301, 420–426.
122. Haight, E. C., and King, W. K., 1971, Stability of parametrically excited vibrations of an elastic rod, Development of Theoretical and Applied Mechanics 5, 677-714.
123. Handoo, K. L., and Sundararajan, V., 1971, Parametric instability of a cantilevered column with end mass, Journal of Sound and Vibration 18, 45-53.
124. Hastings, G.G., and Book, W.J., 1987, A linear dynamic model for flexible robotic manipulators, IEEE Control Systems Magazine, 61– 64.
125. He, G. P., and Lu, Z., 2005, Nonlinear dynamic analysis of planar flexible underactuated manipulators, Chinese Journal of Aeronautics 18, 78-82.
126. Heidari, A., 2005, Maximum Dynamic Load Carrying Capacity For Flexible Robot Manipulators With Finite Element Approach, M. Sc. Thesis, Mechanical Engineering Department, Iran University Science and Technology, Tehran, Iran.
127. Heidari, A., and Nikoobin, A., 2007, Maximum allowable dynamic load of flexible manipulators with imposing residual vibration constraint, IEEE International Conference on Robotics and Biomimetics (ROBIO '07), 1457-1462.
128. Heidari, A., and Nikoobin, A., 2007, Maximum allowable dynamic load of flexible manipulators with imposing residual vibration constraint, Proceedings of the IEEE International Conference on Robotics and Biomimetics December 15 -18,
129. Hermle, M., and Eberhard, P., 2000, Control and parameter optimization of flexible robots, Mechanics of Structures and Machines 28, 137–168.

130. Hillsley, K.L., and Yurkovich, S., 1991, Vibration control of a two-link flexible robot arm, Proceedings of the IEEE International Conference on Robotics and Automation , 2121–2126.
131. Hou, X., and Tsui, S.K., 1998, A control theory for Cartesian flexible robot arms, Journal of Mathematical Analysis and Applications 225, 265–288.
132. Hua, W., and Zhang, D., 2007, Modeling of impact dynamics of flexible robots, Chinese Journal of Mechanical Engineering 43, 222-228.
133. Huang, J. S., and Hung, L.H., 1984, Dynamic stability for a simply supported beam under periodic axial excitation, International Journal of Nonlinear Mechanics 29, 287-301.
134. Hwang, Y.L., 2005, A new approach for dynamic analysis of flexible manipulator systems, International Journal of Nonlinear Mechanics. 40, 925–938.
135. Hyun, H., and Yoo, H.H., 1999, Dynamic modeling and stability analysis of axially oscillating cantilever beams, Journal of Sound and Vibration 228, 543–558.
136. Inoue, T., and Ishida, Y., 2008, Nonlinear forced oscillation in a magnetically levitated system: the effect of the time delay of the electromagnetic force, Nonlinear Dynamics 52, 103-113.
137. Ji J. C. and Leung, A. Y. T., 2002, Bifurcation control of a parametrically excited duffing system**,** Nonlinear Dynamics 27, 411–417.
138. Jin, Y., and Hu, Y., 2007, Principal resonance of a Duffing oscillator with delayed state feedback under narrow-band random parametric excitation, Nonlinear Dynamics 50, 213–227.
139. Kargarnovin, M.H., Younesian, D., Thompson, D.J., and Jones, C.J.C., 2005, Response of beams on nonlinear viscoelastic foundations to harmonic moving loads, Computers and Structures 83, 1865–1877.
140. Karimi, H.R and Yazdanpanah, M.J., 2006, A new modeling approach to single-link flexible manipulator using singular perturbation method, Electrical Engineering 88, 375–382.

141. Khalil, W., and Gautier, M., 2000, Modeling of mechanical systems with lumped elasticity, Proceedings of the IEEE International Conference on Robotics and Automation 4, 3964–3969.
142. Kim, H.S., and Tsai, L.W., 2003, Design optimization of a Cartesian parallel manipulator, Trans. ASME, Journal of Mechanical Design 125, 43–51.
143. Kojima, H., and Nagaya, K., 1985, Nonlinear forced vibration of a beam with a mass subjected to alternating electromagnetic force, Bulletin of the Japan Society of Mechanical Engineers 28, 468–474.
144. Korayem, M.H., and Basu, A., 1994a, Formulation and numerical solution of elastic robot dynamic motion with maximum load carrying capacity, Robotica 12, 253–261
145. Korayem, M.H., and Basu, A., 1994b, Dynamic load carrying capacity for robotic manipulators with joint elasticity imposing accuracy constraints, Robotics and Autonomous Systems 13, 219–229
146. Korayem, M.H., and Basu, A., 2005, Dynamic load carrying capacity of mobile-base flexible joint manipulators, The International Journal of Advanced Manufacturing Technology 25, 62–70.
147. Korayem, M.H., and Ghariblu, H., 2003 Maximum allowable load on wheeled mobile manipulators imposing redundancy constraints, Robotics and Autonomous Systems 44,151–159
148. Korayem, M. H., Heidari A., and Nikoobin A., 2008, Maximum allowable dynamic load of flexible mobile manipulators using finite element approach, International Journal of Advanced Manufacturing Technology 36, 1010-1021.
149. Krishnamurthy, K., and Chao, M.C., 1992, Active vibration control during deployment of space structures, Journal of Sound and Vibration 152, 205–218.
150. Krishnamurthy K., Chandrashekhara, K., and Roy S., 1990, A study of single-link robots fabricated from orthotropic composite materials, Computers and Structures 136, 139–146.

151. Kumar, R., Berkelman, P., Gupta, P., Barnes, A., Jensen, P.S., Whitcomb, L.L., and Taylor, R.H., 2000, Preliminary experiments in cooperative human/robot force control for robot assisted micro-surgical manipulation, Proceedings of the IEEE International Conference on Robotics and Automation.

152. Kumar, R., Dwivedy, S.K., and Dixit, U.S., 2004, Shape optimization of Cartesian flexible manipulator, Proceedings of the 49th Congress of Indian Society of Theoretical and Applied Mechanics, (ISTAM), NIT Rourkela, India.

153. Kumar, R., Dwivedy, S.K., and Dixit, U.S., 2005, Shape optimization of a flexible robot manipulator, in: Proceedings of National Conference on Industrial Problems in Machines and Mechanisms (IPROMM-05), IIT Kharagpur, India..

154. Lee, H.P., 1995, Stability of a cantilever beam with tip mass subjected to axial sinusoidal excitations, Journal of Sound and Vibration 183, 91–98.

155. Lee, C. K., and Hu, Y. M., 2000, Sliding mode control of a single-link flexible robot arm robust to payload variations, Modeling Measurement & Control B: Solid & Fluid Mechanics & Thermics, Robotics Mechanical Systems, Civil Engineering 69, 1-21.

156. Lee, W.K., Lee, K.S., and Pak, C.H., Stability analysis for nonplanar free vibrations of a cantilever beam by using nonlinear normal modes, Nonlinear Dynamics 52, 217–225.

157. Lee, U., and Oh, H., 2005, Dynamics of an axially moving viscoelastic beam subject to axial tension, International Journal of Solids and Structures 42, 2381–2398.

158. Lee, J.D., and Wang, B.L., 1988, Optimal control of a flexible robot arm, Computers and Structures 29, 459–467.

159. Lew, J.Y., and Trudnowski, D.J., 1996, Vibration control of a micro/macro-manipulator system, IEEE Control System Magazine 16, 26–31.

160. Li, D., Zu, J.W., and Goldenberg, A.A., 1998, Dynamic modeling and mode analysis of flexible-link, flexible-joint robot, Mechanism and Machine Theory 33, 1031–1044.
161. Liu, Q., 1993, Dynamic Analysis of a Spatial Robot Manipulator with a Flexible Prismatic Link, Ph.D. Thesis, Mechanical Engineering, West Virginia University, Morgantown, VA..
162. Liu, M. F., and Chang, T.P., 2005, Vibration analysis of a magneto-elastic beam with general boundary conditions subjected to axial load and external force, Journal of Sound and Vibration 288, 399–411.
163. Liu, S., Wu, L., and Lu, Z., 2007, Impact dynamics and control of a flexible dual-arm space robot capturing an object, Applied Mathematics and Computation185, 1149-1159.
164. Loudini, K., Boukhela, D., and Tadjine, M., 2007, Comprehensive mathematical modeling of a lightweight flexible link robot manipulator, International Journal of Modeling, Identification and Control 2,313-321.
165. Love, L., Kress, R., and Jansen, J., 1997, Modeling and control of a hydraulically actuated flexible-prismatic link robot, Proceedings of the IEEE International Conference on Robotics and Automation 1, 669–675.
166. Lu, Q. S., To, C.W.S., and Huang, K. L., 1995, Dynamic stability and bifurcation of an alternating load and magnetic field excited magneto-elastic beam, Journal of Sound and Vibration, 181, 873–891.
167. Lv, Y. G., Wei, Y. D., and Chen, Z. C., 2007, Active control on coupled bending-torsion vibration of two link space flexible component, Journal of Zhejiang University 41,715-719.
168. Maccari, A., 2001, Bifurcation analysis of parametrically excited Rayleigh–Liénard oscillators, Nonlinear Dynamics 25, 293–316.
169. Maccari, A., 2006, Vibration control for parametrically excited Liénard systems, International Journal of Non-Linear Mechanics 41, 146–155.

170. Magee, D.P., and Book, W.J., 1993, Eliminating multiple modes of vibration in a flexible manipulator, Proceedings of the IEEE International Conference on Robotics and Automation 2, 274–279.
171. Mahmoodi, S. N., Jalili, N., and Khadem, S. E., 2008, An experimental investigation of nonlinear vibration and frequency response analysis of cantilever viscoelastic beams, Journal of Sound and Vibration 311, 1409–1419.
172. Mahmoodi, S.N., Khadem, S.E., and Esmailzadeh, E., 2005, Equations of nonlinear motion of viscoelastic beams, ASME, International Design Engineering Technical Conferences and Computers and Information in Engineering Conference 1, 231-235.
173. Mahmoodi, S.N., Khadem, S.E., and Kokabi, M., 2007, Non-linear free vibrations of Kelvin–Voigt visco-elastic beams, International Journal of Mechanical Science 49, 722–732.
174. Mailybaev, A.A., Yabuno, H., and Kaneko, H., 2004, Optimal shapes of parametrically excited beams, Structural and Multidisciplinary Optimization 27, 435–445.
175. Martins, J., Botto, M.A., and Sa da Costa, J., 2002, Modeling flexible beams for robotic manipulators, Multibody System Dynamics 7, 79–100.
176. Martins, J.M., Mohamed, Z., Tokhi, M.O., Sa da Costa, J. and Botto M.A., 2003, Approaches for dynamic modelling of flexible manipulator systems, IEE, Proceedings of Control Theory Applications, 140 (4), 401-411.
177. Marynowski, K., 2002, Non-linear dynamic analysis of an axially moving viscoelastic beam, Journal of Theoretical and Applied Mechanics 40, 465–482.
178. Marynowski, K., 2004, Non-linear vibrations of an axially moving viscoelastic web with time-dependent tension, Chaos, Solitons, and Fractals 21, 481–490.

179. Marynowski, K., 2006, Two-dimensional rheological element in modeling of axially moving viscoelastic web, European Journal of Mechanics A Solids 25, 729–744.
180. Marynowski, K., and Kapitaniak, T., 2002, Kelvin–Voigt versus Bugers internal damping in modeling of axially moving viscoelastic web, International Journal of Non-Linear Mechanics 37,1147–1161.
181. Marynowski, K., and Kapitaniak, T., 2007, Zener internal damping in modeling of axially moving viscoelastic beam with time-dependent tension, International Journal of Non-Linear Mechanics 42, 118–131.
182. Md-Zain, M.Z., Tokhi, M.O., and Mohamed, Z., 2006, Hybrid learning control schemes with input shaping of a flexible manipulator system, Mechatronics 16, 209–219.
183. Meckl, P.H., and Seering, W.P., 1990, Experimental evaluation of shaped inputs to reduce vibration of a Cartesian robot, ASME Journal of Dynamic Systems, Measurement, and Control 112,159–165.
184. Megahed, S.M., and Hamza, K.T., 2004, Modeling and simulation of planar flexible link manipulators with rigid tip connections to revolute joints, Robotica 22, 285–300.
185. Meggiolaro, M.A., and Dubowsky, S., 2001, Improving the positioning accuracy of powerful manipulators with application in nuclear maintenance, Proceedings of the 16th Brazilian Congress of Mechanical Engineering, (COBEM) on Robotics and Control 15, 210–219.
186. Miya, K., Hara, K., and Someya, K., 1978, Experimental and theoretical study on magneto-elastic buckling of ferro-elastic cantilevered beam-plate, Journal of Applied Mechanics 45, 355–360.
187. Moallem, M., Patel, R.V., and Khorasani, K., 2000, Flexible-link robot manipulators: control techniques and Structural Design, Springer-Verlag, London.

188. Moallem, M., Patel, R.V., and Khorasani, K., 2001, Nonlinear tip position tracking control of a flexible-link manipulator: theory and experiments, Automatica 37, 1825–1834.
189. Mockensturm, E.M., and Guo, J., 2005, Nonlinear Vibration of parametrically excited viscoelastic axially moving strings, Tran. ASME, Journal of Applied Mechanics 72, 374-380.
190. Mohamed, Z., Martins, J.M., Tokhi, M.O., Costa, J. S.D., and Botto, M.A., 2005, Vibration control of a very flexible manipulator system, Control Engineering Practice 13, 267–277.
191. Mohamed, Z., and Tokhi, M.O., 2004, Command shaping techniques for vibration control of a flexible robot manipulator, Mechatronics 14, 69–90.
192. Monje, C.A., Ramos, F., Feliu V., and Vinagre B.M., 2007, Tip position control of a lightweight flexible manipulator using a fractional order controller, IET Control Theory & Applications 1, 1451–1460.
193. Moon, F.C. and Pao, Y.H., 1968, Magneto-elastic buckling of a thin plate, Trans. ASME, Journal of Applied Mechanics 37, 53–58.
194. Moon, F.C. and Pao, Y.H., 1969, Vibration and dynamic instability of a beam-plate in a transverse magnetic field, Journal of Applied Mechanics 36, 92–100.
195. Morgul, O., 1990, On the boundary control of a flexible robot arm, in: IEEE International Workshop on Intelligent Motion Control, Istanbul, Turkey, 519–522.
196. Morris, A.S., and Madani, A., 1996, Inclusion of shear deformation term to improve accuracy in flexible link robot modeling, Mechatronics 6, 631–647.
197. Munasinghe, S.R., Nakamura, M., Aoki, S., Goto, S., and Kyura, N., 1999, High speed precise control of robot arms with assigned speed under torque constraint by trajectory generation in joint co-ordinates, Proceedings of IEEE International Conference on Systems, Man, and Cybernetics 2, 854–859.
198. Murrugarra, C., Grieco, J., Fernandez, G., and De Castro, O., 2006, Design of a PD position control based on the Lyapunov theory for a robot

manipulator flexible-link, IEEE, International Conference on Robotics and Biomimetics -ROBIO2006, 890-895.

199. Muscolino, G., and Palmeri, A., 2007, Response of beams resting on viscoelastically damped foundation to moving oscillators, International Journal of Solids and Structures 44,1317–1336.
200. Naganathan, G., and Soni, A.H., 1986, Non-linear flexibility studies for spatial manipulators, Proceedings of the IEEE International Conference on Robotics and Automation 3, 373–378.
201. Nagaraj, B.P., Nataraju, B.S., and Chandrasekhar, D.N., 2001, Nondimensional parameters for the dynamics of a single flexible link, in: International Conference on Theoretical, Applied, Computational and Experimental Mechanics (ICTACEM) Kharagpur, India.
202. Nayfeh, A, H., 1987, Parametric excitation of two internally resonant oscillators, Journal of Sound and Vibration 119, 95-105.
203. Nayfeh, A. H., 1993, Method of Normal Forms, New York: Wiley-Interscience.
204. Nayfeh, A. H., and Balachandran, B., 1995, Applied Nonlinear Dynamics—Analytical, Computational and Experimental Methods, Wiley, Canada.
205. Nayfeh, A. H., and Jebril, E. S., 1987, The response of two-degree of freedom systems with quadratic and cubic nonlinearities to multifrequency parametric excitations, Journal of Sound and Vibration 118, 83-101.
206. Nayfeh, A. H., and Mook, D.T., 1995, Nonlinear Oscillations, Wiley, New York.
207. Nayfeh, A.H., and Pai, P. F., 1989, Nonlinear nonplanar parametric responses of an inextensional beam, International Journal of Nonlinear Mechanics 24, 139-158.
208. Nayfeh, A.H., and Zavodney, L. D., 1986, The response of two degree-of-freedom systems with quadratic non-linearities to a combination parametric resonance, Journal of Sound and Vibration 107, 329-350.

209. Neal, H. L., and Nayfeh, A. H., 1990, Response of a single-degree- of-freedom system to a non-stationary principal parametric excitation, International Journal of Nonlinear Mechanics 25, 275-284.
210. Ng, L., and Rand, R., Nonlinear effects on coexistence phenomenon in parametric excitation, Nonlinear Dynamics 31, 73–89.
211. Nissing, D., 2000, A vibration damped flexible robot: identification and parameter optimization, Proceedings of the American Control Conference Chicago, Illinois.
212. Oden, J. T., and Bhandari, D. R., 1972, Variational Principles in Nonlinear viscoelasticity, International Journal of Solids and Structures 8, 1017–1026.
213. Onsay, T., and Akay, A., 1991, Vibration reduction of a flexible arm by time optimal open-loop control, Journal of Sound and Vibration 147, 283–300.
214. Ower, J.C., and Van De Vegte, J., 1987, Classical control design for a flexible manipulator: modeling and control system design, Journal of Robotics and Automation 3, 485- 489.
215. Oz, H. R., 2001, On the vibrations of an axially traveling beam on fixed supports with variable velocity, Journal of Sound Vibration 239, 556–564.
216. Oz, H. R., and Pakdemirli, M., 1999, Vibrations of an axially moving beam with time dependent velocity, Journal of Sound Vibration 227, 239–257.
217. Ozkaya, E., and Pakdemirli, M., 2000, Vibrations of an axially accelerating beam with small flexural stiffness, Journal of Sound Vibration 234, 521–535.
218. Oz, H.R., Pakdemirli, M., and Boyaci, H., 2001, Non-linear vibrations and stability of an axially moving beam with time-dependent velocity, International Journal Non-Linear Mechanics 36, 107–115.
219. Oz, H.R., Pakdemirli, M., and Ozkaya, E., 1998, Transition behaviour from string to beam for an axially accelerating material, Journal of Sound Vibration 215, 571–576.
220. Ozkaya, E., and Oz, H. R., 2002, Determination of natural frequencies and stability regions of axially moving beams using artificial neural networks method, Journal of Sound Vibration 254, 782–789.

221. Ozkaya, E., and Pakdemirli, M., 2000, Vibrations of an axially accelerating beam with small flexural stiffness, Journal of Sound and Vibration 234, 521–535.

222. Pai, P.F., and Nayfeh, A.H., 1990, Non-linear non-planar oscillations of a cantilever beam under lateral base excitations, International Journal of Nonlinear Mechanics 25, 455-474.

223. Pal, S., Stephanou, H.E., and Cook, G., 1989, Optimal control of a single-link flexible manipulator, Journal of Intelligent and Robotic Systems 2, 187–199.

224. Park, H., and Cho, H., 1991, General design conditions for an ideal robotic manipulator having simple dynamics, The International Journal of Robotics Research 10, 21–29.

225. Pan, Y.C., Scott, R.A., and Ulsoy, A.G., 1990, Dynamic modeling and simulation of flexible robots with prismatic joints, Trans. ASME, Journal of Mechanical Design 112, 307–314.

226. Pan, Y.C., Ulsoy, A.G., and Scott, R.A., 1990, Experimental model validation for a flexible robot with a prismatic joint, Trans. ASME, Journal of Mechanical Design 112, 315–323.

227. Parker, R.G., and Lin, Y., Parametric instability of axially moving media subjected to multifrequency tension and speed fluctuations, Trans. ASME, Journal of Applied Mechanics 68, 49–57.

228. Parks, T.R., and Pak, H.A., 1991, Effect of payload on the dynamics of a flexible manipulator modeling for control, Trans. ASME, Journal of Dynamic Systems, Measurement, and Control 113, 409–418.

229. Payo, I., Ramos, F., Cortazar, O. D., and Feliu, V., 2005, Experimental validation of nonlinear dynamic models for single-link very flexible arms, Proceedings of the 44th IEEE Conference on Decision and Control, and the European Control Conference, CDC-ECC '05, 5304-5309.

230. Pelicano, F., and Vestroni, F., 2000, Non-linear dynamics and bifurcations of an axially moving beam, ASME Journal of Vibration and Acoustics 122, 21–30.

231. Pellicano F., and Vestroni, F., 2002, Complex dynamic of high-speed axially moving systems, Journal of Sound and Vibration 258,31–44.
232. Pfeiffer, F., and Gebler, B., 1988, A multistage approach to dynamics and control of elastic robots, Proceedings of IEEE, International Conference on Robotics and Automation 1, 2-8.
233. Poppelwell, N., and Chang, D., 1996, Influence of an offset payload on a flexible manipulator, Journal of Sound and Vibration 190, 721–725.
234. Qian, W. T., and Ma, C. C. H., 1992, A new controller design for a flexible one-link manipulator, Trans of IEEE, Automatic Control 37, 132–137.
235. Raghothama, A., And Narayanan, A, 2002, Periodic response and chaos in nonlinear systems with parametric excitation and time delay, Nonlinear Dynamics 27, 341–365.
236. Rakhsha, F., and Goldenberg, A.A., 1985, Dynamic modeling of a single link flexible robot, Proceedings of the IEEE International Conference on Robotics and Automation, 984–989.
237. Rattan, K.S., Feliu, V., and Brown, H.B., 1988, Identification and control of a single-link flexible manipulator, Proceedings of the IEEE International Conference on Robotics and Automation 3, 2278–2279.
238. Rosado, V.O.G., and Yuhara, E.A.O., 1999, Dynamic modeling and simulation of a flexible robotic manipulator, Robotica 17, 523–528.
239. Russell, J.L., 1995, Optimization Models for Flexible Manipulators, Ph.D. Dissertation, Department of Systems and Industrial Engineering, University of Arizona, Tucson.
240. Saito, H., and Koizumi, N., 1982, Parametric vibrations of a horizontal beam with a concentrated mass at one end, International Journal of Mechanical Sciences, 24,755-761.
241. Saito, H., and Otomi, K., 1979, Parametric response of viscoelastically supported beams, Journal of Sound and Vibration 63,169–178.

242. Sanchez, N. E., and Nayfeh, A. H., 1990, Prediction of bifurcations in a parametrically excited Duffing oscillator, International Journal of Non-linear Mechanics 25, 163-176.

243. Sang, H. K., Chang, P.H., and Eunjeong, Lee., 2004, Stability analysis of nonlinear bang-bang impact control for a one degree of freedom robotic manipulator, Proceedings of the IEEE International Conference on Mechatronics 2004 (IEEE Cat. No.04EX899), 84-91.

244. Shaheed, M.H., and Tokhi, M.O., 2002, Dynamic modelling of a single-link flexible manipulator: parametric and non-parametric approaches, Robotica 20, 93–109.

245. Sharan, A.M., Jain, J., and Kalra, P., 1992, Efficient methods for solving dynamic problems of flexible manipulators, ASME Journal of Dynamic Systems, Measurement, and Control 114, 78–88.

246. Shih, Y.S., and Yeh, Z.F., 2005, Dynamic stability of a viscoelastic beam with frequency-dependent modulus, International Journal of Solids and Structures 42, 2145–2159.

247. Shirahatti, U.S., and Sinha, S.C., 1994, On the stability of perfect viscoelastic columns, Journal of Sound and Vibration 117, 57–68.

248. Siciliano, B., and Book, W.J., 1988, A singular perturbation approach to control of light weight flexible manipulator, The International Journal of Robotics Research 7, 79–90.

249. Simo, J.C., and Vu-Quoc, L., 1986a, On the dynamics of flexible beams under large overall motions the plane case: Part 1, Trans. of ASME, Journal of Applied Mechanics 53,849–854.

250. Simo, J.C., and Vu-Quoc, L., 1986b, On the dynamics of flexible beams under large overall motions– the plane case: Part II, Trans. of ASME,Journal of Applied Mechanics 53, 855–863.

251. Singer, N.C. and Seering, W.P.,1990, Reshaping command inputs to reduce system vibration, ASME Journal of Dynamic Systems, Measurement and Contro112 (1) ,76-82.

252. Singh, T., 1991, Dynamics and Control of Flexible Arm Robots, Ph.D. Thesis, Mechanical Engineering, Waterloo University, Canada.
253. Sinha, S. C., Redkar, S., Deshmukh, V., and Butcher, E.A., 2005, Order reduction of parametrically excited nonlinear systems: techniques and applications, Nonlinear Dynamics 41, 237–273.
254. Soliman, M.S., 1994, Global transient dynamics of nonlinear parametrically excited systems, Nonlinear Dynamics 6, 317-329.
255. Son, I. S., Uchiyama, Y., Lacarbonara, W., and Yabuno, H., 2008, Simply supported elastic beams under parametric excitation, Nonlinear Dynamics 53, 129–138.
256. Soon, L.T., and Jaw, J.Y., 1992, Shear deformation effect in design considerations of flexible manipulators, Robotica 11, 83–92.
257. Stevens, K. K., 1966, On the parametric excitation of a viscoelastic column, American Institute of Aeronautics and Astronautics Journal 4, 2111-2116.
258. Stevens, K. K., 1969, Transverse vibration of a viscoelastic column with initial curvature under periodic axial load, Trans. of ASME, Journal of Applied Mechanics 36, 814-818.
259. Stevens, K. K., and Evan-Iwanowski, R. M., 1969, Parametric resonance of viscoelastic column, International Journal of Solids and Structures 5, 755-765.
260. Subudhi, B., and Morris, A. S., 2002, Dynamic modeling, simulation and control of a manipulator with flexible links and joints, Robot Automation Systems 4, 257–270.
261. Suire, G. and Cederbaum, G., 1995, Periodic and chaotic behavior of viscoelastic nonlinear bars under harmonic excitations, International Journal of Mechanical Science 37, 753–772.
262. Szemplin'ska-Stupnicka, W., 1990, The Behaviour of Non-linear Vibrating Systems, Vols. 1 and 2, Kluwer Academic Publishers, London.

263. Tadikonda, S.S.K., and Baruh, H., 1992, Dynamics and control of a flexible beam with a prismatic joint, Trans. of ASME Journal Dynamics, Measurement and Control 114, 422–427.

264. Theodore, R.J., Arakeri, J.H., and Ghosal, A., 1996, Modelling of axially translating flexible beam, Journal of Sound and Vibration 191, 363-376.

265. Theodore, R.J., and Ghosal, A., 1995, Comparison of the assumed modes and finite element models for flexible multilink manipulators, The International Journal of Robotics Research 14, 91-111.

266. Theodore, R.J., and Ghosal, A., 1997, Modeling of flexible-link manipulators with prismatic joints, IEEE Transactions on Systems, Man, and Cybernetics, Part B: Cybernetics 27, 296–305.

267. To, C. W.S., 1982, Vibration of a cantilever beam with a base excitation and tip mass, Journal of Sound and Vibration 83, 445-460.

268. Tokhi, M.O., Mohamed, Z., and Shaheed, M.H., 2001, Dynamic characterisation of a flexible manipulator system, Robotica 19,571–580.

269. Tokhi, M.O., Mohamed, Z., Amin, S.H.M., and Mamat, R., 2000, Dynamic characterization of a flexible manipulator system: theory and experiments, Proceedings of TENCON 3, 167–172.

270. Tomei, P., and Tornambe, A., 1988, Approximate modeling of robots having elastic links, IEEE Transactions on Systems, Man and Cybernetics 18, 831–840.

271. Tso, S.K., Yang, T.W., Xu, W.L., and Sun, Z.Q., 2003, Vibration control for a flexible link robot arm with deflection feedback, International Journal of Non-Linear Mechanics 38, 51–62.

272. Tu, Q., and Rastegar, J., 1994, Effects of payload on the vibrational excitation of robot manipulators during motion, Proceedings of ASME, Conference on Machine Elements and Machine Dynamics, 17-24.

273. Tylikowski, A., 2003, Stabilization of parametric vibrations of a nonlinear continuous system, Meccanica 38, 659–668.

274. Tzes, A.P., Yurkovich, S., Siemens, F.D.L., 1989, A method for solution of the Euler–Bernoulli beam equation in flexible-link robotic systems, Proceedings of the IEEE International Conference on Systems Engineering , 557–560.

275. Tzou, H.S., 1989, Nonlinear structural dynamics of space manipulators with elastic joints, International Journal of Analytical and Experimental Modal Analysis 4, 117–123.

276. Wang, F.Y., 1994, On the extremal fundamental frequencies of one-link flexible manipulator, The International Journal of Robotics Research 132, 162–170.

277. Wang, X., Chen, F., and Zhou, L., 2008, Stability and bifurcation for a flexible beam under a large linear motion with a combination parametric resonance, Nonlinear Dynamics, DOI 10.1007/s11071-008-9382-y.

278. Wang, F.Y., and Guan, G.G., 1994, Influence of rotary inertia, shear deformation and loading on vibration behaviours of flexible manipulators, Journal of Sound and Vibration 171, 433–452.

279. Wang, F.Y., and Gao, Y., 2003, Advance Studies of Flexible Robotic Manipulator: Modeling, Design, Control and Application. Series in Intelligent Control and Automation, vol. 4, World Scientific Publishing Co. Pte. Ltd., Singapore.

280. Wang, X., and Lee, J. S., 2006, Dynamic stability of ferromagnetic beam-plates with magnetoelastic interaction and magnetic damping in transverse magnetic fields, ASCE, Journal of Engineering Mechanics 4, 363-375.

281. Wang, D., Liu, Y., and Meng, M., 1999, A study of limit cycles and chaotic motions of a single-link robot manipulator during slow motion, IEEE Conference Proceedings on Systems, Man, and Cybernetics 2, 884–888.

282. Wang, D., Meng, M., and Liu, Y., 1999, Influence of shear, rotary inertia on the dynamic characteristics of flexible manipulators, in: IEEE Pacific Rim Conference on Communications, Computers and Signal Processing, 615–618.

283. Wang, L.T., and Ravani, B., 1988a, Dynamic load carrying capacity of mechanical manipulators part I Problem formulation, ASME Journal of Dynamic Systems, Measurement, and Control 110, 46–52.
284. Wang, L.T., and Ravani, B., 1988b, Dynamic load carrying capacity of mechanical manipulators part II: Computational procedure and applications, ASME Journal of Dynamic Systems, Measurement, and Control 110, 53–61.
285. Wang, F.Y., and Russel, J.L., 1965, Optimum shape construction of flexible manipulators with total weight constraint, IEEE Transactions on Systems, Man and Cybernetics 25, 605–614.
286. Wang, F.Y., and Russel, J.L., 1992, Optimum shape construction of flexible manipulators with tip loads, Proceedings of the IEEE Conference on Decision and Control 1, 311–316.
287. Wang, F.Y., and Russel, J.L., 1997, Minimum weight robot arm for a specified fundamental frequency, Journal of Robotic Systems 13, 157–161.
288. Wang, P.K.C., and Wei, J. D., 1987, Vibration in a moving flexible robot arm, Journal of Sound and Vibration 116, 149–160.
289. Wallerstein, D.V., and Peach, M.O., 1972, Magneto-elastic buckling of beams and thin plates of magnetically soft material, Journal of Applied Mechanics 39, 451–455.
290. Wei, Y. D., Lu, Y. G., Lu, C. Y., Wen, Y.H., and Chen, Z.C., 2005, Active torsional vibration control of flexible manipulator, Zhejiang Daxue Xuebao (Gongxue Ban)/ Journal of Zhejiang University (Engineering Science) 39, 1761-1764.
291. Wickert, J.A., and Mote Jr., C.D., 1988, Current research on the vibration and stability of axially-moving materials, The Shock and Vibration Digest 20, 3–13.
292. Wickert, J.A., and Mote Jr., C.D., 1990, Classical vibration analysis of axially moving continua, Journal of Applied Mechanics 57, 738–744.

293. Wu, G. Y., 2005a, Transient vibration analysis of a pinned beam with transverse magnetic fields and thermal loads, ASME, Journal of Vibration and Acoustics 127, 247-253.

294. Wu, G.Y., 2005b, The analysis of dynamic instability and vibration motions of a pinned beam with transverse magnetic fields and thermal loads, Journal of Sound and Vibration 284, 343–360.

295. Wu, G. Y., 2007, The analysis of dynamic instability on the large amplitude vibrations of a beam with transverse magnetic fields and thermal loads, Journal of Sound and Vibration 302, 167-177.

296. Wu, G. Y., Tsai, R., and Shih, Y.S., 1997, The analysis of dynamic stability and vibration motions of a cantilever beam with axial loads and transverse magnetic fields, Journal of the Acoustical Society of ROC 4, 40–55.

297. Yabuno, H., and Nayfeh, A. H., 2001, Nonlinear normal modes of a parametrically excited cantilever beam, Nonlinear Dynamics 25, 65–77.

298. Yagasaki, K., Sakata, M., and Kimura, K., 1990, Dynamics of a weakly nonlinear system subjected to combined parametric and external excitation, ASME, Journal of Applied Mechanics 57, 209-217.

299. Yang, G.B., and Donath, M., 1988, Dynamic model of a one link robot manipulator with both structural and joint flexibility, Proceedings of the IEEE International Conference on Robotics and Automation, 476–481.

300. Yang, X.D., and Chen, Li. Q., 2005, Bifurcation and chaos of an axially accelerating viscoelastic beam, Chaos, Solitons & Fractals 23, 249–258.

301. Yang, X.D., and Chen, L.Q., 2006, Stability in parametric resonance of axially accelerating beams constituted by Boltzmann's superposition principle, Journal of Sound and Vibration 289, 54–65.

302. Yoon. G. S., and Kyu, T. L., 2006, An adaptive tracking controller for vibration reduction of flexible manipulator, International Journal of Precision Engineering and Manufacturing 7, 51-55.

303. Yu, C.S., and Yuan, T.J., 2008, Study on a new nonlinear parametric excitation equation: Stability and bifurcation, Journal of Sound and Vibration, doi:10.1016/j.jsv.2008.04.055.

304. Yue, S., Tso, S. K., and Xu, W. L., 2001, Maximum dynamic payload trajectory for flexible robot manipulators with kinematic redundancy, Mechanism and Machine Theory 36, 785–800

305. Yuh, J. and Young, T., 1991, Dynamic modeling of an axially moving beam in rotation: simulation and experiment, ASME Journal of Dynamic Systems, Measurement, and Control 113, 34-40.

306. Yuh, J., Young, T., and Baek, Y.S., 1989, Modeling of flexible link having a prismatic joint in robot mechanism-experimental verification, Proceedings of the IEEE International Conference on Robotics and Automation 2, 722–727.

307. Zhang, P., and Li, Y., 2007, Position/force control of two manipulators handling a flexible payload based on finite-element model, IEEE International Conference on Robotics and Biomimetics (ROBIO '07), 2178-2182.

308. Zhang, W., and Meng, G., 2005, Nonlinear dynamical system of micro cantilever under

combined parametric and forcing excitations in MEMS, Sensors and Actuators A 119,

291–299.

309. Zhang, W., Wang, F., and Yao, M., Global bifurcations and chaotic dynamics in nonlinear

nonplanar oscillations of a parametrically excited cantilever beam, Nonlinear Dynamics

40, 251–279.

310. Zhang, D.G., and Zhou, S.F., 2006, Dynamic analysis of flexible link and flexible joint

robots, Applied Mathematics and Mechanics 27, 695-704.

311. Zhao, W.J., and Chen, L.Q., 2002, A numerical algorithm for non-linear parametric vibration analysis of a viscoelastic moving belt, International Journal of Nonlinear Science and Numerical Simulation 3 (2), 139–144.

312. Zavodney, L.D., and Nayfah, A.H., 1988, The response of a single-degree-of-freedom system with quadratic and cubic non-linearities to a fundamental parametric resonance, Journal of Sound and Vibration 120, 63-93.

313. Zavodney, L.D., and Nayfah, A.H., 1989, The non-linear response of a slender beam carrying a lumped mass to a principal parametric excitation: theory and experiment, International Journal of Nonlinear Mechanics 24, 105-125.

314. Zavrazhina, T.V., 2007, Influence of the flexibility of links on the dynamics of a multilink robot manipulator, International Applied Mechanics 43, 577-585.

315. Zhou, D., 1997, The vibrations of a cantilever beam carrying a heavy tip mass with elastic supports, Journal of Sound and Vibration 206, 275–279.

316. Zhou, C.L., Fang, X.Q., and Su, X. Y., 2004, Dynamic analysis and strength of a flexible robot manipulator, Gongcheng Lixue/Engineering Mechanics 21, 11-15.

317. Zhu, G., Ge, S.S., and Lee, T.H., 1999, Simulation studies of tip tracking control of a single-link flexible robot based on a lumped model, Robotica 17, 71–78.

318. Zuev, A.L., 2005, Control of a flexible manipulator within the framework of the Timoshenko beam model, International Applied Mechanics 41, 1418-1425.